First Evidence for Ultrahigh Pressure Metamorphism on Gossa, Western Gneiss Region, Norway

MSc thesis
Willem Dabekaussen

October 2009
Faculty of Geosciences
Utrecht University

Supervisors:
Dr. H.L.M. van Roermund
Dr. A. Barnhoorn

Abstract

Ultrahigh pressure (UHP) metamorphism takes place in rock at depths within the coesite stability field. In the Western Gneiss Region (WGR) in Norway, three domains are present where UHP metamorphic rocks occur. In the northern UHP domain, evidence for UHP is concentrated in three distinct areas. In between these areas lies the island of Gossa. This island is often included in the northern UHP domain, but this is based on extrapolation of lithologies around Gossa and no direct evidence exists that these rocks have experienced UHP metamorphic conditions. Some authors dispute the existence of one UHP domain, and explain the UHP outcrops as small UHP thrust nappes within a single larger lower pressure domain. The aim of this research is to constrain the peak metamorphic conditions of the rocks on Gossa, which places this part of the WGR either within or outside the northern UHP domain.

Fieldwork was carried out on Gossa during the summer of 2008. One of the lithologies that are found here is orthopyroxene (opx) bearing eclogite, enclosed as lenses within basement gneisses. This lithology is sampled for determination of peak metamorphic conditions by evaluating the Al_2O_3 content of opx in contact with garnet. Granulites and basement gneisses have been sampled to constrain the retrograde pressure and temperature (PT) path. All samples are analysed by optical microscopy for determination of their metamorphic facies based on their mineral content. Pressure and temperature are calculated for eclogites and granulites by various geothermobarometric methods, using major element mineral chemistry obtained by analysis of the samples by Electron Microprobe.

Al_2O_3 contents in opx of 0.26 and 0.30 wt% are measured in eclogites from two different outcrops. These very low Al_2O_3 contents indicate UHP conditions, probably within the diamond stability field, with pressures of >37kbar and temperatures of 780-1000ºC. The PT path, based on optical microscopy as well as geothermobarometry, shows isothermal decompression after the peak metamorphic stage until 8-10 kbar. This is followed by cooling without significant change in pressure until ±500ºC. This PT path shows a good correlation with published PT paths of the surrounding area. These results indicate that the northern UHP domain forms one coherent body instead of small scale thrust nappes, and Gossa can be included in this domain.

Index

1 Introduction

In the Western Gneiss Region (WGR) of SW Norway (figure 1.1) mid- to late Proterozoic gneisses are exposed, defining the Western Gneiss Complex (WGC). The WGC forms a window that is overlain by allochthonous Nappes called Lower, Middle, Upper and Uppermost Allochthons (Carswell and Cuthbert, 2003). The WGR is in particular interest to geologists because of the evidence that some parts have undergone ultrahigh pressure metamorphism (UHPM). At many places in the WGR ultrahigh pressure (UHP) metamorphic conditions are demonstrated. UHP occurrences are not evenly distributed across the WGR, but are found in three distinct domains that are referred to as the Northern, Middle and Southern UHP domain (see figure 1.1). More or less in the central part of the northern UHP domain lies the island of Gossa. At three distinct locations around this island outcrops of UHPM rocks are recognised (see figure 2.11). Some authors explain these UHP occurrences by placing them in one large UHP domain (e.g. Spengler, 2006; Vrijmoed et al., 2006) while others (e.g. Terry et al., 2000b) think that the UHP occurrences are in fact thrust nappes, brought to structurally higher levels and therefore are now located in a non-UHP environment. In these different theories Gossa is placed either within or outside the northern UHP domain, based on extrapolation of evidence from other locations.

The main object of this master thesis is to place the metamorphic rocks exposed at the island of Gossa either inside or outside the northern UHP domain. The pressure and temperature (PT) history of the rocks on Gossa will be the most important clue. The maximum PT conditions will reveal whether UHP metamorphic conditions are experienced by the rocks on Gossa. If the rocks on Gossa are part of the northern UHP domain, it is expected that PT paths of rocks on Gossa and other parts of the northern UHP domain show a similar pattern. The PT path of the rocks on Gossa will therefore be compared with published PT paths from UHP metamorphic occurrences in other parts of the northern UHP domain.

This thesis first treats the regional geological setting of the WGR and the position of the northern UHP domain, and deals with the basics of evaluating PT conditions (chapter 2). This creates a reference for the lithologies that are found during the fieldwork and the kind of rocks that are suitable for detecting UHP conditions. Fieldwork has been performed to construct a geological map of Gossa, gather structural data and collect samples of rocks on Gossa (chapter 3). Thin sections are constructed from the most important samples and used for further analysis. Optical microscopy results (chapter 4) supply the different lithologies with a rough PT estimate based on their mineral assemblage. Some samples are analysed by electron microprobe (EMP) to gather detailed data about mineral composition. This data is used to calculate PT conditions by geothermobarometric principles (chapter 5 and 6). All data that is collected in chapter 3 to 6 will be brought together to construction a single PT path (chapter 7), which will then be compared with published PT paths of other parts of the northern UHP domain (chapter 8). In this chapter it will become clear whether Gossa can be included in the northern UHP domain.

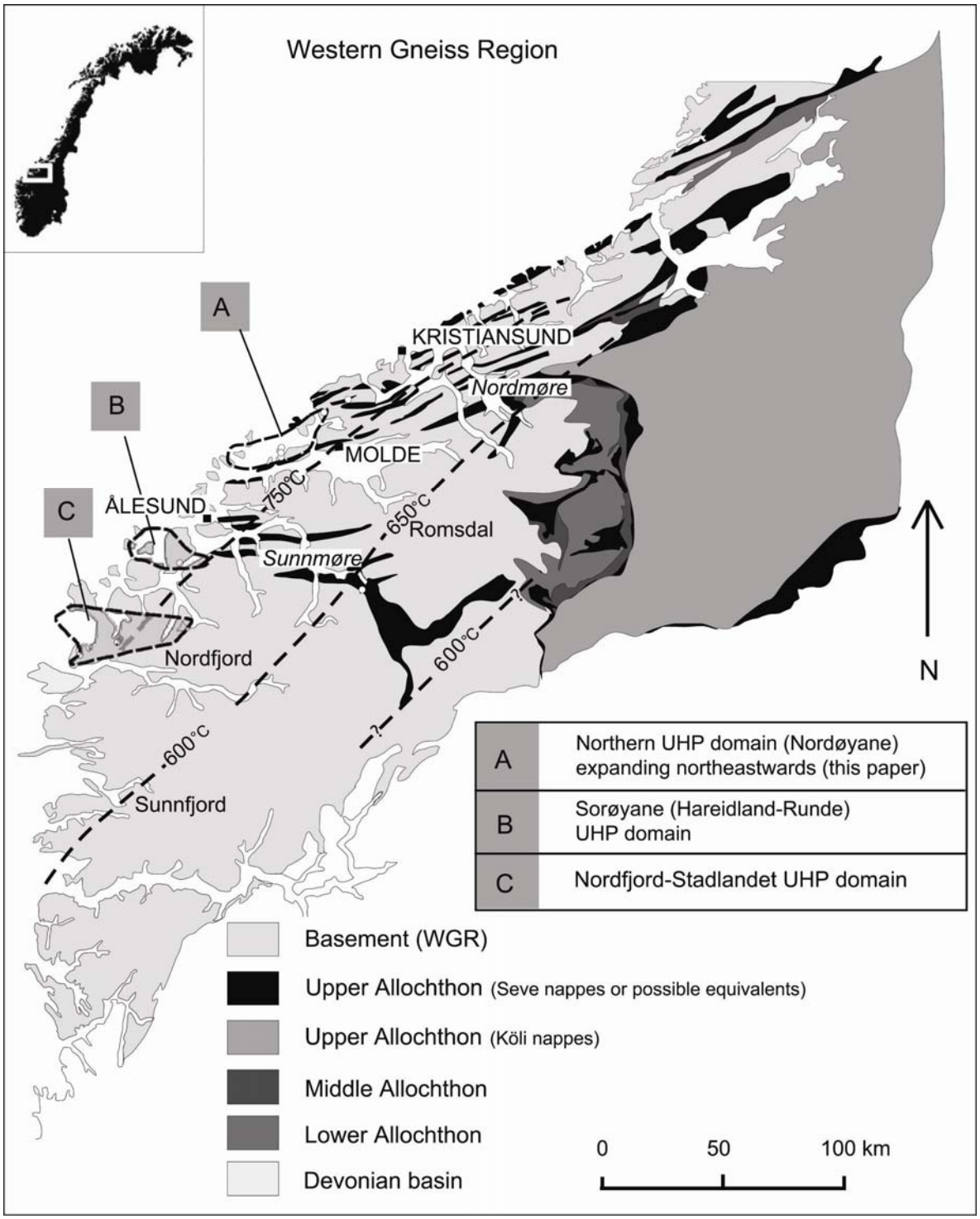

Figure 1.1. Geological map of the WGR. Indicated in light grey are the basement rocks, along the coast 3 UHP domains are illustrated, indicated A, B and C. Regional temperature gradient across the Western Gneiss Region, based on Fe^{2+}/Mg^{2+} partitioning between garnet and omphacite in eclogites (Griffin et al., 1985). Modified image from Vrijmoed et al. (2006).

2 Previous Research

Over the last decades there has been a large interest in the geology of the WGR. To create a framework for the results of this study a summary of essential knowledge of the WGR will be given in this chapter. In section 2.1 the regional geology of the WGR and the rocks occurring in the WGC will be presented, after which the geodynamic models will be discussed that explain the history of the WGR on a large scale. The geological setting of northern UHP domain will be presented in more detail section 2.2, with particular focus on the known UHP occurrences and the expected geology on Gossa. Section 2.3 deals with the basics of PT evaluation techniques, which will be important for the kind of rocks that are sampled in the field and therefore essential for the rest of this study.

2.1 The Western Gneiss Region

2.1.1 Geological setting of the Western Gneiss Region

During the Scandian phase (430-400 Ma) of the Caledonian orogeny the leading edge of the Baltic Plate experienced a short lived but deep subduction beneath the Laurentian Plate (details of tectonic models are discussed in section 2.1.4). The Caledonides became fragmented after break-up of the super-continent Pangea, and can now be found on different continents: the American Appalachians, Greenland Caledonides, British Caledonides and the Scandinavian Caledonides (Spengler, 2006).

The Scandinavian Caledonides are made up of autochthonous basement, covered by a thick stack of allochthonous thrust sheets (Walsh and Hacker, 2004). The allochthons are grouped into the Lower, Middle and Upper Allochthon (see figure 2.1). The WGR is located In the southwestern part of the Scandinavian Caledonides. In the WGR a tectonic window causes the autochthonous basement to be exposed. The basement in this region is called the WGC (note the distinction between the WGR, an area, and the WGC, a rock unit). Within the Scandinavian Caledonides the WGR contains the largest exposure of basement rock (Carswell and Cuthbert, 2003). This thesis mainly deals with rocks from the WGC, because in this unit evidence for UHPM is found.

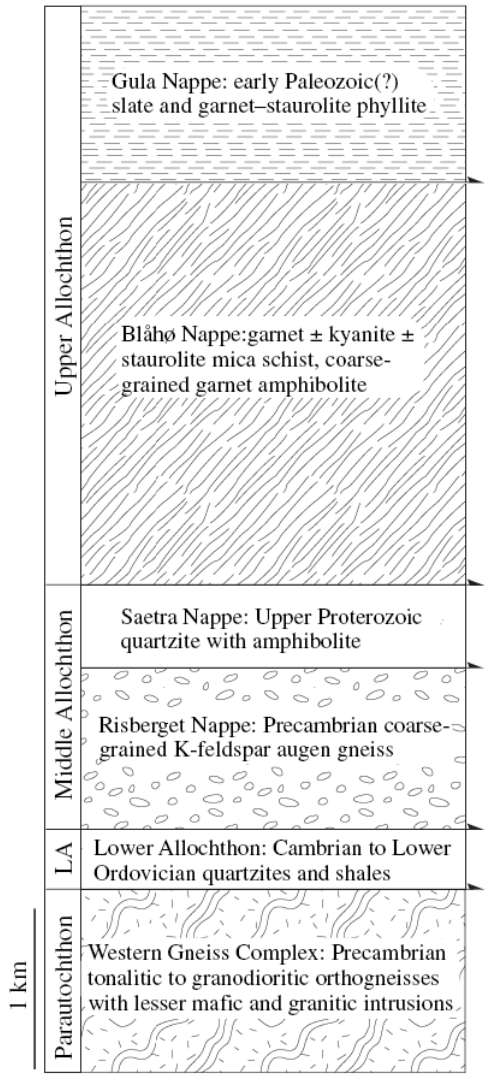

Figure 2.1. Tectonostratigraphic column of autochthon and the allochthonous units of the Scandinavian Caledonides (Walsh and Hacker, 2004)

2.1.2 Definition of UHPM

Over the last decades there has been a large interest by geologists in the WGR. Reason for this is the evidence that (some) rocks of the WGC have witnessed UHP metamorphic conditions. UHP metamorphic conditions are reached when coesite (coe), the high pressure polymorph of quartz (qtz), is stable. The stability field of coesite in PT space is illustrated in figure 2.2. The UHP field , defined by the coesite - quartz transition, therefore lies between 90 and 110 km depth, depending on temperature. At even higher pressures the graphite (gr) - diamond (dia) transition is encountered. This transition is located between 90 and 150km, depending on temperature. Also shown in figure 2.2 are the boundaries of the metamorphic facies fields (dashed lines). The eclogite facies field extends to high pressures in PT space and includes the UHP field.

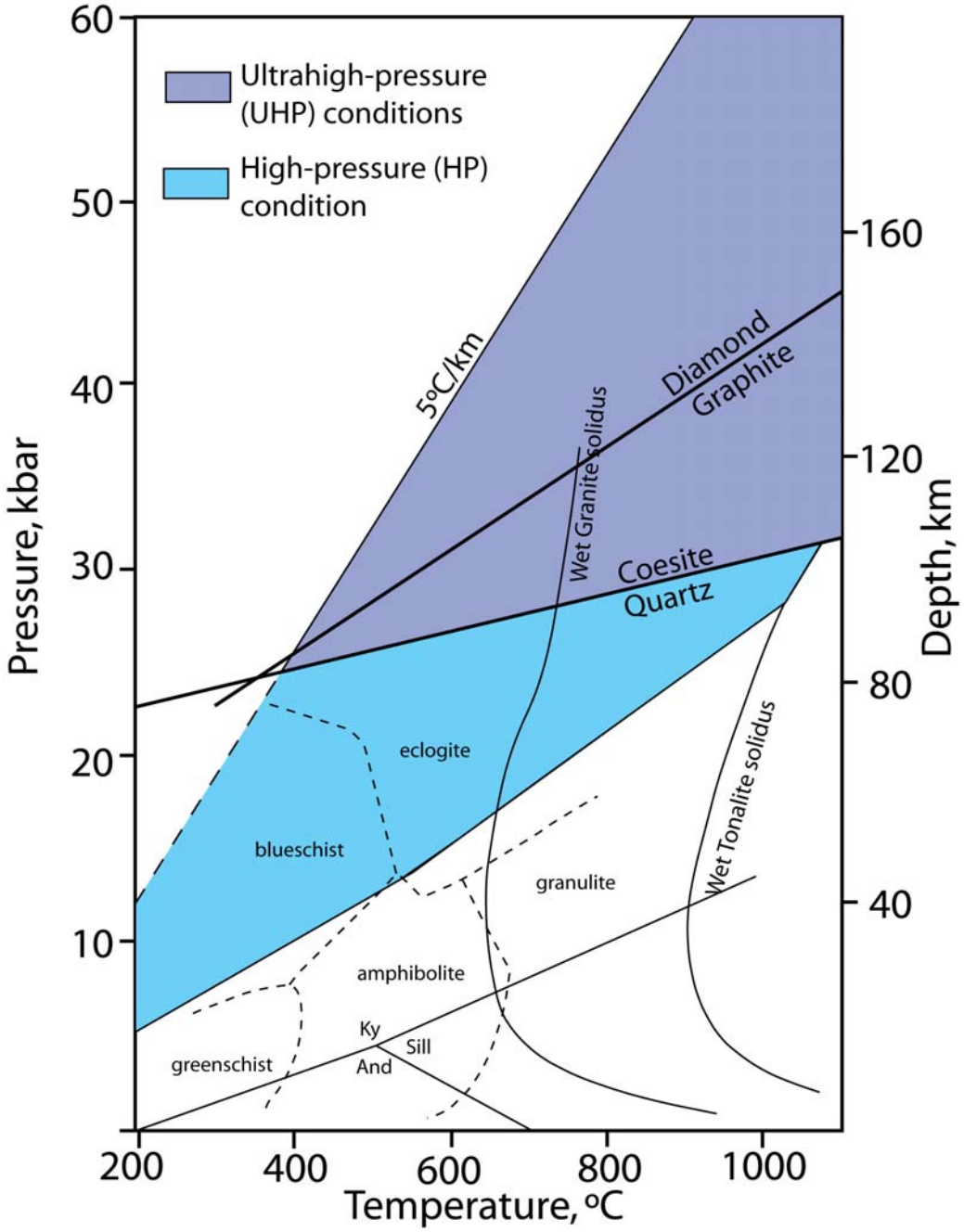

Figure 2.2. PT diagram for metabasic rocks indicating the domains of HP and UHP conditions, quartz-coesite and graphite-diamond transition lines, and metamorphic facies fields. Modified image after Ernst and Liou (2008), And-Sill-Ky transitions from Bucher and Frey (2002).

The first description of UHPM in the WGR was given by Smith (1984), who described the occurrence of coesite within pods of eclogite. At many places in the WGR ultrahigh pressure (UHP) metamorphic conditions have since been demonstrated. UHP occurrences are not evenly distributed across the WGR, but are found in three distinct domains that are referred to as the northern, middle and southern UHP domain (see figure 1.1). A description of important UHP occurrences will be given for the northern UHP domain in section 2.2.1.

2.1.3 Rock units of the Western Gneiss Complex

The autochthonous basement that is exposed in the WGR consists of gneisses with enclosed mafic and ultramafic lenses. Gneisses, mafic and ultramafic lenses all have different mineral assemblages, their classification is done by using different classification diagrams.

The gneisses can be classified according to the classification diagram illustrated in figure 2.3. Tonalitic to granodioritic gneissic rocks make up the bulk of the basement rocks (Krabbendam and Dewey, 1998).

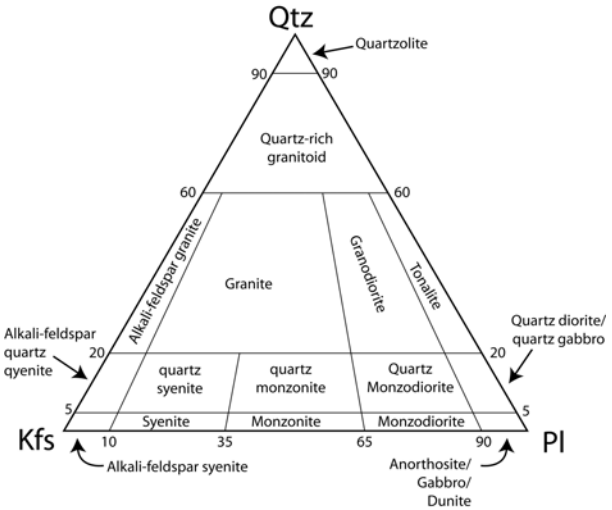

Figure 2.3. Classification diagram of felsic rocks (SiO_2 wt% ≥ 60), image modified after (Alden, 2009).

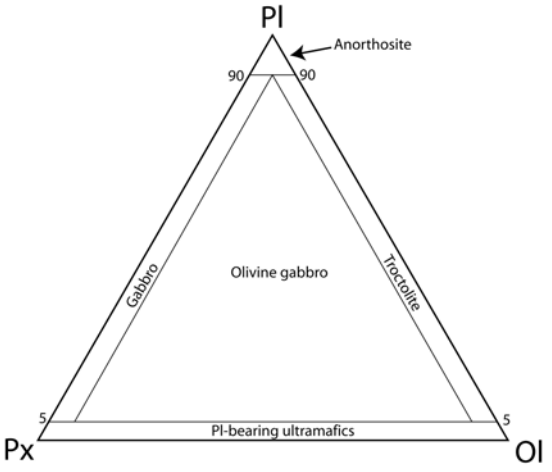

Figure 2.4. Classification diagram of mafic rocks (SiO_2 wt%: 50-60), image modified after (Alden, 2009).

By far the most evidence for UHPM in the WGR comes from mafic and ultramafic lenses enclosed within the basement gneisses. The mafic lenses present within basement gneiss are amphibolites, granulites or eclogites, the ultramafic lenses are peridotites (Vrijmoed et al., 2008). Lenses range in size from centimeters to hundreds of meters. Figure 2.5 shows an example of a lens of eclogite enclosed within basement gneisses.

Mafic magmatic rocks can be classified according to the classification diagram illustrated in figure 2.4. The mafic lenses are classified as melt-gabbro, although their mineral assemblage is different and depends on the metamorphic grade. They are named by their metamorphic rock names amphibolite, granulite and eclogite, corresponding with increasing metamorphic grade. The change of mineral assemblage with metamorphic grade will be discussed in more detail in chapters 3 and 4.

Figure 2.5. Eclogite pod composed of garnet (red) and clinopyroxene (green) with a rim of darker amphibolite, enclosed within the grey basement gneisses, Fjørtoft (Carswell and Cuthbert, 2003).

The ultramafic lenses that are enclosed within the basement gneisses are peridotites. Peridotites are easily recognised by their brown weathering colour, an example is given in figure 2.6. Peridotites can be classified according to the classification diagram illustrated in figure 2.6. Peridotites have a mineralogy of olivine + pyroxene together with an aluminium phase, which can be plagioclase (pl), spinel or garnet (grt) depending on PT conditions.

Figure 2.6. Garnet peridotite from an outcrop at Helgehornsvatn, southern WGR (Beyer et al., 2001)

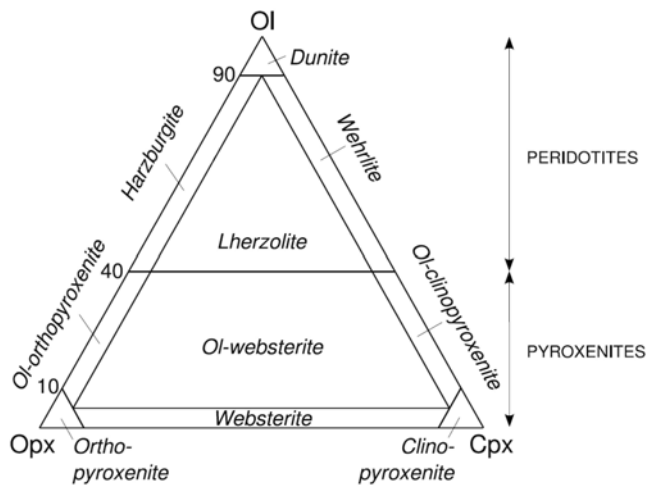

Figure 2.7. Classification diagram of ultramafic rocks (SiO_2 wt% ≤ 50%), (Spengler et al., 2006).

2.1.4 Geodynamic models of the WGR

The tectonic models

The early tectonic models of the WGR were based on the existence of eclogites and peridotites. This was before the discovery of microdiamond, so there was no need to explain extreme depths. Several models from the early '90's (e.g. Andersen and Jamtveit, 1990; Austrheim, 1991; Cuthbert and Carswell, 1990) are all based on the idea that with continent-continent collision one continent is subducted below the other, or a mixed stack of both continents is created, resulting in a stack of maximum twice the thickness of normal continental crust. This means that the lowest part will extend to a depth of about 100 kilometers, a depth where eclogitisation of lower crust will occur and which is in the coesite stability field. Peridotites, consisting of mantle material, were thought to be inserted in the subducted continental crust. Some eclogites and peridotites will be part of the resultant light continental and the crust will be exhumed buoyancy driven.

With the discovery of microdiamond, majoritic garnet and evidence of deeper subduction by geothermobarometry, tectonic models that explain subduction to >120km were needed. In the 'dunk tectonics' model by Brueckner and Van Roermund (2004) continental crust is subducted well into the mantle (figure 2.8a). As subduction of an oceanic plate continues when a continent reaches the subduction zone, slab pull by the oceanic plate creates a drag that can pull down the continental plate. This will cause subduction of the continental plate into the diamond stability field, eclogitisation will occur and peridotites are inserted from the hanging wall mantle wedge. After break-off of the oceanic plate from the subducting continental plate and delamination of the underlying continental lithosphere from the subducting continental crust, the lighter continental crust will be exhumed buoyancy driven until mid-crustal levels (figure 2.8b). This will eventually result in deeply subducted rocks lying next to non- or shallow subducted rocks, and thus a tectonic contact will exist between UHP and low pressure (LP) rocks with a very abrupt pressure gap (figure 2.8c).

Before the continent-continent collision of Baltica and Laurentia, the Iapetus ocean was located in between these continents. The Iapetus ocean closed during a stage of convergence. In this period islands, micro-continents and slabs of oceanic crust were thrusted on top of Baltica. Figure 2.9 shows a geological map where positions and ages of the HP and UHP terrains are indicated. The allochthonous units are distributed in more or less NE-SW oriented bands, with the lower allochtons to the east and the upper allochtons to the west. The ages of these HP and UHP terrains show an increase from 400-418Ma (Scandian orogeny) for the structurally lowest basement unit, to 450Ma (Jämtlandian orogeny), to a maximum of 500Ma (Finnmarkian orogeny) for the upper allochthons. The allochthonous nappes that are now present in the WGR thus represent the islands and micro-continents that are trusted on top of Baltica during several separate events of subduction. The basement represents the outermost tip of Baltica, as it subducted beneath Laurentia during the Scandian. Figure 2.10 shows the configuration of Laurentia and Baltica, with the allochthonous units thrusted on top of Baltica, at the Scandian stage of the collision. In this model deep subduction of the Baltic basement takes place after thrusting of the fossil subduction zones on top of Baltica (Spengler, 2006).

After the last stage of continental collision during the Scandian, extension has affected the Scandinavian Caledonides. Spengler (2006) distinguishes three different stages in exhumation:

1. With the buoyancy driven rise of the UHP rocks, doming of the units above it causes extension (Brueckner and van Roermund, 2004). This has lead to exhumation of the WGC to 40-60km depth at very fast rates of 10mm/yr (Labrousse et al., 2002; Terry et al., 2000a).
2. Ductile orogen parallel extension takes place during convergence at lower crustal levels. This caused sub-horizontal amphibolite facies lineations dipping to the west, with lineation parallel folding (Terry and Robinson, 2004).

3. The last phase of exhumation is related to the ductile-brittle extensional shear, which takes place after convergence has ended. This ultimately caused overprinting of many earlier structures, and resulted in sub-vertical foliations in the northern WGR (Vrijmoed et al., 2006).

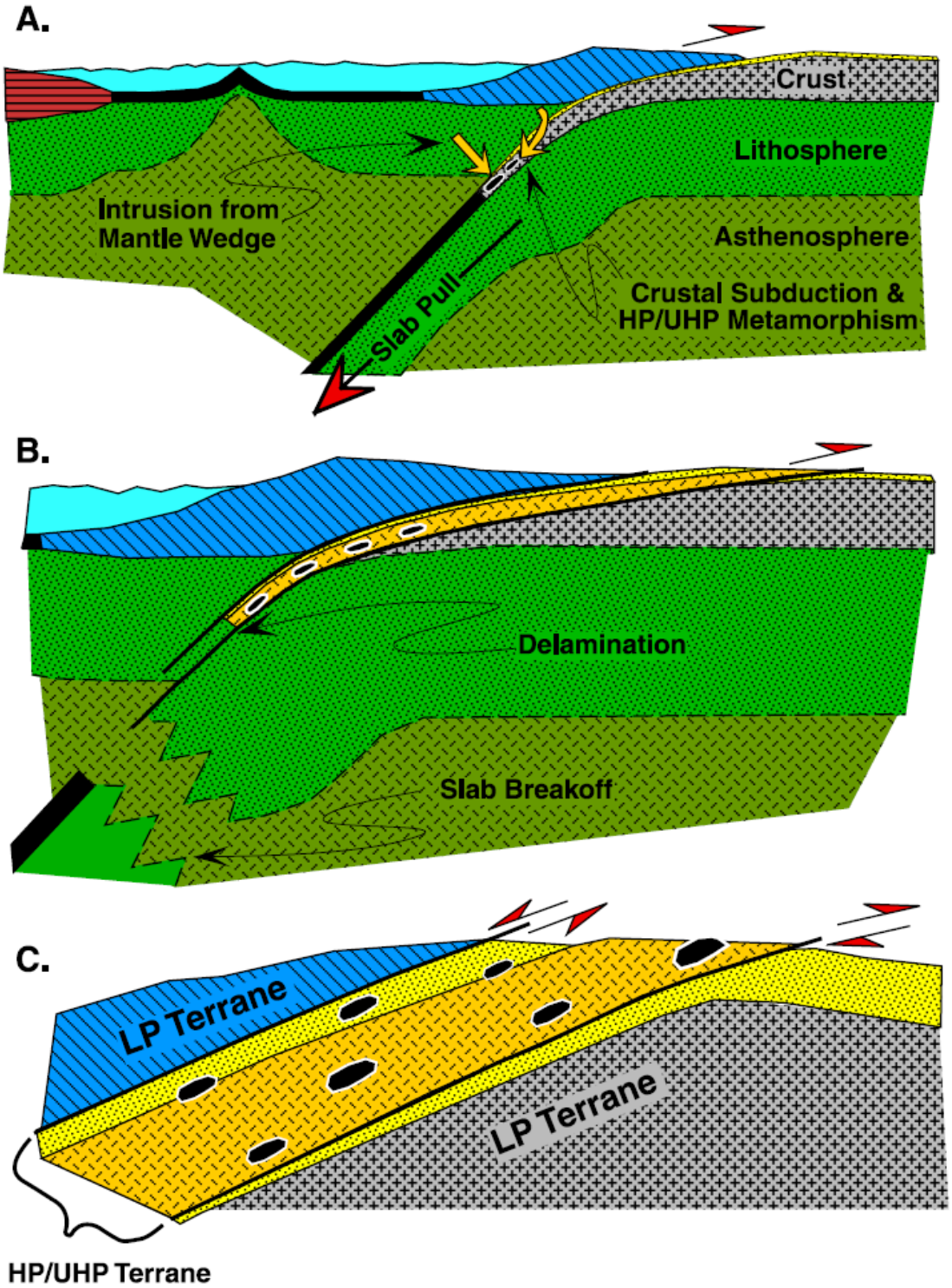

Figure 2.8. The dunk tectonics model proposed by Brueckner and Van Roermund (2004) to explain the UHP origin of the Caledonian basement units. A) deep subduction of the continental crust into the mantle driven by slab pull, B) slab break off and delamination of the crust and underlying lithosphere allows the crust to return upwards buoyancy driven until mid crustal levels, C) after complete exhumation the UHP rocks will be juxtaposed to LP rocks with tectonic contacts in between.

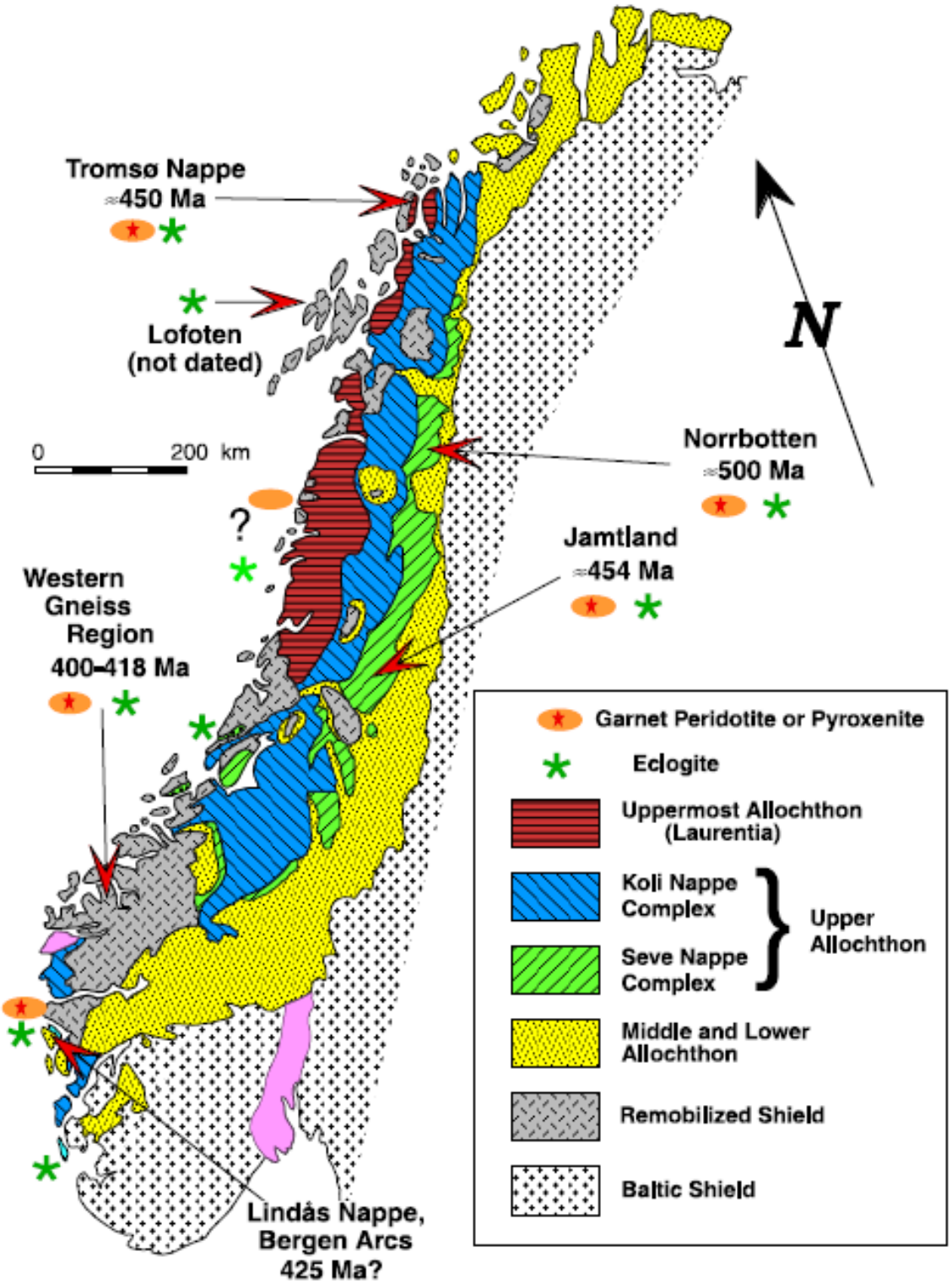

Figure 2.9. Map showing the location and ages HP and UHP terrains. Note that the age of autochthonous and allochthonous units increases from low to high structural levels (Brueckner and van Roermund, 2004).

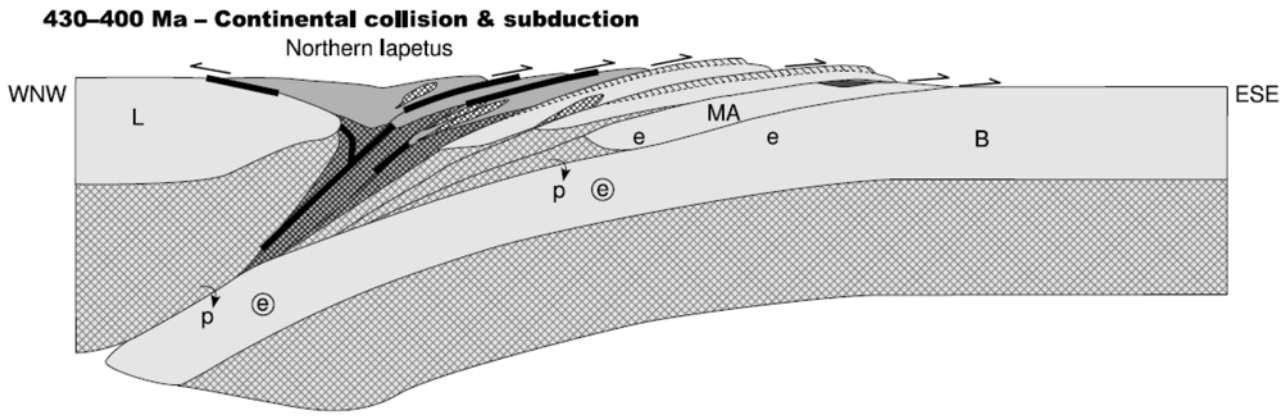

Figure 2.10. Continental collision between Laurentia and Baltica during the Scandian, after relics of earlier subduction events are thrusted on top of the Baltic crust. B=Baltica, L=Laurentia, MA=Middle Allochthon, e=HP eclogite, (e)=UHP eclogite, p=peridotite (Spengler, 2006).

Tectonics or differential retrogression

The basement gneisses are of amphibolite facies, but (some) eclogite and peridotite lenses enclosed in the gneisses are shown to have witnessed UHP conditions. Because of the enormous pressure contrast between the pods of UHP eclogite/peridotite and the gneisses on only cm-scale, Smith (1995) argued that the (U)HP lenses where inserted in lower pressure gneisses. There are, however, two lines of evidence against this reasoning:

1. The occurrence of microdiamond (Dobrzhinetskaya et al., 1995) and coesite (Wain, 1997) within the basement gneisses is shown on the island of Fjørtoft.
2. The existence of a temperature and pressure gradient along the WGR. Figure 1.1 shows the temperature as recorded by the Fe^{2+}/Mg partitioning between garnet and omphacite in eclogite. There is a steady increase in temperature from 600ºC in the SE to 750ºC in the NW. This trend is matched by an increase in pressure in the same direction, although the rocks where the pressure has been measured are much more scattered, and this gradient is therefore more speculative. The gradient indicates that the NW of the WGR has been subducted deepest, and the SE was the shallowest.

The direct evidence of microdiamond in gneisses might be a strong argument in favour of UHP conditions experienced by basement gneisses, but it is only found sporadically. The PT gradient seems a better argument in favour of the idea that both the pods of eclogite and peridotite and the gneisses have been to UHP conditions. If the eclogites have been to UHP conditions and later tectonically inserted into the gneisses, it seems unlikely that tectonic forces have not disturbed the initial PT gradient.

If the basement gneisses were subducted to UHP conditions like the eclogites and peridotites, then why do they lack evidence of UHP conditions? Apparently the different mineralogy of the rocks causes a different reaction to lower PT conditions that they witnessed on their way to the surface. Complete metamorphic reworking of the gneisses has caused the earlier (U)HP mineralogy, that the gneisses must have had, to be overprinted by an amphibolite-facies mineral assemblage (Carswell and Cuthbert, 2003; Carswell et al., 2006). Thus the difference in composition has caused the eclogites and peridotites to withstand lower PT conditions, while the gneisses have completely recrystallized. Looking again at the eclogite pod of figure 2.5, the mineralogy of the rim of the eclogite can be seen to be amphibolite-facies while the core has preserved the eclogite mineralogy. Retrogression of the eclogite thus has started at its rim, but is far from complete. The surrounding gneisses show complete amphibolite facies mineralogy. Differential retrogression is thought to be the cause of the loss of an earlier UHP imprint in the gneisses, while the UHP mineralogy in mafic pods has survived (Wain, 1997; Wain et al., 2001).

This leads us to an important observation in the geodynamic models of the WGR. As we have seen, there are three distinct UHP domains (figure 1.1). The question whether the gneisses next to UHP eclogites have witnessed UHP conditions is here repeated on a larger scale: did the basement (with gneisses and enclosed eclogites) in between the UHP domains experienced UHP conditions and lost this imprint by retrograde reactions, or are the UHP domains separate domains that are tectonically put beside lower pressure rocks? According to Wain et al. (2000) there is a difference between UHP eclogites that are found in the UHP domains, and HP eclogites that are found in between the UHP domains. The garnet minerals in HP eclogites show a prograde zoning pattern and amphibolite facies inclusions without coesite, while the UHP eclogites show flat element profiles with eclogite facies inclusions and with coesite. These different eclogites have a markedly different peak pressures and temperatures, but are found very close to each other. Therefore Wain et al. (2000) place tectonic boundaries in between these different eclogite domains. On the other hand Carswell and Cuthbert (2003) and Cuthbert et al. (2000) state that the two eclogite categories are impossible to tell apart because HP and UHP eclogites have been observed within the same lithology, and HP and UHP characteristics can sometimes even be found within one sample. Also no signs of increased strain and temperature are found in between at the hypothetical tectonic boundaries. Therefore the difference in peak pressures of the eclogites is, like with the gneisses, explained by differential retrogression between eclogites in the different areas.

Consequently there is considerable uncertainty about the mechanisms behind the formation, preservation, exhumation and age of UHP rocks in the WGR. Tectonic models that explain the UHP occurrences in the WGR can be divided into three groups:

1. Those that argue in favour of small UHP thrust nappes tectonically put next to lower pressure units (e.g. Smith, 1984; Terry and Robinson, 2004; Wain et al., 2000)
2. Those that argue in favour of WGR as one coherent mass. The absence of UHP occurrences in between the UHP domains is explained by differential retrograde reactions (e.g. 2004; Carswell et al., 2003; Young et al., 2007)
3. The third category has not yet been discussed. Most models assume that pressure equals lithostatic pressure (the burden of rock above it). However, some argue that pressure in rocks is not only dependent on depth, but can be increased during deformation. For viscous materials this tectonic overpressure is thought to increase linearly with strain rate. As a consequence UHP rocks could be created at lower depths than what is commonly assumed if only lithospheric pressures are taken into account (e.g. Mancktelow, 2008). If tectonic overpressure is a real and substantial force in subduction zones, then the depths that are calculated by geobarometric techniques and the depths of the coesite and diamond transitions might be meaningless. All tectonic models that are based on these depths then would have to be revised. Also the conversion of the PT conditions that will be calculated in this study to depths will be meaningless. However, the significance of tectonic overpressure is still poorly understood and the opponents argue that metamorphic rocks are too weak to sustain the stresses needed to create significant tectonic overpressure (e.g. Green, 2005). Therefore this concept will not be taken into account any further in this study.

Finding evidence for either the first or second group is difficult because those that argue for an UHP origin of all rocks in the WGR use differential retrogression as their main argument, which destroys the inferred UHP imprint. Evidence for either theory could be:

1. Findings of coesite or microdiamond relicts at many places in the basement gneisses would be a strong argument in favour of a coherent WGR.
2. If the UHP domains represent tectonic thrust sheets, faults or shear zones should bound these domains.
3. If the UHP domains represent tectonic nappes, different PTt paths would be expected for the different nappes. High resolution PTt paths for many places in the WGR could be a strong argument for either scenario.

2.2 The northern UHP domain

2.2.1 Geological setting of the northern UHP domain

UHP conditions in the northern UHP domain have been established on the islands Otrøy, Fjørtoft and Flemsøy, located at the southwest of Gossa, and the mainland to the east of Gossa. A summary of the most important findings of UHP occurrences is given in figure 2.11.

The first discovery of UHPM in the northern part of the WGR came from microdiamonds in basement gneisses on the island Fjørtoft (Dobrzhinetskaya et al., 1995). These microdiamonds were uncovered by a total rock digestion method using an unknown chemical solution. No other labs were able to reproduce the results casting sincere doubt. The discovery therefore was questionable, until microdiamonds where discovered in a nearby peridotite as well (Roermund et al., 2002).

On the island of Otrøy the first evidence of UHP was in the form of majoritic garnet in peridotite (Roermund and Drury, 1998). Majoritic garnet is a type of grt that contains more Si than 'normal' grt, and is only stable at pressures ≥ 3.5 GPa. If this type of garnet forms it will form exsolution lamellae of orthopyroxene (opx) after decompression, and these lamellae are regarded as evidence of a precursor majoritic garnet (Chopin, 2003).

The first evidence for UHP conditions on the mainland was found near Tornes, by low Al contents of opx in peridotites (Vrijmoed et al., 2006). This method relies on the decrease of Al in opx in contact with garnet, when pressure increases. Later the UHP metamorphism has been confirmed by the discovery of microdiamonds within the same peridotite body (Vrijmoed et al., 2008).

The text above offers only a short description of the first and most important UHP discoveries in the northern domain of the WGR. A more complete list, with references and locations, is shown in figure 2.11.

Based on the known UHP outcrops an area n can be outlined within which UHP rocks can be found. The size of this UHP domain is a matter of debate, and is best explained by the situation on the Nordøyane islands Fjørtoft and Flemsøy. Here Terry et al. (2000b) have performed a geothermobarometric study. Figure 2.12 shows their geological map. UHP conditions have been confirmed in kyanite bearing eclogites that are found on the north of Fjørtoft and in one location on Flemsøy, called Nogva. There is no indication of UHP on other locations of Fjørtoft and Flemsøy, and the authors explained this by thrusting of the two UHP areas onto HP units. There is no indication of zones where the thrusting is accommodated, the thrusting scenario is based entirely on the UHP/HP transition that apparently takes place over a very short distance.

Figure 2.11 shows the outlines of the northern UHP domain as given by Terry and Robinson (2004), Vrijmoed et al. (2006) and Spengler at al. (2006). It illustrates the differences in the area that is thought to make up the northern UHP in recent papers. It should be noted that Terry and Robinson (2004) do not indicate the UHP extent outside Nordøyane, and the size of their UHP domain only applies to the local extend on Fjørtoft and Flemsøy. Terry and Robinson (2004) argue for a small area of the northern UHP, because they regard the local UHP occurrences as thrust sheets. On the other hand Vrijmoed et al. (2006) draw the conclusion that the gneisses on Fjørtoft and Flemsøy are in fact all part of an UHP unit, but the UHP is largely overprinted by later HP/LP metamorphism.

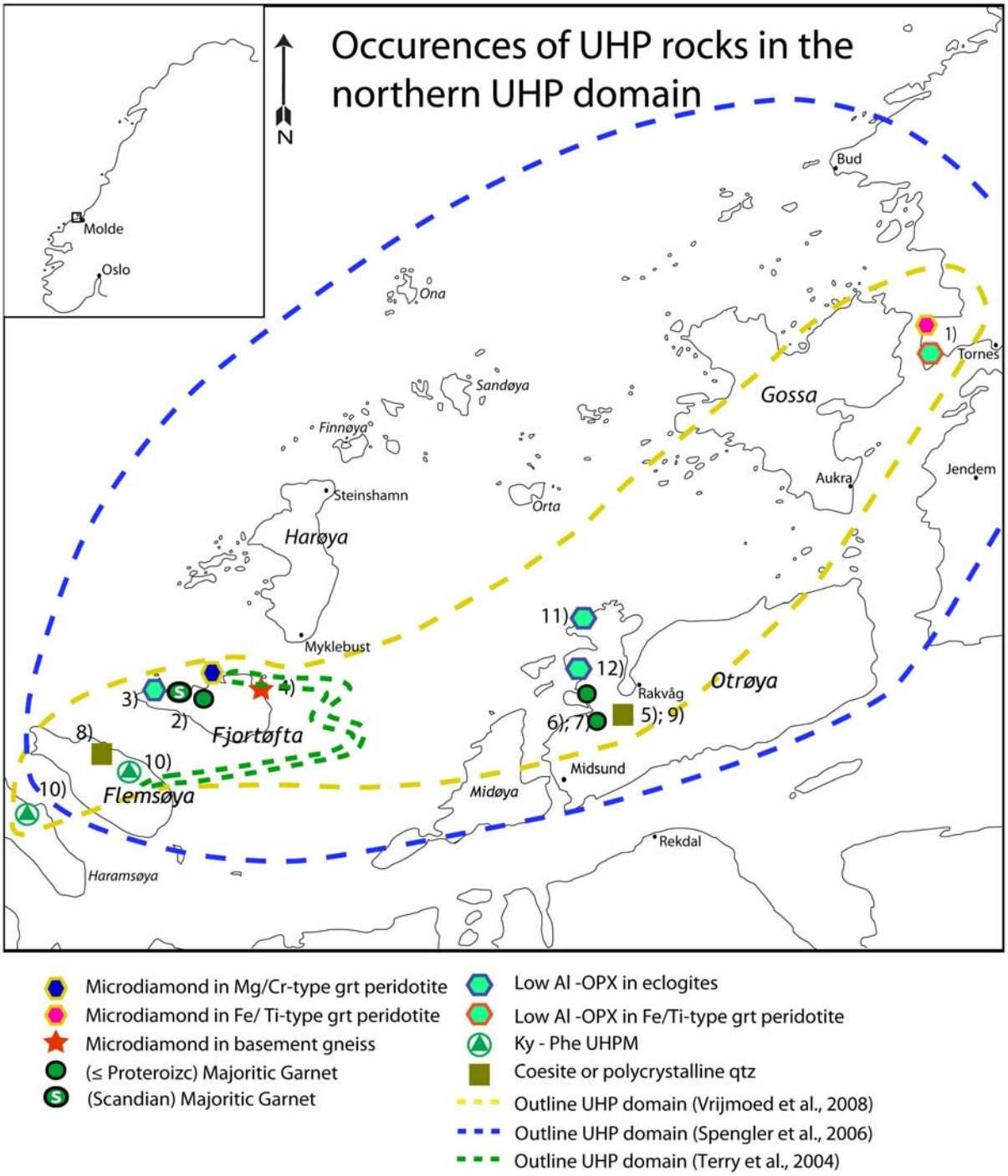

Figure 2.11. Identified occurrences of UHP rocks in the vicinity of the island of Gossa. Numbers refer to: 1) Vrijmoed et al. (2006) 2) Scambelluri et al. (2008) 3) Van Roermund et al. (2002) 4) Dobrzhinetskaya et al. (1995) 5) Smith (1995) 6) Van Roermund and Drury (1998) 7) Van Roermund et al. (2000) 8) Terry et al. (2000a) 9) Spengler et al. (2006) 10) Robinson et al (2008) 11) Carswell and Van Roermund (2003) 12) Van Roermund et al (2005).

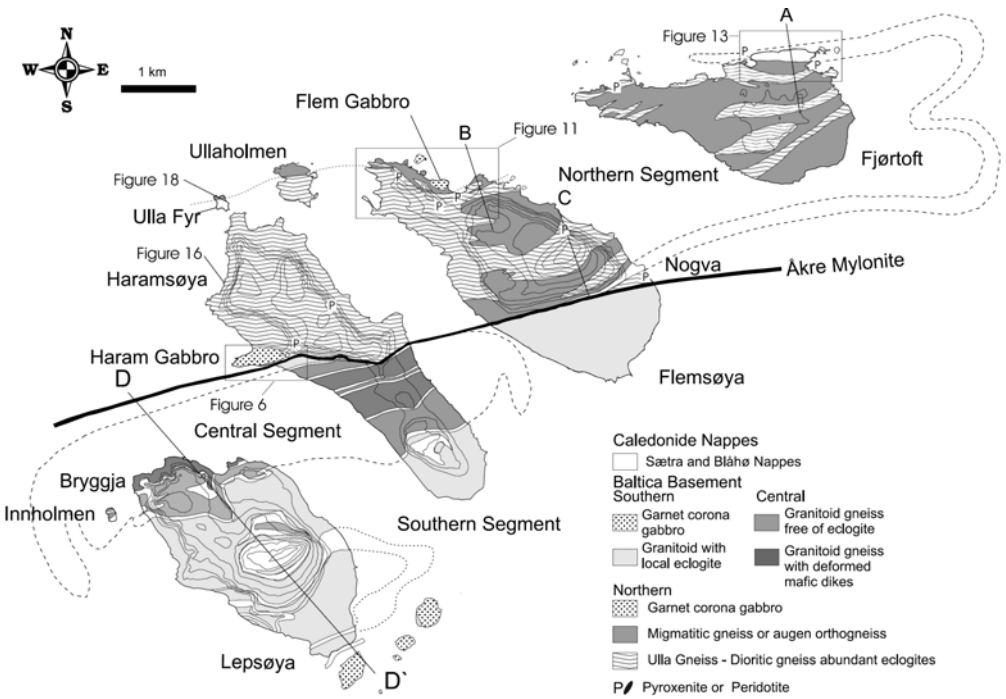

Figure 2.12. Geological map of Nordøyane (Terry and Robinson, 2004; Terry et al., 2000b).

2.2.2 Expected geological setting on Gossa

Two geological maps are available of the island of Gossa. One is given in Terry et al. (2000b) and the other is provided by the Norwegian Geological Survey (NGU, 2009).

The map by Terry et al. (2000b), see figure 2.13, displays two different geological units: basement and the tectonic cover. The tectonic cover is equivalent to the allochthonous units. A simple division is present where the NE part of Gossa consists of tectonic cover and basement in the south (see inset figure 2.13).

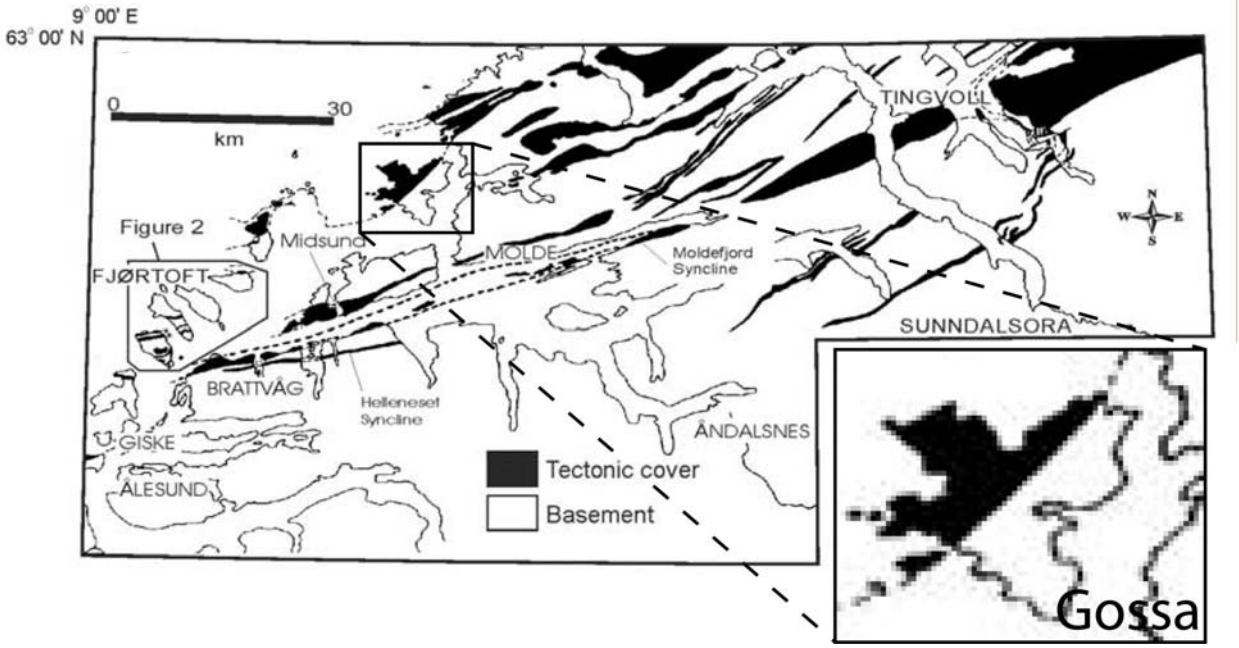

Figure 2.13. Map of Gossa and surrounding areas by Terry et al. (2000b), Gossa is divided in tectonic cover (NW) and basement (SE).

In contrast the geological map of the NGU (2009), see figure 2.14, shows three different geological units exposed on Gossa. Like the map by Terry et al. (2000b) a basement and allochthonous unit are exposed in approximately the same position. The NGU map is more detailed in the west and northwestern parts, where outcrops of basement are recognized as well. Eclogite is identified as a third unit and is present in the western part of Gossa in between the allochthonous and basement units (see inset figure 2.14).

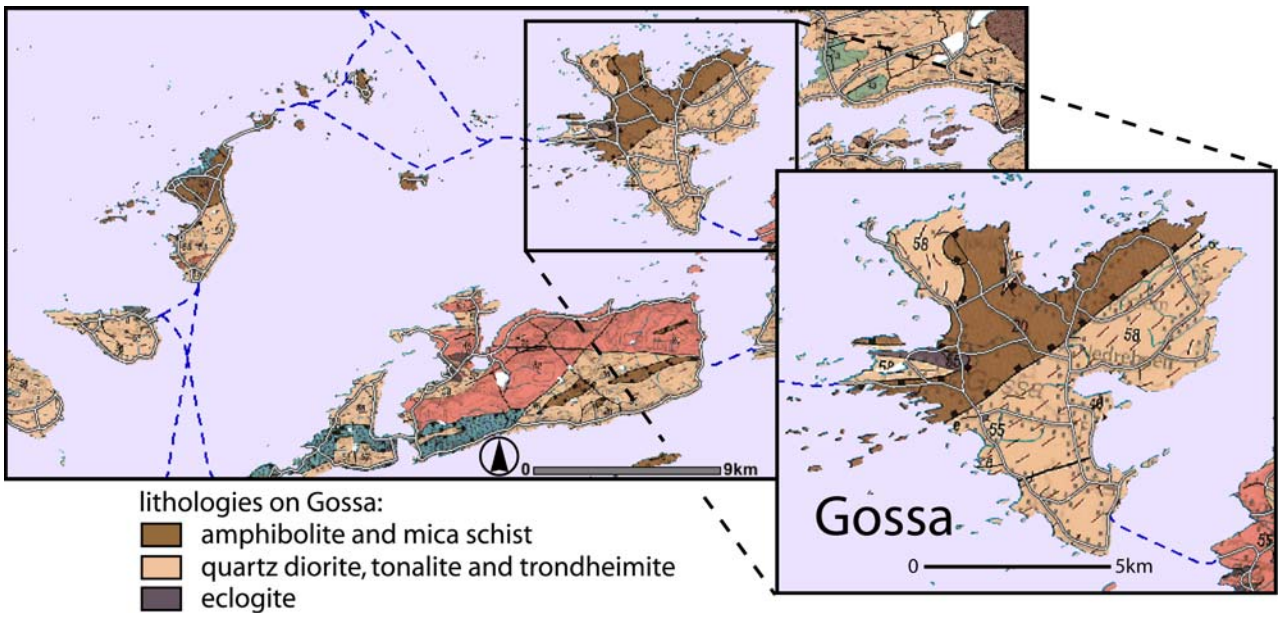

Figure 2.14. Geologic map of Gossa, modified after (NGU, 2009).

The allochthonous unit that is found on Nordøyane and on the Bud-Tornes area is correlated to the Blåhø en de Sætre nappe (Terry and Robinson, 2004). As is shown in figure 2.1, these units are part of the upper and middle allochthonous unit. Because Gossa is situated in between Nordøyane and the Bud-Tornes area, and this unit has a NE-SW orientation, it is very likely that these allochthons are present on Gossa as well (see figure 2.13 and figure 2.14).

The basement gneisses are identified as the Ulla Gneiss in both Nordøyane and the Bud-Tornes area (Terry and Robinson, 2003; Vrijmoed et al., 2006). It is reported as a melange of coarse grained eclogite boudins and hornblende (hbl) ± clinopyroxene (cpx) + grt + biotite (bt) + pl + qtz gneiss. The basement gneisses also show a NE-SW trend on a large scale, and therefore the Ulla Gneiss is expected to be present on Gossa as well (see also figure 2.13 and figure 2.14).

2.3 Techniques to determine PT conditions

There are several ways to determine the PT conditions that rocks have witnessed in the past. What method to choose depends on the rock that is being investigated. This research focuses on finding signs of UHPM and to establish the retrograde PT path that shaped the rocks on their way back to the surface. Roughly there are three methods that can be used to determine the grade of metamorphic conditions. These will be discussed below to understand why certain rocks are collected and some geological occurrences are mapped in higher detail during fieldwork (chapter 3).

Method 1: Mineral assemblages
Certain combinations of minerals are stable under a specific range of PT conditions. The stable mineral assemblages (as present in different bulk rock compositions) together define the metamorphic field in PT space. The size of this metamorphic facies field can be large, and this method is only suitable for a rough PT estimations. In order to obtain a complete PT-record, it is vital to collect a wide range of samples with different bulk rock compositions. Determination of metamorphic facies field of the collected samples will be performed by optical microscopy (chapter 4).

Method 2: geothermobarometry
Exact PT conditions can be obtained using geothermobarometry. This method uses the PT dependence of the composition of minerals that are stable together. Both a geothermometer and a geobarometer should be used to pinpoint PT conditions. The UHP conditions experienced by rocks of the WGR that have been proven by geothermobarometry, are found in eclogites and peridotites. The search for UHP on Gossa should therefore concentrate on one of these lithologies. Eclogites are the most widely occurring rock type. For eclogites a range of geothermometers is available, but only two geobarometers are normally used:

1. The aluminium content of opx grown together with garnet (Carswell et al., 2006; Vrijmoed et al., 2006).
2. The assemblage kyanite (ky) + phengite (phen) + grt + cpx + qtz/coe (Ravna and Terry, 2004).

Eclogites form from mafic rocks during (U)HP conditions. They are characterized by their composition of grt + omphacite (omph), with omph being a high grade variation of cpx. This poses a problem, as is it not possible to apply geothermobarometry on this composition. But as for all rocks there can be considerable variation in the bulk rock composition, resulting in some extra minerals that can be formed in eclogites. shows an ACF diagram for mafic rocks (modified from Bucher and Frey, 2002). From this diagram it is apparent that an enrichment in Al_2O_3 will cause phen and ky to form (ky is the high grade form of the aluminosilicates) while an enrichment in FeO will cause opx to form. Figure 2.16 shows a polished slab of an opx-bearing eclogite. To make geothermobarometry possible, sampling of the eclogites focuses on eclogites that contain either opx or ky + phen as 'extra' minerals. Determination of PT conditions by geothermobarometry will be presented in chapters 5 and 6.

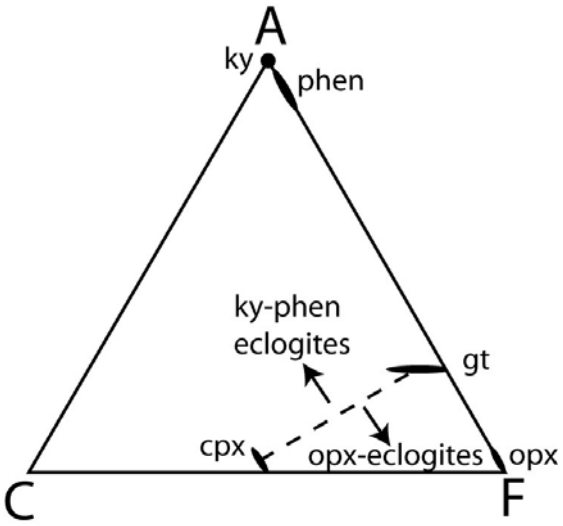

Figure 2.15. ACF diagram (Al_2O_3-CaO-FeO) showing possible variation in mineralogy of eclogites. Aluminium-rich eclogites can contain ky and phen, Fe/Mg-rich eclogites can contain opx (modified from Bucher and Frey, 2002).

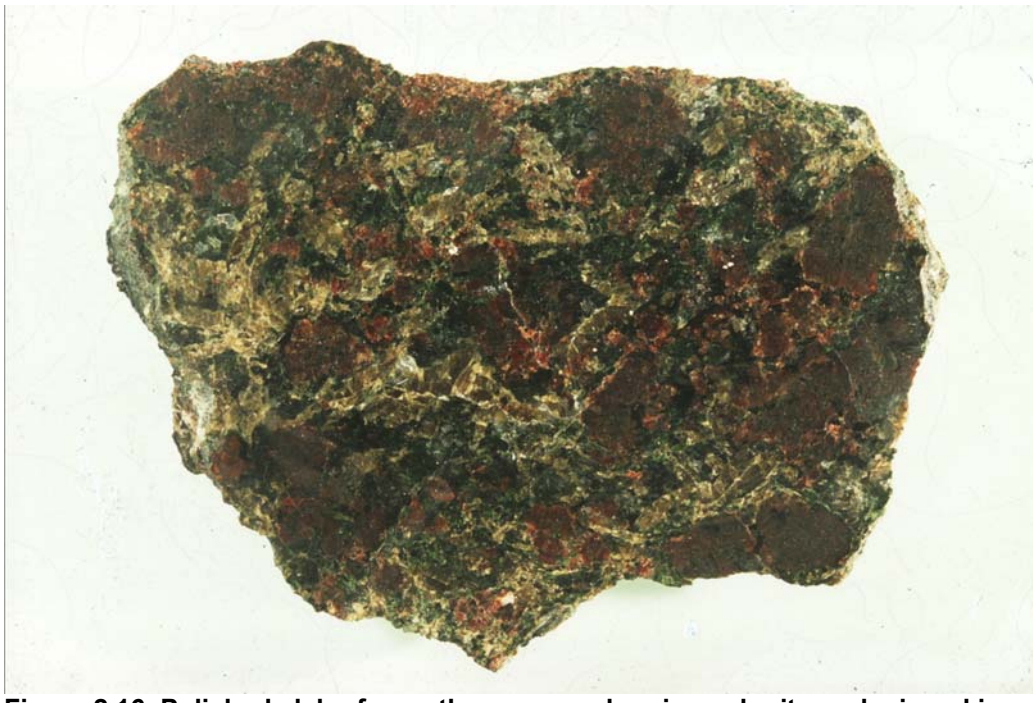

Figure 2.16. Polished slab of an orthopyroxene bearing eclogite, red mineral is grt, bright green mineral is cpx, brown mineral is opx (Carswell and Cuthbert, 2003).

Method 3: index minerals

In a rock, polymorphic mineral reactions can take place above or below certain pressures. Finding evidence for the reaction products will therefore be useful for making minimum/maximum pressure estimates. Mineral reactions that are indicative of UHPM are the transformation of qtz to coesite and graphite to microdiamond. Because these minerals are mainly found in eclogites and peridotites the same samples that are used for geothermobarometry can also be used to look for these index minerals. As coesite and microdiamond are very small and mainly found as inclusions in container minerals there is no possibility to identify such features in the field. Possible findings of these minerals are presented in chapters 4, 5 and 6.

3 Geological setting on Gossa

3.1 Fact maps

Observations that have been made of lithologies and foliations on Gossa that are collected during the fieldwork are given in the fact maps, figure 3.2 to figure 3.6. It has been tried to show as many observations as possible, but in some cases simplification can not be avoided. The resolution at which individual features can be observed on the map scale is about 50 meters, so lithological changes and changes of foliation that occur below this resolution limit are not given. Instead, in those cases an average of the lithology and/or foliation is presented. The maps show the coastline, roads and UTM map grid for reference.

On the fact maps the following lithologies are shown: granodioritic basement, tonalitic basement, allochthon (=supracrustals), eclogite and granulite. Mafic lenses are generally too small to show them on the map, but because of their importance for PT-evaluation their locations are given in symbols. Lithologies will be discussed in section 3.4. Structural data is presented as foliations, lineations and high strain zones, these will be discussed in section 3.5. Approximate positions where observations have been made are marked with data points.

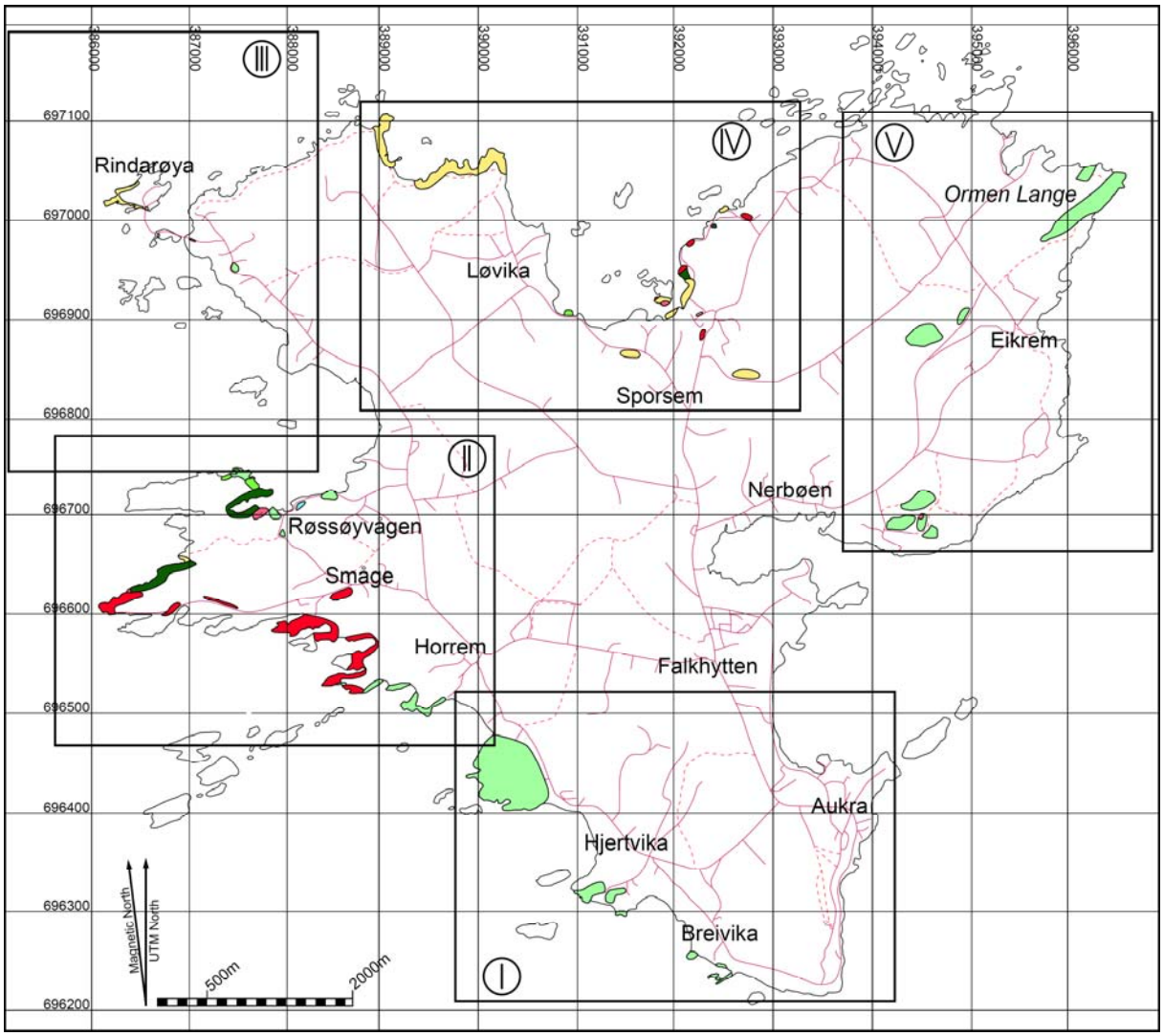

Figure 3.1. Overview fact map of Gossa. Superposed black squares numbered I to V refer to maps illustrated in figure 3.3 to figure 3.6, for legend figure 3.2

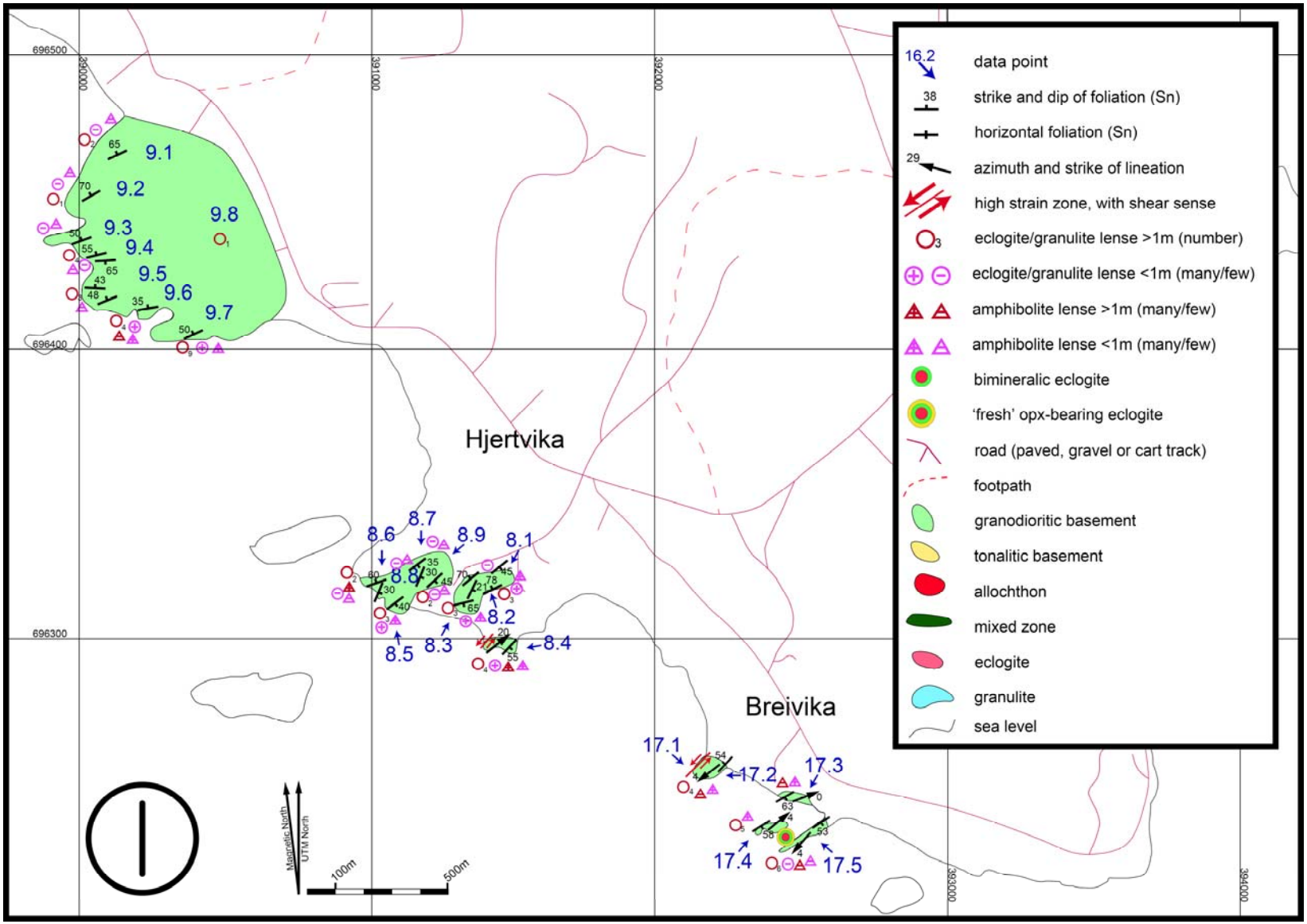

Figure 3.2. Fact map I (southern part of Gossa) for location see figure 3.1.

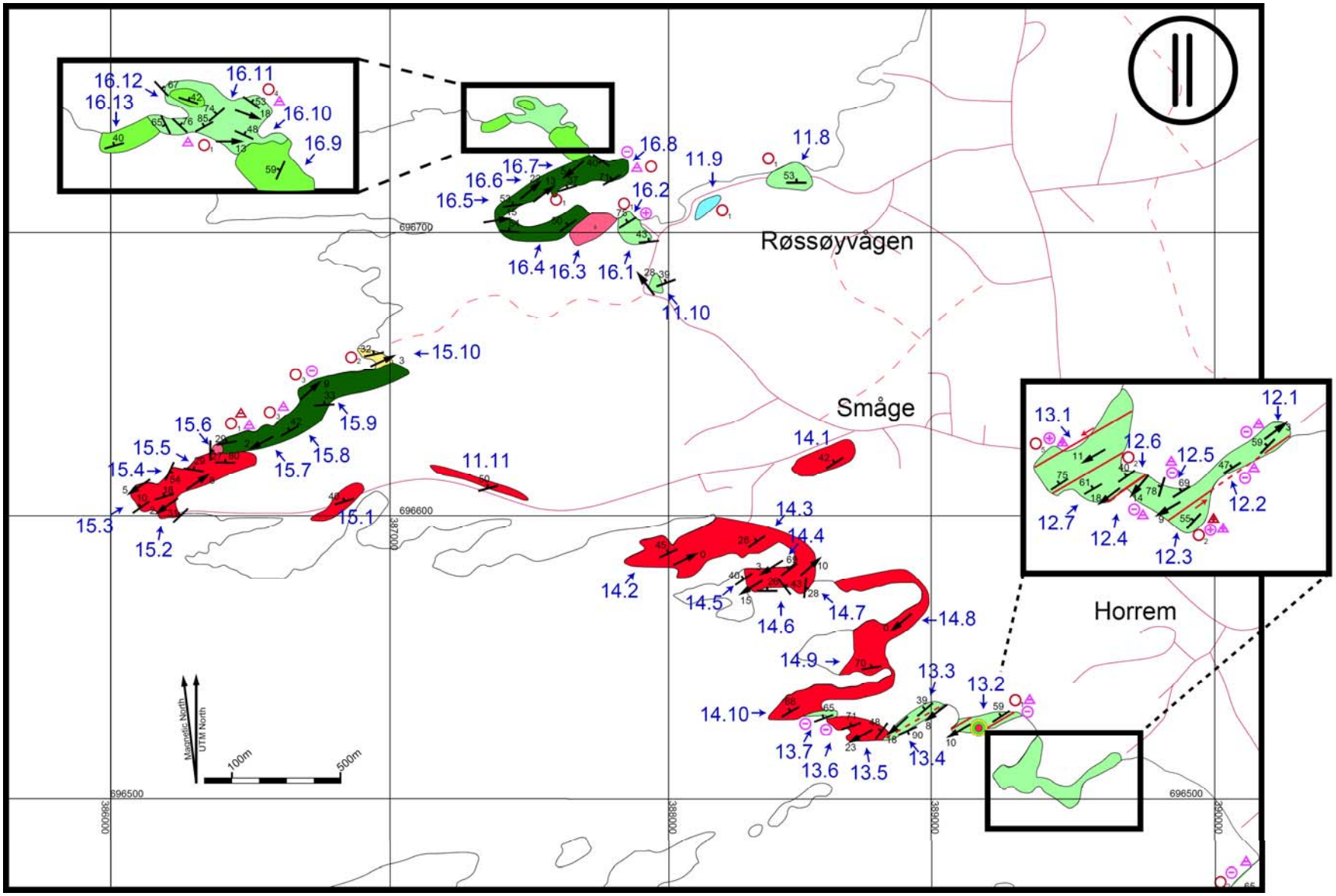

Figure 3.3. Fact map II (western part of Gossa) for location see figure 3.1, legend is given in figure 3.2.

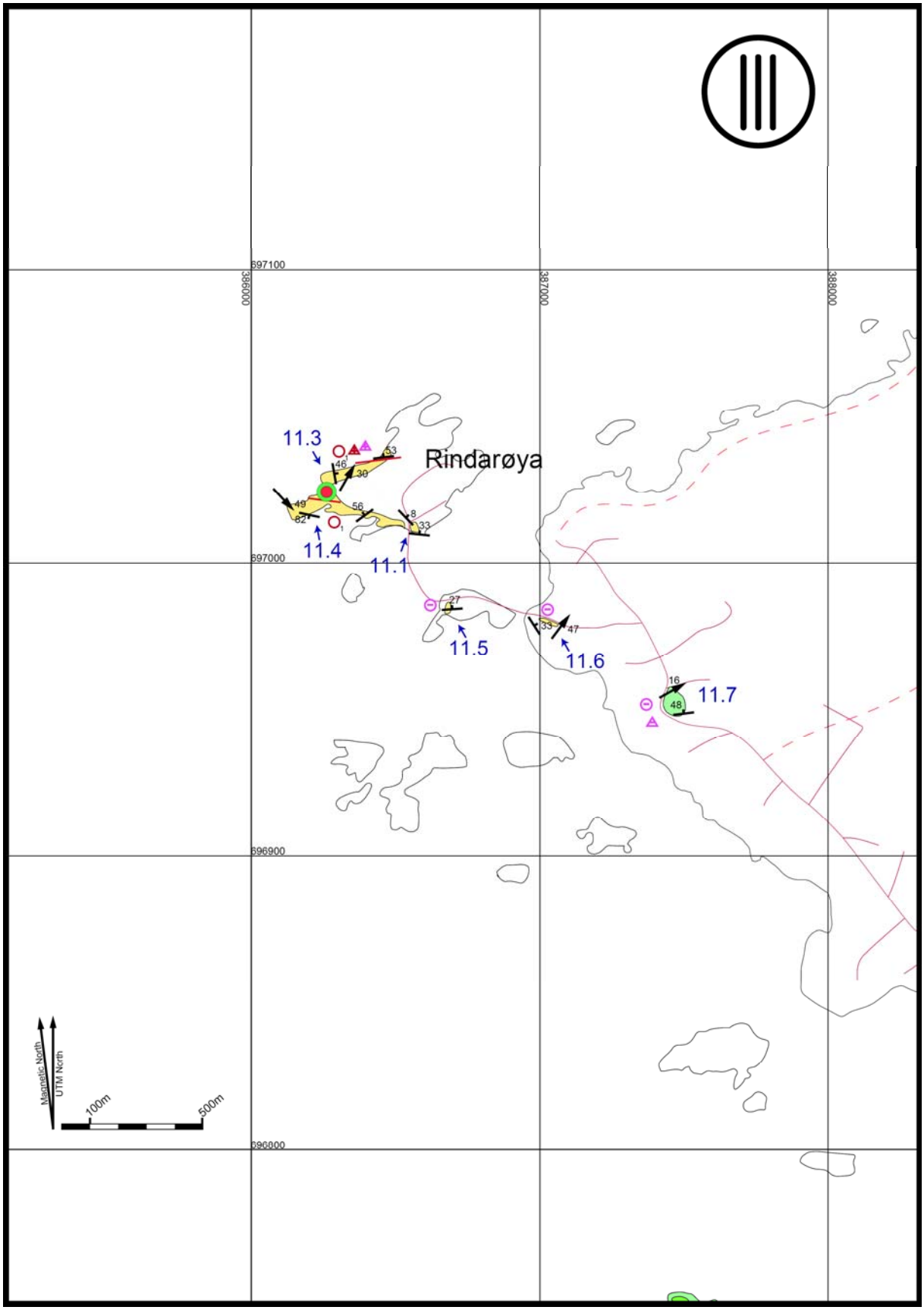

Figure 3.4. Fact map III (northwestern part of Gossa) for location see figure 3.1, legend is given in figure 3.2.

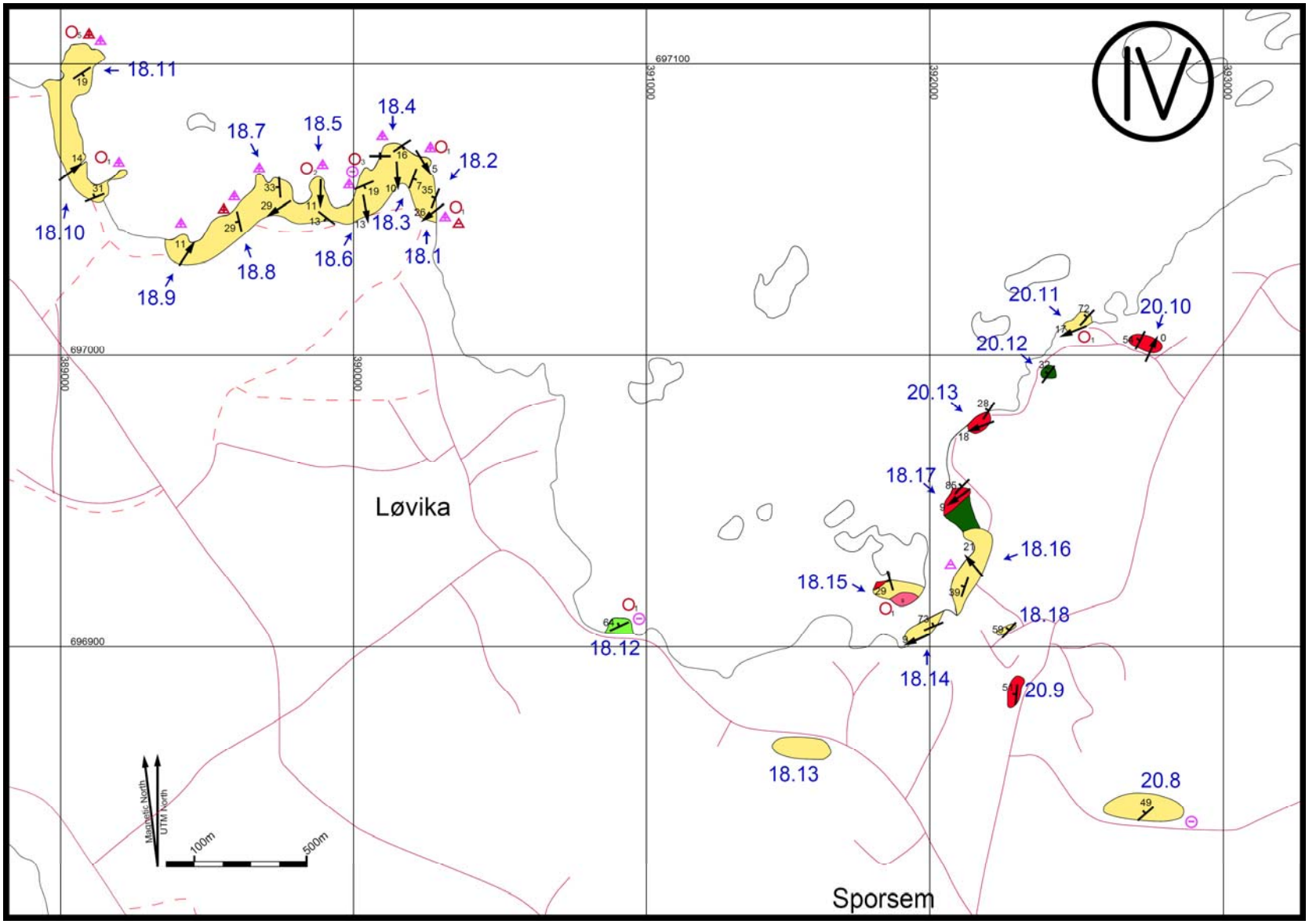

Figure 3.5. Fact map IV (northern part of Gossa) for location see figure 3.1, legend is given in figure 3.2.

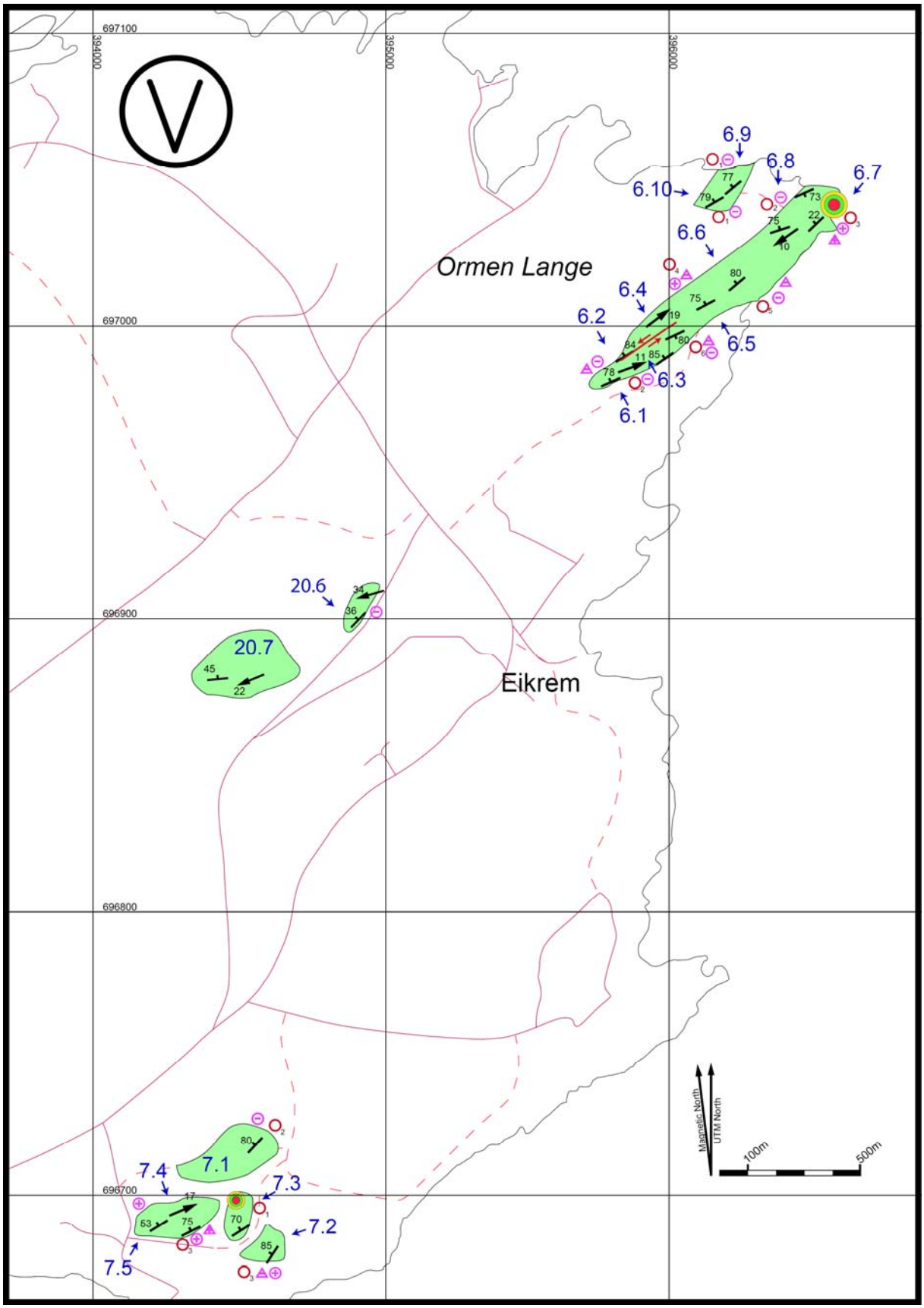

Figure 3.6. Fact map V (northeastern part of Gossa) for location see figure 3.1, legend is given in figure 3.2.

3.2 Samples: description and locations

In chapters 4, 5 and 6 samples are used that are collected during the fieldwork. The location of these samples is given in figure 3.7, and correspond to the data points on the fact maps (figure 3.2 to figure 3.6). The samples include 6 basement samples, 4 granulites and 2 opx bearing eclogites.

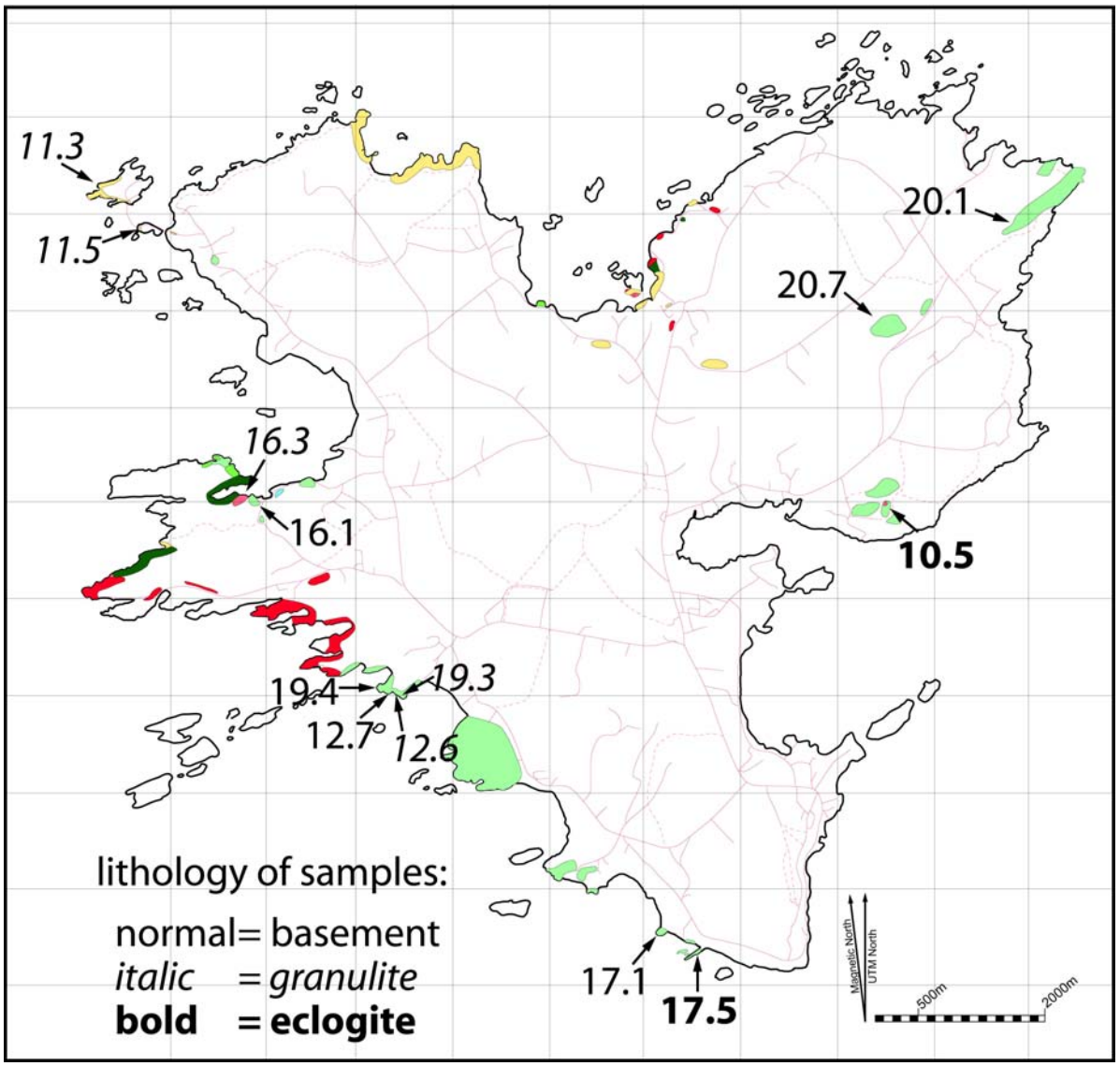

Figure 3.7. Topographic map indicating the name and location of samples. Only samples that are used to determine PT conditions are shown.

3.3 Interpreted geological map

Figure 3.8 shows an interpreted geological map based on field observations presented in figure 3.2 to figure 3.6. Dashed boundaries are supplied with a '?' and are based on very little evidence. The interpreted geological map has been made under the assumptions that:

1. In the southern basement only granodioritic rocks are observed, with the exception of one outcrop at data point 20.8. This means that a small area is classified as tonalitic, with an unknown size and unknown boundary with the granodioritic gneisses. The rest of the southern basement is completely classified as granodioritic gneiss.
2. In the northern basement only tonalitic gneisses have been found, except for the area north of the supracrustals, in the SW part of Gossa.

3. The boundary between the supracrustals and the northern basement is the mixed zone in the SW part of Gossa. This boundary has been extrapolated to the NE, where the boundary between these units is very poorly exposed.
4. Because of the lack of good outcrop and low accessibility no data has been collected in the northern part of the, inferred, supracrustals. This area has been interpreted based on the previously published geological maps by (NGU, 2009; Terry et al., 2000b).
5. A small area within the supracrustals is classified as tonalitic gneiss. However, in this area gneisses and supracrustals are found in equal amounts. The reason that a small area of tonalitic gneiss is drawn inside supracrustals, instead of a small area of supracrustals inside tonalitic gneisses, is based on extrapolation of the supracrustals in the SW towards the NE.

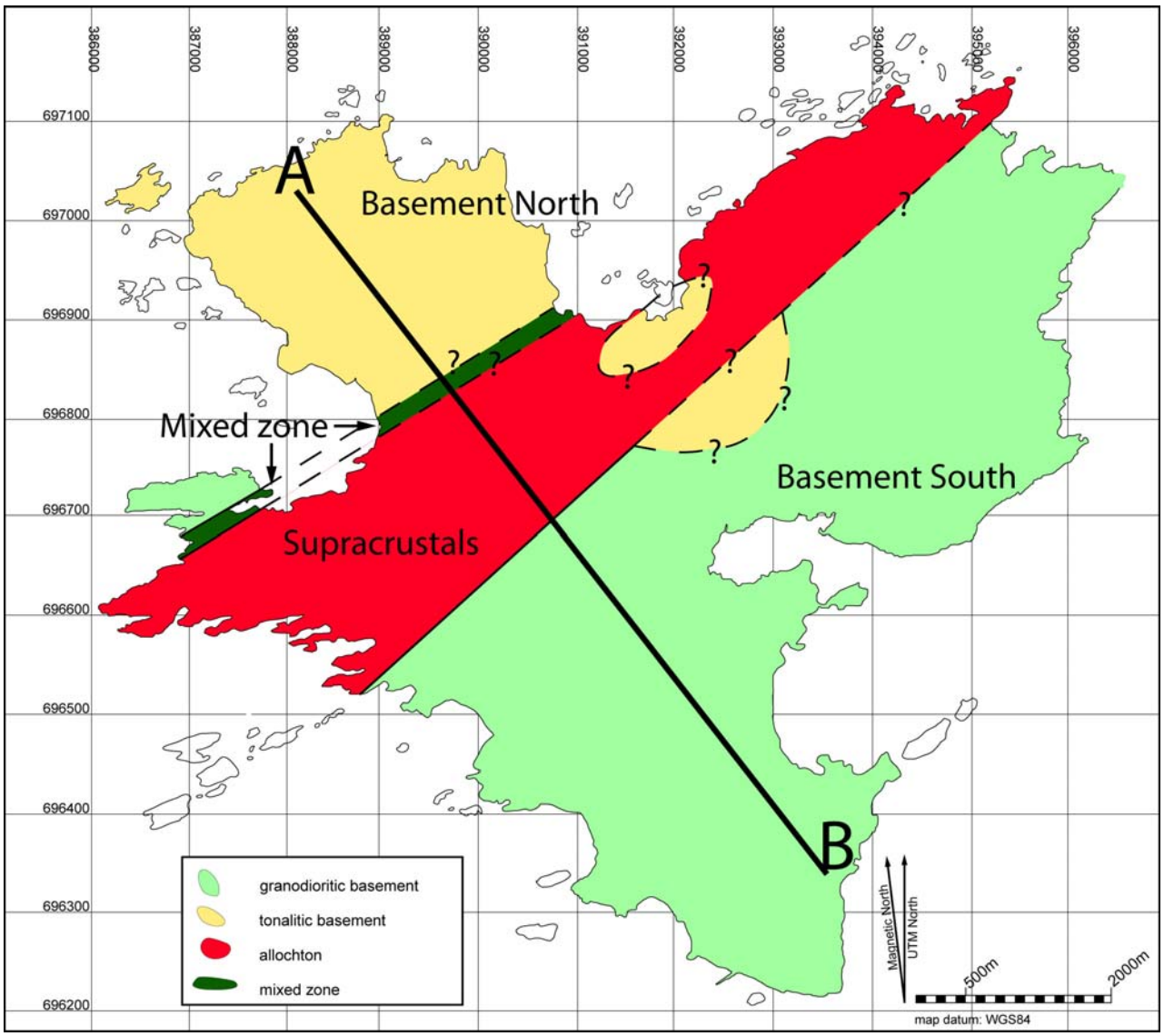

Figure 3.8. Interpreted geological map of Gossa, based on data as given in the fact maps (figure 3.2 to figure 3.6).

3.4 Lithologies

The characteristics of the rock types that on Gossa are presented in this section. These are the basement gneisses (section 3.4.1), mafic lenses (section 3.4.2) and supracrustals (section 3.4.3). Migmatic veins and intrusions that occur within both basement gneisses and supracrustals are discussed in section 3.4.4. The contact between the basement and supracrustals is treated in section 3.4.5.

3.4.1 Basement gneiss

The lithology that covers the largest area on Gossa is basement gneisses. Based on their mineralogy the basement has been subdivided in two different types (see figure 2.3 for classification diagram):

Tonalitic gneiss: qtz + pl + amphibole (amph) ± grt
Granodioritic gneiss: qtz + pl + k-feldspar (kfs) + bio ± grt

Granodioritic gneiss (figure 3.9) and tonalitic gneiss (figure 3.10) are characterised by a fine to medium grain size. Garnet is only locally present in both units. It has a larger grain size with up to cm-sized crystals. Most garnet crystals are one or more mm's large. Typical basement garnet is shown in figure 3.11, where the garnet crystals are the small red dots clustered just above the pencil.

Distinguishing between granodioritic and tonalitic gneiss is not always straightforward. The minerals qtz, pl and kfs can be very alike, having similar colours, and it is hard to distinguish between these minerals especially when the grain-size is small. Identification has mostly been done by distinguishing between bio and amph. These minerals are somewhat easier to identify because of the 'flaky' structure of bio, opposed to the '3-D' structure of amph. Unfortunately the crystal shape is harder to see when grain sizes are small and then these minerals become almost indistinguishable as well.

Basement is found in the northwest and the southwest of Gossa. These two areas are referred to as the basement north and basement south, respectively (figure 3.8). Granodioritic gneisses have mainly been found in the southern basement (green colour in figure 3.8), while the northern basement unit consists of tonalitic gneisses (yellow colour in figure 3.8).

Figure 3.9. Foliated granodioritic gneiss (data point 6.3).

Figure 3.10. Strongly foliated tonalitic gneiss (data point 3.7).

Figure 3.11. Garnet in mica-rich foliated granodioritic basement (data point 8.1).

Figure 3.12. Mafic lens enclosed in basement gneiss, blue handle of hammer for scale (data point 7.4).

3.4.2 Mafic lenses

Within the basement, abundant mafic lenses are present, while no mafic lenses have been found in the supracrustal rocks. The number and the size of the mafic lenses per unit area is highly variable across the island. The mafic lenses are shown in the fact map with symbols (see figure 3.2 to figure 3.6). Lenses greater than 1 meter are indicated with a red symbol, smaller than 1 m with a pink symbol. Eclogite/granulite lenses are indicated with circles, amphibolite lenses with triangles. Only for large eclogites and granulites the lenses the number next to the symbol refers to number of lenses that can be found at the particular data point. For the other categories the symbol '+' or '-' indicates if a large or a small number of lenses can be found at a particular data point.

Based on their mineralogy the mafic lenses can be subdivided into three categories:

Eclogite: grt + cpx ± opx
Granulite: grt + cpx + pl + amph ± opx
Amphibolite: amph + pl ± grt

These three mineral assemblages correspond to different metamorphic facies, as will be discussed in chapter 4. Mafic lenses vary in size from cm's to many tens of meters. Large lenses that can be mapped are present at data points 7.3, 15.6, 16.3 and 18.15, but mostly the lenses do not exceed a diameter of about 10 meter. The lenses occur as pods enclosed within the basement gneiss. Figure 3.12 is a good example where this structure can be observed in 3-D.

Small lenses mostly have amphibolite facies mineralogy. Larger mafic lenses consist of granulite, mostly with a rim of amphibolite. Figure 3.13 shows the outer edge of a larger mafic lens. Towards the core (left) the red and green colours refer to the presence of grt and cpx, defining the eclogite mineralogy. More to the right darker colour is characteristic for the mineralogy of amphibolite. On the right side of the image the white band refers to basement gneiss. Figure 3.14 shows a similar situation as figure 3.13, but here the core of the mafic lens is made up of granulite, and the transition to the broad amphibolite rim is sharper.

Figure 3.13. Detail of outer part of mafic lens in basement gneiss (data point 4.2). Note the transition from eclogite on the left, to amphibolite on the right in the mafic lens.

Figure 3.14. Mafic body inside basement gneiss (white). The mafic body consists of an eclogite core (red-green) surrounded by an amphibole rim (dark), data point 9.6

Most eclogites are not 'fresh', meaning that they have undergone retrograde reactions. Garnet crystals are then rimmed by amph and/or pl and amph grows in the eclogite matrix as well. Black (amph) and white (pl) colours are then added to the characteristic red and green appearance of fresh lenses, as is shown in figure 3.15.

In the AFC diagram of figure 2.15 the possible mineralogical variation of fresh eclogites are illustrated. Most eclogite bulk rock compositions plot in such ACF diagram on the tie-line cpx-grt. This means that the eclogite will be a bimineralic eclogite consisting of these two minerals (+qtz). In contrast bulk rock chemistries that plot more to the Al side of the diagram will have in addition kyanite and/or phengite. If the bulk rock chemistry of the eclogite plots towards the Fe/Mg end opx will appear in the assemblage. Both are important for geothermobarometry and fresh eclogites have been investigated in detail for their mineral assemblage. For example, sample 10.5 (from data point 7.3) is taken from a fresh eclogite lens that has an outcrop size of about 1200m^2 (30x40m). This outcrop shows areas where the eclogite is very fresh, but also regions that have undergone retrograde mineral growth. In the fresh parts the mineralogy is essentially bimineralic. Only after a long search two small patches, half covered in soil, where found to be fresh and to contain opx (see figure 3.16). Locations like this have been used to sample opx bearing eclogites. These outcrops are classified as opx-bearing eclogites on the fact map because of their importance for geothermobarometry, even though the actual fresh, opx bearing part may be only a small part of a large, essentially bimineralic eclogite outcrop. Opx-bearing eclogites are found at data point 17.5, 13.2, 6.7, 7.3

Figure 3.15. A retrograde eclogite: garnet (red mineral) is rimmed by plagioclase (white mineral). In matrix abundant amphibole (black mineral) is present (data point 4.3).

Figure 3.16. Fresh coarse grained opx-bearing eclogite, right before the moment of sampling (data point 7.3).

3.4.3 Supracrustals

The mineralogy of the supracrustal rocks is:

grt + hbl ± bio ± kfs ± pl ± muscovite (musc) ± ky ± sill

Supracrustal rocks are found in the central part of Gossa in a strip running from SW to NE. They are coloured red on the geological maps (figure 3.1 to figure 3.8). Compared to the basement rocks they are generally coarser grained. A conspicuous characteristic is the occurrence of abundant large crystals of garnet, giving rise to the nickname ‘current loaf’. Figure 3.17, figure 3.18 and figure 3.19 show field photographs of the supracrustal rocks, in all of them garnet can be seen to be present in much greater quantities and with a larger grain size than garnet in basement rocks (compare with figure 3.11).

Figure 3.17. Close-up photograph of foliated garnet-plagioclase-amphibole-biotite gneiss (data point 3.4).

.

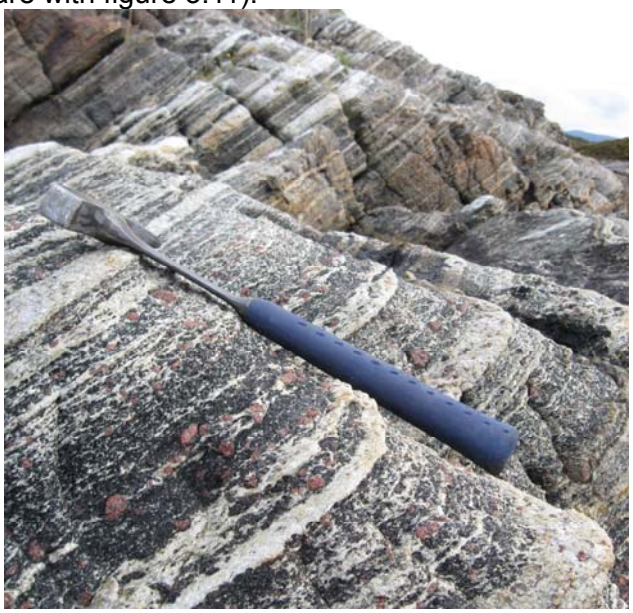

Figure 3.18. Foliated garnet-plagioclase-amphibole-biotite gneiss (data point 14.2)

Figure 3.19. Large kyanite crystals in supracrustals (data point 18.17).

Figure 3.20. Migmatic character of granodioritic basement gneiss (data point 8.3)

3.4.4 Melting

Signs of melting are found in all rock units on Gossa. This feature is not shown on the geological maps. Parts of the basement rocks, in the north and in the south, have a migmatic character. The migmatic character in granodioritic gneiss is shown in figure 3.20. The pinkish coloured layers near the bottom of the image have a granitic composition and consist of kfs + pl + qtz occurring in bands parallel to the main foliation in the gneiss. The migmatic character in the tonalitic gneiss is shown in figure 3.21. These melt veins are different in composition compared to the veins in granodioritic gneisses, consisting of qtz + pl. The lower half of the image shows folded migmatite veins which are cut by straight veins in the upper half of the image.

The supracrustals show a strong compositional layering (figure 3.18). Very pl-rich white layers alternate with darker grt-bio-rich layers. This is probably caused by partial melting of the supracrustals. However, the compositional layering is much more regular than in the basement gneisses, and features like cross-cutting veins are not observed. Therefore a sedimentary layering can not be excluded as the origin of the compositional variation.

The migmatic veins that are described above range in thickness from 1-10 cm. Granitic intrusions, with a mineral composition of qtz + kfs + pl ± bio ± musc, are generally larger with thicknesses of dm's to m's. They are present in all lithologies but scatter in their regional occurrence. Like the migmatic veins, deformation of the intrusions is variable. Figure 3.22 shows folded intrusions in granodioritic basement gneisses, figure 3.23 shows intrusions that cut through mafic lenses within the basement gneisses. Figure 3.24 shows a large, undeformed, granitic intrusion that cuts the supracrustal foliation at right angles.

Figure 3.21. Two generations of melt veins in tonalitic gneisses (data point 11.5).

Figure 3.22. Folded granitic intrusions (data point 17.2).

Figure 3.23. Granitic intrusions cutting through retrograde eclogite with amphibolite rim (data point 12.2).

Figure 3.24. Granitic intrusion cutting through supracrustals (data point 14.10)

.

3.4.5 Contact between basement and supracrustals

The contact between the basement rocks and the supracrustals is especially well exposed on the southeastern side of Gossa, where an almost continuous outcrop is present starting from the southern basement, to the supracrustals, and on to the northern basement.

The contact between the southern basement and supracrustal rocks is marked by the occurrence of many high strain zones within the basement rocks. These zones are given by red lines on the geological fact maps (figure 3.2 to figure 3.6). High strain zones are usually a couple of meters wide and characterized by an intense penetrative foliation. Figure 3.25 shows an example of the high strain zone which is located a couple of hundreds of meters south of the boundary between basement and supracrustals (data point 13.1). No high strain zones are observed in the supracrustals. The actual contact between the basement and supracrustals is normally easy to find because change in mineral assemblage and mineral grain size. Such a contact is shown in figure 3.26, with the highly migmatic, fine grained basement rocks in the upper half of the image, and coarser grained supracrustal rocks with large garnet crystals in the lower half.

The contact between the supracrustals and northern basement rocks is not as clear as it is on the southern side. A wide zone where basement and supracrustals occur together is present. Some places in this zone clearly represent supracrustals, while others are clearly basement, and at many places the categorisation to either basement or supracrustals is unclear. This is why we have named in the 'mixed zone' (coloured green on the geological maps, figure 3.2 to 3.6). The boundaries between the lithologies in the mixed zone are more fuzzy, instead of the sharp contact as is shown in figure 3.26. The mixed zone is best described as a melange of basement and supracrustal rocks where the individual lithologies are hard to discern.

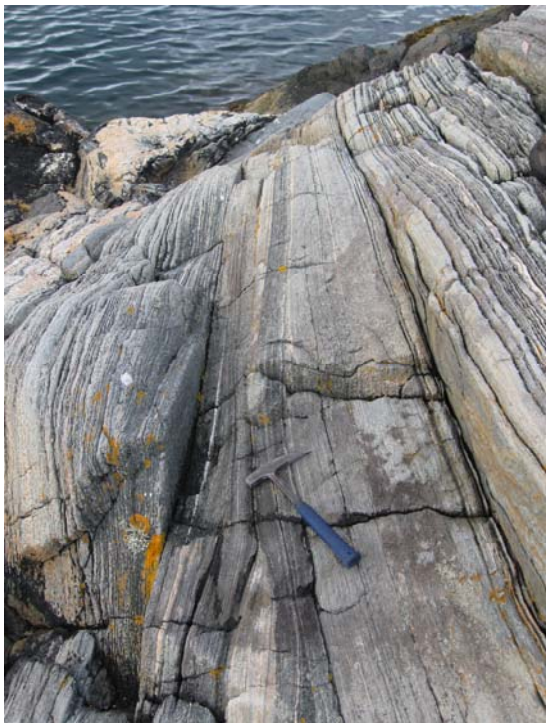

Figure 3.25. A high strain zone in the southern basement near the contact with supracrustals, looking SW (data point 13.1).

Figure 3.26. Interpreted contact between basement (top) and supracrustals (bottom), data point 18.17

3.5 Structures

The structural geology on Gossa is presented in this section. Structural features that are distinguished are the high strain zones (section 3.5.1), S and Z folds (3.5.2), foliations (0) and lineations (3.5.4).

3.5.1 High strain zones

High strain zones are present in basement rocks. They occur both in the northern and southern basement, with an especially high density near the southern contact between supracrustals and southern basement (see figure 3.3). The supracrustals are free of high strain zones.

All high strain zones have been investigated on signs of shear sense. Shear sense is indicated with an arrow next to the high strain zone on the geological fact maps (figure 3.2 to figure 3.6). The arrows show the relative movement of the rocks on both sides of the high strain zone. This relative sense of shear has in all cases been identified making use of sigma clasts, an example is shown in figure 3.27. The asymmetric shape of the white 'layer' reveals a relative movement of the upper part of the image to the left with respect to the lower half: a sinistral shear sense. In all high strain zones where the shear sense could be determined, a sinistral shear sense was found.

Figure 3.27. σ-clasts in high strain zone indicate a sinistral shear sense (data point 13.1).

3.5.2 S/Z-folds

In heavily deformed terrain like the northern and southern basement, small scale structures can be used to make interpretations about the larger scale. We have recorded the orientation of 15 S- and Z-folds on Gossa. An example of an S-fold is given in figure 3.28, a Z-fold is a mirror image of this structure. If folds are present the S- and Z-folds can be used to determine the vergence. The observation of an equal amount of S- and Z-folds could therefore imply that the symmetric folds are present on a larger scale, and a larger amount of either one could imply asymmetric folds. In a shear zone the S- and Z-folds can also be sheath folds, in which case they can be used to determine the shear sense. The number of observations is, however, too low to draw any meaningful conclusions and these observations are not given on the fact map.

Figure 3.28. S-fold in basement rocks (data point 12.2).

Figure 3.29. Intensely deformed basement rocks (data point 18.2).

3.5.3 Foliations

A penetrative foliation is present in all basement and supracrustal rocks, as comes forward from images already shown of this lithology (e.g. figure 3.9 to figure 3.11 and figure 3.18). Complicating this foliation is the folding, that has affected the basement. Figure 3.29 shows an example of intensely deformed basement rocks. There is a high variation in folding of the basement foliation. Areas with almost straight, unfolded foliation interchange with areas where open or tight folds are present.

Mafic lenses enclosed in basement gneisses do not always contain foliation. Foliation in amphibolite lenses is always present and is orientated identical to the surrounding basement gneisses (see figure 3.30). In contrast, most granulite and virtually all eclogite lenses are free of foliation. At a few locations foliation of granulite has been observed (figure 3.31), and very sporadically there is also foliation present in eclogite (figure 3.32).

Where the orientation of the foliation of amphibolite lenses is in line with the surrounding gneisses, the granulite and eclogite foliation show contrasting orientation compared to the surrounding basement gneisses. Figure 3.33 shows the typical relation of the basement foliation and mafic lenses, with the foliation wrapping around the lens. This relation has been observed at granulites and eclogites at a scale from cm's to many tens of meters.

Figure 3.30. Foliated amphibolite lens (data point 6.9).

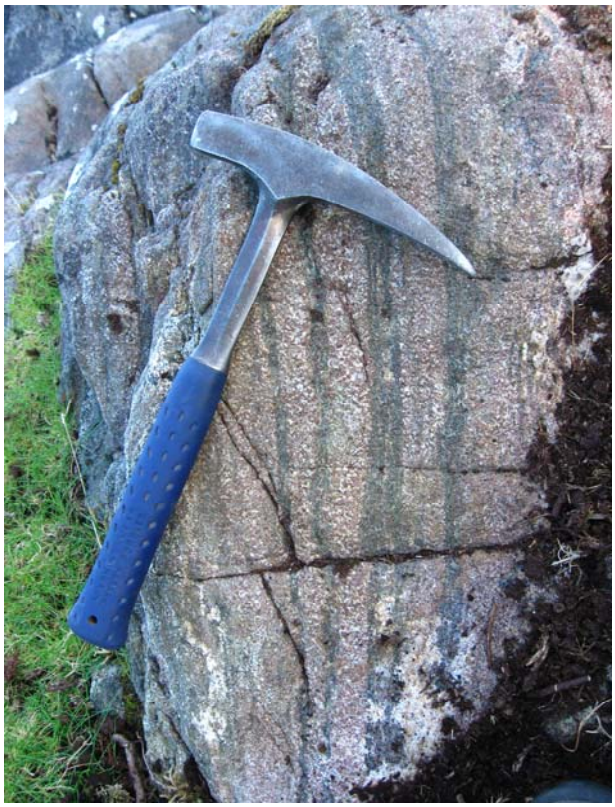

Figure 3.31. Foliated granulites (data point 16.9).

Figure 3.32. Rare example of a foliated eclogite lens (data point 9.6).

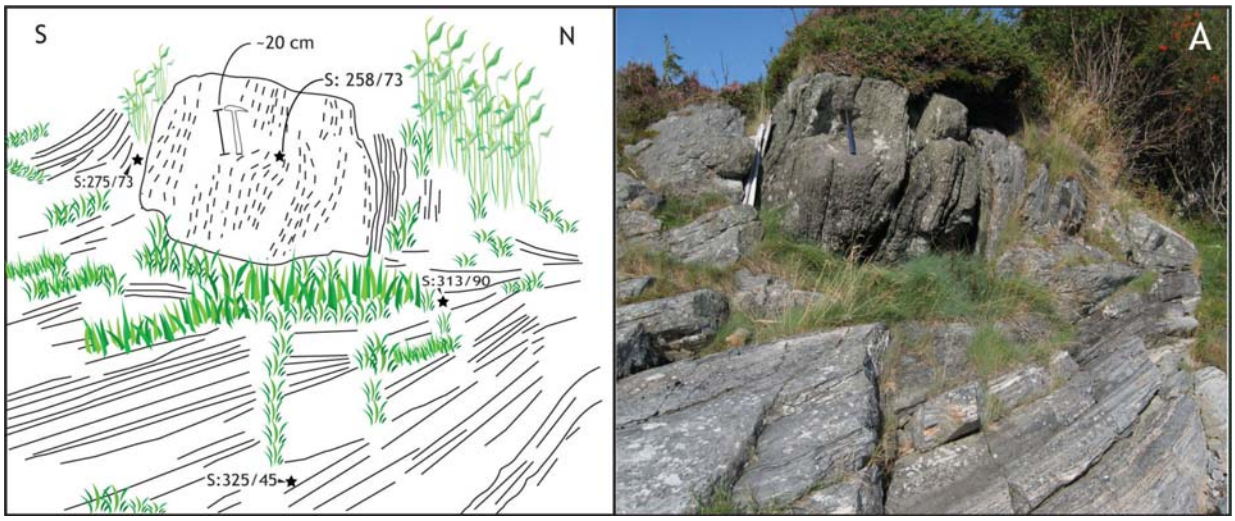

Figure 3.33. Foliated eclogite lens. The basement foliation wrapped around it (location 12.6).

Foliation measurements are grouped according to the rock type in which they occur. The foliation in granulite and eclogite lenses is invariably cut-off by the foliation of surrounding basement gneisses. Therefore the basement foliation is inferred to be a younger feature than granulite and eclogite foliation. The basement foliation, as well as the similar oriented foliations of supracrustals and amphibolite lenses are grouped into Sn. The eclogite and granulite foliation are grouped into Sn-1. A further subdivision has been made based on rock type in which foliations are formed and geographical location. Measurements of foliations are graphically shown in Wulff-nets. Separate plots are given for granodioritic gneisses of the southern basement (figure 3.34) tonalitic gneisses of the northern basement (figure 3.35), supracrustals (figure 3.35), the mixed zone (figure 3.35) and eclogites and granulites (figure 3.36).

Foliation measurements of the southern basement indicate orientations with a constant strike (SW-NE) and variable dip ranging between horizontal and vertical. There are more NW dipping foliations than SE dipping foliations. The supracrustals have on average the same strike as the southern basement, but their dip is more constant and clusters about 45º to the NW. Not many measurements from the mixed zone are taken, but the pattern seems to be the same as for the supracrustals. Measurements in the northern basement rocks show a very different pattern, with orientations of the foliation being more scattered and dipping more to the NNW on average.

3.5.4 Lineations

Lineations have been measured in all rock units that contain Sn foliations. Lineations are not observed in granulites and eclogites. Measurements of lineations are given in dip and dip direction of the lineation. Measurements of lineations are graphically shown in Wulff-nets, separate plots are given for granodioritic gneisses of the southern basement (figure 3.34) tonalitic gneisses of the northern basement, supracrustals and the mixed zone (figure 3.35). Foliation in the basement rocks is often folded. In some cases, where the fold is visible in an outcrop in 3-D, this enables the measurement of fold axes. Measurements of fold axes are graphically shown in figure 3.37, with the location of each measurement indicated. These fold axes are primarily measured in the southern basement.

Lineations present in the southern basement are oriented in line with the strike of foliations, with (sub)horizontal dips. In supracrustals lineations are also more or less in line with the strike of foliations, and almost horizontal. In contrast the lineations of the northern basement are almost randomly distributed. The orientation of the fold-axes, mostly measured in the southern basement, are more or less in line with lineations in this southern basement.

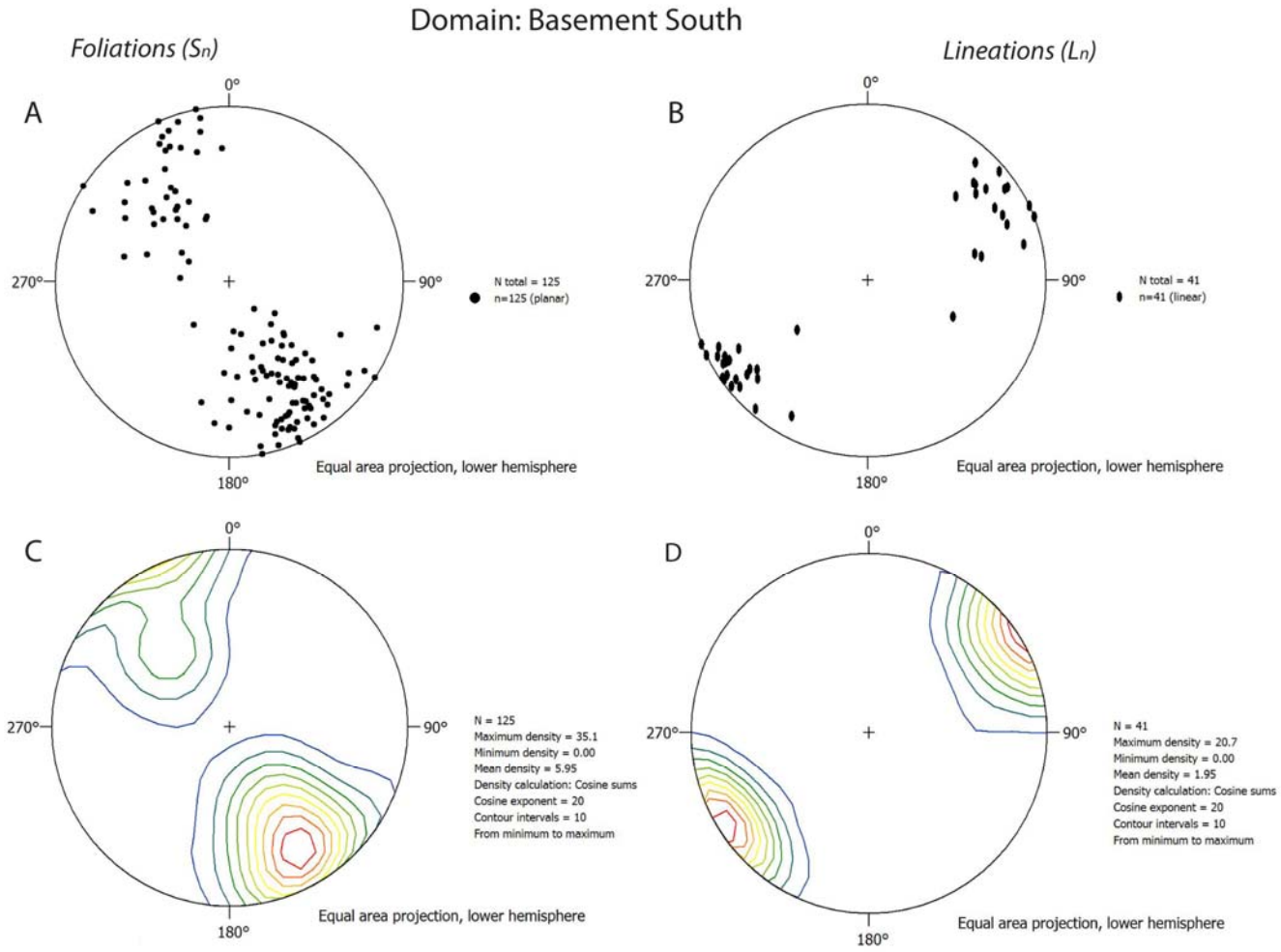

Figure 3.34. Wulff-net, equal area, lower hemisphere projection of poles to foliation and of lineations in the granodioritic gneisses of the southern basement. 0º equals orientation to North. A) normals to the foliation planes, B) lineations, C) density distribution of foliations, D) density distribution of lineations.

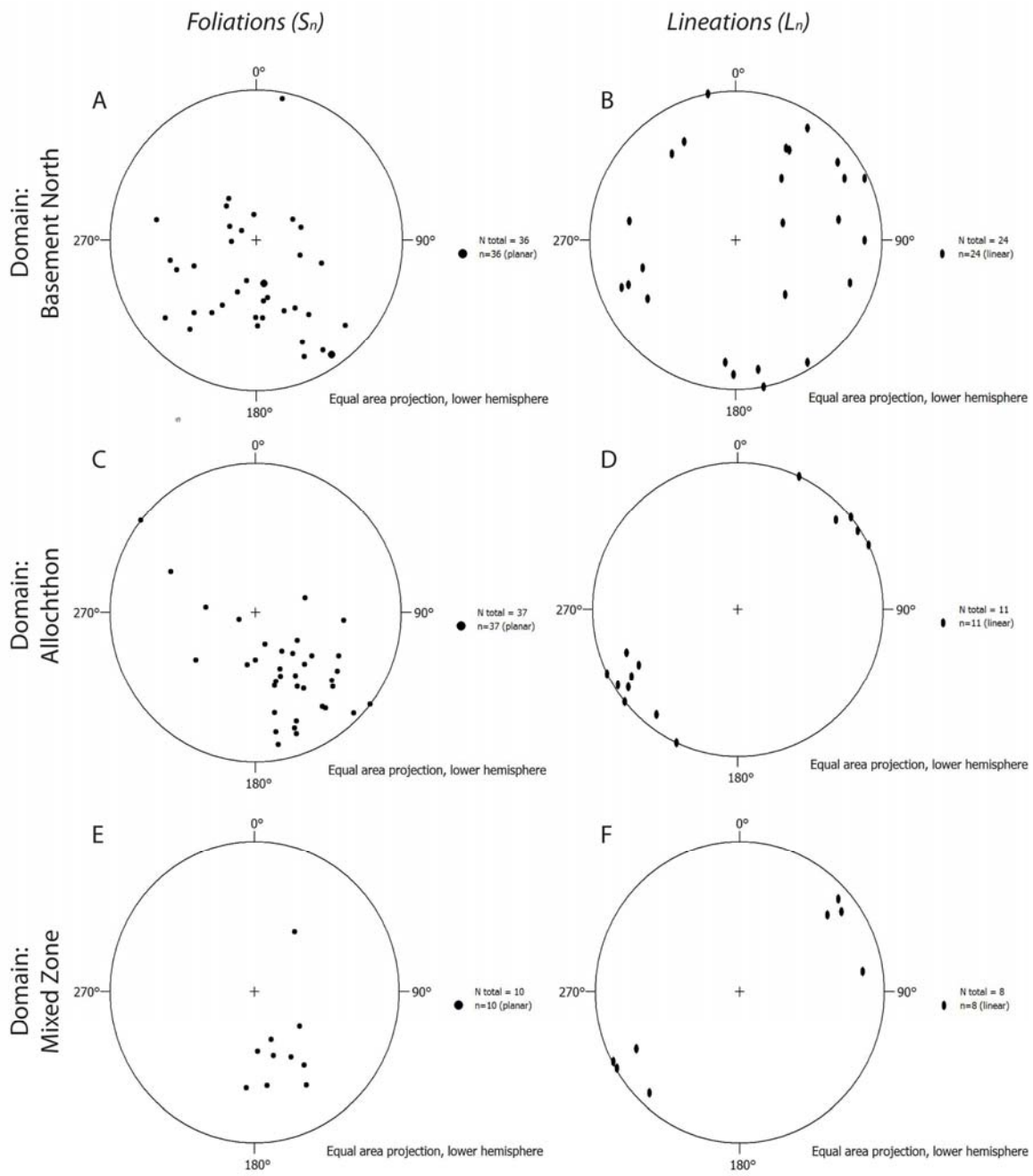

Figure 3.35. Wulff-net, equal area, lower hemisphere projection of poles to foliation and of lineations. 0º equals orientation to North. A, B) tonalities gneisses of the northern basement. C, D) supracrustals. E, F) mixed zone.

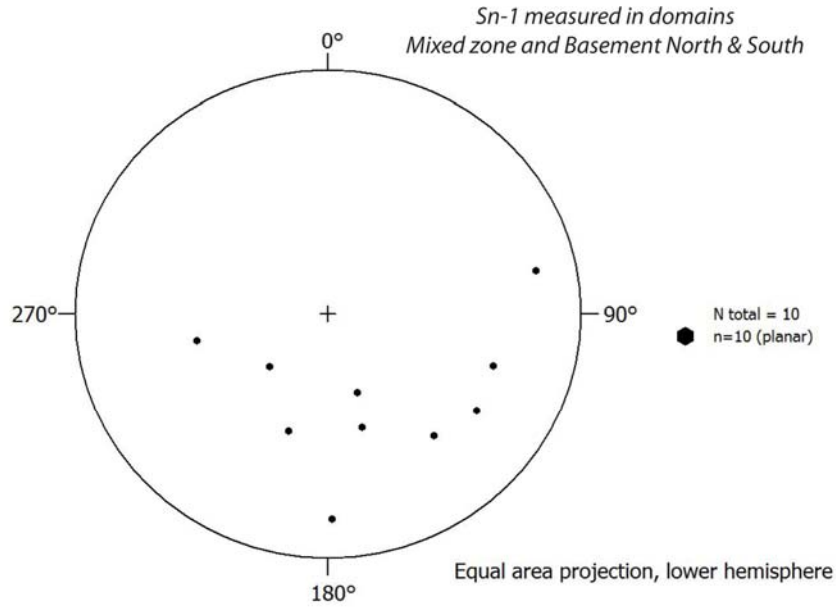

Figure 3.36. Wulff-net, equal area, lower hemisphere projection of poles to foliation in eclogites and granulites from basement north and south and the mixed zone. 0º equals orientation to North.

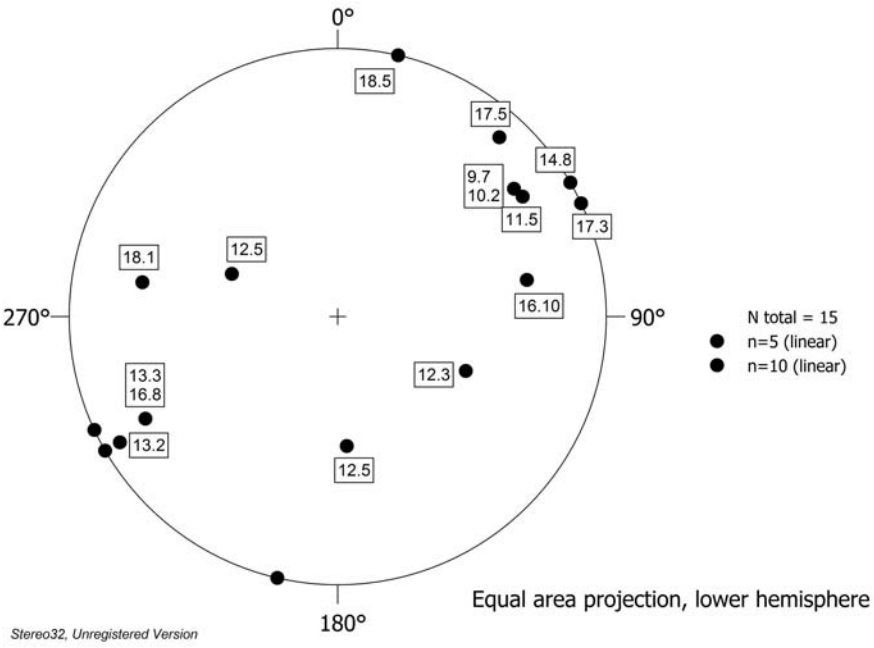

Figure 3.37. Wulff-net, equal area, lower hemisphere projection of fold axes in basement gneisses. Measurements are mostly from the southern basement, numbers indicate the data point of each measurement. 0º equals orientation to North.

3.6 Geological and structural summary

For clarity the most important characteristics of the four geological units, all discussed in text above, are summarized in table 3.1.

	Basement North	***Supracrustals***	***Mixed Zone***	***Basement South***
Lithologies	• Tonalitic gneiss	• garnet-mica schist	• interchanging of basement gneisses and supracrustals	• Granodioritic gneiss
Mafic Lenses?	• yes, also eclogites	• no	• yes	• yes, few eclogites
Foliations	• NNE-SSW strike, but variable • dips to NNW	• NNE-SSW strike • dips to NNW	• NE-SW strike • dips to NW	• NE-SW strike • variable dip, larger population dipping NW
Lineations	• scattered orientation • (sub)horizontal dip	• NE-SW • horizontal dip	• NE-SW • horizontal dip	• NE-SW • (sub)horizontal dip
Fold structures	• Intense folding • Tight/isoclinal folds	• None to gentle open folds	-	• Intense folding • Tight/isoclinal folds
Fold Axes	• mainly NE-SW strike • mainly (sub)horizontal dip	• no	-	• mainly NE-SW strike • mainly (sub)horizontal dip
Migmatic character	• high, both deformed and undeformed	• high, mainly undeformed	-	• high, both deformed and undeformed
High strain zones	• Yes	• no	• no	• yes

Table 3.1. Summary of most important characteristics of the four geological units.

3.7 Discussion and cross sections

Lithologies

As discussed in chapter 2, the Ulla Gneiss is characterized by Terry and Robinson (2003) as a melange of coarse grained eclogite boudins and hbl ± cpx + grt + bt + pl + qtz gneisses. It is found on the Nordøyane islands Fjørtoft and Flemsøy and in the mainland at the Bud-Tornes area (Vrijmoed et al., 2006). Gossa is located in between these locations, and the lithological description is in agreement with both the northern and the southern basement rocks. This makes it very likely that the basement gneisses that are found on Gossa are indeed part of the Ulla Gneiss.

The allochthon is mapped by the NGU (2009) as mica schists. According to Terry and Robinson (2004) the allochthon in the northern UHP domain is equivalent to the Blåhø en de Sætre nappe, of which the Blåhø nappe consists of grt ± ky ± staurolite (stau) mica schists (Walsh and Hacker, 2004). This descriptions show indeed a very good correlation with the supracrustals that we mapped on Gossa.

The resultant interpreted geological map (figure 3.8) shows improvements with respect to the preciously published maps. The basement gneisses have been subdivided into granodioritic

and tonalitic gneisses. The boundary of the supracrustals, especially on the northwestern side of Gossa, is different from the published maps. However, the map by the NGU is found to be quite accurate. For the search of UHP conditions on Gossa, the biggest improvement of our mapping is the identification of locations of mafic lenses that are given in the fact maps, and the search for peridotites. Although peridotites are found to be absent on Gossa, it might be useful for future research to know that there is no need to look for this lithology on Gossa.

Structural relation between northern- and southern basement and supracrustals

The question whether the northern and southern basement are structurally the same unit cannot be answered with certainty. It is uncertain whether the supracrustals are folded into the basement or thrusted, or a combination of both. If the supracrustals are folded into the basement then on a large scale the basement rocks would form a syncline, with the supracrustals in its centre. This situation is graphically shown in figure 3.38. If the basement form a large scale fold, then the southern basement foliation would be expected to be dipping to the NW, while the northern basement dips to the SE. However, tight isoclinal folding or the occurrence of parasitic folds could cause a complication and result in the northern and the southern basement showing the same foliation pattern.

If the supracrustals are a thrust slice in between two basement blocks, a situation shown in figure 3.39, it might be expected that the foliation changes towards the boundary according to the existence of a hanging wall syncline and footwall anticline. Also mylonites (high strain zones) will be present in between the basement and the supracrustals.

All of this is, of course, under the assumptions that the current day foliations are indeed related to the emplacement of the supracrustals and basement gneisses. However, there is little evidence to support this. The foliation in supracrustals and southern basement is found to be about parallel to the boundary between the basement and supracrustal units, which might imply a link between emplacement and foliation. However, such a correlation can also be achieved when large scale shearing or stretching takes place with high strains, because then all foliations and contacts will eventually reach a (sub)parallel position with respect to each other. As discussed in chapter 2 the current day foliations and high strain zones are possibly related to the latest stage of extension (Vrijmoed et al., 2006), which does not have to represent the emplacement of supracrustals and basement next to each other.

There is no evidence that the lineations and foliations are related to the emplacement of the supracrustals next to the basement. Even so, the NE dipping foliations and randomly scattered lineations of the northern basement agree with neither the folding or thrusting theory. The occurrence of high strain zones in the basement at the contact between the supracrustals and the southern basement is in favour of the thrusting scenario. However, his line of evidence in too thin too rule out the folding scenario. Therefore the question about the emplacement of supracrustals next to basement and whether the northern and southern basement can be classified as the same unit remains open.

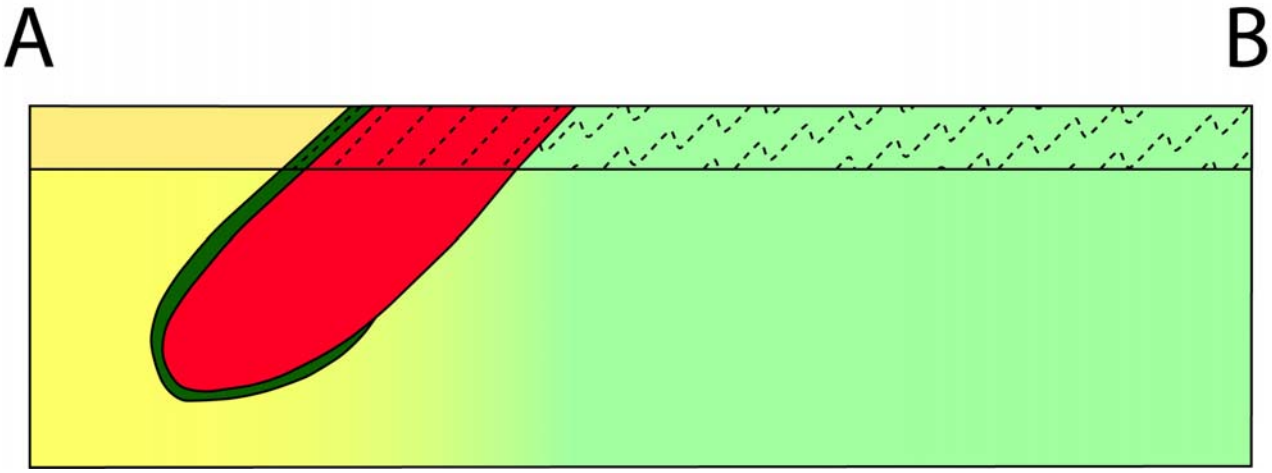

Figure 3.38. NW-SE cross section across Gossa with supracrustals folded in the basement in a tight syncline, for location of cross section see figure 3.8.

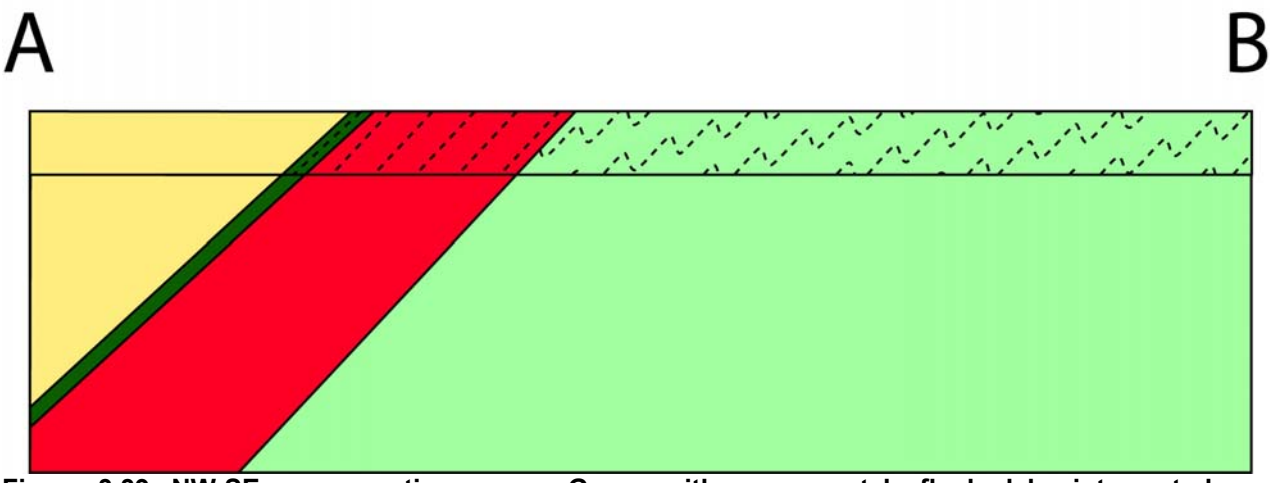

Figure 3.39. NW-SE cross section across Gossa with supracrustals flanked by interpreted thrust contacts with southern basement. For location of cross section see figure 3.8.

Foliations

Foliation are observed in all lithologies. The foliation of eclogites, granulites and the basement rocks will be shown in the following chapter to have formed during very different pressure and temperature conditions and at a different time. At least three different phases of foliation can be discerned. The Sn-1 foliation is defined by both the granulite mineral assemblage (figure 3.31) and the eclogite mineral assemblage (figure 3.32). Because the granulite and eclogite mineral assemblages require different PT conditions to form, the Sn-1 foliations defined by granulites and eclogites are formed at a different time. The Sn foliation of the basement gneisses wraps around and cuts off the foliation in mafic lenses (figure 3.33), which implies that the Sn-1 foliation is older than Sn.

The basement foliation is folded itself at many locations. Possible explanations for this folding are that the basement is deformed in a later, fourth deformation event. Prolonged deformation, with high strain rates, can also have caused both the foliation and the folding of this foliation. If the latter is the case, then the folds could be sheath folds. In a rock that experiences very high shear strains, folds will gradually be transformed into sheath folds. Newly developed folds will have a fold axis that is within the plane of foliation but perpendicular to the main direction of transport. With increasing strain these folds will rotate, and fold axes will rotate towards the direction of transport. This means that sheath folds can be identified based on the parallel relation between fold axes and lineations. Comparison between the orientation of the fold axes (figure 3.37) and the orientation of lineations in the southern basement, where most fold axes measurements are taken (figure 3.37) shows that this parallel relation might exist. This observation can not be made with high certainty because of the higher scatter of the fold axes and the relative low number of fold axis measurements.

In summary, based on the observed foliations in eclogites, granulites and the basement gneisses there are at least three different deformation events. A possible fourth deformation event that has affected the basement could be the same event that caused the main basement foliation.

Migmatites and granitic intrusions

Both deformed and undeformed migmatic veins and granitic intrusions are found in all units. The undeformed veins and intrusions can be expected to have formed after the main deformation of the rocks in Gossa, i.e. after the formation of the basement foliation. The deformed veins and intrusions are affected by strain, and thus formed at or before the formation of the basement foliation. This means that melting happened before/during and

after the deformation event on Gossa. There must have been at least two different generations veins and intrusions, and thus two generations of melting, or melting took place during prolonged time that extended from the time of deformation until deformation had stopped.

The granitic intrusions show a mineral assemblage that is the same in both the tonalitic gneisses and the granodioritic gneisses. In contrast the mineral assemblage of the migmatic veins changes is different in tonalitic gneisses form those found in granodioritic gneisses. This implies a local origin for the migmatic veins, with partial melting of their host rock. The granitic intrusions are from an external source.

4 Optical microscopy

Hand-sized samples have been collected during fieldwork and are used for further analysis at Utrecht University. The 12 investigated include 6 samples from basement gneisses, 4 granulites and 2 opx-bearing eclogites. Locations where the samples have been taken are given in figure 3.7. Investigated samples have been cut (figure 4.1), and cuttings used for preparation of thin sections. In this chapter not all thin sections that have been made will be discussed. Especially the eclogite samples, of which initially all opx-bearing outcrops have been sampled, turned out not all to be useful for further analysis. Only samples taken at data points 10.5 and 17.5 are judged to be fresh enough after an initial analysis by optical microscopy. All thin sections are from different hand samples, with a number corresponding to the data point where they are collected. If multiple samples have been taken from one outcrop they are assigned a letter. Different hand samples taken at the same outcrop usually been taken a few meters apart.

Pressure and temperature conditions of eclogite and granulite samples will be determined by geothermobarometry (chapter 5 and 6). It is, however, still useful to use optical microscopy on these samples to determine the exact mineral assemblage and select the mineral grains most suitable for further analysis by Electron Microprobe (EMP). PT conditions of the basement samples has not been determined by geothermobarometry. Instead, a more detailed analysis of their mineralogy will follow in this chapter to constrain PT conditions.

Figure 4.1. Cuttings of eclogite sample 17.5a.

4.1 Eclogites

The percentages of minerals present in the eclogite samples are shown in table 4.1. The percentages are rough estimates, and there can easily be a 5% error in the assigned values. Omph and phlogopite (phlog) are the high pressure equivalents of cpx and bio, these mineral names will all be used.

Sample	grt	cpx	opx	bio	hbl	qtz	rutile	apatite
10-5A	10%	40%	30%	<5%	<5%	<5%	<1%	<1%
10-5B	20%	45%	25%	<5%	-	<5%	<1%	-
10-5C	30%	35%	25%	-	5%	<1%	<1%	-
10-5D	15%	40%	30%	<5%	5%	<5%	<1%	-
10-5E	40%	15%	35%	<5%	0%	5%	<1%	-
17-5A	10%	50%	25%	<5%	<5%	<5%	<1%	-
17-5B	40%	35%	15%	<1%	5%	5%	<1%	-
17-5C	20%	50%	20%	<5%	<5%	<5%	<1%	-

Table 4.1. Mineral composition of the eclogite samples

Eclogite mineral composition
Eclogites mainly consist of garnet, opx and omp. The high percentage of opx is mainly the result of the sampling procedure, because in the field the eclogites with the highest amount of opx are collected. The typical opx-bearing eclogite mineralogy is shown in figure 4.2, microphotographs from sample 10-5A. Garnet is easily recognisable because it appears black in cross polarized light (XPL) and because of its many inclusions. Cpx is greenish in plain polarized light (PPL) and has higher colours in XPL than opx. Omph appears pinkish in PPL, which is approximately the same colour as garnet in PPL.

Garnet is not very angular but has roundish shapes. The large minerals grt, cpx and opx, show on average nice, smooth grain boundaries with triple junctions. The amphibole that is present in some thin sections (not shown in figure 4.2) have boundaries that are more wiggly without nice crystal shapes.

In general the samples that are collected at the same outcrop are very much alike. Of course the amount of grt, omph and opx can vary between the thin sections due to the variation that occurs in a rock on cm scale. For example, grains of garnet can be relatively large (up to half of the width of the thin section), and by chance these grains can be incorporated or left out in the thin sections, hence the variation between 10-40% in the same outcrop. Small minerals (bio, qtz, hbl, rutile, apatite) are more evenly distributed on the scale of the thin section, therefore variation of these minerals is much smaller.

Kelephytic rim
There is some difference between the samples from 10-5 and the samples from 17-5, that is not readily apparent from the mineral distribution. Figure 4.3 shows the outer part of a garnet grain, in contact with both cpx and omph. The outer rim of the garnet is not in direct contact with the pyroxenes, but a thin line made up of very fine-grained crystals is in between the garnet and the pyroxenes. This is a kelephytic rim, and it is present around every garnet from outcrop 17-5. The minerals that make up the kelephytic rim are too small for mineral determination under the optical microscope. It is important to realize that the small grain size and the occurrence at the outer edge of the garnets reveals that the kelephytic rim is a break-down product of garnet, as garnet became unstable at lower PT-conditions. Samples from outcrop 10-5 generally lack this kelephytic rim, or locally it is present with only a fraction of the thickness of the garnets from 17-5 (compare figure 4.2 with figure 4.3). The lack of kelephytic garnet rims in outcrop 10-5 compared to 17-5 means that these samples have undergone less retrograde reaction, and are therefore ‘fresher’ eclogites.

Cpx symplectites
Cpx that grows at high PT conditions will become unstable at low PT conditions. This results in fine-grained symplectites to form at the grain boundaries between grains of cpx (Joanny et al., 1991). When the retrograde reaction is complete, the entire cpx crystal will be replaced by symplectites. This reaction can be seen in figure 4.4. Here different grains of cpx are locally in direct contact with each other, but mostly the grains are separated by symplectites. The cpx symplectites are therefore analogous to the garnet kelephytic rim, and the amount of cpx that has been replaced by symplectites is a measure of the amount of retrograde reaction that has taken place in a rock. Indeed, the samples taken at outcrop 10-5 show (almost) no cpx symplectites, while it is a common feature in all samples from 17-5. Based on the symplectites the same can be said about the freshness of the eclogite samples: Samples from outcrop 10-5 have undergone less retrograde reaction than samples from outcrop 17-5.

Cpx exsolution needles
A very high percentage of the grains of cpx from outcrop 17-5 show small, needle like features within the crystal. The needles are evenly distributed in the core of a crystal, but are mostly absent at the cpx rim. They are always preferentially orientated, with only one orientation occurring within a grain. A good example is shown in figure 4.5, but it can also be observed in figure 4.4, figure 4.6. The distribution within the core of the cpx crystals makes it very different from cpx symplectites, that occur concentrated at the grain boundaries. The needles in cpx are virtually absent in cpx from samples from outcrop 10-5. The occurrence of needles in cpx will be discussed in section 4.4.

Fluid inclusions
Samples from both 10-5 and 17-5 locally show fluid inclusions. Examples are given in figure 4.6. The fluid inclusions can be distinguished from the cpx exsolution because of their uneven distribution, round shape, and tendency to cross grain boundaries. The occurrence of fluid inclusions will be discussed in section 4.4.

Quartz
Samples from both outcrop 10-5 and 17-5 contain some quartz. As one of the main targets of this research is to find evidence for a possible UHP origin, all eclogites have been extensively investigated for signs of radial cracks or other signs of polycrystalline quartz (PCQ). However, none of these features have been convincingly observed in eclogite samples. There are many examples within these samples where some cracks are seen that 'radiate' away from possible quartz grains, but none of them are very convincing. Figure 4.7a shows a typical example of a quartz grain, in this case within a grain of opx. No radial cracks can be seen and the internal structure of the quartz grain shows no subdivisions to indicate PCQ. Quartz grains do show some undulose extinction. Characteristics of PCQ are discussed in section 4.4.

Twinning in cpx
Twinned cpx grains have been observed in a few grains within sample 10-5A. It is thus not a common feature in the eclogite samples. An example is given in figure 4.7.

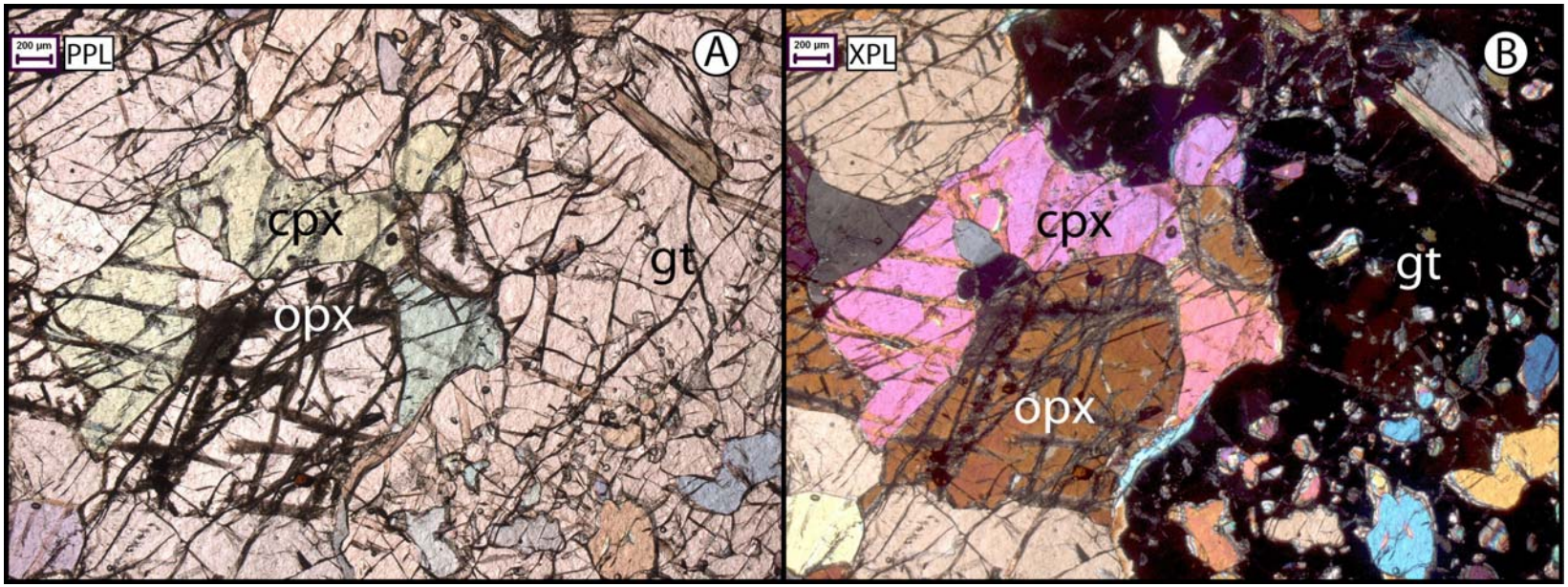

Figure 4.2. Eclogite sample 10.5B. Typical mineralogy of opx-bearing eclogite. A) PPL, B) XPL

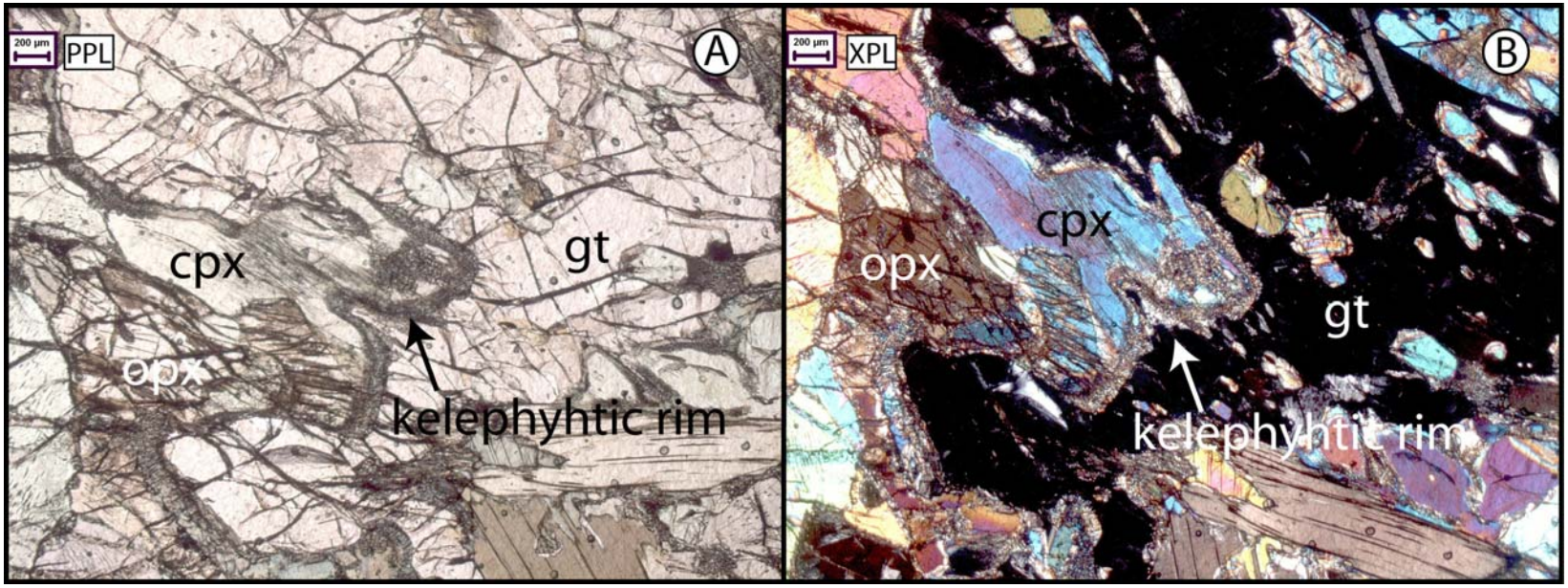

Figure 4.3. Eclogite sample 17.5A. Note kelephytic rim around garnet. A) PPL, B) XPL

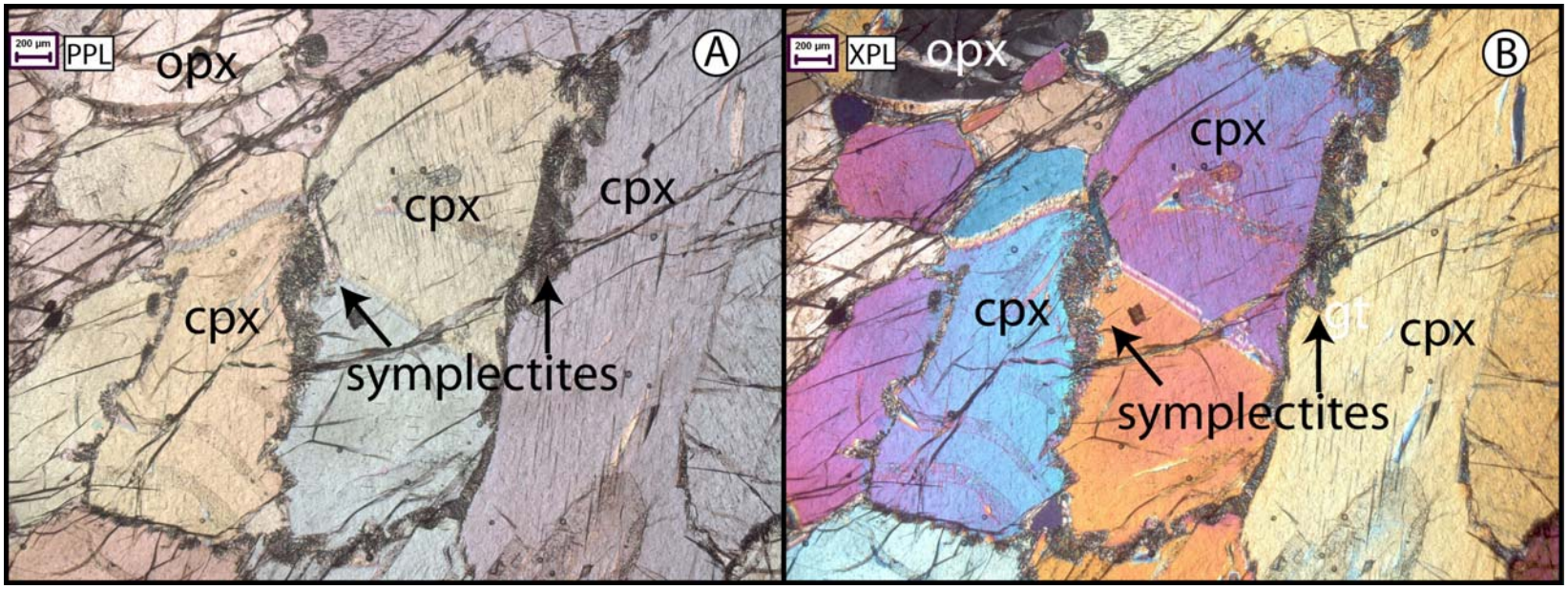

Figure 4.4. Eclogite sample 17.5C. Note cpx symplectites and cpx exsolution. A) PPL, B) XPL

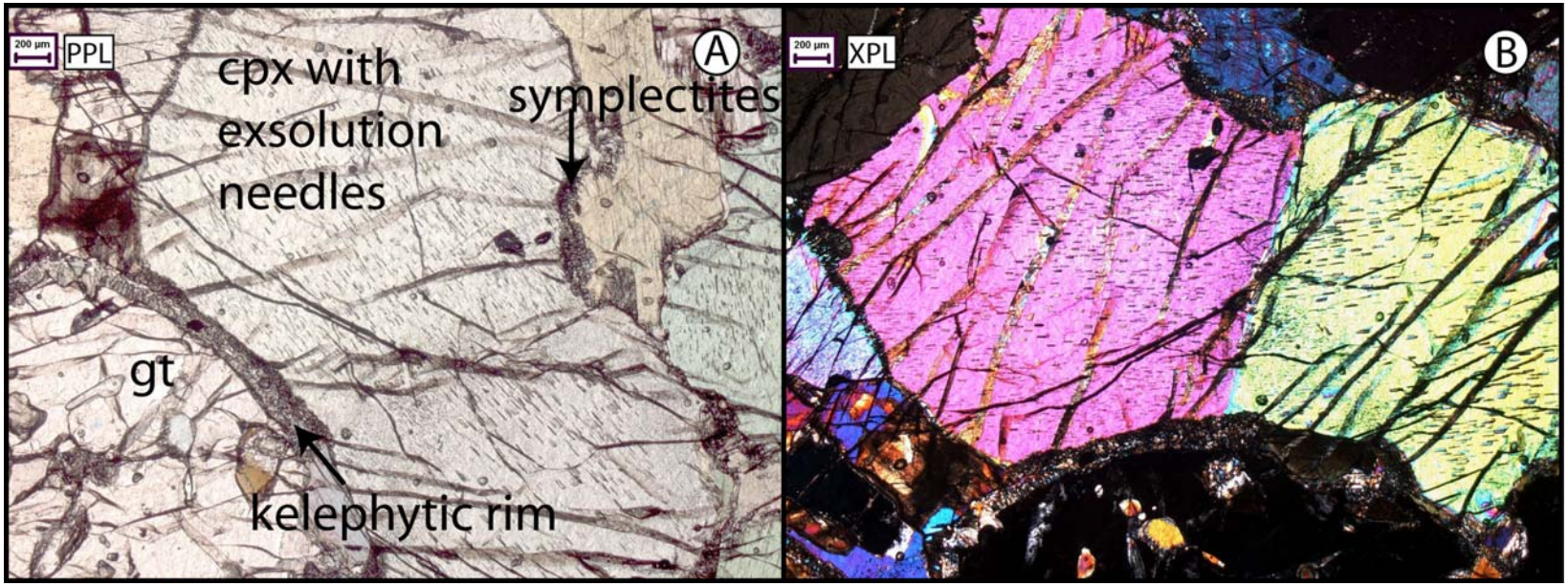

Figure 4.5. Eclogite sample 17.5A. Note cpx with exsolution needles, also visible are kelephytic rim around garnet and cpx symplectites. A) PPL, B) XPL

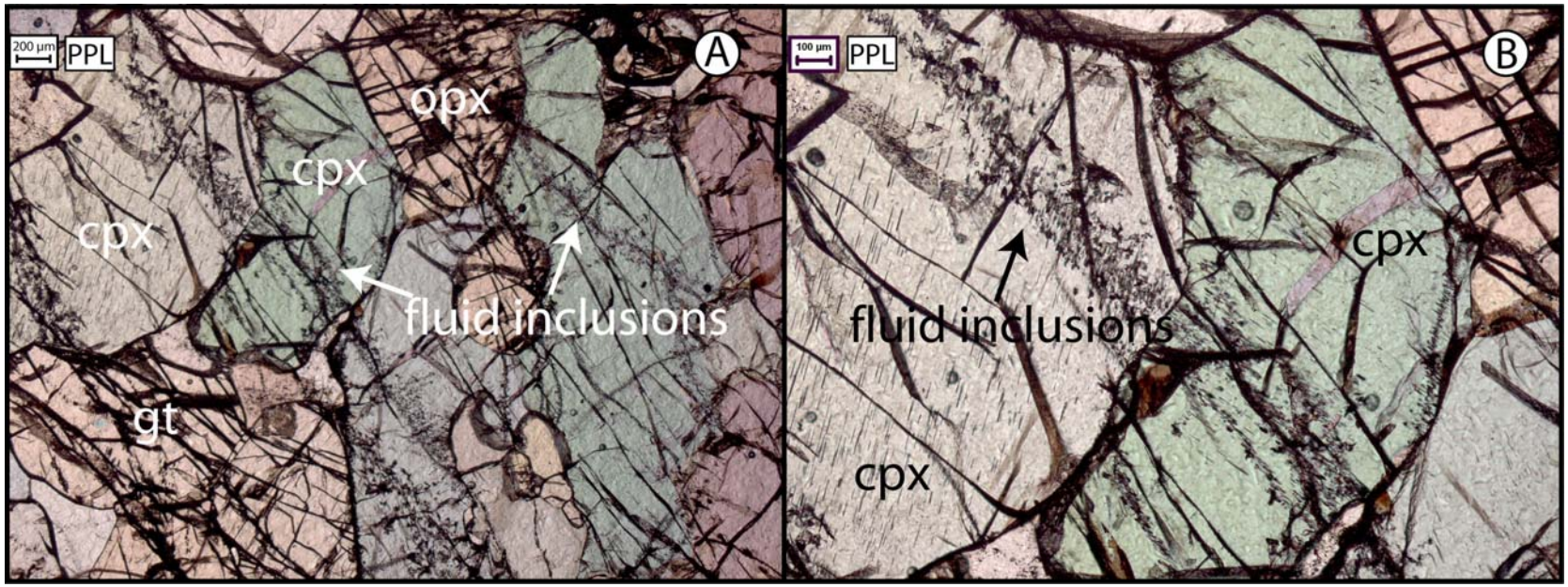

Figure 4.6. A,B) Eclogite sample 10.5A. Fluid inclusion in pyroxenes. B) is enlargement of inclusions in A)

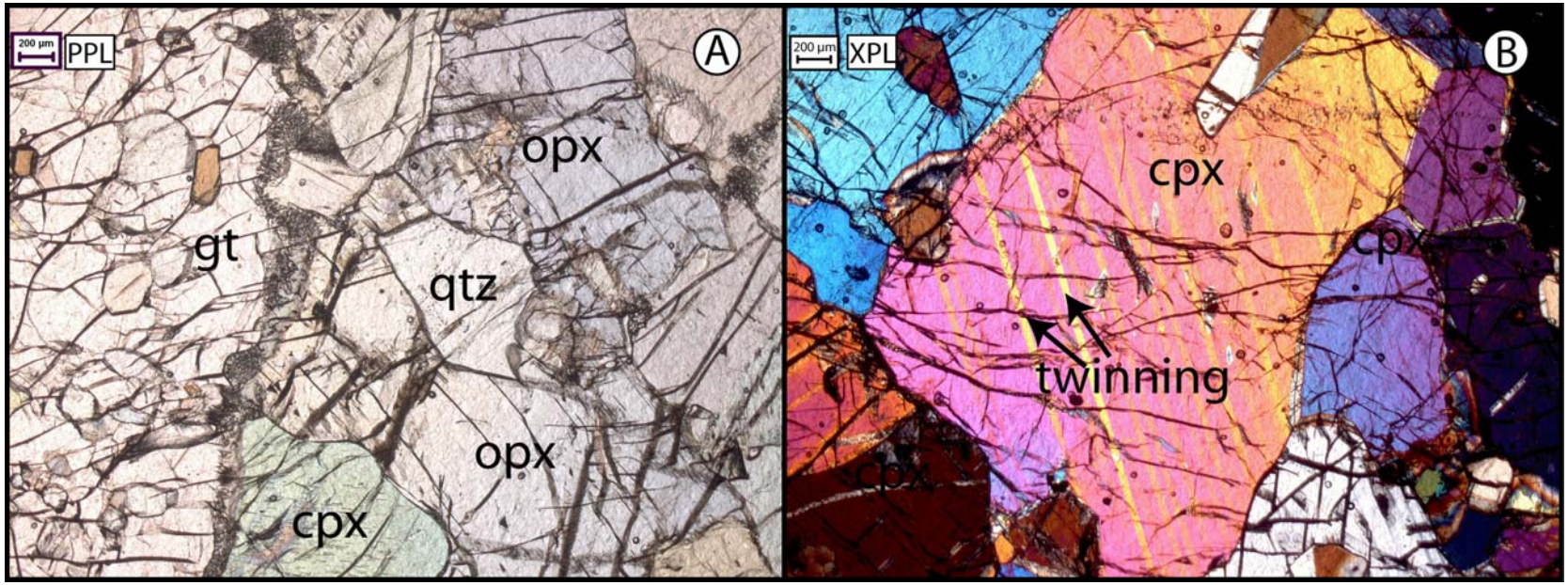

Figure 4.7. A) Eclogite sample 17.5C, qtz in eclogite opx. B) Eclogite sample 10.5A. Note twinning in cpx

4.2 Granulites

sample	grt	cpx	qtz	pl	amph	bio
11-3B	25%	25%	5%	25%	15%	5%
11-5	35%	10%	10%	25%	15%	5%
12-6C	15%	45%	5%	10%	20%	5%
16-3A	40%	20%	10%	20%	10%	-
19-3A	35%	25%	5%	10%	20%	<5%

Table 4.2. Mineral composition of the granulite samples

Granulite mineral composition
The mineralogy of granulites is different from eclogites. The granulites contain plagioclase, which is absent in eclogites, and amphibole, which is present in the eclogites in very minor amounts. The amount of quartz is also a somewhat higher, but as quartz and plagioclase can be hard to distinguish in thin sections, the proportions can show some deviation from the true value. The granulite samples contain no opx. A typical granulite example is given in figure 4.8, where all phases grt, cpx, qtz, pl, amph and bio are present. The chaotic character of the granulites is eminent, when compared to the eclogites. Grain boundaries are much more wiggly and crystal shapes are far from perfect.

Cpx symplectites
The cpx symplectites in granulite samples are much more developed than in eclogites. Generally the grain size of the symplectites is much higher, and a greater part of the original cpx grain has been converted to symplectites. Figure 4.9 shows a cpx crystal that has not yet been completely converted to symplectites (50% symplectite), while figure 4.10 shows completely recrystallized grains (100% symplectite). So not all cpx has undergone the retrograde reaction to the same degree.

'Fresh' garnet
In the eclogites we have seen that some garnets show a kelephytic rim, indicating retrograde reactions in the sample. As the cpx in granulites shows extensive recrystallization to symplectites, it might be expected that the garnet would show very thick kelephytic rims, possibly extending towards the garnet cores. Instead, garnets in the granulites shows no sign of a kelephytic rim. The grain size is much smaller compared to eclogites: mm's instead of cm's, and are relatively free of inclusions. Figure 4.11 shows examples of such garnet grains.

Coesite
Structures that resemble radial cracks and PCQ sub-grains are sporadically found in the eclogite samples, as well as in some granulites. The most promising example is shown in figure 4.12. This possible coesite relict is an inclusion in cpx, and fractures radiate away from the inclusion. This particular example is investigated by EMP and will be further discussed in the next chapter.

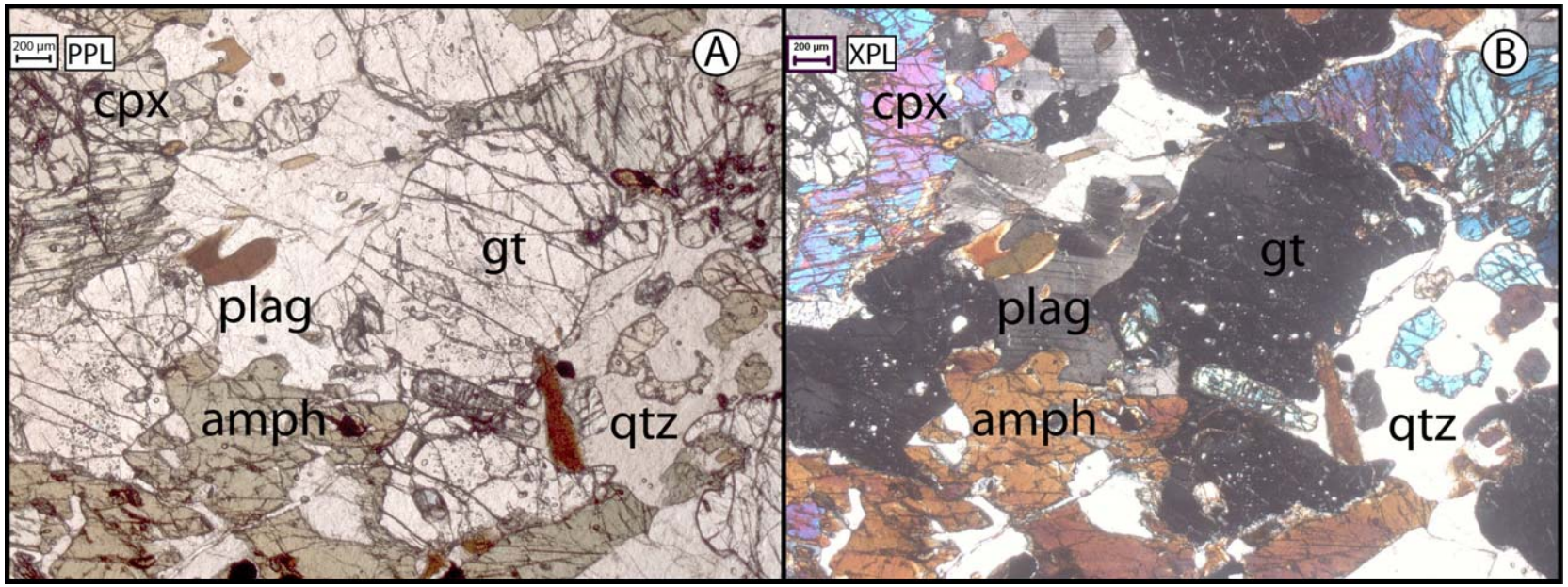

Figure 4.8. Granulite sample 11.3B. Typical mineralogy of granulite samples, with grt, pl, amph, qtz and cpx. A) PPL, B) XPL

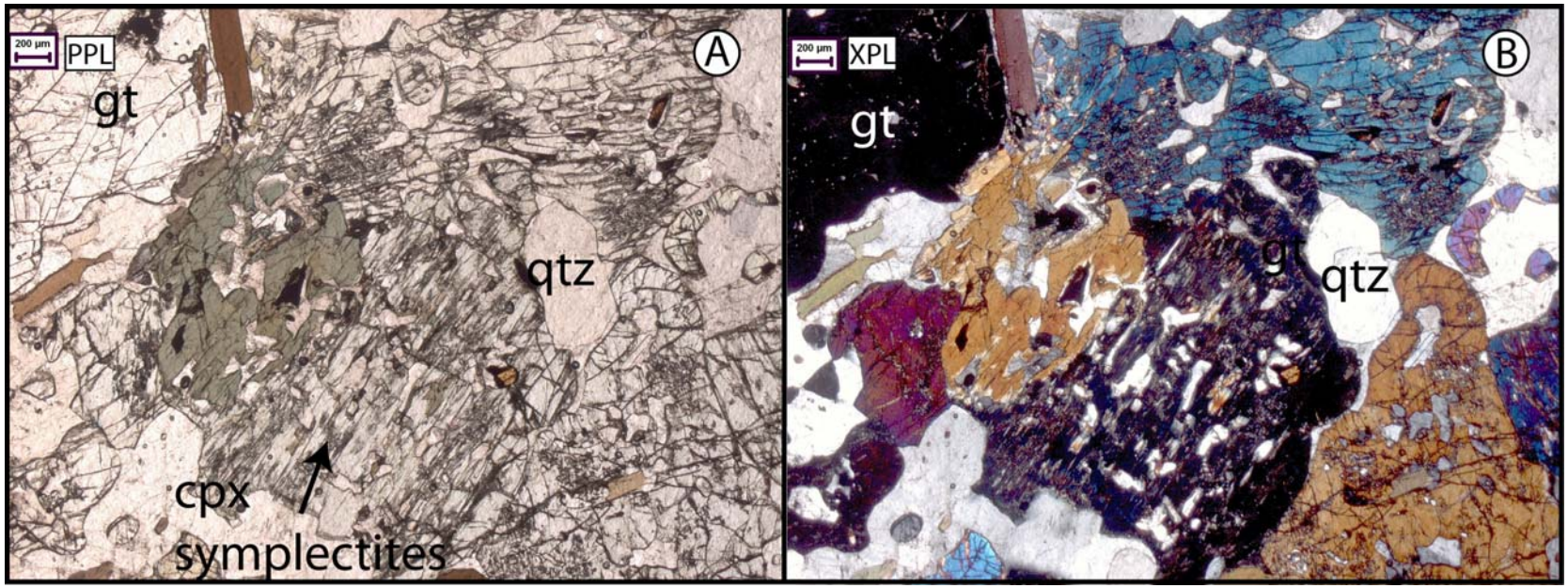

Figure 4.9. Granulite sample 11.3B. Note 50% cpx symplectites. A) PPL, B) XPL

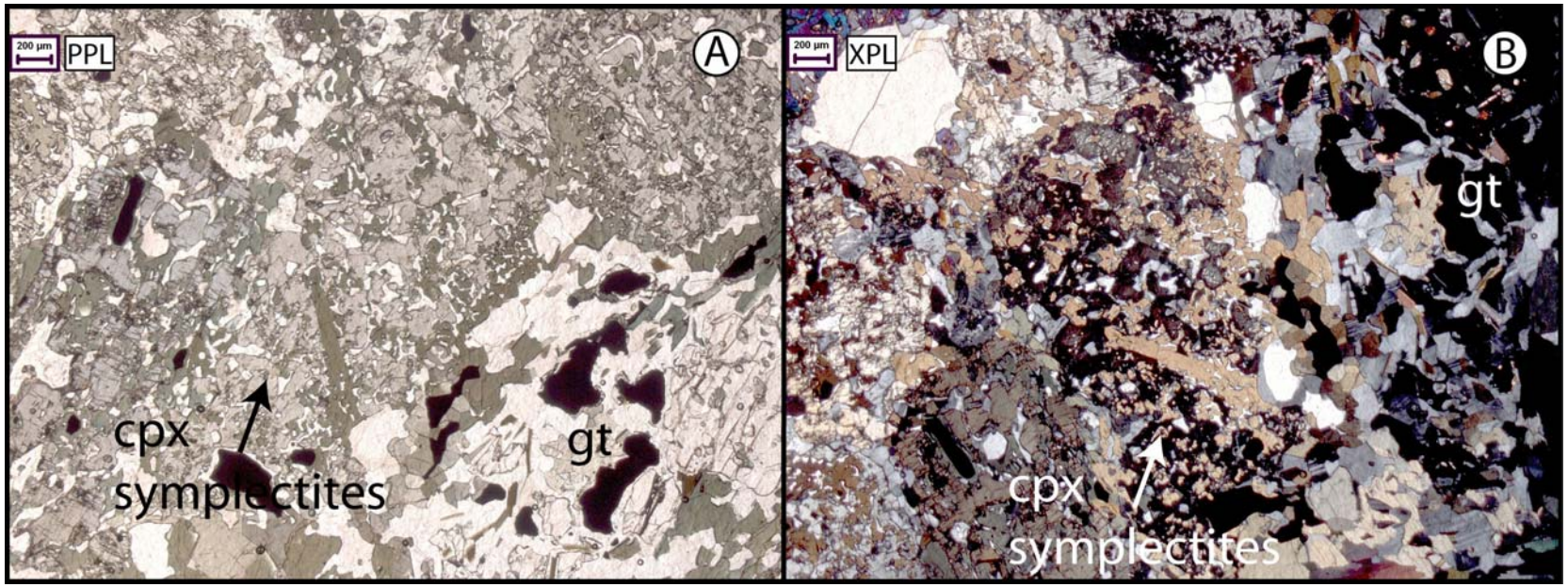

Figure 4.10. Granulite sample 12-6C. Note 100% cpx symplectites. A) PPL, B) XPL

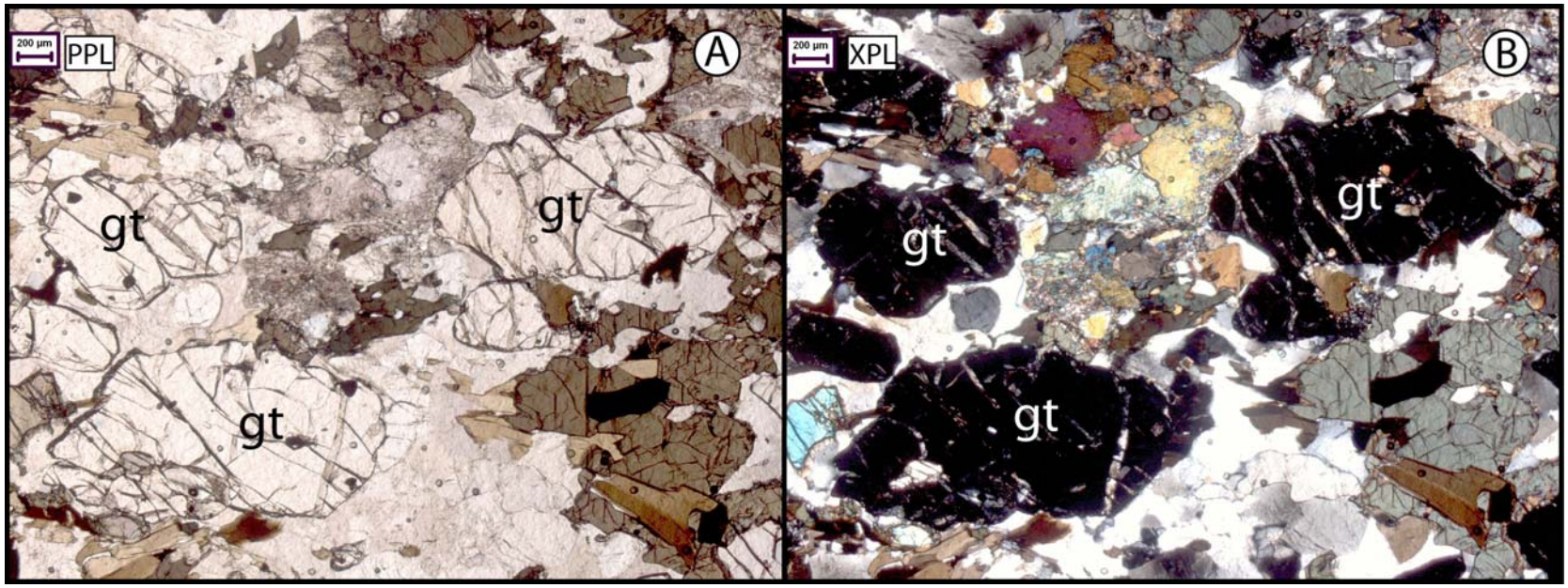

Figure 4.11. Granulite sample 11.5. Note fresh garnet. A) PPL, B) XPL

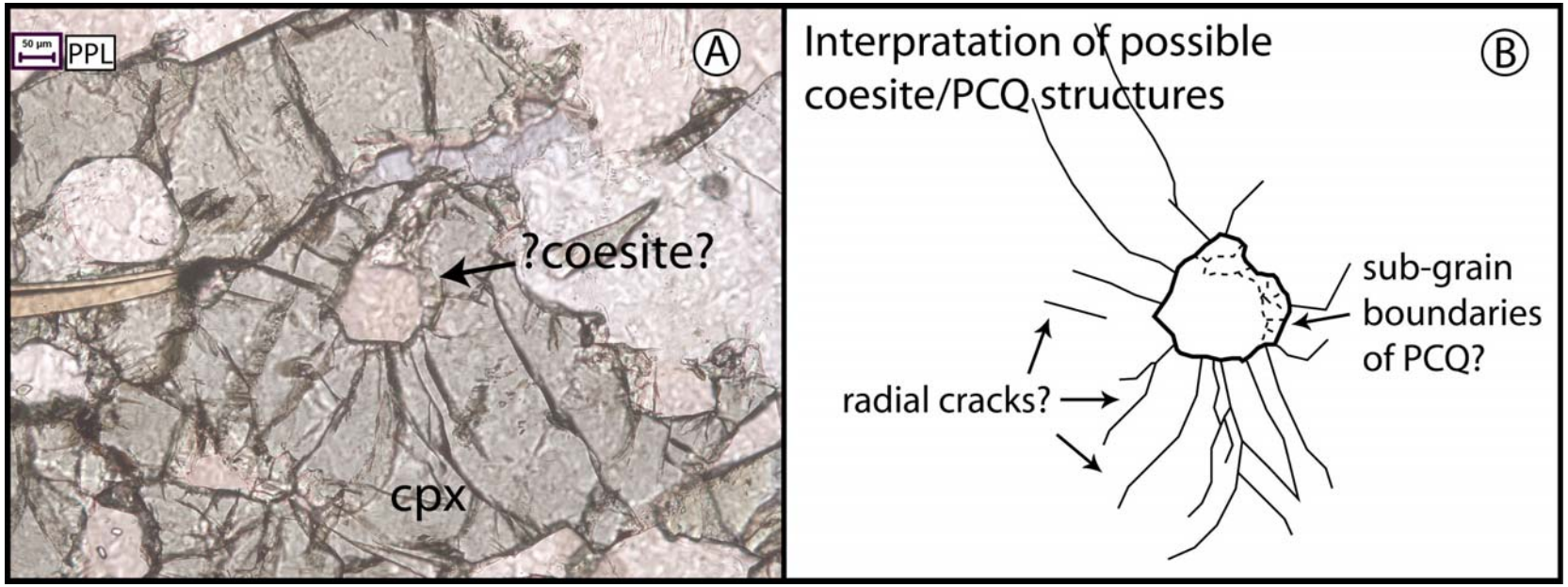

Figure 4.12. Granulite sample 11.5, A) possible coesite as inclusion in cpx, B) interpretation of inferred radial cracks and PCQ sub-grains

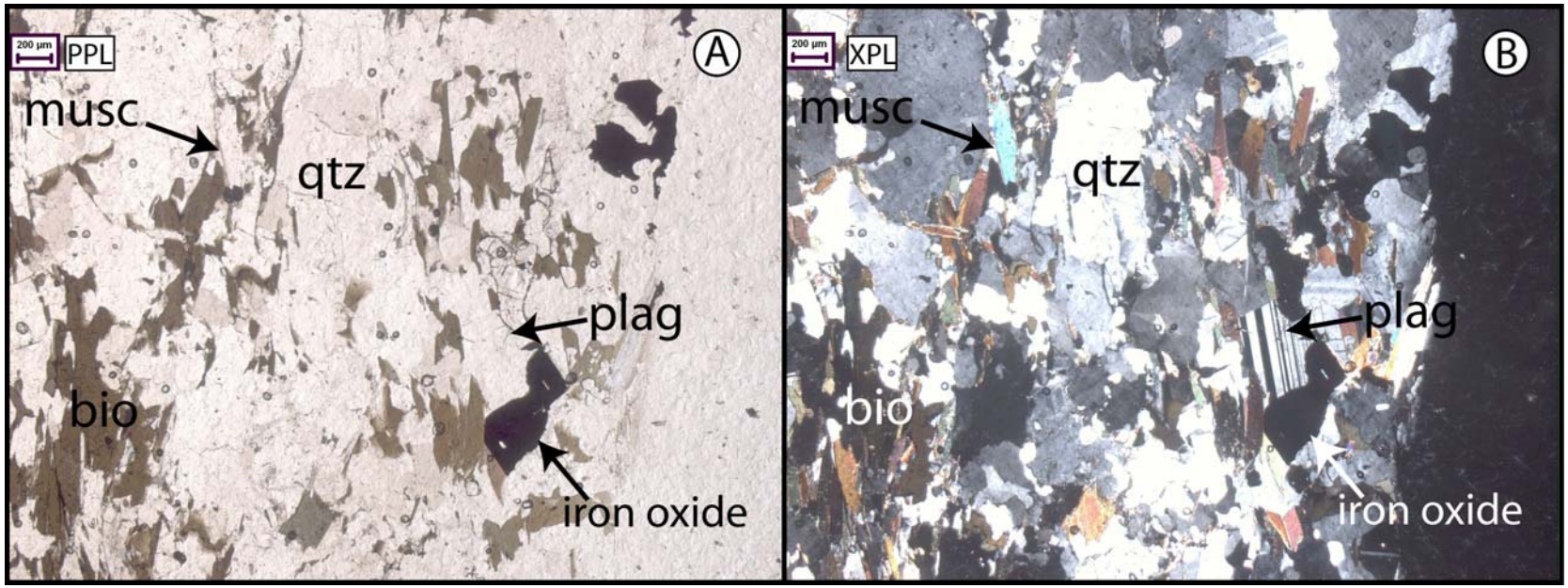

Figure 4.13. Basement sample 20-7. Typical mineralogy of granodioritic basement. A) PPL, B) XPL

4.3 Basement

sample	qtz	grt	kfs	pl	amph	bio	musc
12-7	35%		30%	15%	<5%	5%	<5%
16-1B	35%	5%	25%	15%	5%	15%	
17-1B	40%		20%	10%		10%	5%
19-4	25%	5%	25%	20%	10%	15%	
20-1A	30%		25%	15%		15%	15%

Table 4.3. Mineral composition of the basement samples

Basement mineral composition
All basement samples are taken in the southern granodioritic basement and thus are not representative for the northern tonalitic basement gneisses (figure 3.7). In all samples qtz, kfs, pl and bio are present. An example of the typical granodioritic basement mineral assemblage is given in figure 4.13.

Sillimanite is present in some samples, in significant quantities. Figure 4.14 shows well developed sillimanite grains in sample 12-7. Grain sizes for all minerals are much smaller than for the eclogite and granulite samples. Garnet is present in some samples (figure 4.16) and shows signs of instability. Recrystallization to other minerals has taken place at the garnet rim, but also to within the garnet core and has broken up the grain in separate parts.

Foliation defining minerals
Foliation is a dominant characteristic of the basement gneisses. Figure 4.15 shows sample 17-1B where foliation is particularly well developed. Minerals that define this foliation can be seen to be bio, sill, qtz and pl. in samples where muscovite is present, it has a random orientation. So muscovite does not define the foliation.

Overprinting relations
When garnet is present in the basement, it is unstable (see figure 4.16) and replaced by other minerals.

Muscovite is present in some basement samples. Where it is present it is observed to be a replacement mineral for other minerals. The following reactions are observed:

1. Muscovite replacing sillimanite. Figure 4.17 shows this replacement reaction. The fibrous minerals, best seen in PPL, are sillimanite. The translucent or slightly pinkish mineral in PPL with bright blue birefringence colours is muscovite. The sillimanite is present on both sides of the grain of muscovite, and the structure of sillimanite clearly shows that both sides used to be part of one structure.
2. Muscovite replacing biotite. Figure 4.18 shows this replacement reaction. Again muscovite is the mineral that appears slightly pinkish in PPL and clear blue in XPL. Biotite is a dark shade of brown in PPL. The XPL images show two parts of biotite going extinct at exactly the same orientation, and thus have an identical crystal orientation. The shape of the two parts also indicates that this once one single grain of biotite. Muscovite has grown right through, and thus replacing, biotite.
3. Muscovite replacing kfs (no figure available to illustrate this)

The replacement reactions are determined by assuming that if two parts of the same mineral that belong to the same grain are separated by second mineral, the second mineral has replaced the first mineral. Some caution here is needed, because the situation is observed in 2 dimensions. If mineral B grows partly around mineral A, it is possible that a cross-section shows mineral A in the centre, with mineral B on both sides. If this is interpreted as mineral A replacing mineral B, this interpretation is wrong because mineral B grew after mineral A. For

the present replacement reactions of musc replacing sill and bio, this is no problem. Biotite is a platy mineral that will grow in a straight tabular form, and will not curve. The above possibility of biotite growing around muscovite will therefore not occur. Sillimanite is very fibrous and by the orientation of its fibres it is easy to determine if they are cut-off by muscovite.

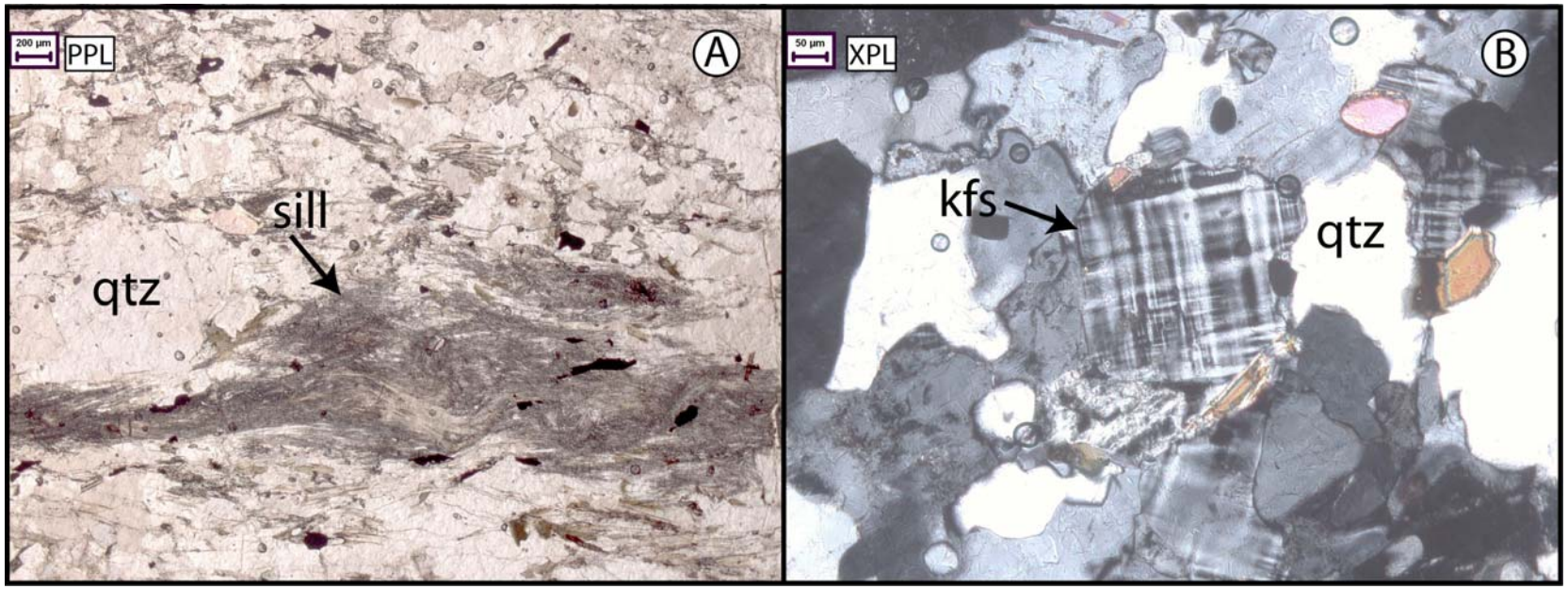

Figure 4.14. Basement sample 12-7, A) Note fibrous sillimanite, B) tartan twinning of k-feldspar notable in XPL

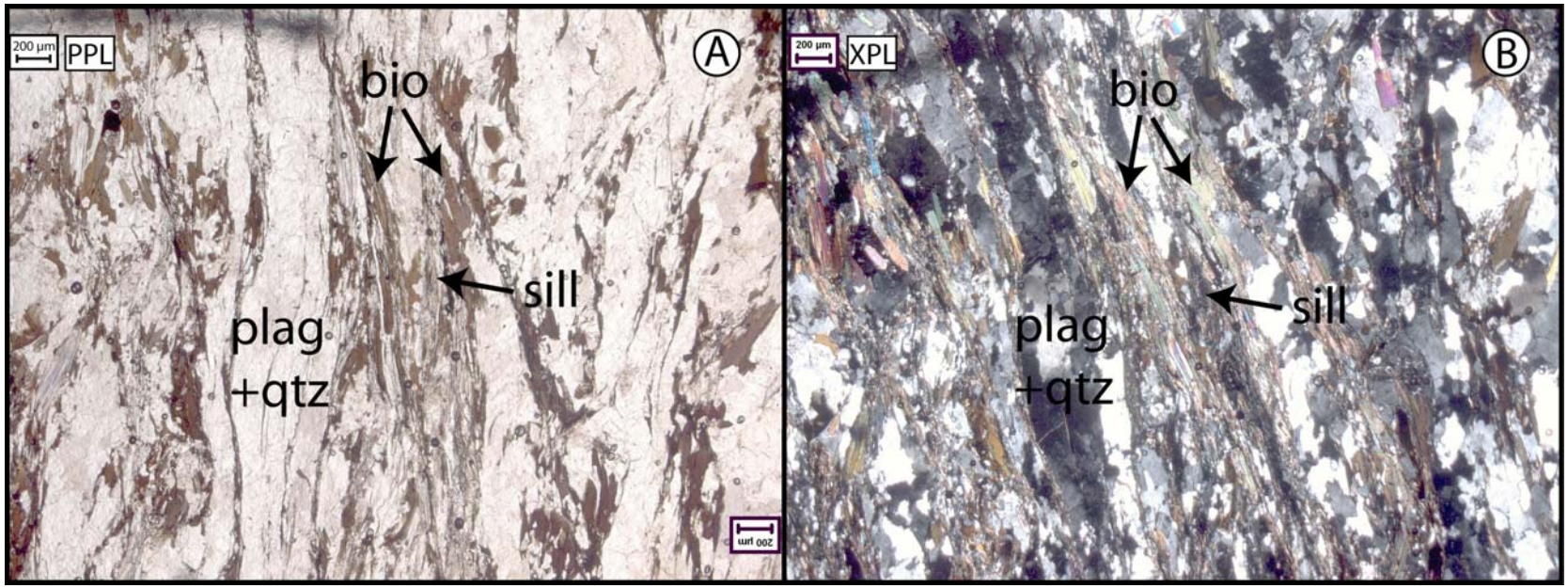

Figure 4.15. Basement sample 17.1B. Foliation defined by bio, sill, pl and qtz. A) PPL, B) XPL

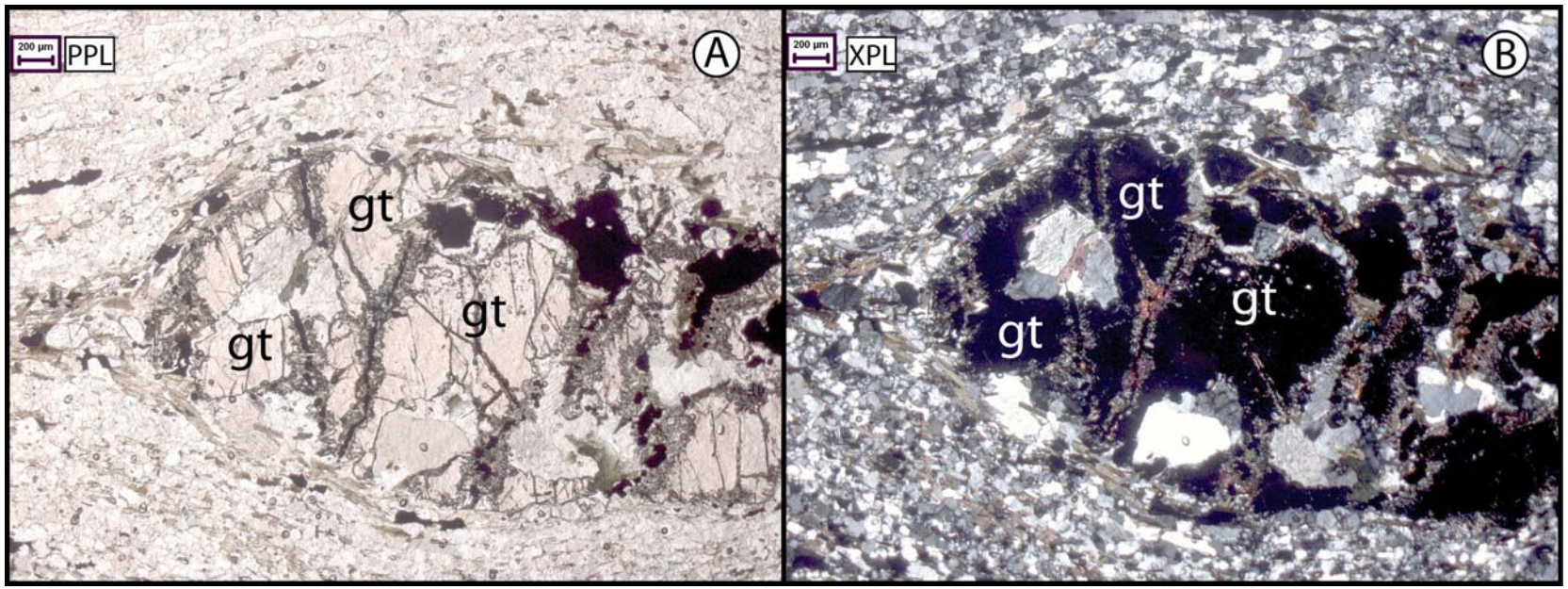

Figure 4.16. Basement sample 19-4. Garnet is unstable and replaced by other fine grained minerals. A) PPL, B) XPL

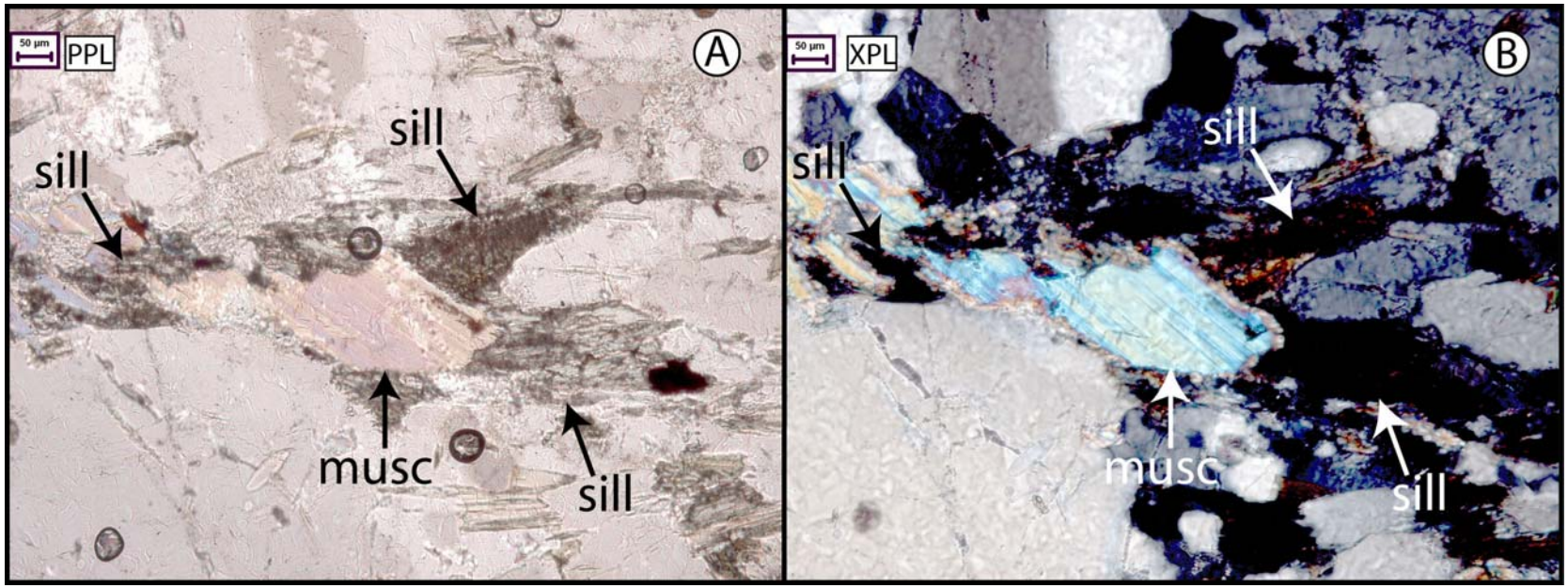

Figure 4.17. Basement sample 12-7. Sillimanite is replaced by muscovite. A) PPL, B) XPL

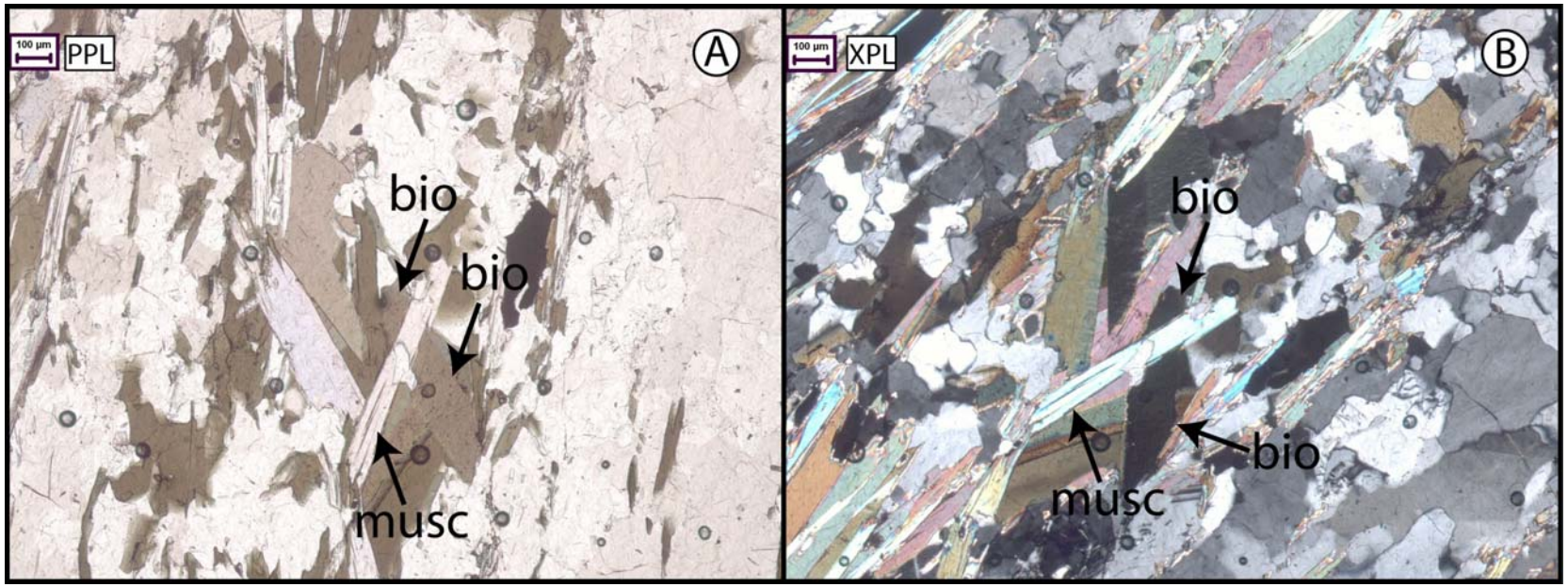

Figure 4.18. Basement sample 20-7. Muscovite overgrows a grain of biotite. Both parts indicated are two parts of originally the same biotite grain, because they have the same crystal orientation and a matching shape. A) PPL, B) XPL

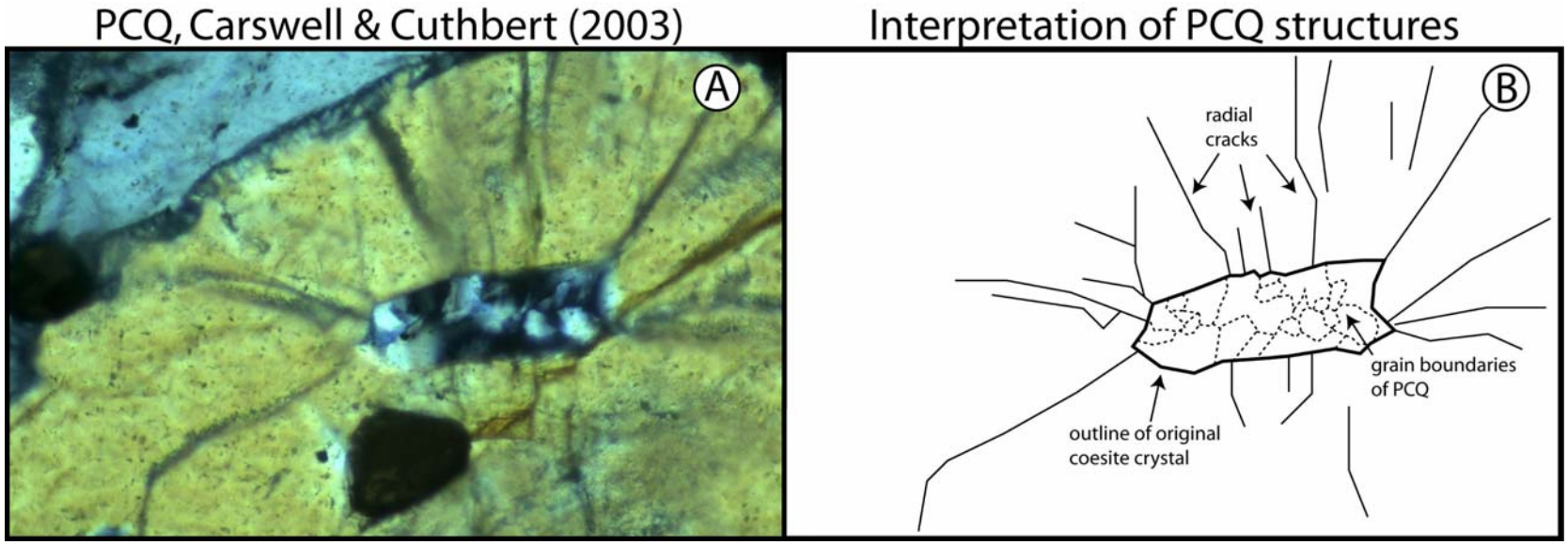

Figure 4.19. A) image of PCQ inclusion in omphacite, found in a ky-phen eclogite, field of view ±2mm (Carswell and Cuthbert, 2003), B) interpretation of the PCQ structures following the explanation by (Carswell and Cuthbert, 2003)

4.4 Implications for PT conditions

Indications of UHP
Because UHPM occurs in the coesite stability field, the occurrence of coesite means a rock has experienced UHP metamorphic conditions. Figure 4.19a shows a coesite inclusion in an omphacite grain, found in a ky-phen eclogite (Carswell and Cuthbert, 2003). An interpretation of this image is made in figure 4.19b. Coesite is the high pressure polymorph of quartz. Because coesite is a denser mineral than quartz, a coesite crystal will increase in volume when it transforms (back to) quartz at lower pressure conditions. If the coesite crystal is an inclusion mineral in another mineral, the host mineral will 'break' because of the increased volume of the inclusion mineral, resulting in radial cracks (Liou et al., 1998). The internal structure of a coesite crystal is different from normal quartz, such that after coesite transforms to normal quartz, the resultant quartz grain will consist of many different sub-grains, hence the name polycrystalline quartz.

Comparing the PCQ inclusion of figure 4.19 with the possible PCQ from granulite sample 17.5C (figure 4.12), the radial cracks look similar in appearance but the internal structure does not show sub-grains. Only at the far right side of the inclusion some features are seen that are possibly PCQ sub-grains. This inclusion is one of the best examples of a possible coesite relict in the analysed samples, but even here there is no certainty whether we are indeed looking at a former coesite inclusion. This possible coesite/PCQ inclusion is analysed by EMP, see section 6.3.

Another feature that is often taken as typical UHP reactions is the precipitation of quartz in omphacitic clinopyroxene. Such an example, from Chopin (2003), is shown in figure 4.20. Oriented quartz needles are present within cpx. The density, distribution and orientation show a good similarity with the exsolution needles that are observed in cpx from outcrop 17.5, as shown in figure 4.5. These exsolution features are analysed by EMP to reveal the minerals that form these needles (section 5.3.1).

The fluid inclusions that are observed in the eclogite samples (see figure 4.6) can be caused by decompression. Fluid inclusions that have been incorporated in a mineral at depth can 'explode' during decompression. This can result in many smaller fluid inclusions that cross grain boundaries (Touret and Frezzotti, 2003). This means that the eclogites have come from higher pressure conditions, but that does not have to indicate an UHP origin.

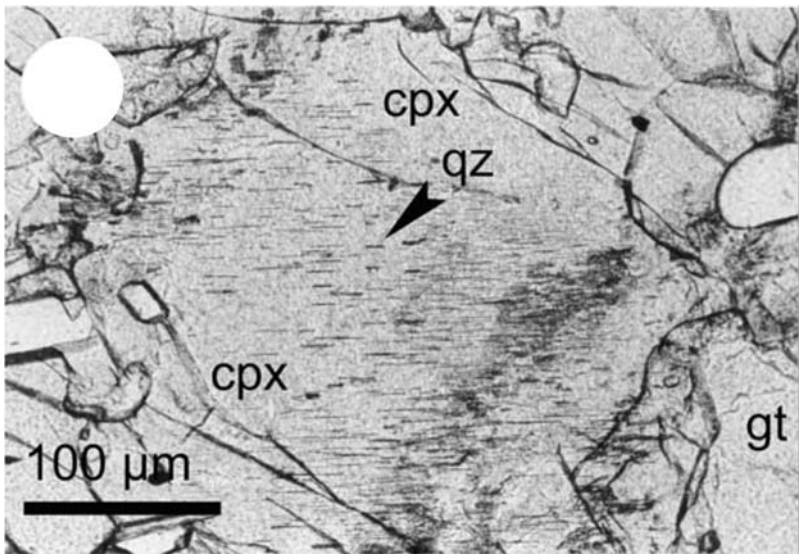

Figure 4.20. Oriented quartz needles precipitated within omphacitic clinopyroxene (Chopin, 2003).

PT-conditions

Defining the metamorphic facies field of samples from mafic lenses is performed by using diagrams from Bucher and Frey (2002), see figure 4.21. ACF triangles show the change in stable minerals assemblages with changing PT conditions. The exact PT conditions at which certain mineral assemblages become unstable is not shown in this PT-grid, but as these samples will be used for PT analysis by geothermobarometry, the exact PT-field of mineral combinations is not important right now.

Eclogites mainly consist of grt, omph and cpx. Amph is present as well, but its shape reveals that was not part of the original equilibrium assemblage. The assemblage of grt + omph + opx is only stable in ACF diagram 19 (see figure 4.21). If the omph would be 'normal' cpx crystals, than it would still be expected that some pl would be present in the eclogites. This is not the case, therefore the eclogite mineral assemblage is indeed characteristic for the eclogite metamorphic facies field. Granulites have the assemblage grt + cpx + qtz + pl + amph ± bio. This is the assemblage that is stable in ACF diagram 7 of figure 4.21. This is approximately at the granulite/amphibolite transition, around 700ºC and 8kbars. The higher granulite diagram 9 shows stability of grt + cpx + pl, but without hbl. Diagrams in the pyroxene granulite fields also have pl and cpx stable together, but at these low pressures grt becomes unstable.

The grain size of symplectites is correlated with the temperature of their formation (Joanny et al., 1991). Because of the smaller grain size of symplectites in eclogites compared to the granulites (compare figure 4.4 and figure 4.10) the retrograde reactions in eclogites might have taken place at lower temperatures than in the formation of the granulites. Minerals in the eclogite samples show better developed crystal shapes than minerals in granulite samples. The symplectites show that original cpx crystals are completely transformed and this might indicate recrystallization from an instable original higher pressure variance of cpx. The garnet, on the other hand, is smaller than in eclogites shows no sign of recrystallization at all.

Basement samples are no mafic rocks and because of their composition cannot be represented by the diagram of figure 4.21. The mineralogy of the basement samples is best represented by diagrams for metapelites. Figure 4.22 shows the reactions that involve mica's. In the thin sections the reactions sill → musc (figure 4.17), kfs → musc and bio → musc (figure 4.18) are observed. Reaction 26 in figure 4.22 shows the position in PT-space of the reaction line kfs + als → musc. Als (aluminosilicate) at these PT conditions is sill. The basement samples have thus made the transition from the right side of reaction 26 to the left side of reaction 26, within the stability field of sill. Garnet is shown to be unstable in basement samples. This is in accordance with this PT range, as the sillimanite field is below the stability field of grt (Poli and Fumagalli, 2003). The reaction biotite → musc is not shown in figure 4.22 as bio is stable in this entire PT range. Possibly the biotite that has been observed to be unstable are higher pressure equivalents of bio that have become unstable at lower pressures, and where involved in the formation of musc. This shall not be investigated any further because it will put no further constraints on the PT conditions of the basement.

The PT conditions based on optical microscopy are summarized figure 4.23. The eclogite samples are somewhere in the eclogite metamorphic facies field, an upper pressure limit cannot be given. The granulite samples have PT conditions of approximately 700ºC and 8 kbars. For the basement samples it is known that they cross the als + kfs → musc line, from right to left, within the stability field of sill.

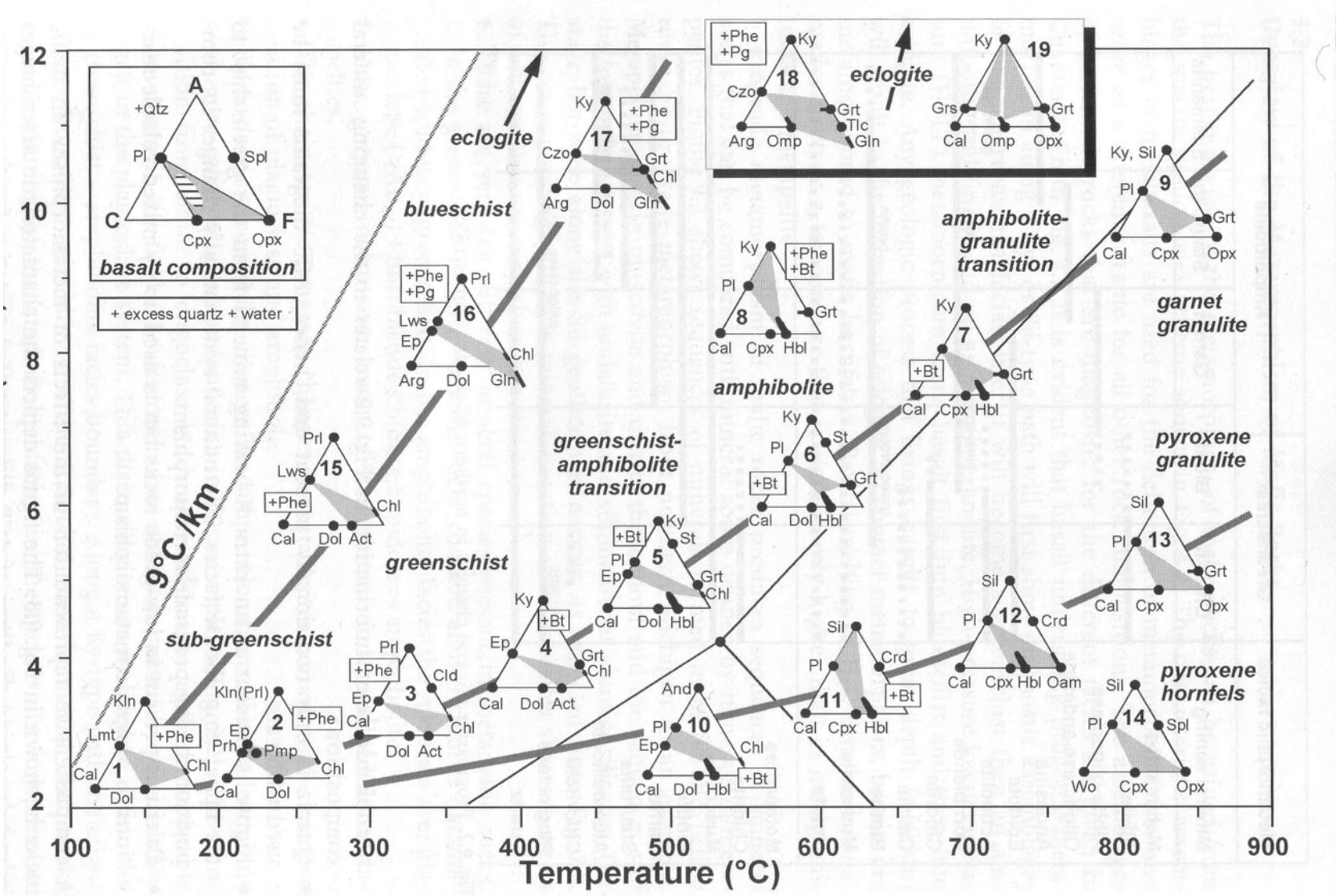

Figure 4.21. Stability fields of metamorphic mineral assemblages of rocks with a mafic composition (Bucher and Frey, 2002).

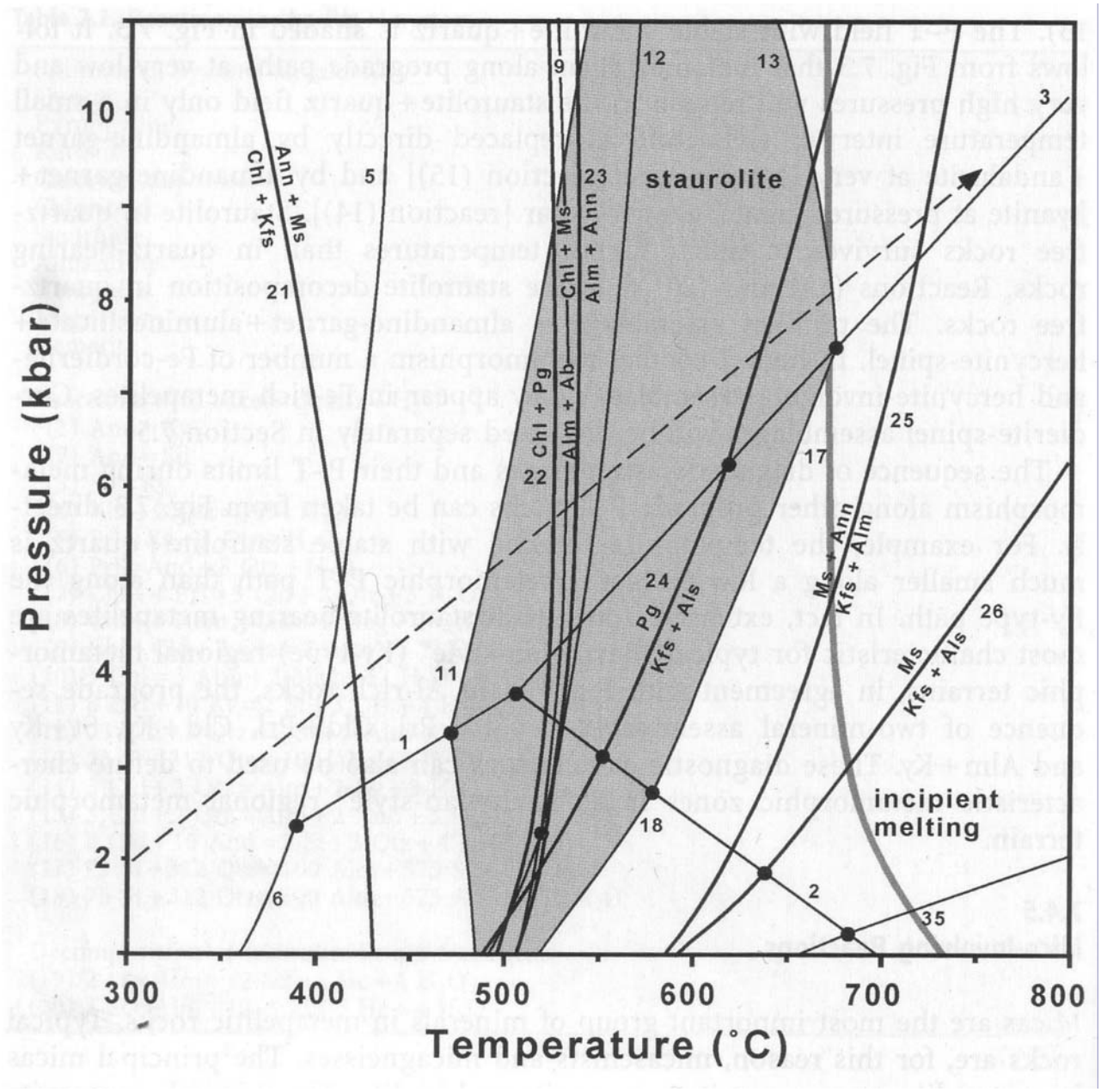

Figure 4.22. Mica reactions in metapelites (Bucher and Frey, 2002).

Stress, strain and foliations

The eclogites show some signs of strain. Twinning is observed in some cpx grains in sample 10-5A (figure 4.7) and quartz in all samples show some signs of undulose extinction. However, the evidence for strain in the eclogites is minimal. The same holds for granulite samples where only some undulose extinction of quartz has been observed. Both eclogites and granulites show no sign of any foliation.

The basement samples do show evidence of very high strain as a penetrative foliation is well developed in most samples. The minerals that define the foliation are bio, sill, qtz and pl, but not musc. This means that the foliation has formed before the appearance of musc, and therefore before the basement crossed the sill + kfs → musc line (see figure 4.23). Because (unstable) garnet is present in basement samples the PT conditions of the basement have experienced higher PT conditions of at least in the garnet stability field.

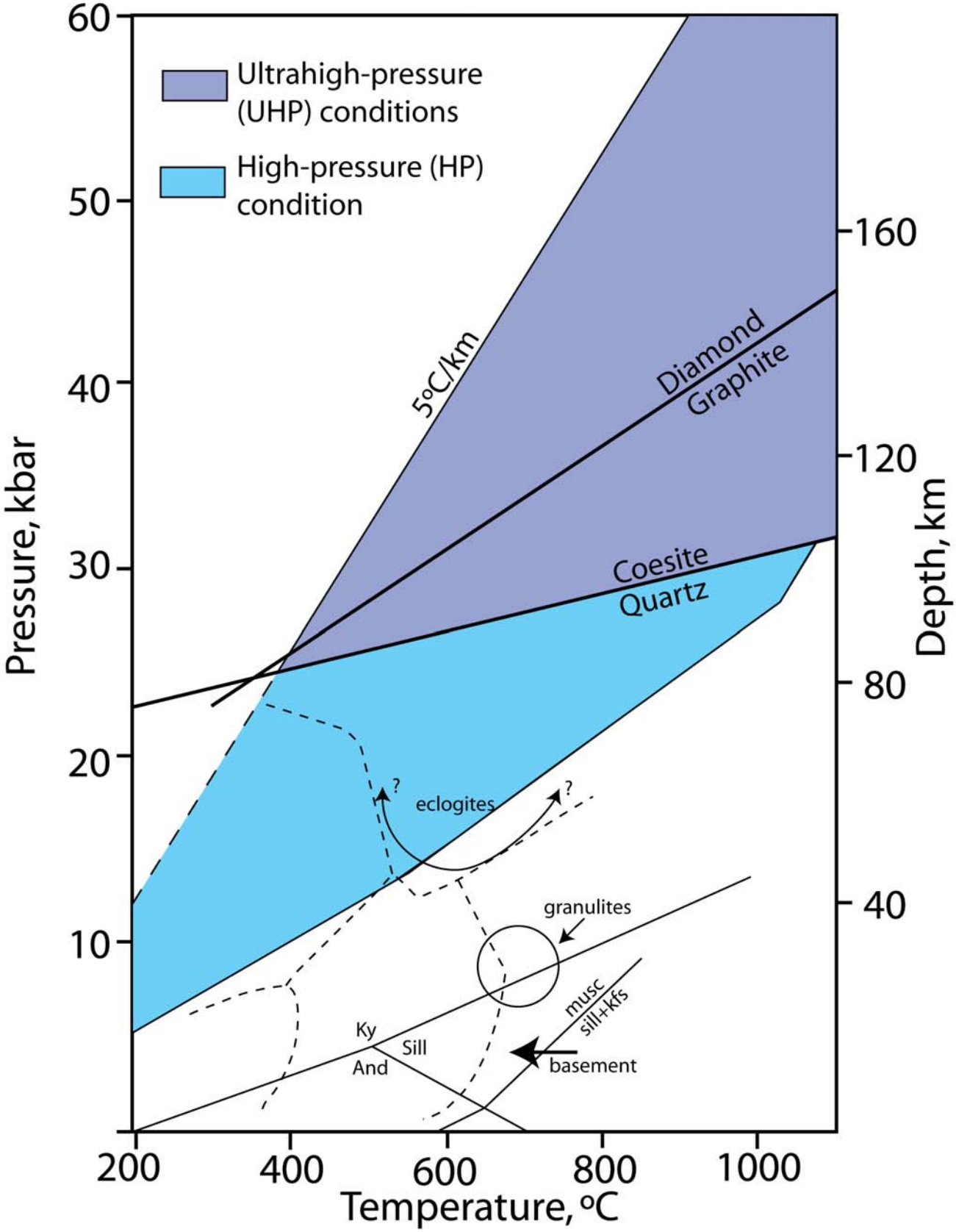

Figure 4.23. PT diagram indicating the positions in PT space for eclogite, granulite and basement samples, modified after Ernst and Liou (2008). Facies names as in figure 2.2.

5 PT analysis of eclogite facies rocks

5.1 Methods

Seven eclogite and four granulite samples have been analysed at Utrecht University with an Electron Microprobe (EMP), a JEOL JXA-8600 Superprobe, with operating conditions of 15kV accelerating voltage and 20 nA beam current. The EMP provides data in compound weight percentages for selected elements at one point in a sample. What elements should be measured depends on the kind of mineral that is being investigated. For the minerals in eclogites and granulites this means that some analyses are done with, and some without measuring the element K. Software is available that calculates PT conditions from the compound weight percentages. It is, however, important what measurements are chosen for PT calculations. The composition of a mineral can show variation from core to rim, and calculations based on different measurements may give a very different PT result as well. For this reason linescans have been made for all analysed minerals. With a linescan the EMP makes a number of measurements between two preset points, e.g. from rim to core to rim. Because the mineral composition is most conveniently expressed as percentages of the mineral end-members (e.g. garnet can be expressed in pyrope, grossular, almandine and spessartine) all EMP data has been converted to the appropriate end-members. There is a software programme that can convert large quantities of EMP data to mineral end-member compositions. This programme, Calcmin (Brandelik, in press) has the disadvantage that amphibole end-members cannot be calculated. Also at the time that the calculations in this study have been performed it was unknown what procedure Calcmin follows in making the calculations, which means that it is not always clear what the end-members represent. Currently an accompanying paper of this program is in press in which additional information is given, probably making Calcmin more useful. But at the time that EMP data had to be converted to end-member data this paper was not yet available, therefore the excel-sheets ‘End-member calculation, with K’ and ‘End-member calculation, without K’ have been constructed that can handle large quantities of EMP data and convert it to mineral end-members. These excel sheets plot the original EMP compound weight percentage data in graphs, give the element per formula unit, the end-members, and plot the end-members in graphs. In this excel sheet the compound weight percentages for each element should be loaded, after which the kind of mineral has to be filled in for each measurement (grt, cpx, opx, pl or amph). The end-members for each measurement will then be calculated automatically. This excel-sheet is given in digital format accompanying this thesis, the manual for this excel-sheet and the formula’s that are behind the calculations are given in appendix I.

All linescans of which a measurement is used for PT calculations are given in appendix V. The positions of the linescans is plotted in images taken with the EMP, and the position of the EMP image is indicated in scans of the thin-sections. This information makes it possible to relocate every measurement within a thin section, and easily determine the relation of a measurement to the position in the mineral where it is taken, and the position of the mineral with respect to other minerals. All this can be found in appendix III and IV. Although this procedure is rather elaborate, it is chosen so that maximum transparency is available for the data on which the calculations are based. In order not to overwhelm the reader with data, in this chapter only representative data, linescans and images are given. For a complete list of all data, see appendix V.

Error margins for EMP analyses are 1% for the major elements (with compound wt% >5%) and about 5-10% for the other elements. This can cause some errors in the geothermobarometric calculations, especially if the cumulative error of more elements is taken into account. To reduce these errors only ‘good’ EMP measurements have been used, with total wt% between 98.5 and 101.5.

5.1.1 Geothermo- and geobarometers

There are three reaction that are important for geothermobarometry (Bucher and Frey, 2002):

1. Net-transfer reactions. One (or more) mineral(s) reacts to form one (or more) other mineral(s). At least one of the involved minerals should be part of a solid solution. This kind of reaction is mainly dependent on pressure, and thus can be used for geobarometry.
2. Solvus thermometry. Some solid solutions are temperature dependent, a shift in temperature will cause a shift in the end-member concentration. These reactions can be used for geothermometers.
3. Exchange reactions. Here similar elements can be exchanged between different minerals. Elements that are about the same size and have the same charge are involved in these reactions. This reaction is mainly dependent on temperature, and can be used for geothermometers.

All of the above reaction are to some extend dependent on both pressure and temperature (Ravna and Paquin, 2003). This means that the line in PT space along which the reaction will take place will be steep for barometer, and shallow for thermometers. Both a barometer and a thermometer have always to be used, and the intersection of these two lines then given a single point in PT space.

For PT calculations of the eclogites the excel-sheet ptexl3 is used (Köhler, 2007). With this excel-sheet a number of different geothermo- and barometers can be selected with which to perform the PT calculations. This study is not meant to be an evaluation of the available geothermo-and barometers, therefore different calibrations that are available in ptexl3 will be used on the same analyses. An argument against this method might be that that ptexl3 uses many calibrations that are from article the article by Brey and Kohler (1990), which may give a limited view on all available calibrations. However, the calibrations used by ptexl3 are widely accepted (e.g. according to the overview of excepted geothermo- and barometers and calibrations by Ravna and Terry (2004)).

The geothermo- and barometers that are discussed below all involve the minerals grt and/or cpx and/or opx. They are therefore excellent for PT calculations of eclogites, because these minerals make up the bulk of the eclogite samples.

Net-transfer reactions

Garnet-clinopyroxene

The most popular geothermometers for eclogites are based on the exchange of Fe^{2+}-Mg between grt and cpx. They are all based on the reaction:

$$\tfrac{1}{3} Mg_3Al_2Si_3O_{12} + CaFeSi_2O_6 = \tfrac{1}{3} Fe_3Al_2Si_3O_{12} + CaMgSi_2O_6$$

pyrope + hedenbergite = almandine + diopside

Four different calibrations are used:

- T(EG79) Ellis and Green (1979)
- T(Powell85) Powell (1985)
- T(Ravna88) Ravna (1988)
- T(KroghRavna00) Ravna (2000).

Although Ravna (2000) is the newest version, the older versions are still in use, and therefore will be used in this study as well.

Garnet-orthopyroxene
The geothermometers based on the exchange of Fe^{2+}-Mg between grt and opx is less popular. It is based on the reaction:

$$\frac{1}{3}Mg_3Al_2Si_3O_{12} + \frac{1}{2}Fe_2Si_2O_6 = \frac{1}{3}Fe_3Al_2Si_3O_{12} + \frac{1}{2}Mg_2Si_2O_6$$

pyrope + ferrosilite = almandine + enstatite

For this reaction the calibration by Harley (1984) is used.

- T(Harley84) Harley (1984)

Solvus thermometry
Clinopyroxene-orthopyroxene
Two different calibrations, by Wells (1977) and Brey and Kohler (1990) are used. The amount of opx in cpx, and the amount of cpx in opx is used for the calculations:

- T(Wells77) Wells (1977)
- T(BKN90) Brey and Kohler (1990)

Ca in orthopyroxene
This geothermometer is based on the Ca content present in opx. One calibration will be used:

- T(OpxBK90) Brey and Kohler (1990)

Na in clinopyroxene and orthopyroxene
This method is based on the Na content of both opx and cpx. This not a widely used method and only the calibration by will be used:

- T(NaPxBK90) Brey and Kohler (1990)

overview on geothermometers
For clarity the effect of compositional variation of different minerals for the geothermometers is given in table 5.1. For example: the calculated temperature with T(Krogh88) will be higher if the Mg# in grt is higher, when all other variables in this calibration, Mg# in cpx and Ca in grt, are constant. Table 5.1 gives a quick overview what variables are involved in the different calibrations and effect they have on calculated temperatures.

	Change of T with higher value for …							
	Mg#, grt	Mg#, cpx	Mg#, opx	Ca, grt	Mn, grt	Ca, opx	Na, cpx	Na, opx
T(KroghRavna00)	H	L	-	H	H	-	-	-
T [Krogh88]	H	L	-	H	-	-	-	-
T [Powell85]	H	L	-	-	-	-	-	-
T [EG79]	H	L	-	-	-	-	-	-
T [Harley84]	H	-	L	H	-	-	-	-
T [BKN90]	-	L	H	-	-	-	-	-
T [Wells77]	H	-	L	-	-	-	-	-
T [OpxBK90]	-	-	-	-	-	L	-	-
T [NaPxBK90]	-	-	-	-	-	-	H	L

Table 5.1. Compositional variation that influences the different calibrations of the geothermometers. With higher value for a certain element, the calculated temperature will be higher (H) or lower (L).

Exchange reactions
Al in orthopyroxene

$$Mg_2Si_2O_6 + \mathrm{MgAl_2SiO_6} = \mathrm{Mg_3Al_2Si_3O_{12}}$$
enstatite + Mg-Tsermakite = pyrope

- P(BKN90) Brey and Kohler (1990)
- P(BBG08) Brey et al. (2008)

The Al in orthopyroxene barometer is the most widely used geobarometer in eclogites. There are some different calibrations, but the calibration P(BKN90) is the most widely used and most reliable according to the overview article by Ravna and Paquin (2003). Recently a new calibration is proposed, P(BBG08). This new calibration is an updated version of BKN90, calibrated at higher pressures. It should be an improvement of BKN90, and both BKN90 and BBG08 shall be used.

The formula's behind the Al in opx geobarometers are quite complex. The most important factor is the amount of Al that is present in the M1 sites of orthopyroxene which is the Mg-Tsermakite component of opx, with a lower amount leading to higher pressures. There are, however, different methods to calculate Al^{M1} in opx. Brey and Kohler (1990) and Brey et al. (2008) use a method to calculate the amount of Al^{M1} in opx by Nickel and Green (1985). Another method by Carswell (1991) is used, not surprisingly, by Carswell et al. (2006). The calculation of Al^{M1} in opx by Carswell (1991) gives lower Al^{M1} in opx than does Nickel and Green (1985), and thus leads to higher pressures. The reasoning and formula's behind both methods are explained in appendix II. Like with the use of different thermometers, also these two different methods to calculate Al^{M1} in opx are used. The method by Carswell (1991) has been implemented in the ptexl3 excel-sheet, so that both BKN90 and BBG08 can be calculated with both methods to calculate Al^{M1} in opx.

5.1.2 The Fe^{3+} problem

The EMP is able to calculate the compositions of a mineral based on the weight of different elements. This is a very accurate method, but the downside is that different isotopes of the same element cannot be detected. Iron is a major constituent of many minerals, and, as we have seen, many geothermometers depend on the Fe^{2+}-Mg proportion between minerals. The Fe^{3+}/Fe_{tot} proportion in the minerals that occur in eclogites normally ranges from 0.03 in garnet, 0.03-0.1 in opx to 0.2-0.4 in cpx (Carswell et al., 2000). There are two different methods to calculate the Fe^{3+}/Fe^{tot} proportion of an EMP analysis. One by Droop (1987) and one by Schumacher (1991). The formula's behind both methods are given in appendix I. Unfortunately, the correction for Fe^{3+} is very sensitive to the accuracy of the EMP analysis. Both methods for Fe^{3+} correction are based on charge balance. So a small error in the amount of measured SiO_2 will give a large error in calculated Fe^{3+}, even in the accurate WDS mode of the EMP (Carswell and Zhang, 1999). This makes Fe^{3+} calculations very sensitive to errors in measurements, and many analyses will simply not be good enough to make a correct correction. Carswell and Zhang (1999) argue that 100ºC error margin solely due to the Fe^{3+} problem is present for the Fe^{2+}-Mg grt-cpx geothermometers.
According to Bucher and Frey (2002) the Fe^{3+}/Fe^{2+} proportion should not deviate by more that 5%, because an equilibrium situation is normally assumed. If the Fe^{3+} calculations do not work out, the best guess that can be made is to assume $Fe_{tot}=Fe^{2+}$, and therefore $Fe^{3+}=0$.
Vrijmoed et al. (2006) makes all calculations with both Fe^{3+} calculated and with $Fe_{tot}=Fe^{2+}$.
According to Carswell et al. (2006) it is best to make calculation with $Fe_{tot}=Fe^{2+}$, because Fe^{3+} is often overestimated, which will cause an underestimation of temperature.

It should be noted that the Fe^{3+} problem is especially present in the geothermometers that use the Fe^{2+}-Mg exchange in grt and cpx, it is a smaller problem in the Fe^{2+}-Mg in grt and opx geothermometers, while the solvus thermometers are unaffected by the problem. Also for this reason nine different geothermometers are selected, because it will give a clue when wrong Fe^{3+} show the Fe^{3+} sensitive geothermometers to deviate from the Fe^{3+} insensitive geothermometers.

5.1.3 Finding the peak assemblage

PT calculations of the eclogite samples are performed because this lithology is assumed to have retained a composition that represents the highest PT conditions. The rocks have been collected at surface level, which means that they have travelled from eclogite facies PT conditions to very much lower PT condition. How much have these rocks been affected by retrograde reactions during their ascent to the surface? We have seen that some amphiboles have grown in between the original equilibrium eclogite assemblage of grt + cpx + opx (section 4.1). Thus growth of new minerals has taken place at lower PT conditions than the eclogite facies. This in itself poses no problem, because we are interested in measuring grt, cpx and opx to obtain the peak PT conditions. Minerals can, however, change composition by diffusion. For example, at high temperatures the Mg# in grt will be relatively high, while the Mg# in cpx will be relatively low (see table 5.1). If these minerals cool, they will exchange Fe and Mg at their grain boundaries, causing a decrease of the Mg# in garnet and an increase in the Mg# in cpx compared to the original composition. Depending on temperature, grain size and time, the diffusion will effect the grains from the rim all the way to the core. This problem is generally dealt with by making linescans across the minerals which gives some insight in the amount of diffusion that has taken place. If the composition changes from rim to core it is essential to a take core measurement for peak PT calculations, avoiding the rim where the Fe-Mg equilibrium has been changed at lower temperatures (e.g. Carswell et al., 2006; Vrijmoed et al., 2006).

To calculate the pressure of the eclogites, the Al content in opx is especially important. The same reaction as stated above will also be valid for Al in opx: during decompression the Al content in opx will become higher, a process that starts from the rim. An example from Carswell et al. (2006) is given in figure 5.1. 10 analyses across a grain of opx show the variation in Al_2O_3 from rim to core to rim. The Al_2O_3 shows a clear U-shaped pattern from ±1.2 wt% at the rims to ±0.3 wt% in the opx core. The high values at the opx rim are assigned to retrograde reactions that have taken place after the peak PT conditions. So, in this case the analysis with an Al_2O_3 content of 0.3% should be taken for the PT calculations, because it closest resembles the inferred original Al_2O_3 content of the opx grain. In general large grains of opx will have a higher chance that the original Al_2O_3 content is still present within the core, if it is still present at all.

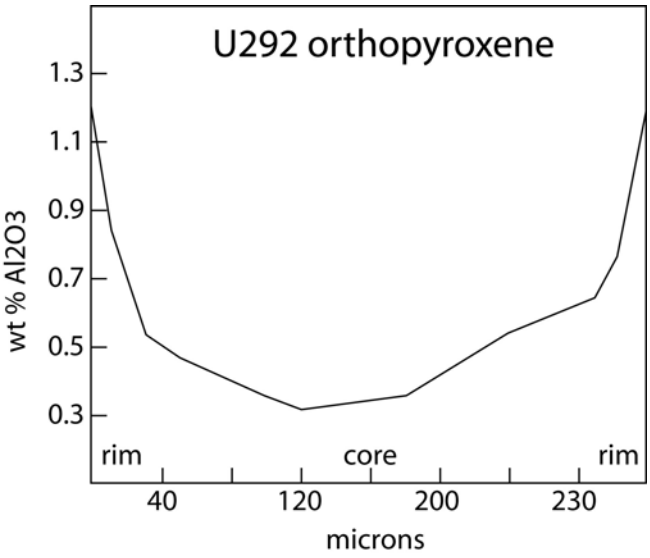

Figure 5.1. Linescan across an opx grain from Ugelvik, Otrøy (Carswell et al., 2006).

5.2 Results

5.2.1 Thin section 10-5B (II); procedure of a PT analysis

The peak PT conditions of the eclogites have been calculated at four locations in three different thin sections. The procedure that has been followed to make the calculations will be illustrated by sample 10.5B, location II. PT calculations on other samples are performed by similar methods and only the essential data is given (section 5.2.2). All data that is presented for sample 10-5B is available for the other samples as well, and is given in appendix III, IV and V.

Figure 5.2 shows an image of thin section 10-5B. EMP measurements have been performed on two locations in this thin section. Figure 5.3 shows an EMP image of location II in thin section 10-5B. Four linescans have been made here:

linescan	mineral	# of analyses
W10-5BL7	grt	60
W10-5BL8	opx	15
W10-5BL9	opx	15
W10-5BL10	cpx	10

The starting point of a linescan marked ‘1’, the ending point is marked with the number of the final analysis. All linescans that have been made can be referenced in this way in an image, and the location of every spot# can be roughly estimated. E.g. spot# 5 of W10-5BL8 will be located at one third of the distance between the first and the last point of the linescan.

PT calculations are based on the assumption of chemical equilibrium between the involved minerals. Minerals that are not in direct contact can be in chemical equilibrium by the interactions with fluids in a rock. However, the highest chance that the minerals where in equilibrium is when mineral grains are in direct contact with each other. Therefore it is best only to use grt, opx and cpx that are in direct contact with each other. The mineral combination that is chosen in location II of 10-5B (see figure 5.3) does not obey this rule. Grt and opx, as well as opx and cpx are in direct contact, cpx and grt are, however, separated by opx and hbl. So it can be argued if the cpx that is right above the grt, and separated only by a thin amphibole, would not have made a better analysis. But, as we will see later on, the composition of cpx and grt is fairly constant within one thin section. It is mostly the Al content in opx that is important in choosing where to make the analyses.

Garnet

Linescan W10-5BL7 is shown in figure 5.3 from ± spot# 23 to the finish point. The chemical profile of this linescan is shown in figure 5.4. The inclusions within the garnet are all cpx and amph, and these are left out of the profile. The compound wt% are recalculated to the mineral end-members following the procedure as explained in appendix I. An important reason to make these calculation is that visual inspection of the linescans becomes much easier. The geothermometers that use grt are dependent on the Mg# and/or Ca (see table 5.1). The end-members of garnet are:

Almandine	$Fe_2Al_3(SiO_4)_3$
Grossular	$Ca_2Al_3(SiO_4)_3$
Pyrope	$Mg_2Al_3(SiO_4)_3$

The end-member profile (see figure 5.5) shows that the pyrope content of garnet decreases at the garnet rim and next to inclusions, while the almandine content increases. This is

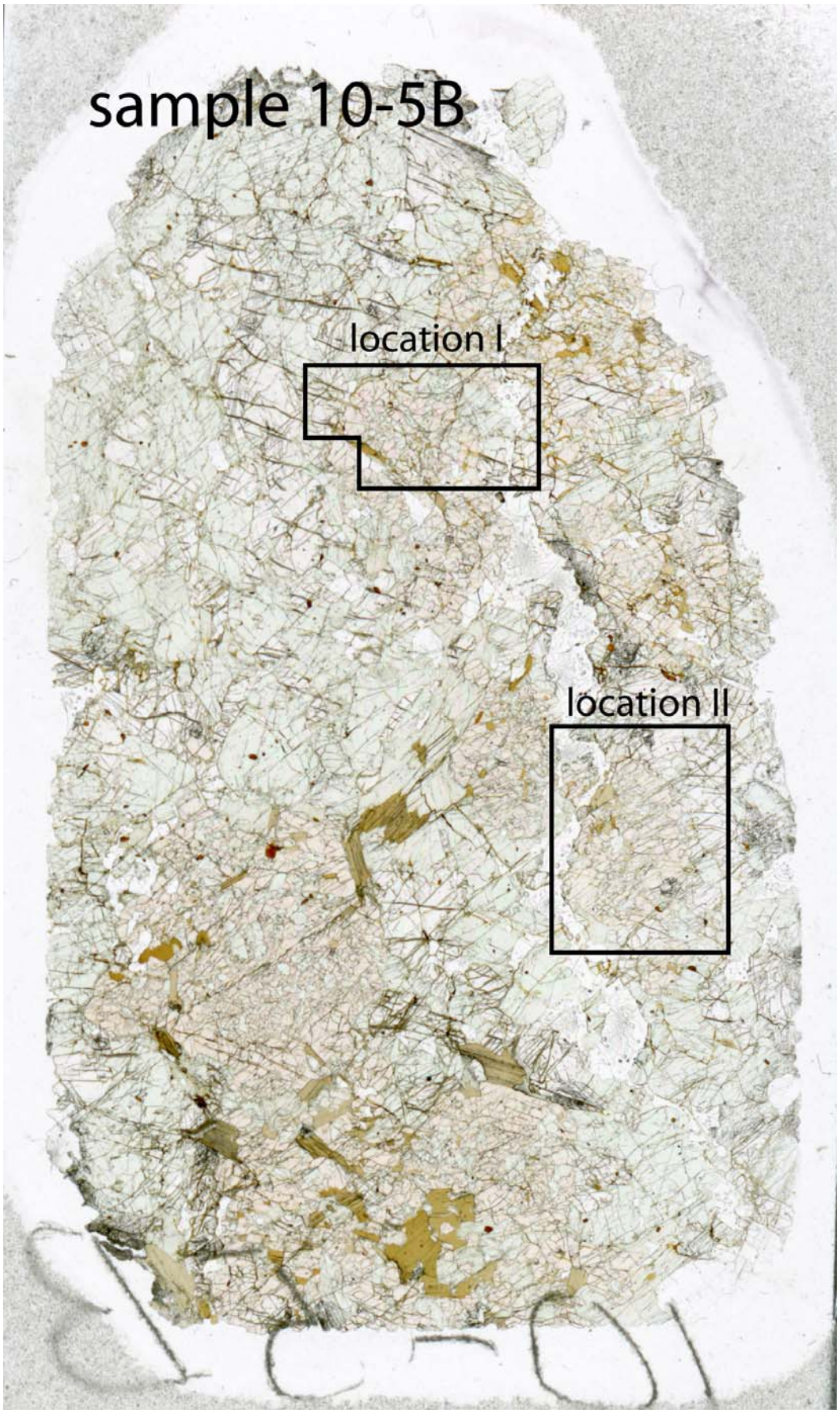

Figure 5.2. Thin section of opx bearing eclogite sample 10-5B. An EMP image of the area marked location II is shown in figure 5.3

equivalent to a decrease in Mg# and a decrease in temperatures that will be calculated (see table 5.1). This relation is much harder to see in the chemical profile. This shift in end-member composition is best explained by equilibration of the garnet with other minerals during lower (P)T conditions during the retrograde path. So for calculations on the peak PT conditions, a garnet analysis should be selected with a low almandine and high pyrope content, and far as possible from the garnet rim or any inclusions. This is thought the best representation of the original garnet composition.

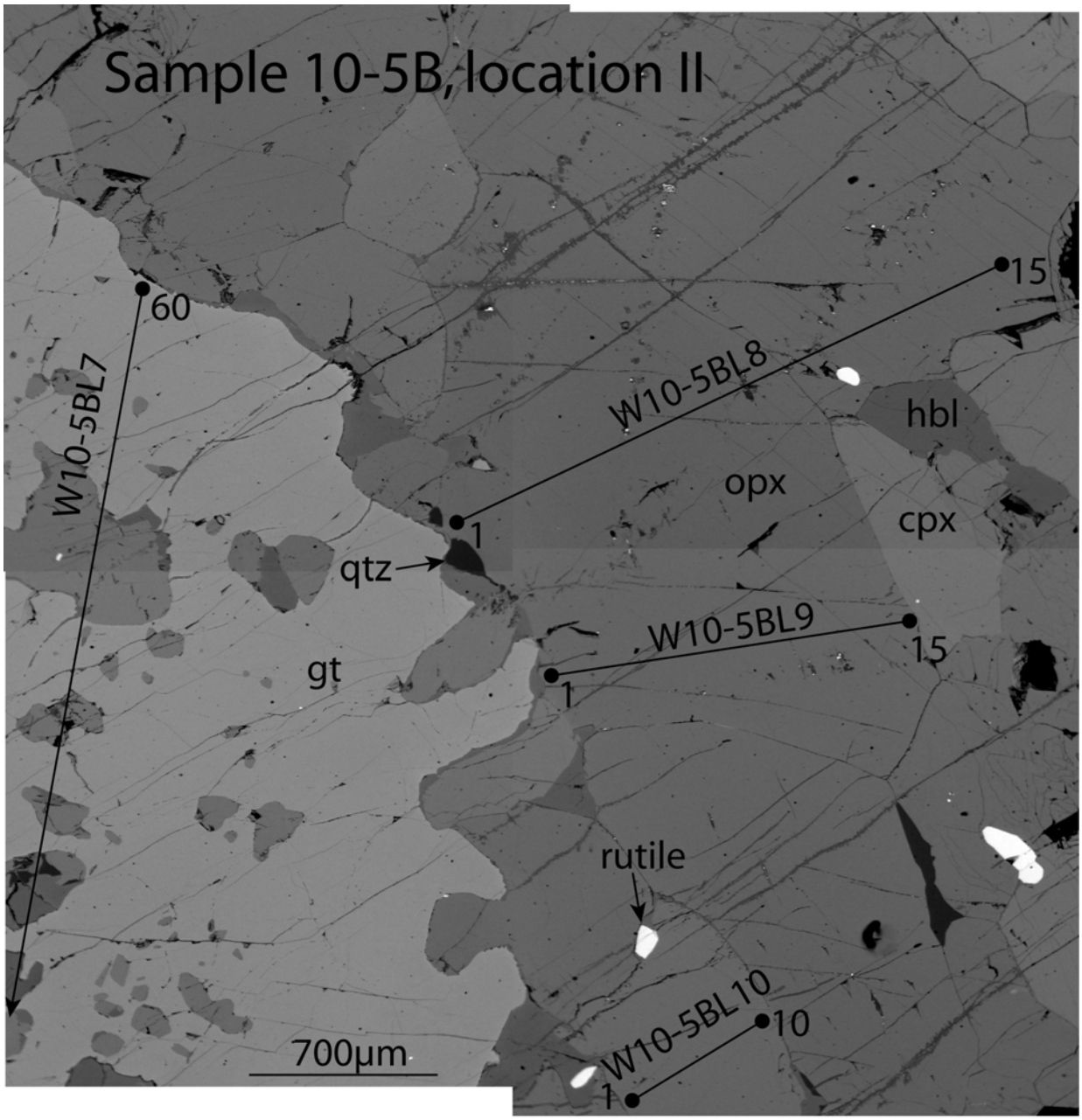

Figure 5.3. EMP image of location II in thin section 10-5B. The location of linescans through grt, opx (2x) and cpx is shown. Minerals that can be seen are, from lightest shade of grey to black: rutile, grt, cpx, opx, hbl and qtz.

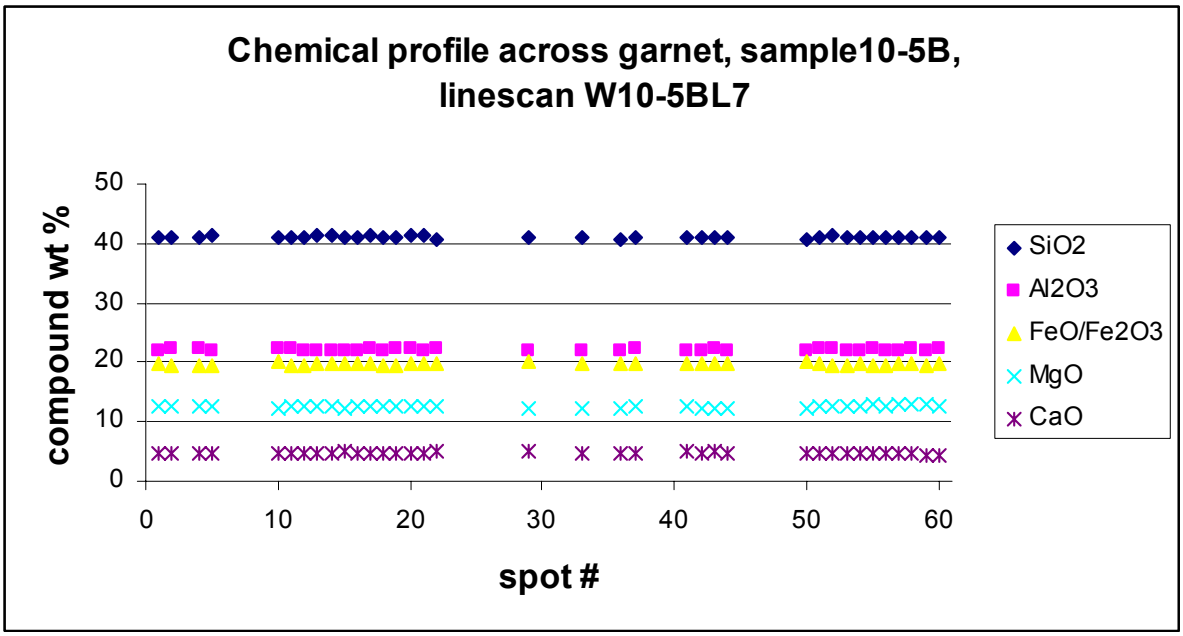

Figure 5.4. Chemical profile across the garnet grain in sample 10-5B, linescan 10-5BL7. Analyses of inclusions within the garnet are left blank.

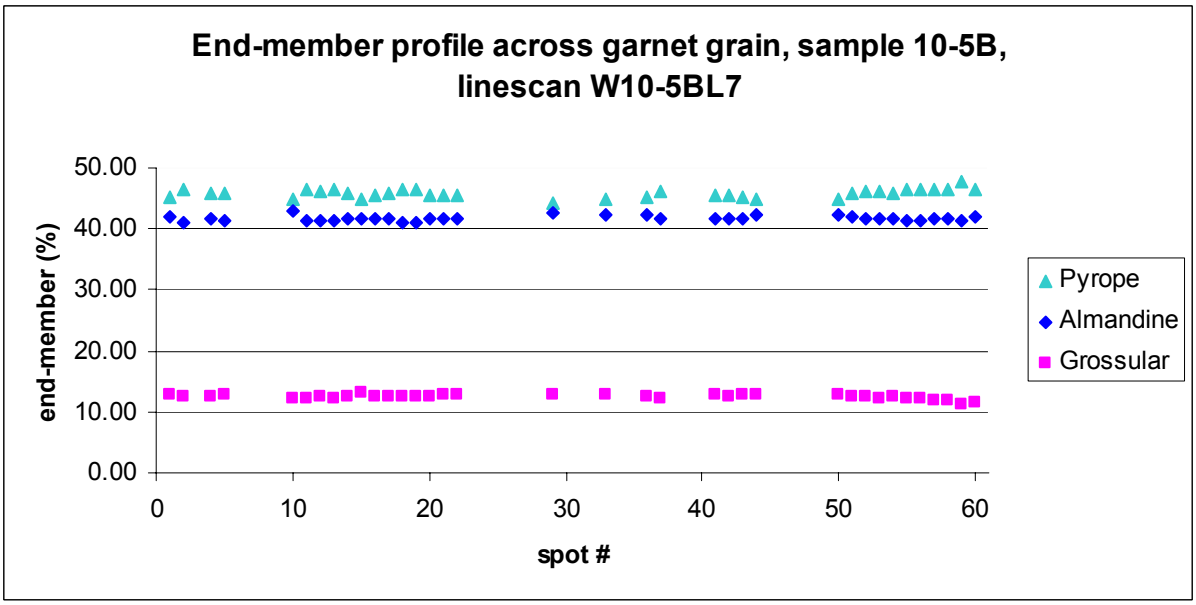

Figure 5.5. End-member profile across the garnet grain in sample 10-5B, linescan 10-5BL7. Analyses of inclusions are left blank.

Clinopyroxene

Figure 5.6 shows the chemical profile across the cpx grain that is shown in figure 5.3, linescan W10-5BL10. The chemical profile shows very little variation. For geothermometry only the Mg# of cpx is important (see table 5.1). The end-members of cpx are:

Enstatite	$Mg_2Si_2O_6$
Ferrosilite	$Fe_2Si_2O_6$
Wollastonite	$Ca_2Si_2O_6$

Figure 5.7 shows the recalculation of the chemical profile to end-member components. There is a minimal variation in the proportion between enstatite and ferrosilite, and for geothermometry it is therefore irrelevant which measurement should be taken. For consistency, core measurements of cpx are always selected.

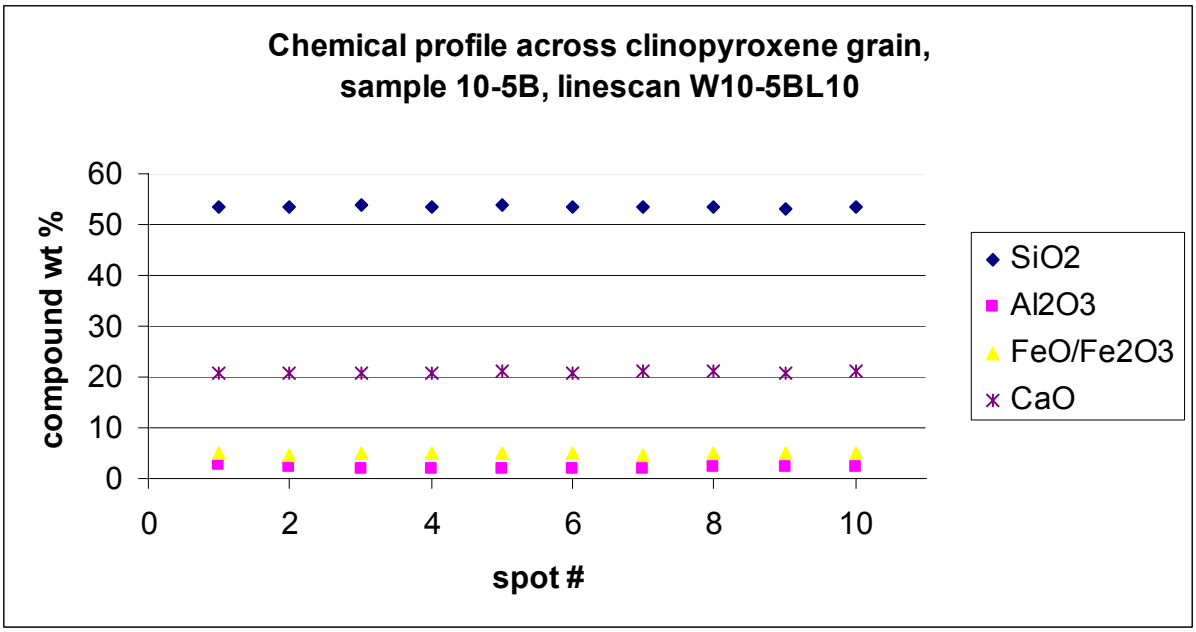

Figure 5.6. Chemical profile across cpx grain in sample 10-5B, linescan 10-5BL10.

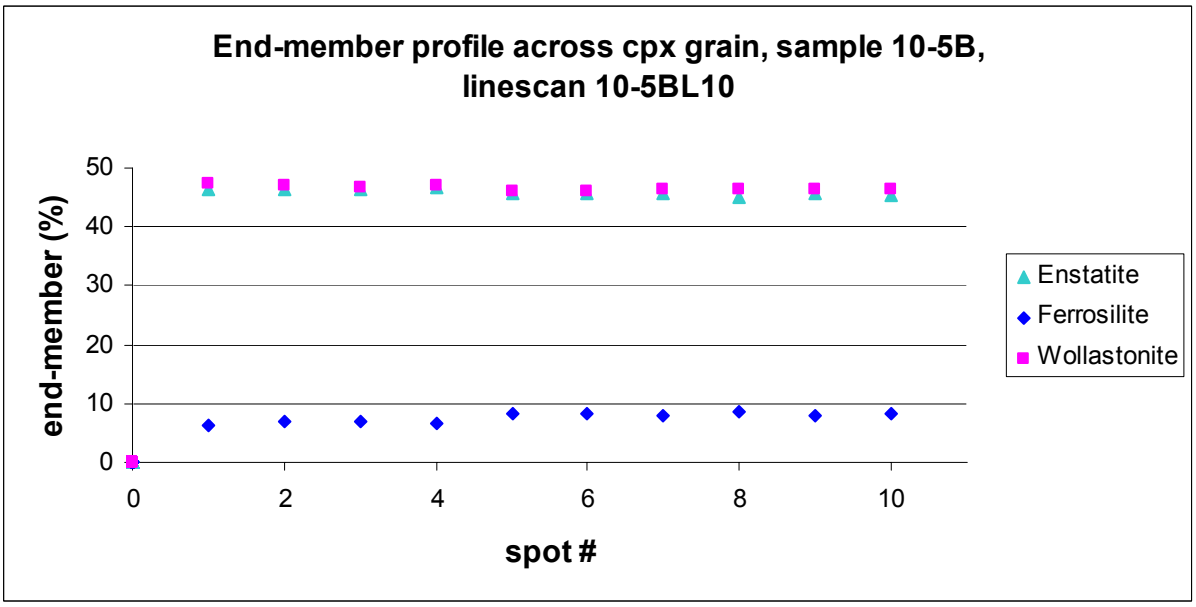

Figure 5.7. End-member profile across cpx grain in sample 10-5B, linescan 10-5BL10.

Orthopyroxene

Figure 5.8 shows the chemical profile across the upper opx linescan (see figure 5.3), W10-5BL7. Like with the cpx, there is little variation in the chemical profile of the major elements. Opx can be expressed with the same end-members as cpx. Important for geothermometry are the Mg# of opx, but also the Ca content. The end-member profile, figure 5.9, shows that there is very little variation of these elements across the grain. There is certainly no U shaped pattern visible from rim to core. So for geothermometry it is unimportant what spot# of the linescan is selected.

For geobarometry the Al content of opx is the most important variable. Figure 5.10 shows the variation in Al_2O_3 of the same linescan. The vertical axis is a different scale, as the concentration of Al_2O_3 is much lower. The pattern that arises is very different than that of the elements used for geothermometry. Spot # 1 has an Al_2O_3 content of about 1.4%, this goes down to about 0.3% at spot # 5-7, then rises again to 1.4% at spot # 9. Spot # 9 is a crack in

the opx grain (see figure 5.3). The Al_2O_3 content then goes down again to about 0.6% in the rest of the grain. This profile is very similar to the one reported by (Carswell et al., 2006), as discussed above. The higher Al_2O_3 concentrations at the opx rim are therefore explained by diffusional reequilibration of Al_2O_3 at lower pressures during the retrograde path. The original Al_2O_3 concentration is best represented by the lowest concentration that is present in the grain.

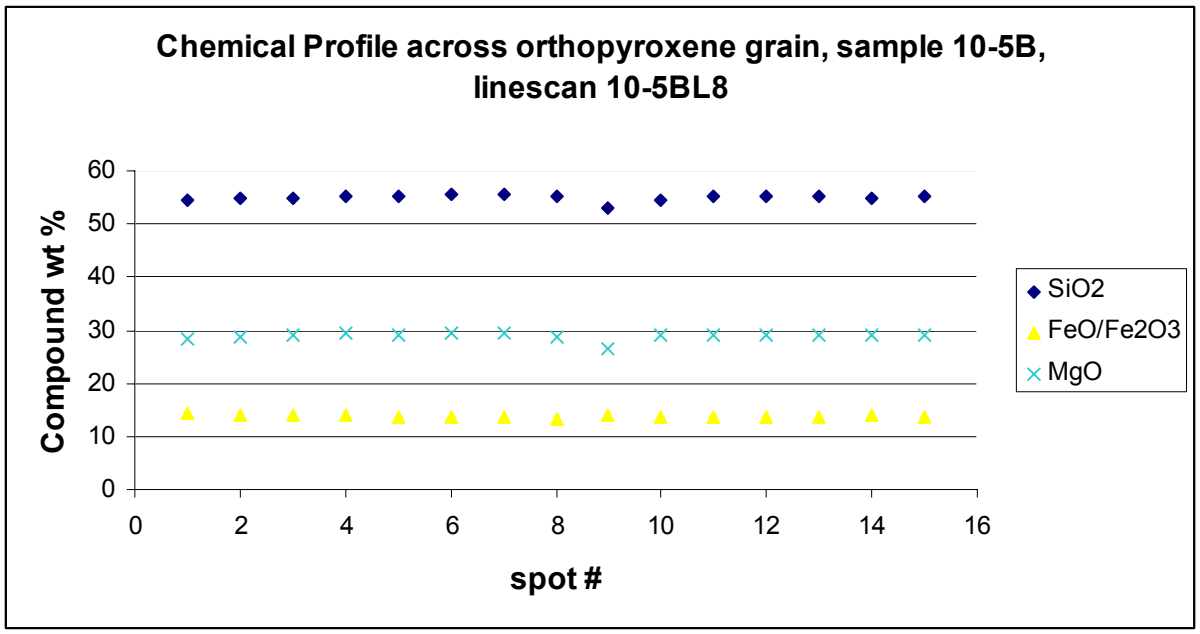

Figure 5.8. Chemical profile across opx grain in sample 10-5B, linescan W10-5BL8.

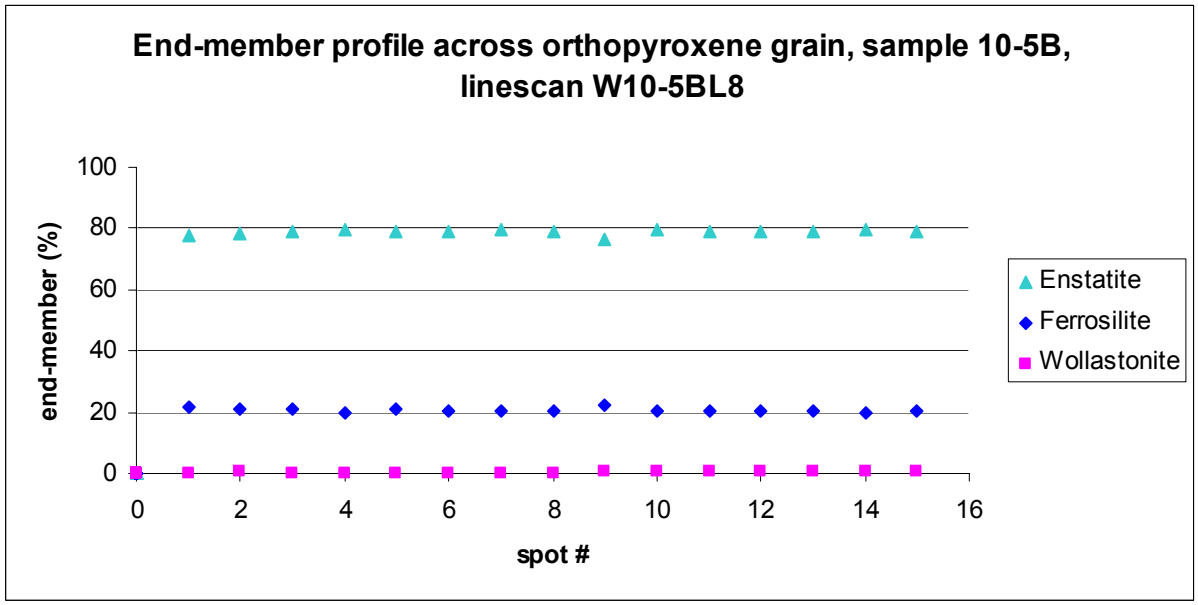

Figure 5.9. End-member profile across opx grain in sample 10-5B, linescan W10-5BL8.

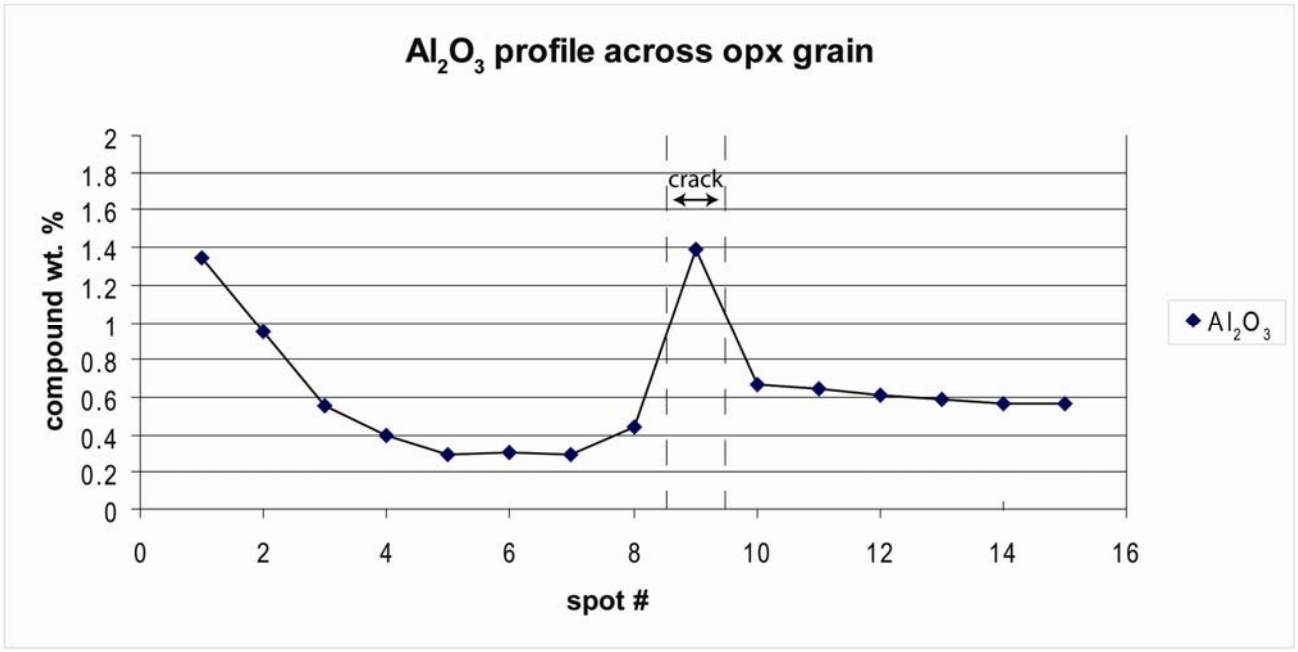

Figure 5.10. Variation in Al_2O_3 in profile across opx grain, sample 10-5B, linescan W10-5BL8.

The PT calculations

The analyses that are selected for grt, cpx and opx are shown in table 5.1 In this table the original EMP measurements (compound wt%), the recalculation to the mol% of the elements (cations per formula unit), and the end-members of the minerals are shown.

The analyses of grt: spot # 15 W10-5BL7, opx: spot# 5 W10-5BL8, cpx: spot# 5 W10-5BL10, are used in ptexl3 for the PT calculations. The input data of ptexl3 is the compound wt%, and the software first calculates the cations p.f.u. The program has the option to make these calculations with $Fe_{tot}=(Fe^{2+} + Fe^{3+})$ or with $Fe_{tot}=Fe^{2+}$. The result of the calculations with Fe^{3+} is shown in table 5.3. Here the intersections of all nine calibrations of five geothermometers with four calibrations of the geobarometer is given. In total nine different calibrations of geothermometers will be used and four calibrations of geobarometers. This will result in 4x9=36 different points in PT space. Of course all these PT points will not give the absolute truth, and there will be a considerable spread in the calculated PT points. In general the geothermometers have an error margin of 50-100ºC, and the geobarometers about 1-2kbar. As we will see, the spread in PT calculations exceeds this error margin, and the points will therefore be plotted without error bars.

A graphic representation of this result is given in figure 5.11. The diagram should be read as follows: the dashed lines are the result of the different calibrations of the geobarometers. Two different calibrations with two different methods to calculate Al^{M1} in opx give four lines in PT space. The five geothermometers, with their different calibrations, result in nine lines in PT space. However, these lines are not shown, but only the intersections with the geobarometers. Every geothermometer has its own colour. For example: T(Harley 84) intersects P(BBG08) with Al calculated according to (Nickel and Green, 1985) at 46.1 kbar and 857ºC. This is the purple circle on line 1.

Sample: W10-5B, location II			
Linescan:	W10-5BL7	W10-5BL8	W10-5BL10
Spot #	15	5	5
Mineral	grt	opx	cpx
compound (wt%)			
SiO_2	40.93	55.36	53.77
Al_2O_3	21.87	0.30	1.92
FeO	19.76	13.63	4.93
MnO	0.63	0.12	0.05
MgO	12.32	29.10	14.97
CaO	5.03	0.18	21.02
Na_2O	-	0.02	1.48
TiO	0.03	0.02	0.04
Cr_2O_3	0.22	-	0.25
Total	100.80	98.73	98.43
cations (p.f.u.)			
Si	3.04	2.00	1.97
Al	1.92	0.01	0.08
Fe^{2+}	1.23	0.41	0.15
Fe^{3+}	-	-	-
Mn	0.04	-	-
Mg	1.37	1.56	0.82
Ca	0.40	0.01	0.83
Na	-	-	0.11
Ti	-	-	0.04
Cr	-	-	-
total	8.00	4.00	4
Mg#	0.53	0.79	0.84
end-members			
Pyrope	45.00	-	-
Almandine	41.80	-	-
Grossular	13.20	-	-
Spessartine	1.30	-	-
Enstatite	-	78.90	45.57
Ferrosilite	-	20.74	8.42
Wollastonite	-	-	46.01
En+Fs+Wo	-	-	90.49
Jadeite	-	-	9.51
Aegirine	-	-	-
Albite	-	-	-
Anorthite	-	-	-

Table 5.2. The selected measurements of grt, cpx and opx in sample 10-5B, location II.

	With Fe3+							
	P(BKN90), Al(NG85)		P(BBG08), Al(NG85)		P(BKN90), Al(C91)		P(BBG08), Al(C91)	
	P (kbar)	T (ºC)	P (kbar)	T (ºC)	P (kbar)	T (ºC)	P (kbar)	T (ºC)
T[KroghRavna00]	23.2	613	26.3	630	24.8	622	28.3	641
T [Krogh88]	24.2	624	26.3	630	25.3	627	27.8	635
T [Powell85]	32.6	714	33.0	715	33.9	717	34.5	719
T [EG79]	36.0	749	35.7	749	37.4	753	37.3	753
T [Harley84]	46.1	857	43.2	842	48.5	869	45.3	853
T [BKN90]	43.4	828	41.8	825	44.8	831	43.3	828
T [Wells77]	42.9	823	41.7	823	44.0	823	42.9	823
T [OpxBK90]	45.4	850	43.1	841	47.4	858	44.9	848
T [NaPxBK90]	31.5	701	32.0	702	32.6	703	33.4	704

Table 5.3. All intersections of four different calibrations of the geobarometer with nine (calibrations of) geothermometers, with Fe^{3+} calculated. P in kbar, T in ºC.

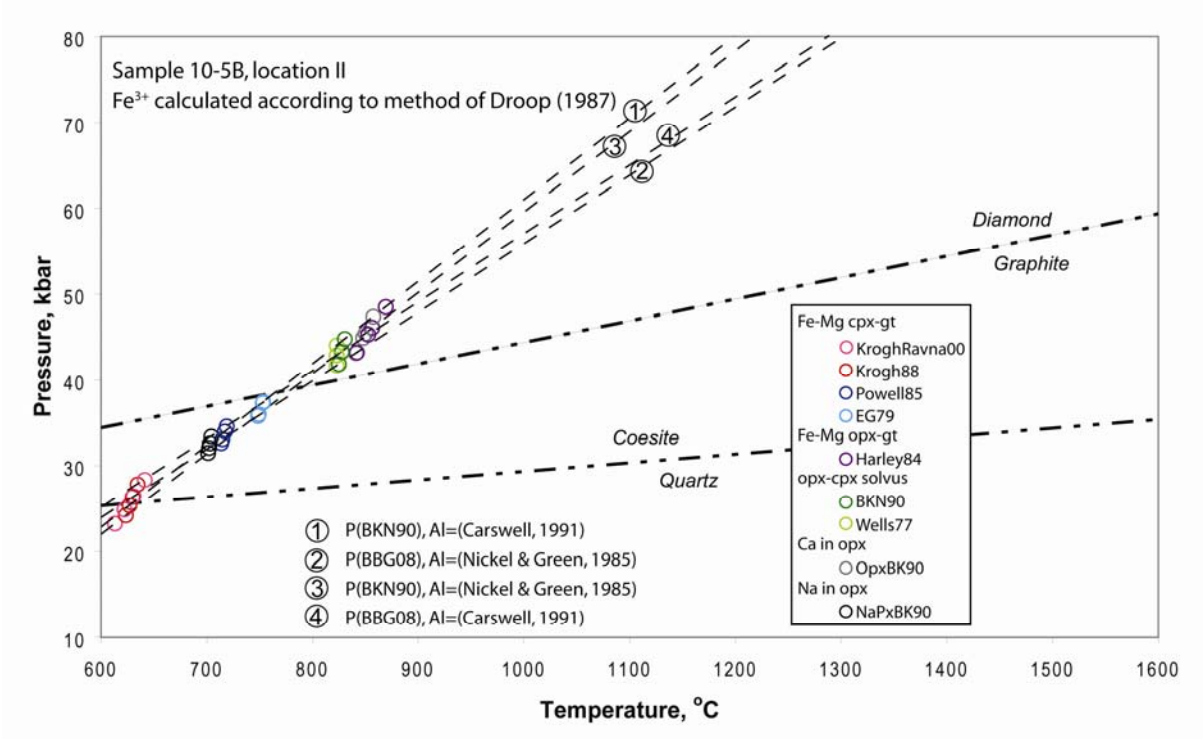

Figure 5.11. PT calculations of sample 10-5B, location II, with data as in table 5.2, with calculation of Fe^{3+}. Four different calibrations of the Al in opx barometer are used, combined with nine different calibration of five geothermometers. The quartz-coesite phase boundary is from Hemingway et al. (1998), the graphite-diamond phase boundary from Kennedy and Kennedy (1976).

The difference in results between the different calibrations of the geobarometer are not very great, compared to the difference between the geothermometers. P(BKN90) combined with Al(C91) gives the highest PT conditions, P(BBG08) combined with AL(NG85) the lowest. This difference is largest for geothermometers with a relatively flat slope, e.g. T(Harley84), and is max. ±5kbar and 25ºC. The difference between geothermometers is of much greater importance. With one geobarometer calibration, e.g. P(BKN90) with AL(NG85), the difference between the highest and the lowest intersection is as much as 23kbar and 245ºC. The lowest PT points are still in the quartz stability field, while the four highest PT points are even in the diamond stability field. It should be noted that the geothermometers that are based on the Fe^{2+}-Mg exchange between grt and cpx and the Na in opx geothermometer, are all below the

diamond stability line and show a large spread. The other geothermometers are all above the diamond stability line and cluster very nicely, with a relatively small difference between the highest and the lowest PT conditions.

The same calculations as above, but now with $Fe_{tot}=Fe^{2+}$ are given in table 5.4 and the graphic representation in figure 5.12. Not all geothermometers are sensitive to the calculation of Fe^{3+}. Only the ones that use the Mg# in cpx will show large difference (see table 5.1), because this is the mineral with the largest amount of iron, and thus the largest source of error. The calculation with $Fe_{tot}=Fe^{2+}$ therefore have a shift of the Fe^{2+}-Mg exchange geothermometers between grt and cpx with respect to the calculations with Fe^{3+} calculated. This results in these thermometers to shift into the diamond stability field, at the approximate position of the geothermometers that where already in this field with Fe^{3+} included. The result is a cluster of seven out of nine geothermometers that show a variation of about 8 kbar and 80ºC. Two geothermometers are outside this cluster: T(Krogh88) and T(NaPxBK90).

	Fetot=Fe2+							
	P(BKN90), Al(NG85)		**P(BBG08), Al(NG85)**		**P(BKN90), Al(C91)**		**P(BBG08), Al(C91)**	
	P (kbar)	**T (ºC)**	**P (kbar)**	**T (ºC)**	**P (kbar)**	**T (ºC)**	**P (kbar)**	**T (ºC)**
T[KroghRavna00]	41.0	802	39.2	792	43.6	818	41.5	806
T [Krogh88]	34.9	738	34.9	738	36.4	743	36.5	743
T [Powell85]	42.7	821	41.2	817	44.4	826	42.8	821
T [EG79]	46.1	857	43.8	850	47.8	862	45.5	855
T [Harley84]	46.1	857	43.2	842	48.5	869	45.3	853
T [BKN90]	43.4	828	41.8	825	44.8	831	43.3	828
T [Wells77]	42.9	823	41.7	823	44.0	823	42.9	823
T [OpxBK90]	45.4	850	43.1	841	47.4	858	44.9	848
T [NaPxBK90]	31.5	701	32.0	702	32.6	703	33.4	704

Table 5.4. As table 5.3, but with $Fe_{tot}=Fe^{2+}$.

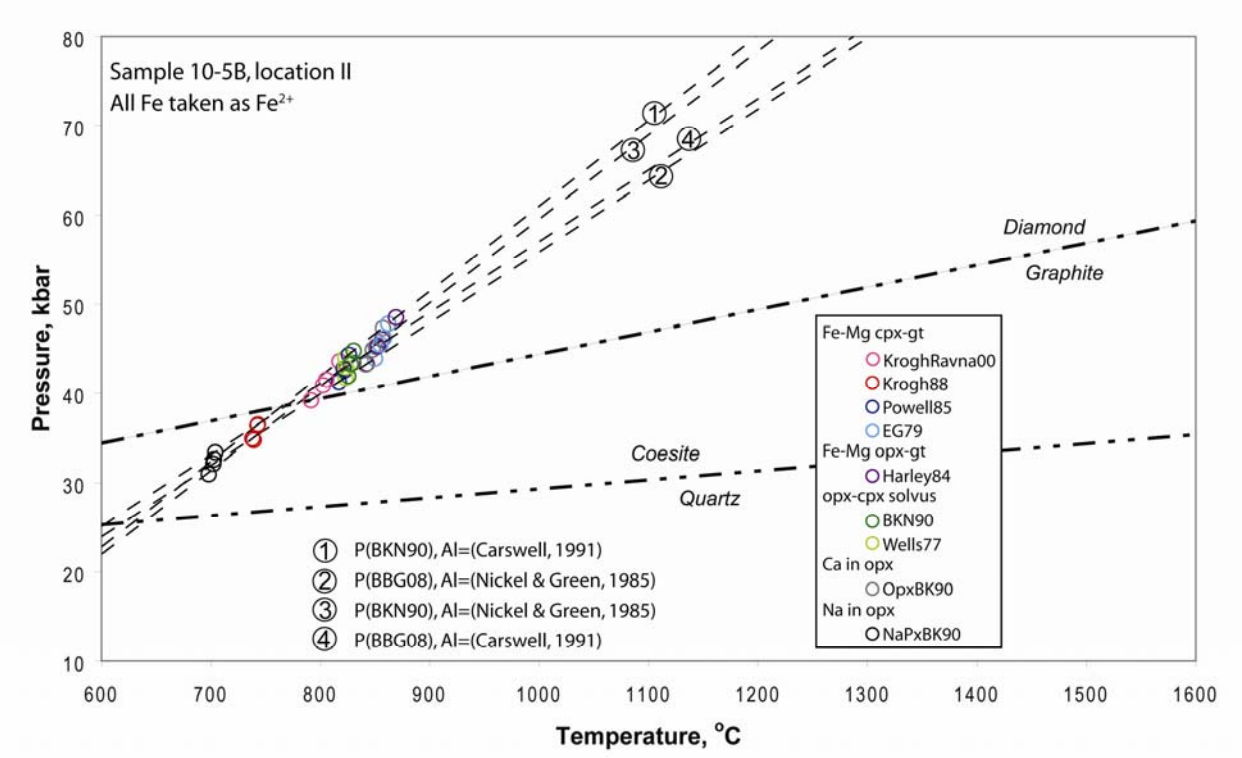

Figure 5.12. As figure 5.11, but with $Fe_{tot}=Fe^{2+}$.

If T(Krogh88) and T(NaPxBK90) are ignored, it follows that the geothermometers that are sensitive to calculation of Fe^{3+} are scattered and at lower PT conditions when Fe^{3+} is calculated compared to calculations under the assumption $Fe_{tot}=Fe^{2+}$. They show higher PT conditions and are in agreement with the geothermometers that are not sensitive to the calculation of Fe^{3+} when Fe^{3+} is not calculated. Based on these observations, it is concluded that the Fe^{3+} correction does not work. Apparently Fe^{3+} is overestimated, which leads to an underestimation of the pressure according to Carswell et al. (2006). If this is the case, then the best guess: $Fe_{tot}=Fe^{2+}$ should be used (Bucher and Frey, 2002).

Now we have a very nice cluster of seven out of nine geothermometers, that all give PT conditions within the diamond stability field. T(Krogh88) and T(NaPxBK90), however, give much lower PT conditions. Because seven out of nine geothermometers give an other result, the odds are that T(Krogh88) and T(NaPxBK90) give a wrong PT point. Maybe the chemical equilibrium of Na in opx has reequilibrated more at lower PT conditions compared to the other chemical systems, leading to the low PT estimation of T(NaPxBK90), or maybe this chemical equilibrium is not applicable to this rock. T(Krogh88) is one of the four Fe^{2+}-Mg grt-cpx exchange geothermometers, and is therefore likely to be a wrong calibration. This is in agreement with an observation done by Ravna and Paquin (2003) who states that his own geothermometer, T(Krogh88), 'yields unrealistic low temperatures on natural rocks'.

Scatter of different geothermo- and barometers is a problem that is not uncommon in geothermobarometry, and there are different ways to cope with it. For example Vrijmoed et al. (2006) encircle all PT-points, stating that the truth must be somewhere in that circle. Carswell et al. (2006) eliminate the PT points that show a large deviation with respect to the other points, and in that way try to limit the PT range. A combination of the two methods is favoured here, because T(Krogh88) and T(NaPxBK90) clearly deviate from the large group but no preference exists for any of the other geothermometers.

The same calculations will be repeated for three other locations in two other samples as well in section 5.2.2. This will be done under the assumptions:

1. $Fe_{tot}=Fe^{2+}$
2. Only the geobarometers P(BKN90) with Al(C91) and P(BBG08) with Al(NG85) will be used, as these give the extreme PT values and the combinations P(BBG08) with Al(C91) and P(BKN90) with Al(NG85) always result in PT values in between.

5.2.2 PT calculation on samples 10-5B (I), 17-5A and 17-5C (I)

The data that is used for the PT calculations of 10-5B, location I, 17-5A and 17-5C, location I, is given in table 5.5. The result of the calculations in table 5.6, with graphical representation in figure 5.13, figure 5.14 and figure 5.15. The analyses have been selected with the same method as described above, for 10-5B, location II. Core measurements of grt and cpx are combined with the opx analysis that has the lowest Al content. At some locations more than one linescan of opx has been made, to capture the lowest Al in opx measurement in a single grain.

	W10-5B, location I			W17-5A			W17-5C, gebied I		
Linescan:	W10-5BL4	W10-5BL3	W10-5BL2	W17-5AL3	W17-5AL2	W17-5AL1	W17-5CL1	W17-5CL6	W17-5CL4
Analysis #	11	4	2	27	9	7	3	9	46
Mineral	grt	cpx	opx	grt	cpx	opx	grt	cpx	opx
compound (wt%)									
SiO_2	40.83	53.17	54.59	41.96	54.4	56.39	41.36	53.67	56.41
Al_2O_3	21.94	2.44	0.35	22.65	5.37	0.51	22.25	5.42	0.26
FeO	19.52	4.98	13.76	16.13	4.31	10.93	16.55	4.23	10.6
MnO	0.62	0.04	0.14	0.74	0.05	0.16	0.83	0.1	0.13
MgO	12.51	14.64	29.04	15.43	12.77	31.58	15.16	12.64	31.49
CaO	4.95	20.93	0.22	3.57	17.56	0.17	3.7	17.87	0.13
Na_2O	0.01	1.47	0.02	0.01	3.81	0.03	0.01	3.74	0.01
TiO	-	0.07	0.01	0.02	0.08	0.01	0.02	0.09	0.02
Cr_2O_3	0.17	0.09	0.01	0.28	0.5	0.02	0.49	0.77	0.02
Total	100.56	97.82	98.13	100.79	98.86	99.82	100.38	98.53	99.07
cations (p.f.u.)									
Si	3.04	1.98	1.98	3.06	1.93	1.99	3.04	1.92	2
Al	1.92	0.11	0.02	1.95	0.22	0.02	1.93	0.23	0.01
Fe^{2+}	1.21	0.12	0.4	0.98	0.13	0.31	1.02	0.13	0.31
Fe^{3+}	-	0.03	0.02	-	-	0.01	-	-	-
Mn	0.04	-	-	0.05	-	-	0.05	-	-
Mg	1.39	0.81	1.57	1.68	0.68	1.66	1.66	0.67	1.66
Ca	0.39	0.83	0.01	0.28	0.67	0.01	0.29	0.69	-
Na	-	0.11	-	-	0.26	-	-	0.26	-
Ti	-	-	-	-	0.1	-	-	0.1	-
Cr	-	-	-	-	-	-	-	-	-
total	8	4	4	8.00	4.00	4.00	8	4	4
Mg#	0.53	0.84	0.79	0.63	0.84	0.84	0.62	0.84	0.84
end-members									
Pyrope	45.7	-	-	56.16	-	-	54.96	-	-
Almandine	41.3	-	-	34.5	-	-	35.38	-	-
Grossular	13	-	-	9.34	-	-	9.66	-	-
Spessartine	1.29	-	-	1.53	-	-	1.71	-	-
Enstatite	-	45.95	79.55	-	45.90	83.81	-	45.37	83.91
Ferrosilite	-	6.81	20.02	-	8.70	15.86	-	8.52	15.85
Wollastonite	-	47.24	-	-	45.40	-	-	46.11	-
En+Fs+Wo	-	87.68	-	-	75.13	-	-	75.29	-
Jadeite	-	7.14	-	-	24.87	-	-	24.71	-
Aegirine	-	3.45	-	-	-	-	-	-	-
Albite	-	-	-	-	-	-	-	-	-
Anorthite	-	-	-	-	-	-	-	-	-

Table 5.5. Selected analyses in sample 10-5B, location I, 17-5A and 17-5C.

	10-5B, location I				17-5A				17-5C, location I			
	P(NNG08), Al(NG85)		P(BKN90), Al(C91)		P(NNG08), Al(NG85)		P(BKN90), Al(C91)		P(NNG08), Al(NG85)		P(BKN90), Al(C91)	
	P (kbar)	T (ºC)	P (kbar)	T (ºC)	P (kbar)	T (ºC)	P (kbar)	T (ºC)	P (kbar)	T (ºC)	P (kbar)	T (ºC)
T[KroghRavna00]	36.8	796	40.2	818	41.0	935	45.6	968	57.6	1034	66.9	1099
T [Krogh88]	33.1	749	34.6	755	34.3	835	37.0	846	44.7	860	47.2	870
T [Powell85]	39.3	830	42.0	838	42.0	950	45.1	960	52.7	968	56.8	982
T [EG79]	41.9	862	45.0	872	44.0	979	47.2	990	55.1	999	59.8	1016
T [Harley84]	40.9	849	44.9	870	35.5	853	38.8	871	45.5	870	48.8	888
T [BKN90]	37.9	811	39.9	815	32.0	802	34.2	807	33.9	713	33.8	713
T [Wells77]	38.3	816	40.1	816	28.1	744	29.8	744	31.8	685	31.4	685
T [OpxBK90]	42.3	868	45.9	882	30.5	779	32.9	789	37.3	760	38.0	763
T [NaPxBK90]	27.8	681	28.2	681	15.6	560	16.9	562	9.5	385	5.2	380

Table 5.6. Result of PT calculations of 10-5B, location I, 17-5A and 17-5C, location I.

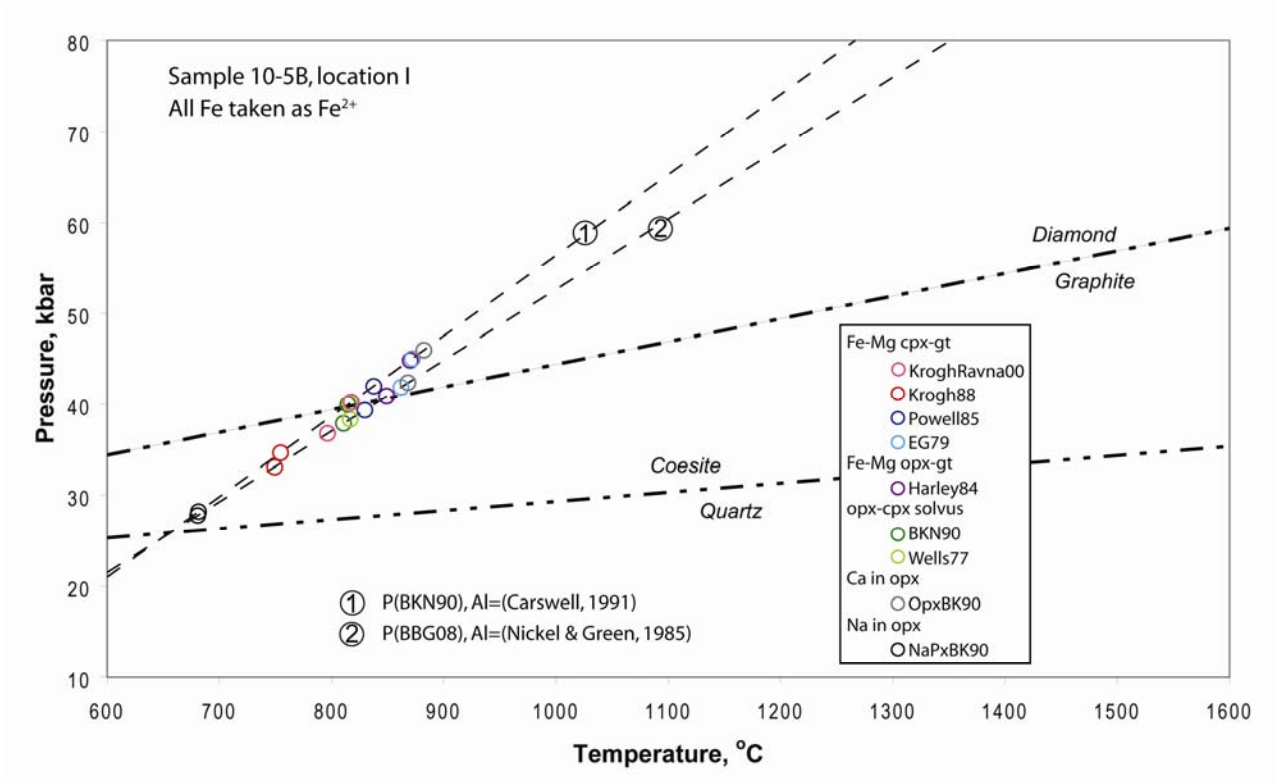

Figure 5.13. PT calculations of sample 10-5B, location I, with analyses as in table 5.5.

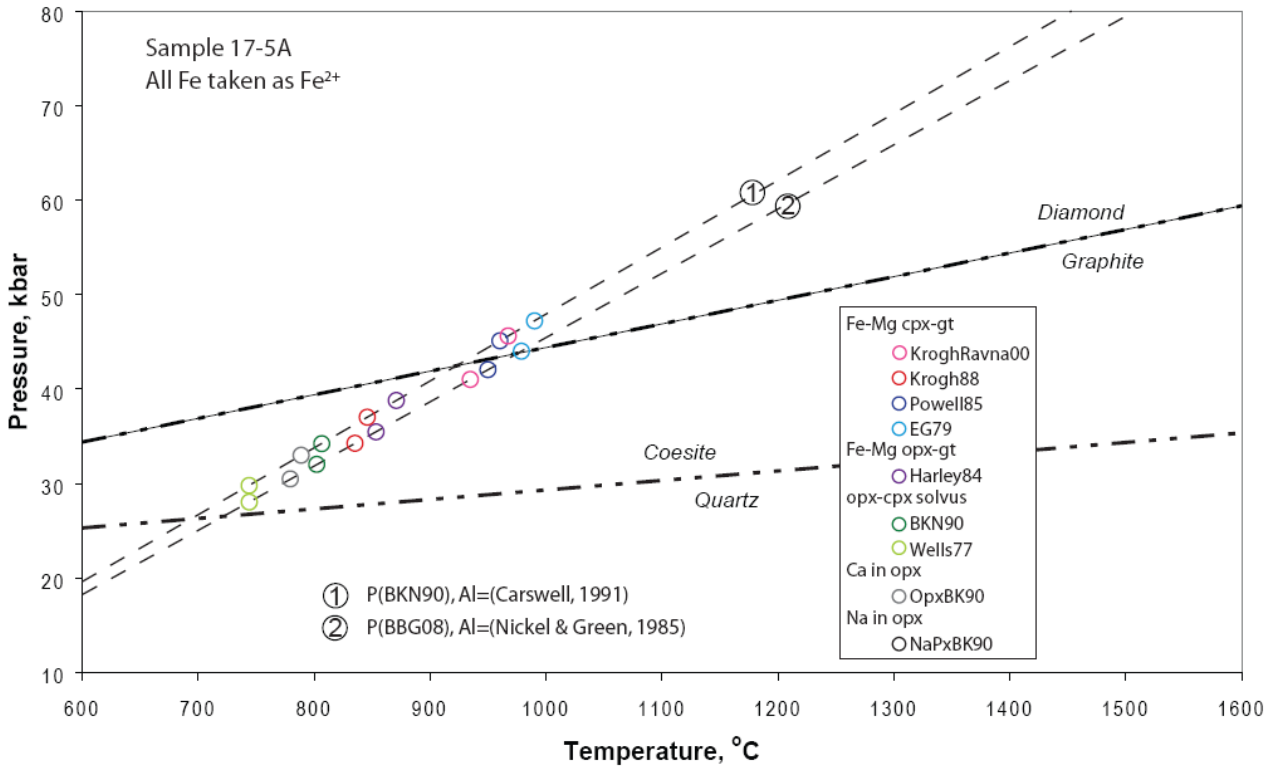

Figure 5.14. PT calculations of sample 17-5A, with analyses as in table 5.5.

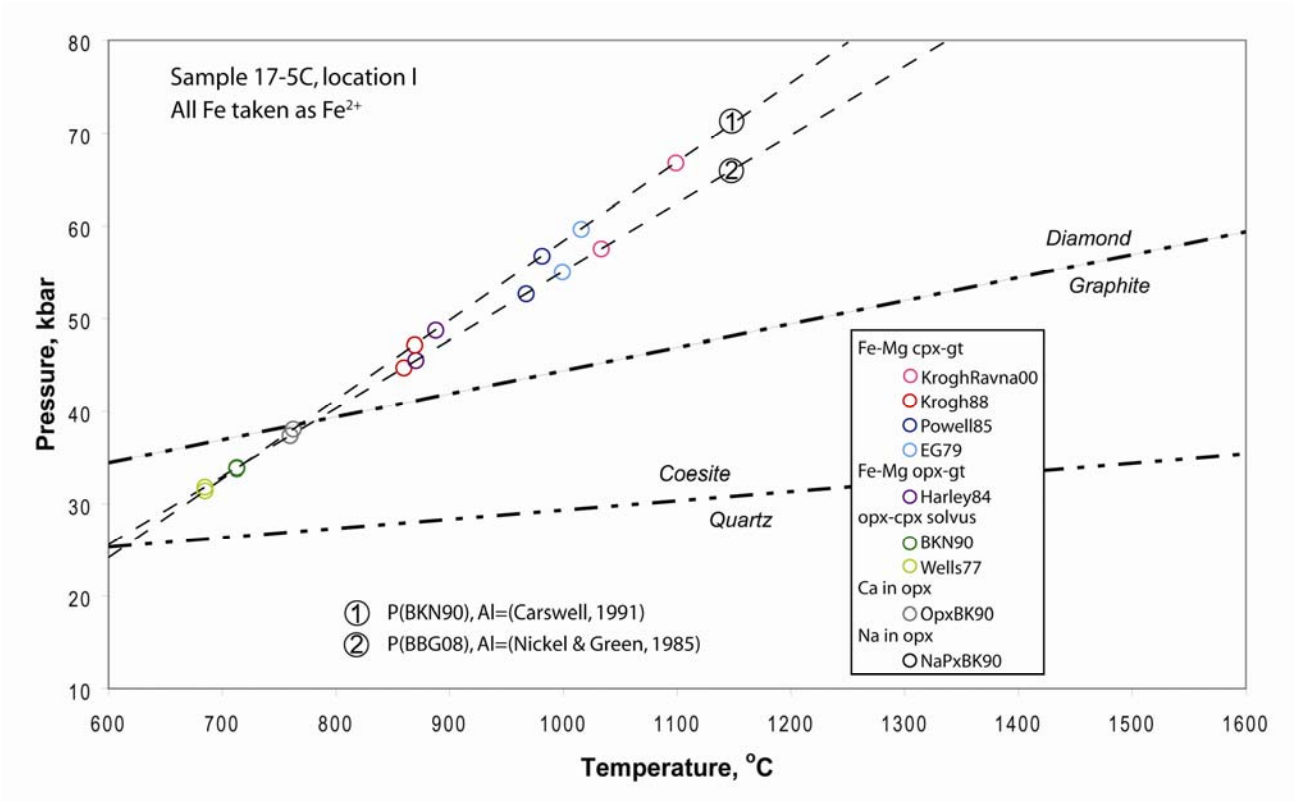

Figure 5.15. PT calculations of sample 17-5C, location I , with analyses as in table 5.5.

5.2.3 Discussion

10-5B, location I
The PT points calculated in 10-5B, location I, are similar to the results of that thin section in location II, but with lower pressures. This makes sense, since the Al_2O_3 content 0.35% in opx is measured, instead of 0.30% in location II. This causes a shift of the location of the geobarometers, but since the elements that influence the geothermometers do not significantly change, the calculated temperatures stay about the same. Like in 10-5B, location II, the geothermometers T(Krogh88) and T(NaPxBK90) give lower PT conditions than the other seven geothermometers that indicate PT conditions around the graphite-diamond transition.

17-5A
At sample 17-5A the lowest Al_2O_3 content in opx is 0.51%. It would be expected that the resultant PT conditions are much lower. Instead, the geothermometers that show the highest PT points are not much lower than the highest PT points in sample 10-5B, location I. This is caused by a difference in Mg# of the garnet. Figure 5.16 shows the end-member profile across a garnet grain in thin section 17-5C, which is representative for all garnets from outcrop 17-5. Compared with the end-member profile from garnet of outcrop 10-5B (see figure 5.5) the pyrope content is higher and almandine lower. This is equivalent to a rise in Mg#, and thus results in higher temperatures as calculated with certain geothermometers (see table 5.1). The lines in PT space of the geobarometers thus have shifted to lower pressures, but the lines of some geothermometers have shifted to that much higher temperatures that the resultant pressure is about the same, but at much higher temperatures. Except for the change in Mg# in garnet, the other elements that influence the geothermometers are quite constant. This causes the geothermometers that are not dependent on the Mg# in grt to indicate much lower PT points, because the geobarometer has shifted to lower pressures because of the high Al content in opx. This causes significant scatter of the PT results between the different geothermometers. Now there is an opposite situation to that of 10-5B, location II, that was calculated with Fe^{3+} (see figure 5.11) because the geothermometers that depend on the Fe^{2+}-Mg exchange between grt and cpx indicate higher PT conditions than the other geothermometers. Calculating Fe^{3+} will cause lower PT results for these thermometers. However, these calculations with Fe^{3+} result in unrealistic low temperatures for this sample below the eclogite facies field.

17-5C
The measurement with the lowest Al_2O_3 content have not been selected for PT calculations, because these have a total compound wt% of <98.5%. These measurements would lead to pressures that are few kbar higher for the highest geothermometers.

Like in 17-5A there is a large spread between the different geothermometers. The Al_2O_3 content of opx is very low, 0.26, which causes overall higher PT results than 17-5A. T(NaPxBK90) results in very low PT conditions, lower visible on this graph.
Although the Al_2O_3 content in opx is lower than in 10-5B, location II, not all geothermometers result in higher PT conditions. The combination of T(KroghRavna00) combined with P(BKN90) with Al(C91) gives P=66.9kbar and T=1099ºC, while T(Wells77) with the same geobarometer gives P=31.4 and T=685ºC. A very large contrast. A division is visible where the geothermometers that use Fe^{2+}-Mg exchange give PT condition (deep) in the diamond stability fields, while the other geothermometers give conditions in between the quartz-coesite and the graphite-diamond stability line.

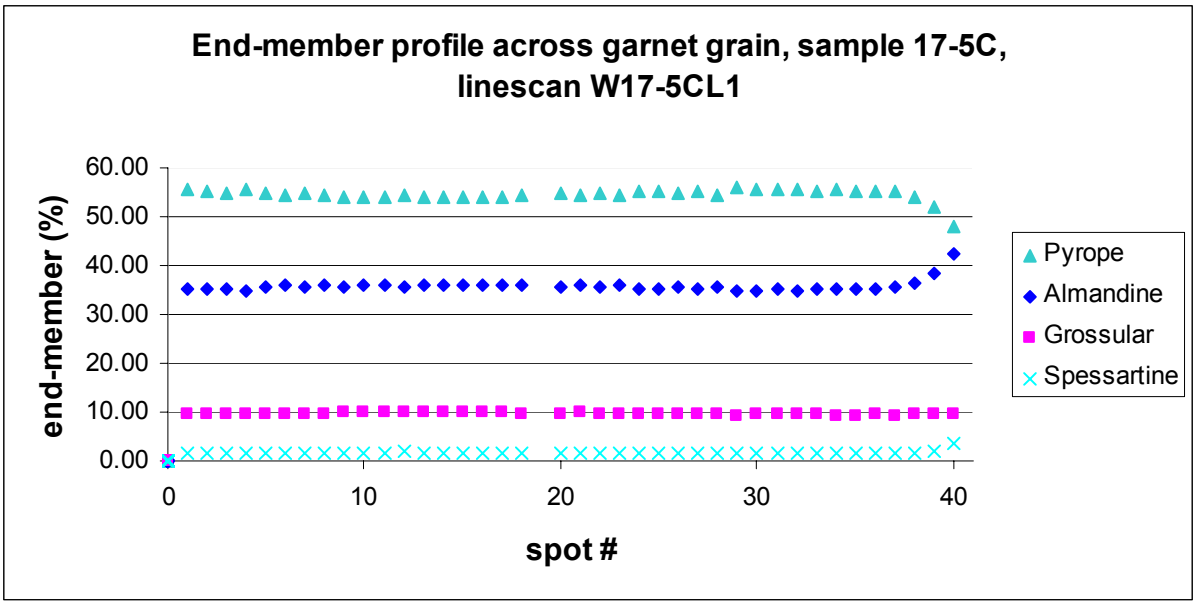

Figure 5.16. End-member profile across grt in 17-5C, location I, linescan 17-5CL1.

Exsolution lamellae in clinopyroxene

The exsolution features that are observed by optical microscopy (see figure 4.5), look very similar to the quartz exsolution lamellae that are reported by (Chopin, 2003), see figure 4.20. Indeed, closer inspection with the EMP reveals that these lamellae do contain quartz, but in combination with hbl (figure 5.17). Every 'needle' is either quartz, hbl or a combination of the two. The larger exsolution 'needle' in the enlargement of figure 5.17 shows that hbl is capped on two sides by qtz. Possibly the other exsolution features are also hbl capped on both sides by qtz, and different 2-D sections through this assemblage cause either one or two of the minerals to be visible. Note that the exsolution is visible in the core of cpx grains, but the rims are relatively exsolution free.

5.3 Additional features: indications for UHP

5.3.1 Qtz and hbl exsolution in clinopyroxene

Qtz lamellae in cpx are thought to be a result of the breakdown of super-silicic cpx. This super-silicic cpx is the non stoichiometric Ca-Eskola component (CaEs) that upon breakdown at lower pressures results in cpx enriched in Ca-Tschermaks component (CaTs) and qtz (Page et al., 2005), following the reaction:

$2Ca_{0.5}\square_{0.5}AlSi_2O_6=CaAl_2SiO_6+3SiO_2$
CaEs=CaTs + qtz

with □ being an empty site

The question then is what pressures are required to form the CaEs component. According to Chopin (2003) super-silicic quartz will only be stable under UHP conditions. Liou et al. (1998) argue that this should even be the diamond stability field. Finding qtz exsolution lamellae is then evidence for the former stability super-silicic cpx, and thus of an UHP (diamond field) origin. These authors do not, however, mention the occurrence of hbl together with qtz as an exsolution product.

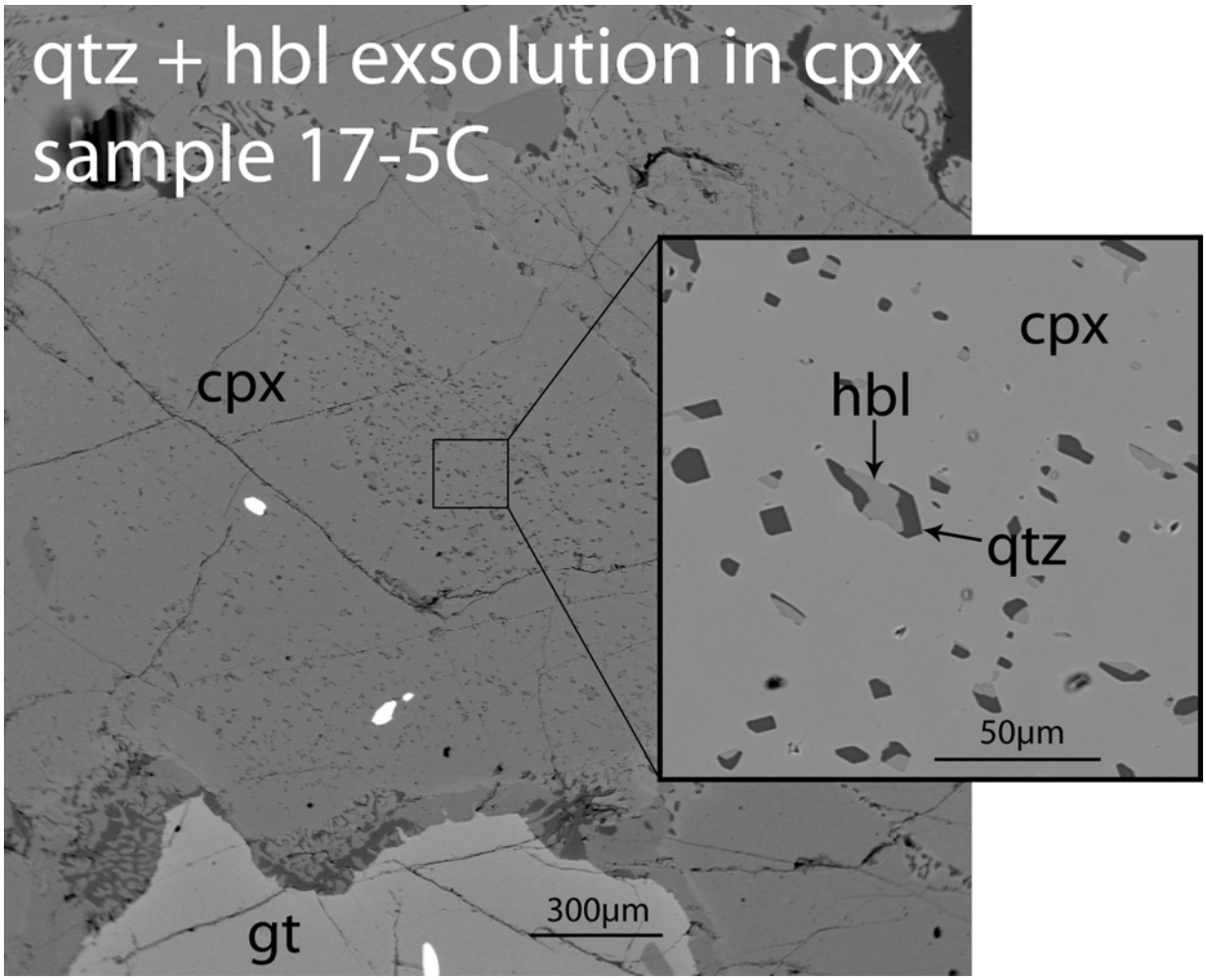

Figure 5.17. EMP image, qtz + hbl exsolution in cpx, sample 17-5A.

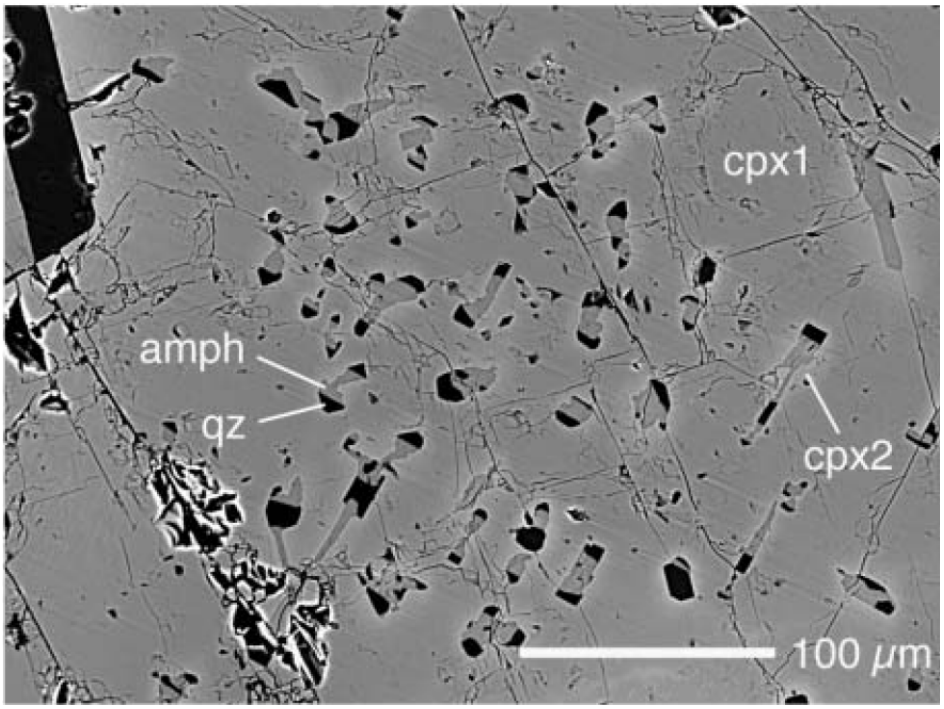

Figure 5.18. BSE image of qtz + amph exsolution in cpx, parallel to cpx c-axis (Page et al., 2005).

Page et al. (2005) report the occurrence of hbl + qtz needles within cpx in an eclogite. An EMP image of these features (figure 5.18) is very similar to the image from sample 17-5A (figure 5.17). It is interpreted to be hbl capped on two sides by qtz, indeed as a breakdown product of CaEs. The reason that many authors only report the presence of qtz exsolution from cpx, instead of hbl + qtz, is attributed to the fact that those observations are done by optical microscopy. With optical microscopy qtz is readily visible, but hbl is almost indistinguishable from the surrounding cpx. Thus according to Page et al. (2005) the qtz exsolution in cpx as reported by other authors is in fact also qtz + hbl exsolution. The exsolution of amphibole is not predicted by the CaEs breakdown reaction as described above. However, according to Bromiley and Keppler (2004) the solubility of water in cpx increases 'drastically' with the presence of CaEs. This would explain the exsolution of amphibole, a water-rich phase, with break-down of CaEs.

The exsolution features as reported by Page et al. (2005) are found in an eclogite which has not experienced UHP conditions. The stability of CaEs solely in the UHP field is therefore questioned. The experiments that have been done to constrain the stability field of CaEs are performed by Gasparik (1985; 1986). According to Page et al. (2005) these experiments have been performed with less chemicals than are present in natural systems, leading to a higher stability field of CaEs in the experiments. CaEs is subsequently misinterpreted by other authors to be an indication of UHPM.

Concluding, the stability field of CaEs has not been determined with a high enough precision. The CaEs component will increase with increasing pressure, which has resulted in the reported qtz exsolution in UHP rocks. The presence of qtz exsolution in UHP rocks does, however, not mean that it is unique to UHPM, and it has been found in HP rocks as well. Therefore the qtz + hbl exsolution lamellae that are found in outcrop 17-5 can not be used as proof of the UHP origin of these eclogites.

5.3.2 Al in opx

The largest influence on PT conditions that are calculated with geobarometry on these eclogites comes from the variation in Al in opx. The samples of outcrop 10-5 have similar grt and cpx compositions, but give different PT results because of difference of the Al content in opx (compare figure 5.11 with figure 5.13). The same holds for outcrop 17-5 (compare figure 5.14 with figure 5.15). For the best approximation of the peak PT conditions the measurement with the lowest Al in opx has to be taken. However, the lowest Al content that is present now, does not have to be the Al concentration that was present at peak PT condition because with retrograde reactions this Al concentration might have gone up. This is illustrated in figure 5.19. Here the current concentration of Al_2O_3 is represented by the solid line, the dotted line t=0 is the inferred concentration at peak PT conditions, and the t=1 line is at a time somewhere in between. The centre of the grain with the lowest concentration is thought to represent the concentration in the entire grain at peak PT conditions, while the concentration of the rest of the grain has gone up since. However, it is unlikely that the Al_2O_3 has changed in the entire grain, except for the place where the lowest concentration are found now. It is possible that there has been a shift in the concentration in the entire grain, with the places near the rim or near cracks are affected most. The peak Al_2O_3 concentrations then might have been lower than the lowest value that is currently present in an opx grain. The t=0 line in figure 5.19, representing peak PT conditions, could therefore is therefore be lower than the current lowest value. For PT conditions this has the implication that the calculated PT conditions are a lower limit, and the peak PT conditions could be even higher.

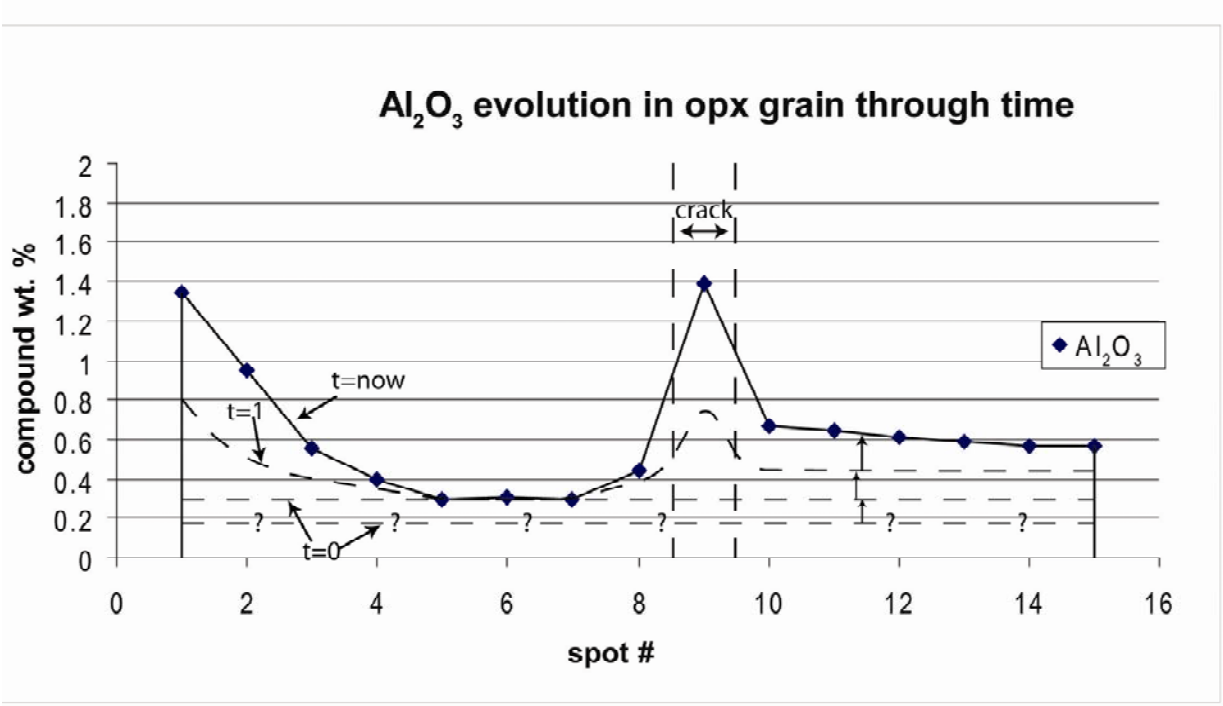

Figure 5.19. Evolution of the Al_2O_3 concentration in opx with t=0 is the concentration at peak PT conditions, t=now is the current concentration, t=1 is at a time somewhere in between, based on linescan W10-5BL7, sample 10-5B.

Another problem is the difficulty which it takes to find the lowest Al_2O_3 that is present within a sample. Figure 5.20 shows the variation in Al_2O_3 in a grain of opx, based on 6 linescans in sample 17-5C. The low concentrations of 0.3 compound wt% or less are restricted to a small area. When random measurements are taken in this grain, there is a high chance that the low concentrations would be missed. Also in samples where the low concentrations are present, it is only in few grains of opx that they are present. Of course a thin section is a 2-D section through the grains. This means that the middle of a grain of opx in a thin section does not have to be the centre of the grain in 3-D, and thus the low Al_2O_3 concentrations might not be present. Only a small percentage of the opx grains that are present do contain the low Al_2O_3 values. For example, samples 10-5C and 10-5E have been investigated on the EMP. In these samples many (±20-30) grains of opx have been measured, but the Al_2O_3 concentrations are mostly ±0.6%, with 0.5% the minimum. Out of the 7 analysed thin sections an Al_2O_3 concentration of 0.3 or less is only found in 2 grains of opx.

Because finding the peak PT conditions requires to find the lowest Al_2O_3 content that are present in an outcrop, some persistence is necessary in measuring opx. Probably the best method is to have multiple samples of one outcrop. In every sample many grains of opx (bordering grt) should be measured in the centre of the grain. If low concentrations are not found, this does not mean that they are not present. Some luck is needed in finding the low concentrations, but measuring the centre of big crystals, some distance from any cracks, and measuring many different grains might increase the chance. In this study linescans have been made across minerals that are found to contain low Al_2O_3 values to find the lowest value that is present in that particular grain.

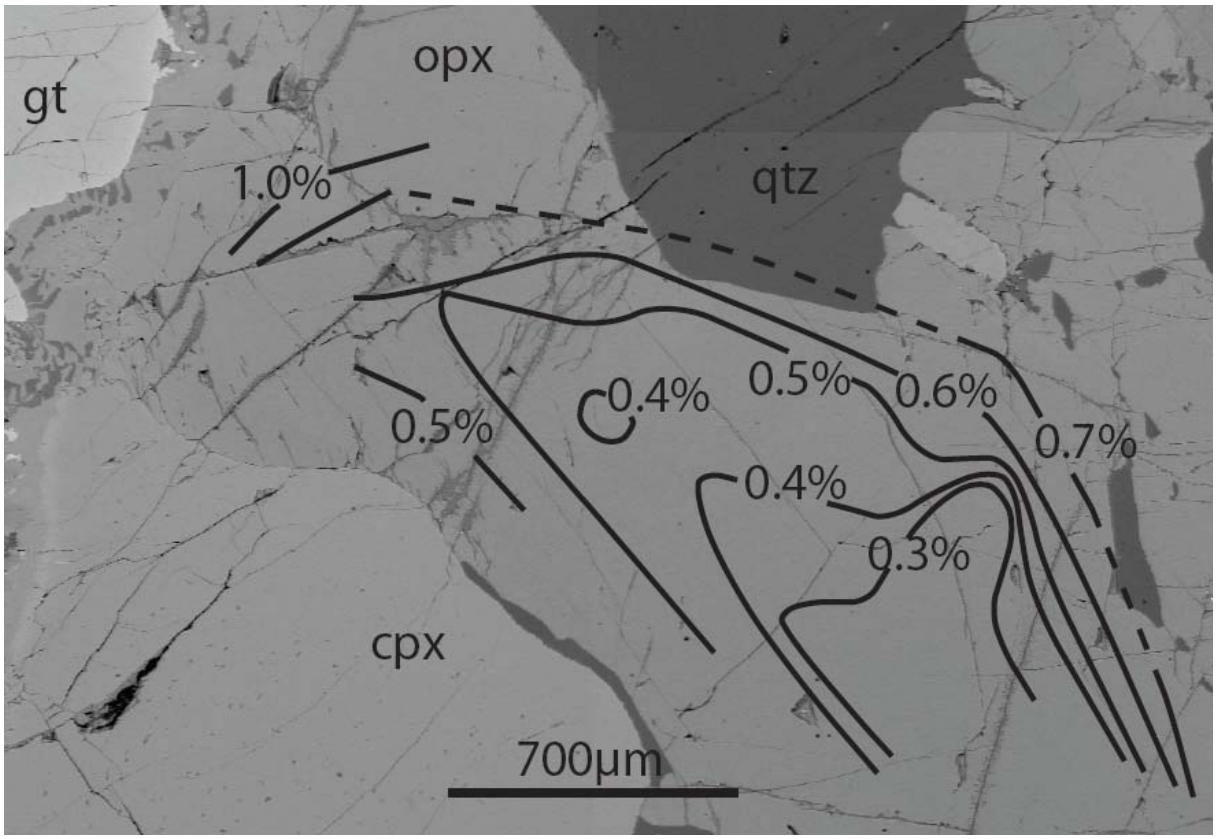

Figure 5.20. EMP image with variation of Al_2O_3 compound wt% within a grain of opx. Based on several linescans as given in Appendix IV, sample 17-5C, location I.

5.3.3 Possible coesite

Figure 5.20 shows a grain of qtz that is bordering opx with very low Al_2O_3 values. If the quartz was already present at peak PT conditions, this should be a grain of coesite or PCQ. With the EMP it is not possible to make a distinction between coesite or quartz. The quartz grain of figure 5.20 is the same as is imaged by optical microscopy, see figure 4.7, but the complete lack of any radial cracks or PCQ structure makes it unlikely that this is coesite or PCQ.

5.4 Results summary

Figure 5.21 gives the summary of all PT calculations in eclogites, as described above. It is constructed by encircling all PT calculations per sample, but ignoring T(Krogh88) and T(NaPxBK90) for reasons already discussed. It can be concluded that the peak PT conditions of the eclogites are indeed in the UHP field (above the quartz-coesite line). Very probably the conditions where within the diamond stability field, as this is the result of sample 10-5B, location II. Some geothermometers even predict conditions deep into the diamond field (max. 66kbar for 17-5C).

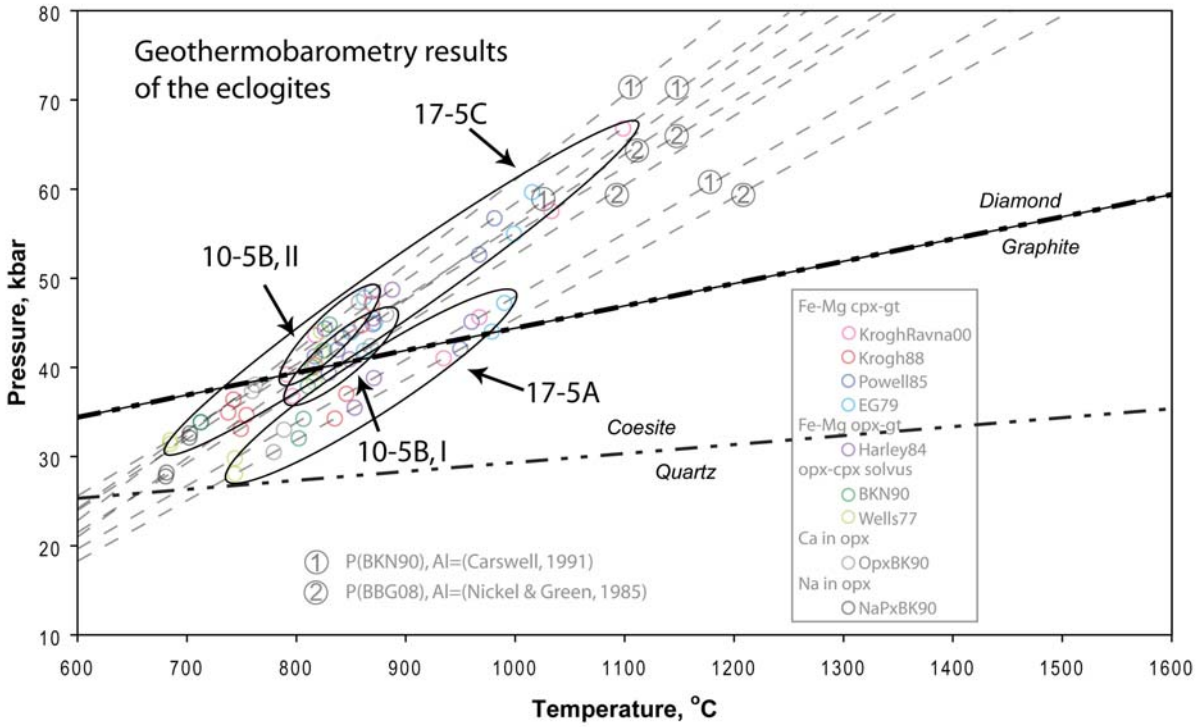

Figure 5.21. Summary of all PT calculations on the eclogites, T(Krogh88) and T(NaPxBK90) are omitted.

6 PT analysis of granulite facies rocks

6.1 Methods

The basics of the EMP analysis of granulite samples is similar to eclogite facies samples (section 5.1), but different geothermo- and geobarometers are used because of the different mineral assemblage.

6.1.1 Geothermo- and geobarometers

The advantage of geobarometry on granulites over eclogites is that on the mineral combination grt + cpx + amph + pl two different barometers can be applied. Both barometers work with different mineral combinations. This means that the result will be more robust because the result of the two different chemical systems, that should result in more or less the same PT conditions, can be compared.
Also the place of the measurements within a mineral can be varied. All of this will lead to significant scatter in the PT results, which makes it too complicated to include many different geothermometers. Therefore the different geobarometers and places of measurement will only be combined with one geothermometer.

All geothermo- and barometers that are used for PT calculations of the granulites are introduced below, the complete formula's are given in appendix II.

The mineral combination grt + cpx + pl:
Geothermometer
The geothermometers that use the Fe^{2+}-Mg exchange between grt and cpx can be used, like with the eclogites. Only one calibration will be used here:

- T(KroghRavna00) (Ravna, 2000)

Geobarometer
The GADS (garnet-anorthite-diopside-SiO_2) geobarometer is based on the reaction:

$$CaAl_2Si_2O_8 + CaMgSi_2O_6 = \tfrac{2}{3}Ca_3Al_2Si_3O_{12} + \tfrac{1}{3}Mg_3Al_2Si_3O_{12} + SiO_2$$

anorthite + diopside = grossular + pyrope + quartz

Two different calibrations will be used:

- P(NP82) (Newton and Perkins, 1982)
- P(EN91) (Eckert et al., 1991)

The mineral combination grt + amph + pl

Geothermometer
Geothermometers that use the exchange of Fe^{2+}-Mg between grt and amph are based on:

$$\tfrac{1}{4}NaCa_2Fe_4Al_3Si_6O_{22}(OH)_2 + \tfrac{1}{3}Mg_3Al_2Si_3O_{12} = \tfrac{1}{4}NaCa_2Mg_4Al_3Si_6O_{22}(OH)_2 + \tfrac{1}{3}Fe_3Al_2Si_3O_{12}$$

ferro-pargasite + pyrope = pargasite + almandine

One calibration of this geothermometer will be used:

- T(GP84) (Graham and Powell, 1984)

Geobarometer
This geobarometer is based on complicated reactions between grt, amph and pl and is given in the appendix. There is one calibration for Mg end-members, and one for Fe end-members:

- P(KS90, Fe) (Kohn and Spear, 1990)
- P(KS90, Mg) (Kohn and Spear, 1990)

6.1.2 The Fe^{3+} problem

Like with the eclogites, the lack of Fe^{3+} data is a problem for geothermobarometry. Calculation of Fe^{3+} is even harder because of the water that is present within the mineral structure of amphibole as OH groups (Bucher and Frey, 2002). Water is not measured by the EMP. This makes the Fe^{3+} calculation more difficult because also assumptions of the water content in amphibole have to be made, before Fe^{3+} can be calculated by charge balance. The best guess that can be made is to calculate Fe^{3+} contents in grt, cpx or pl and assume that this value is valid for amphiboles as well. This is thought to contain too many uncertainties. Fe^{3+} is therefore ignored, and calculations of the granulites are performed with the assumption that $Fe_{tot}=Fe^{2+}$.

6.2 Results

6.2.1 Thin section 11-5A, procedure of a PT analysis

The procedure that has been followed to calculate PT conditions in the granulites will be illustrated with sample 11-5. In this thin section three detailed linescans have been made, which enables the evaluation of compositional change in the minerals. The location of the linescans is given in figure 6.1.

linescan	mineral	# of analyses
W11-5AL1	grt	80
W11-5AL2	cpx + pl	80
W11-5AL4	amph	80

Garnet
The chemical profile of the garnet linescan W11-5AL1 is given in figure 6.2, the end-member profile of the same linescan in figure 6.3. There is a large difference with the garnet composition in eclogites. In eclogites samples 10-5 the pyrope content in garnet is slightly higher than almandine, both between 40 and 45%, and in the samples from outcrop 17-5 the pyrope content is 55% and almandine 35%. The granulite garnets have higher almandine and grossular contents, and lower pyrope. At the rim there is a slight increase in pyrope and decrease in almandine.

Clinopyroxene and plagioclase
Symplectites of clinopyroxene and plagioclase are measured in one linescan. The chemical profile of linescan W11-5AL2 (figure 6.4) is therefore somewhat chaotic. For clinopyroxenes two end-member profiles are constructed. Figure 6.5 gives the end-member profile in the same end-member system that is used for the eclogites, while figure 6.6 also gives the clinopyroxene end-member in the system:

Enstatite+Ferrosilite+Wollastonite	$(Fe, Mg, Ca)_2Si_2O_6$
Jadeite	$NaAlSi_2O_6$
Aegirine	$NaFe^{3+}Si_2O_6$

There is significant compositional variation in the cpx, this is especially apparent in the second end-member profile.

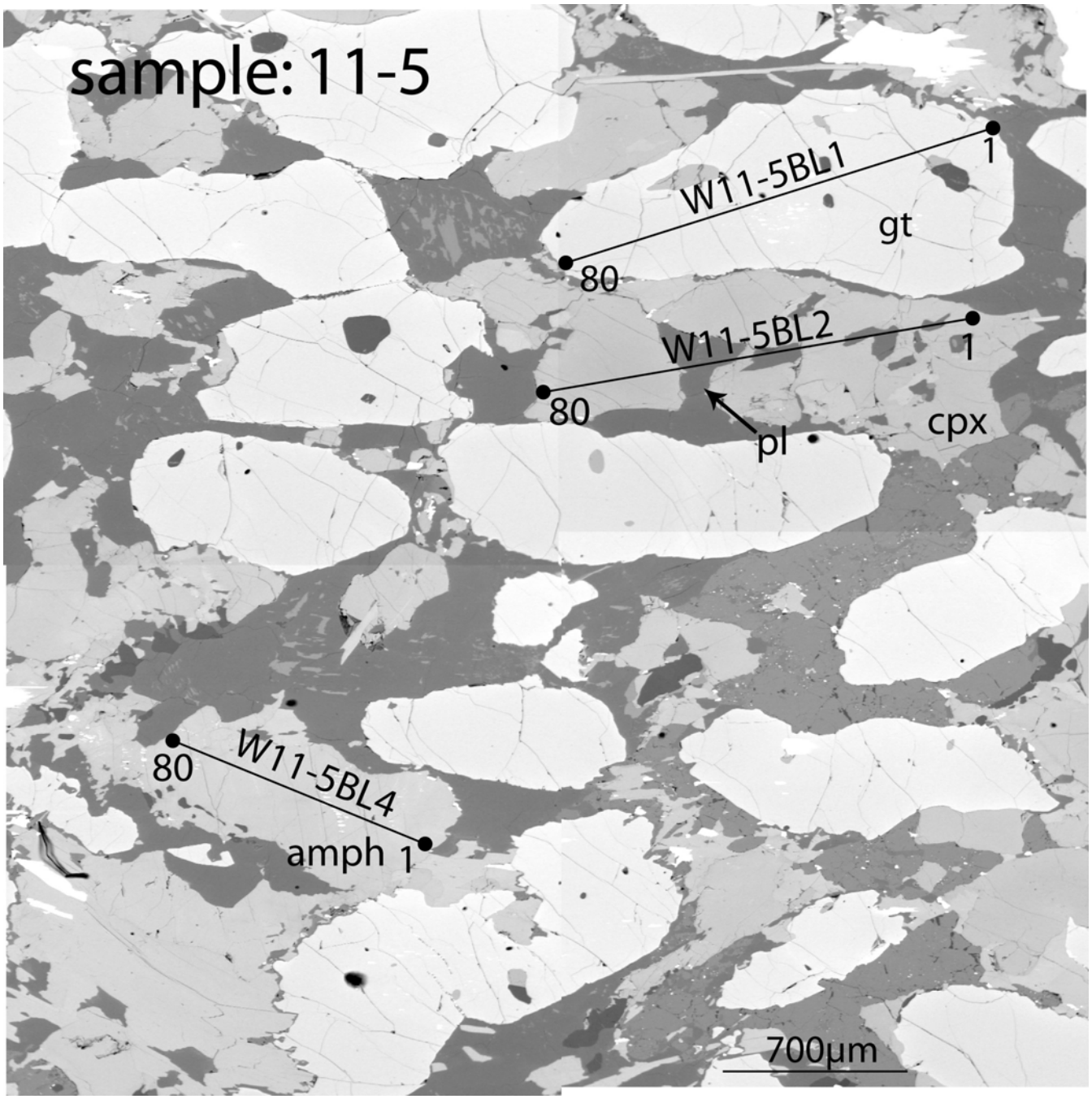

Figure 6.1. EMP image of locations of linescans in sample 11-5A.

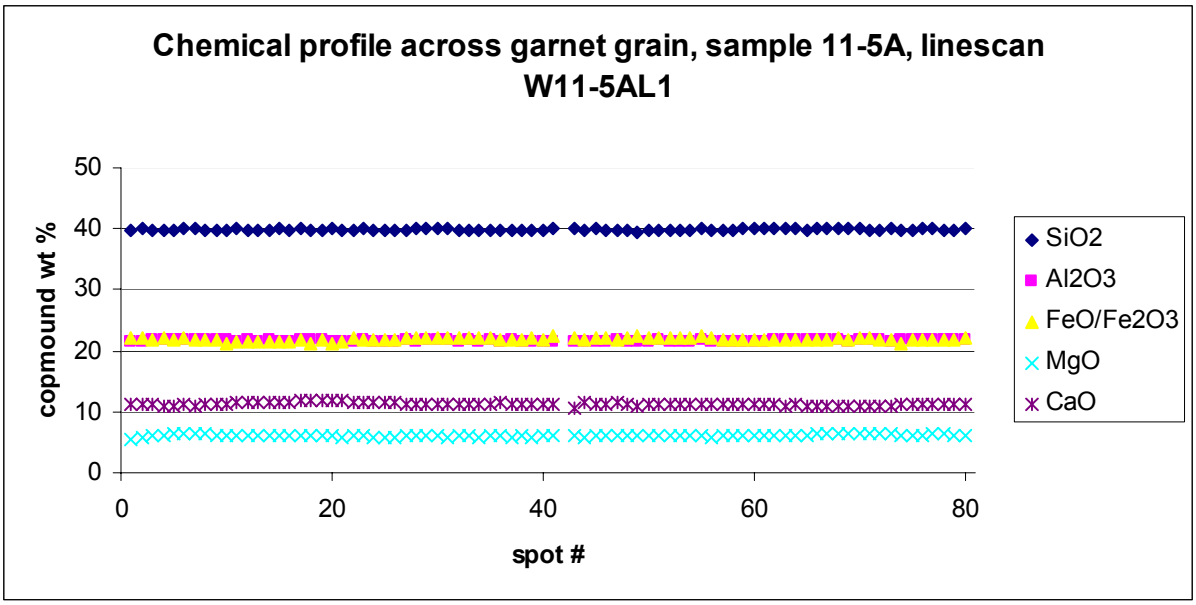

Figure 6.2. Chemical profile across a garnet grain in sample 11-5A, linescan 11-5AL1.

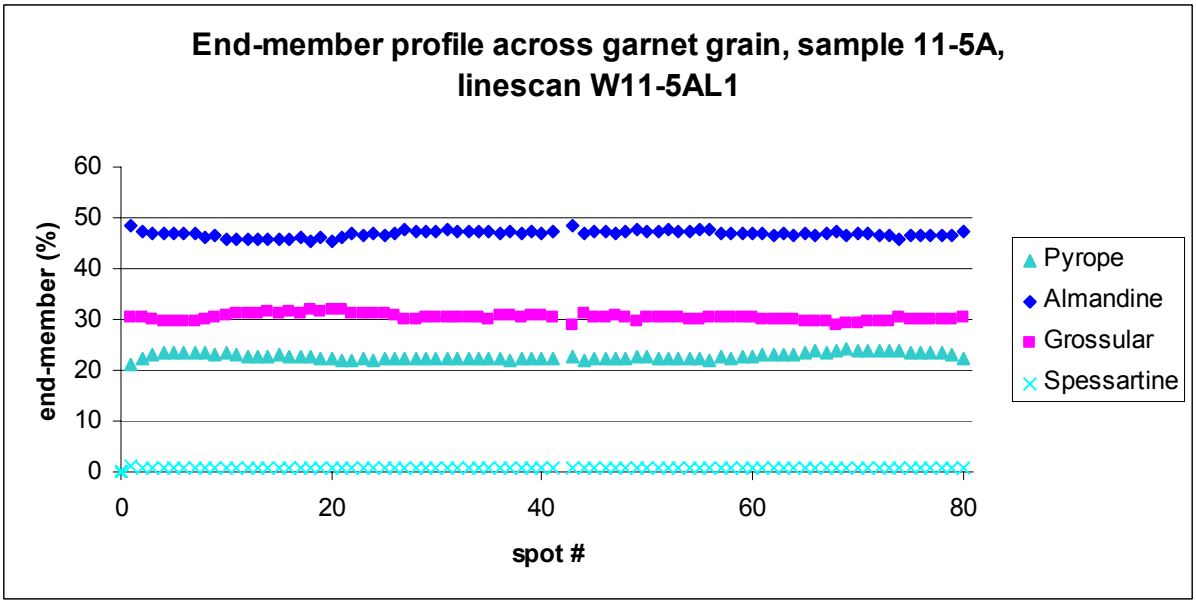

Figure 6.3. End-member profile across a garnet grain in sample 11-5A, linescan 11-5AL1.

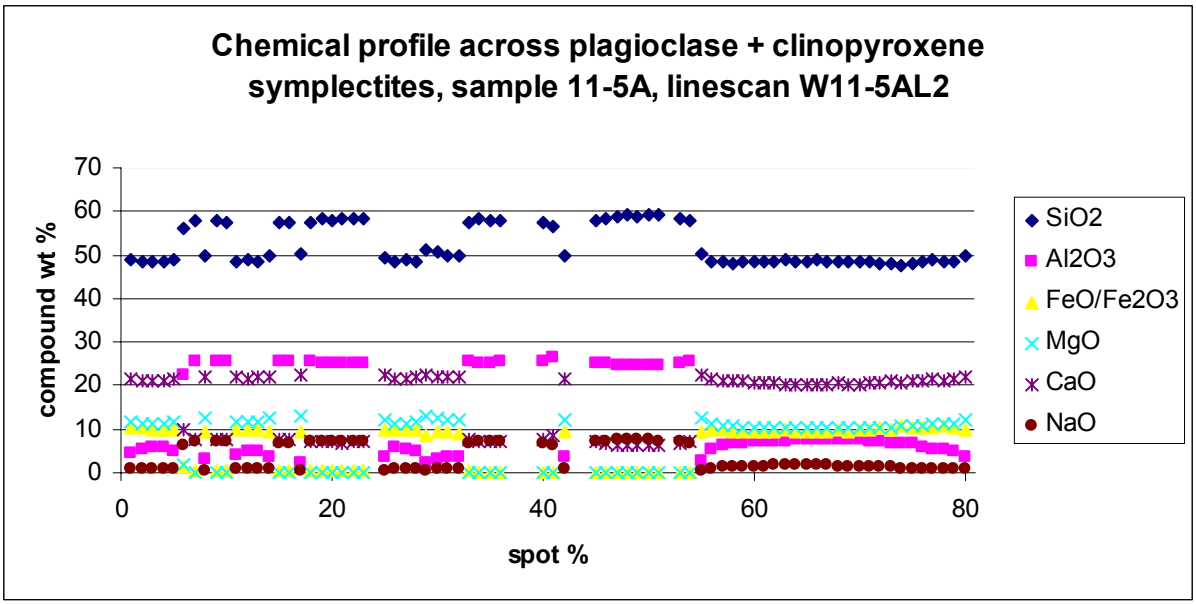

Figure 6.4. Chemical profile across a plagioclase and clinopyroxene symplectite in sample 11-5A, linescan 11-5AL2.

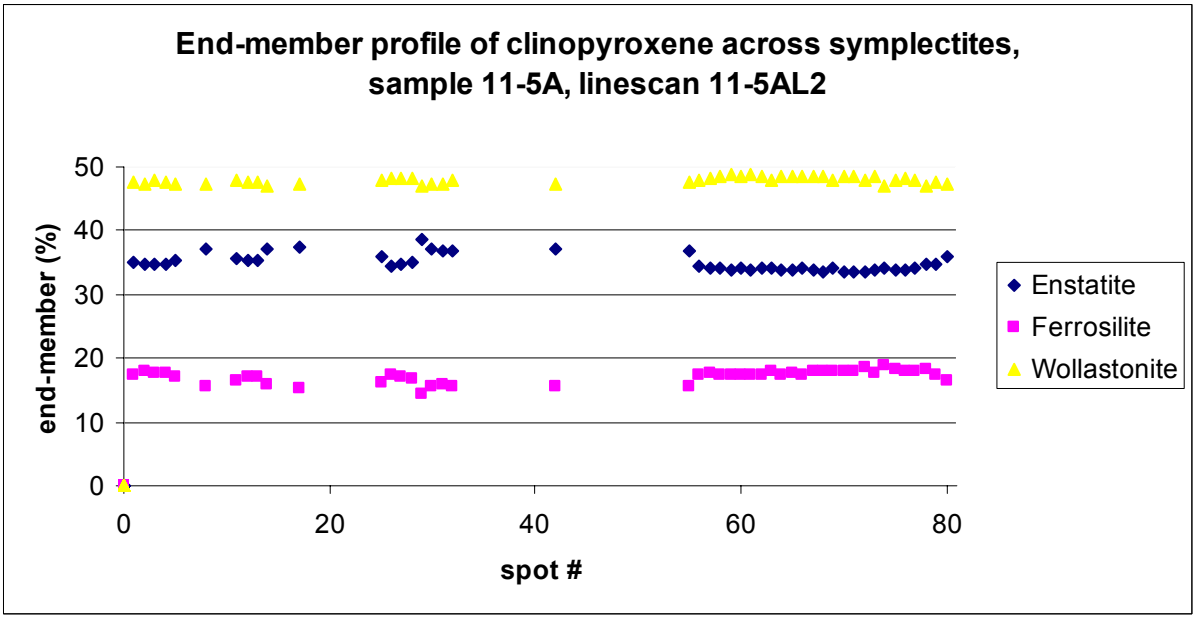

Figure 6.5. End-member profile of clinopyroxene in a plagioclase and clinopyroxene symplectite in sample 11-5A, linescan 11-5AL2.

Clinopyroxene and plagioclase

Symplectites of clinopyroxene and plagioclase are measured in one linescan. The chemical profile of linescan W11-5AL2 (figure 6.4) is therefore somewhat chaotic. For clinopyroxenes two end-member profiles are constructed. Figure 6.5 gives the end-member profile in the same end-member system that is used for the eclogites (see section 5.2.1), while figure 6.6 also gives the clinopyroxene end-member in the system:

Enstatite+Ferrosilite+Wollastonite	$(Fe, Mg, Ca)_2Si_2O_6$
Jadeite	$NaAlSi_2O_6$
Aegirine	$NaFe^{3+}Si_2O_6$

There is significant compositional variation in the cpx, this is especially apparent in the second end-member profile.

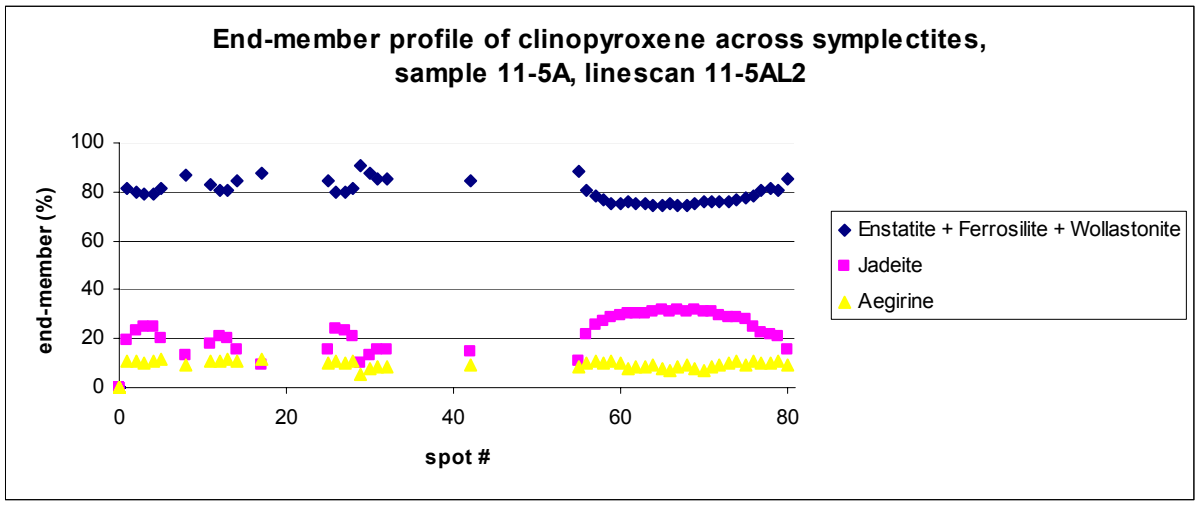

Figure 6.6. End-member profile of clinopyroxene in a plagioclase and clinopyroxene symplectite in sample 11-5A, linescan 11-5AL2.

The end-members of plagioclase are given in the end-member system:

Albite	$NaAlSi_3O_8$
Anorthite	$CaAl_2Si_2O_8$
K-feldspar	$KAlSi_3O_8$

The end-member profile for the plagioclase is given in figure 6.7. Like the cpx, pl also shows considerable variation from its core to the rim. At the rim the anorthite content increases, and the albite content decreases, compared to the core.

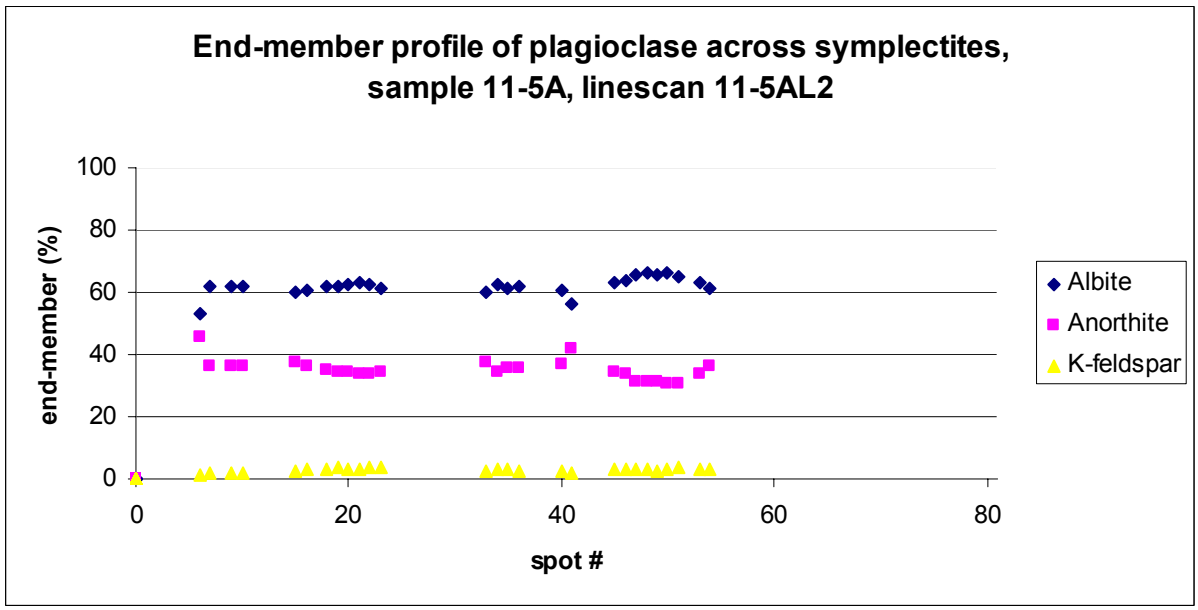

Figure 6.7. End-member profile of plagioclase in a plagioclase and clinopyroxene symplectite in sample 11-5A, linescan 11-5AL2.

Amphiboles

The end-member system for amphiboles is quite complex. The classification scheme by (Leake et al., 1997) is used, which depends on the proportions of a number of elements. Figure 6.8 shows the chemical profile across an amphibole, linescan W11-5AL4, and figure 6.9 the classification diagram for calcic amphiboles. All variation in the amphibole composition is present randomly across the grain, and there is clear difference between core and rim compositions.

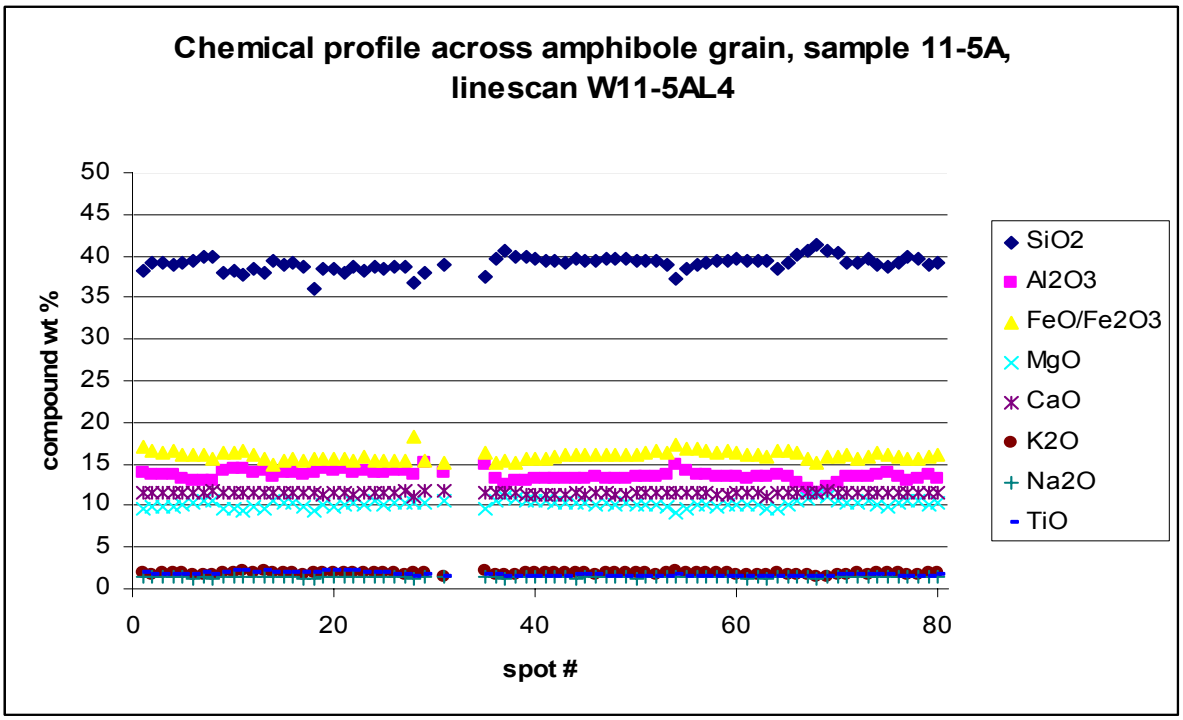

Figure 6.8. Chemical profile across a amphibole grain in thin section 11-5, linescan 11-5AL4.

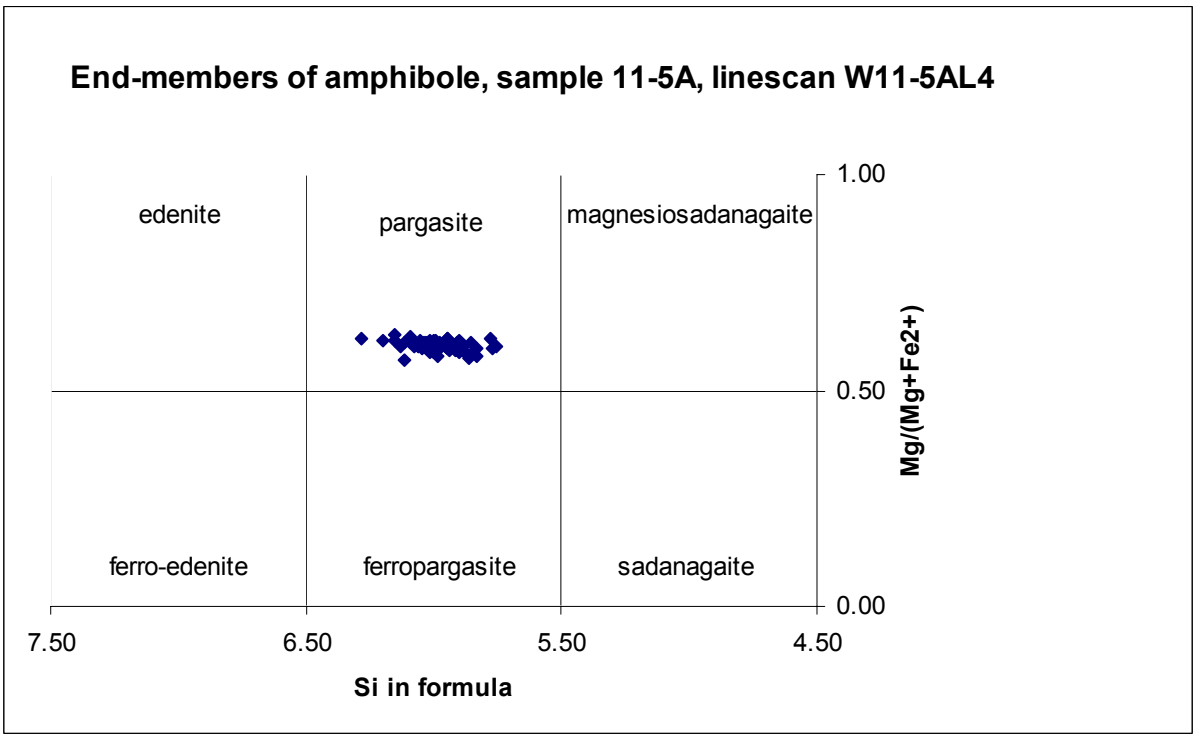

Figure 6.9. End-member profile across an amphibole grain in thin section 11-5, linescan 11-5AL4.

Selecting the measurements

Selecting measurements for geobarometry of granulites is not as straightforward as it is for eclogites. In eclogites the core measurements represent the peak PT conditions. This method is not valid for the granulites, because we are not necessarily interested in maximum PT conditions.

There are two possible origins for the granulites:

1. they are retrograded eclogites, and have been through the same UHP conditions as the eclogites that are measured above. Subsequent recrystallization at granulite facies conditions has changed their mineralogy.
2. The granulites have not experienced the same PT conditions as the eclogites, and their mineralogy is the original mineralogy.

This has implications for the measurements that should be selected for geothermobarometry, because it is necessary to select measurements that represent an equilibrium assemblage. In a geothermobarometric study of granulites Page et al. (2003) make the assumption that the cpx and pl from the symplectites, as well as the amph, are all in equilibrium with the garnet rim. These measurements are then used for PT calculations. This might be a too simplistic view here. Assuming that the granulites are retrogressed eclogites, then the garnets could be relicts of the eclogite stage and the garnet core might have the eclogite facies composition. At lower PT conditions the eclogite cpx recrystallizes to a lower pressure cpx and pl symplectites and new amph grows in the matrix. At those lower PT conditions the garnet rim might change composition. The garnet rim will then be in equilibrium with cpx, pl and amph. However, the cpx and pl symplectites show compositional variation from core to rim. This means that they grew at certain PT conditions, and reequilibrated from their rim at lower PT conditions, or that they have shown continues growth from high to low PT conditions. Either way, it is not known whether the garnet rim is in equilibrium with the core or with the rim of cpx and pl.

Looking at the chemical profile of garnet, there is a large difference with the composition of the garnet in eclogite. Also the garnets look very ‘fresh’, as if there have been very little retrograde reactions (see figure 4.11). This might be an indication that the garnet has recrystallized, and is not the same garnet as that grew at eclogite conditions. In that case the garnet core could very well be in equilibrium with the cpx, pl and amph.

There are thus large uncertainties in what part of which mineral is in equilibrium with what parts of which other minerals. To deal with this problem, two different combinations will be used:

1. combining core measurements of grt, cpx, pl and amph
2. combining rim measurements of grt, cpx, pl and amph

The core measurements give the highest PT conditions, while the rim measurements give the lowest. This method will capture the largest possible spread in PT results, and also represents both possible origins of the granulites (they are either retrogressed eclogites, or they are not). It is of course possible that the grt rim is in chemical equilibrium with the core of cpx, pl and amph, but calculation with these measurements will be in between the PT conditions of all core or all rim measurements. Also the (likely) situation that cpx, pl and amph have not grown at exactly the same time, and thus all are in chemical equilibrium with different parts of the garnet will result in PT points in between the two end-member situations.

The measurements that are selected for 11-5A are given in table 6.1. The EMP analyses are generally not as good as analyses in eclogites, because the total compound wt % of a measurement is often lower than 98.5%. Therefore with these analyses extra care has been

taken to find measurements in between 98.5-101.5%. For both mineral combinations, grt + cpx + pl and grt + amph + pl, two different geobarometer calibrations and one geothermometer are applied to both core and rim measurements. This results in 8 sets of PT results, these are given in table 6.2.

	Sample: 11-5A, core				Sample: 11-5A, core			
Linescan:	W11-5AL1	W11-5AL2	W11-5AL2	W11-5AL4	W11-5AL1	W11-5AL2	W11-5AL2	W11-5AL4
Spot #	69	66	54	44	79	80	50	2
Mineral	grt	cpx	pl	amph	grt	cpx	pl	amph
compound (wt%)								
SiO2	39.92	48.81	57.98	39.60	39.80	49.74	59.25	39.22
Al2O3	21.63	7.54	25.40	13.24	21.69	3.54	24.51	13.69
FeO	21.73	9.31	0.17	16.09	21.73	9.86	0.08	16.49
MnO	0.30	0.03	-	0.11	0.30	0.09	-	0.18
MgO	6.42	10.17	-	10.26	6.17	12.03	-	9.89
CaO	10.87	20.20	7.40	11.42	11.14	21.97	6.26	11.54
K2O	-	-	0.53	1.89	-	-	0.53	1.75
Na2O	-	1.65	6.94	1.31	0.03	0.70	7.54	1.35
TiO	0.04	0.42	-	1.57	0.06	0.19	-	1.72
Cr2O3	-	0.01	-	0.01	-	0.02	0.01	0.01
Total	100.89	98.13	98.43	95.51	100.91	98.15	98.18	95.85
cations (p.f.u.)								
Si	3.04	1.84	2.63	6.04	3.03	1.89	2.69	5.97
Al	1.94	0.34	1.36	2.38	1.95	0.16	1.31	2.46
Fe2+	1.38	0.22	-	1.52	1.38	0.21	-	1.49
Fe3+	-	0.07	0.01	0.66	-	0.10	-	0.69
Mn	0.02	-	-	0.01	0.02	-	-	0.02
Mg	0.73	0.57	-	2.33	0.70	0.68	-	2.25
Ca	0.89	0.82	0.36	1.87	0.91	0.89	0.30	1.88
K	-	-	0.03	0.37	-	-	0.03	0.34
Na	-	0.12	0.61	0.39	0.01	0.05	0.66	0.40
Ti	-	0.01	-	0.18	-	0.01	-	0.20
Cr	-	-	-	-	-	-	-	-
total	8.00	4.00	5.00	15.63	8.00	4.00	5.00	15.62
Mg#	0.34	0.66	0.00	0.53	0.34	0.68	0.00	0.52
end-members								
Pyrope	24.13	-	-	-	23.23	-	-	-
Almandine	46.49	-	-	-	46.59	-	-	-
Grossular	29.38	-	-	-	30.17	-	-	-
Spessartine	0.64	-	-	-	0.64	-	-	-
Enstatite	-	34.00	-	-	-	36.06	-	-
Ferrosilite	-	17.46	-	-	-	16.59	-	-
Wollastonite	-	48.54	-	-	-	47.35	-	-
En+Fs+Wo	-	75.33	-	-	-	85.18	-	-
Jadeite	-	31.37	-	-	-	15.12	-	-
Aegirine	-	6.67	-	-	-	9.59	-	-
Albite	-	-	60.98	-	-	-	66.44	-
Anorthite	-	-	35.94	-	-	-	30.50	-
K-feldspar	-	-	3.08	-	-	-	3.06	-
… amphibole	-	-	-	Calcic	-	-	-	Calcic
Si	-	-	-	6.04	-	-	-	5.97
Mg/(Mg+Fe2+)	-	-	-	0.61	-	-	-	0.60

Table 6.1. Selected measurements for sample 11-5A.

	11-5A			
	core		rim	
	P (kbar)	**T (ºC)**	**P (kbar)**	**T (ºC)**
P(NP82)	14.6	957	11.8	878
P(EN91)	16.7	971	13.9	891
P(KS90,Mg)	12.5	905	11.9	920
P(KS90, Fe)	11.6	905	11.2	920

Table 6.2. PT results for sample 11-5A.

6.2.2 PT calculation on samples 11-3B, 16-3A and 19-3A

Geobarometry has been applied on three other granulite samples: 11-3B, 16-3A and 19-3A. The selected measurements are given in table 6.3, table 6.4 and table 6.5, PT results in table 6.6. A graphical representation of all granulite facies results is given in figure 6.12, figure 6.13, figure 6.14 and figure 6.15. For clarity all results have been given twice: once classified per sample, and once classified per geobarometric method.

11-3B

Cpx and pl are measured without K_20. This error means that the relative proportions of all other elements are overestimated. For geothermobarometric results it only introduces a small error. Calculations performed with representative K_2O values from similar minerals in other granulites indicate that there is only an error of 0-0.2kbar and 0-2ºC. This is negligible compared with the difference in PT results that already arises by using different calibrations. This error will therefore be ignored.

The pl grains in the symplectites of this sample are too small too allow separate core and rim measurements. The same pl measurements have therefore been taken to combine with core and rim measurements of the other minerals.

	Sample: 11-3B, core				Sample: 11-3B, core			
Linescan:	W11-3BL1	W11-3BL3	W11-3BL3	W11-3BL6	W11-3BL1	W11-3BL3	W11-3BL3	W11-3BL6
Spot #	28	43	17	10	50	46	17	20
Mineral	grt	cpx	pl	amph	grt	cpx	pl	amph
compound (wt%)								
SiO2	40.04	50.14	62.82	39.47	39.69	50.57	62.82	40.94
Al2O3	21.76	7.66	23.18	14.53	21.62	4.64	23.18	13.60
FeO	22.56	8.13	0.21	14.21	24.11	8.80	0.21	14.13
MnO	0.43	0.08	-	0.13	0.73	0.08	-	0.11
MgO	7.93	10.56	-	10.93	6.95	11.96	-	11.72
CaO	8.16	19.05	4.04	10.57	7.82	20.58	4.04	10.89
K2O	-	-	-	0.98	-	-	-	0.98
Na2O	0.02	2.32	8.81	2.25	-	1.43	8.81	2.33
TiO	0.02	0.34	-	1.74	0.04	0.34	-	1.78
Cr2O3	-	0.02	-	0.02	-	0.03	-	-
Total	100.92	98.30	99.06	94.83	100.96	98.43	99.06	96.48
cations (p.f.u.)								
Si	3.03	1.85	2.65	5.99	3.03	1.88	2.65	6.10
Al	1.94	0.33	1.15	2.60	1.95	0.20	1.15	2.39
Fe2+	1.43	0.25	0.01	1.15	1.54	0.23	0.01	1.19
Fe3+	-	-	-	0.60	-	0.04	-	0.56
Mn	0.03	-	-	0.02	0.05	-	-	0.01
Mg	0.90	0.58	-	2.47	0.79	0.66	-	2.60
Ca	0.66	0.75	0.18	1.72	0.64	0.82	0.18	1.74
K	-	-	-	0.19	-	-	-	0.19
Na	-	0.17	0.72	0.66	-	0.10	0.72	0.67
Ti	-	0.06	0.28	0.20	-	0.04	0.28	0.20
Cr	-	0.01	-	-	-	0.01	-	-
total	8.00	4.00	5.00	15.64	8.00	4.00	5.00	15.66
Mg#	0.39	0.70	0.00	0.58	0.34	0.71	0.00	0.60
end-members								
Pyrope	29.69	-	-	-	26.20	-	-	-
Almandine	48.33	-	-	-	52.59	-	-	-
Grossular	21.97	-	-	-	21.21	-	-	-
Spessartine	0.91	-	-	-	1.55	-	-	-
Enstatite	-	36.76	-	-	-	38.72	-	-
Ferrosilite	-	15.57	-	-	-	13.39	-	-
Wollastonite	-	47.67	-	-	-	47.89	-	-
En+Fs+Wo	-	75.82	-	-	-	83.00	-	-
Jadeite	-	23.47	-	-	-	10.55	-	-
Aegirine	-	-	-	-	-	4.29	-	-
Albite	-	-	79.80	-	-	-	79.80	-
Anorthite	-	-	20.20	-	-	-	20.20	-
K-feldspar	-	-	-	-	-	-	-	-
… amphibole	-	-	-	Calcic	-	-	-	Calcic
Si	-	-	-	5.99	-	-	-	6.10
Mg/(Mg+Fe2+)	-	-	-	0.68	-	-	-	0.69

Table 6.3. Selected measurements for sample 11-3B

	Sample: 19-3A, core				Sample: W19-3A, rim			
Linescan:	W19-3AL2	W19-3AL3	W19-3AL3	W19-3AL4	W19-4AL2	W19-3AL3	W10-3AL3	W19-3AL4
Spot #	5	8	26	17	1	16	34	2
Mineral	grt	cpx	pl	amph	grt	cpx	pl	amph
compound (wt%)								
SiO2	39.00	48.94	62.73	39.39	38.99	49.73	59.26	39.83
Al2O3	21.16	3.60	22.23	12.35	21.08	2.94	24.46	12.13
FeO	25.38	11.37	0.13	17.93	26.23	11.07	0.16	17.82
MnO	0.44	0.18	-	0.10	0.95	0.18	-	0.12
MgO	4.95	11.08	-	9.05	4.47	11.38	-	9.15
CaO	9.10	21.25	3.79	11.08	8.77	22.14	6.42	11.11
K2O	-	-	1.12	1.44	-	-	0.55	1.39
Na2O	0.01	0.66	8.69	1.64	0.01	0.57	7.62	1.55
TiO	0.04	0.32	-	2.10	0.04	0.33	0.01	1.90
Cr2O3	0.01	0.05	-	0.03	-	0.02	0.02	0.01
Total	100.09	97.44	98.70	95.10	100.55	98.37	98.49	95.01
cations (p.f.u.)								
Si	3.04	1.89	2.82	6.10	3.04	1.90	2.68	6.16
Al	1.94	0.16	1.18	2.25	1.93	0.13	1.30	2.21
Fe2+	1.65	0.28	-	1.74	1.71	0.26	-	1.73
Fe3+	-	0.09	-	0.56	-	0.09	0.01	0.56
Mn	0.03	0.01	-	0.01	0.06	0.01	-	0.02
Mg	0.57	0.64	-	2.09	0.52	0.65	-	2.11
Ca	0.76	0.88	0.18	1.84	0.73	0.91	0.31	1.84
K	-	-	0.06	0.28	-	-	0.03	0.27
Na	-	0.05	0.76	0.49	-	0.04	0.67	0.46
Ti	-	0.01	-	0.24	-	0.01	-	0.22
Cr	-	-	-	-	-	-	-	-
total	8.00	4.00	5.00	15.64	8.00	4.00	5.00	15.60
Mg#	0.26	0.63	0.02	0.47	0.23	0.65	0.00	0.48
end-members								
Pyrope	19.04	-	-	-	17.16	-	-	-
Almandine	55.78	-	-	-	58.61	-	-	-
Grossular	25.18	-	-	-	24.22	-	-	-
Spessartine	0.96	-	-	-	2.07	-	-	-
Enstatite	-	33.85	-	-	-	33.96	-	-
Ferrosilite	-	19.48	-	-	-	18.54	-	-
Wollastonite	-	46.67	-	-	-	47.50	-	-
En+Fs+Wo	-	85.60	-	-	-	87.29	-	-
Jadeite	-	15.64	-	-	-	12.72	-	-
Aegirine	-	8.49	-	-	-	8.62	-	-
Albite	-	-	75.45	-	-	-	66.12	-
Anorthite	-	-	18.18	-	-	-	30.75	-
K-feldspar	-	-	6.37	-	-	-	3.13	-
… amphibole	-	-	-	Calcic	-	-	-	Calcic
Si	-	-	-	6.10	-	-	-	6.16
Mg/(Mg+Fe2+)	-	-	-	0.55	-	-	-	0.55

Table 6.4. Selected measurements for sample 19-3A

	Sample: 16-3A, core			Sample: W16-3A, rim		
Linescan:	W16-3AL1	W16-3AL2	W16-3AL2	W16-3AL1	W16-3AL2	W16-3AL2
Spot #	95	42	32	100	56	59
Mineral	grt	cpx	pl	grt	cpx	pl
compound (wt%)						
SiO2	40.29	51.06	61.33	40.10	52.25	61.15
Al2O3	21.70	2.94	23.57	21.71	1.41	23.81
FeO	20.77	8.52	0.18	21.44	7.47	0.14
MnO	0.39	0.06	0.01	0.46	0.06	-
MgO	7.64	13.98	0.08	7.21	13.93	0.01
CaO	10.22	21.07	4.84	10.01	22.59	5.23
K2O	-	-	0.13	-	-	0.10
Na2O	0.04	0.64	8.40	0.01	0.53	8.48
TiO	0.02	0.23	0.01	0.03	0.02	0.02
Cr2O3	0.02	0.01	-	0.02	0.04	0.01
Total	101.09	98.50	98.54	100.98	98.29	98.96
cations (p.f.u.)						
Si	3.04	1.92	2.76	3.04	1.97	2.74
Al	1.93	0.13	1.25	1.94	0.06	1.26
Fe2+	1.31	0.20	0.01	1.36	0.20	-
Fe3+	-	0.07	-	-	0.04	-
Mn	0.03	-	-	0.03	-	-
Mg	0.86	0.78	0.01	0.81	0.78	-
Ca	0.83	0.85	0.23	0.81	0.91	0.25
K	-	-	0.01	-	-	0.01
Na	0.01	0.05	0.73	-	0.04	0.74
Ti	-	0.01	-	-	-	-
Cr	-	-	-	-	-	-
total	8.00	4.00	5.00	8.00	4.00	5.00
Mg#	0.40	0.75	0.43	0.37	0.77	0.08
end-members						
Pyrope	28.43	-	-	26.99	-	-
Almandine	44.23	-	-	46.05	-	-
Grossular	27.34	-	-	26.96	-	-
Spessartine	0.83	-	-	0.98	-	-
Enstatite	-	41.23	-	-	40.53	-
Ferrosilite	-	14.11	-	-	12.20	-
Wollastonite	-	44.66	-	-	47.27	-
En+Fs+Wo	-	88.17	-	-	93.04	-
Jadeite	-	12.55	-	-	6.17	-
Aegirine	-	6.62	-	-	3.91	-
Albite	-	-	75.28	-	-	74.15
Anorthite	-	-	23.95	-	-	25.27
K-feldspar	-	-	0.77	-	-	0.59
… amphibole	-	-	-	-	-	-
Si	-	-	-	-	-	-
Mg/(Mg+Fe2+)	-	-	-	-	-	-

Table 6.5. Selected measurements for sample 16-3A

	11-3B				16-3A	
	core		rim		core	
	P (kbar)	**T (ºC)**	**P (kbar)**	**T (ºC)**	**P (kbar)**	**T (ºC)**
GADS N&P'82	14.90	879	11.80	768	13.50	840
GADS E&N'91	17.00	893	13.90	781	15.60	853
GHPQ K&S'90, Mg	13.60	826	12.40	734	-	-
GHPQ K&S'90, Fe	12.00	826	11.00	734	-	-

	16-3A		19-3A			
	rim		core		rim	
	P (kbar)	**T (ºC)**	**P (kbar)**	**T (ºC)**	**P (kbar)**	**T (ºC)**
GADS N&P'82	11.20	745	11.70	786	8.00	706
GADS E&N'91	13.30	756	13.80	799	10.00	717
GHPQ K&S'90, Mg	-	-	12.90	797	9.50	749
GHPQ K&S'90, Fe	-	-	12.50	797	9.50	749

Table 6.6. PT results of sample 11-3B, 16-3A and 19-3A

6.2.3 PT conditions of symplectites in eclogite

From optical analysis it is apparent that retrogression has taken place in the eclogites as well. Around the garnets a thin kelephytic rim is present, and some cpx grains are partly replaced by symplectites. Thus the same geothermobarometric methods that are used on the granulites can be applied to these eclogites as well. Figure 6.10 shows grt, amph + pl as the kelephytic rim and cpx + pl symplectites. Figure 6.11 shows an end-member profile of the outermost rim of a garnet grain in eclogite sample 17-5C. It is a detailed linescan, and all changes in chemistry take place in the last ±50 µm of the grain.

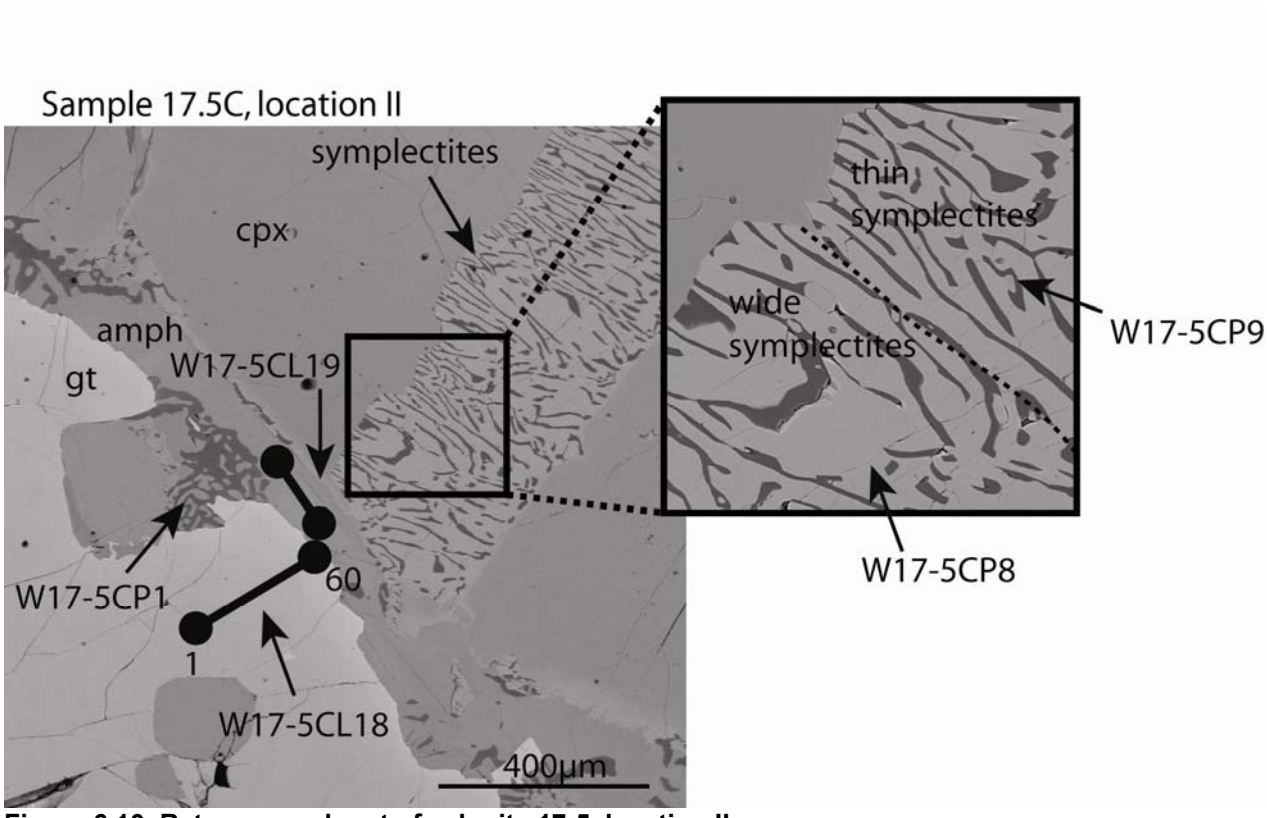

Figure 6.10. Retrogressed part of eclogite 17-5, location II.

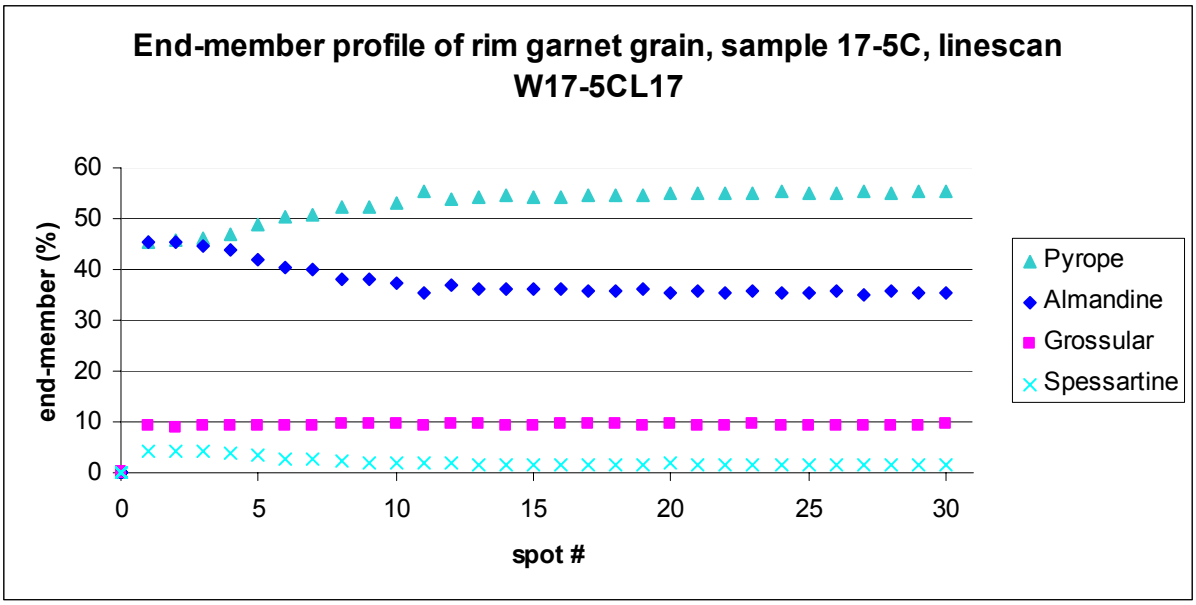

Figure 6.11. Garnet rim in sample 17-5, linescan W17-5CL17.

The width of the symplectites can be seen to be variable. According to Joanny et al. (1991) the width of the symplectite lamellae depends on temperature. The enhanced speed of diffusion and chemical reactions cause wider lamellae to form at higher temperatures and thinner lamellae at lower temperatures. It therefore makes sense that the wide lamellae have grown at higher PT conditions than the small ones. For geobarometry measurements of cpx and pl have been selected from both the wide lamellae (W17-5CP8) and the thin lamellae (W17-5CP9), because they record different PT conditions. These measurement are used in the same way as core and rim measurements in the granulites, so with 'core' measurements of the grt + pl + cpx system it is meant that a core measurement of grt is combined with measurements from wide lamellae of pl and cpx. 'Rim' measurements are the grt rim composition with pl and cpx from thin lamellae.

It should be noted that the smallest symplectite lamellae in sample 17-5C (not visible in figure 6.10) have not been measured, because their size is too small for accurate measurements. The spot size of the EMP is about 3 µm in diameter, so minerals that approach that size cannot be measured, as is the case for some of the thinnest lamellae.

Unfortunately the amph measurements of the kelephytic rim (see figure 6.10) are not good. Geothermobarometry is still possible by combining the pl measurements of the kelephytic rim (W17-5CP1) with measurements of the amphibole grain that is located right next to is (W17-5CL19). The assumption of chemical equilibrium between pl and amph is now somewhat less firm. As we will see the resultant PT conditions calculated with P(KS90, Fe) and P(KS90, Mg) show more deviation than calculations with the other granulites. Possibly this is the result of the poor chemical equilibrium for this mineral combination.

The selected measurements for 17-5C are shown in table 6.8 and PT results in table 6.7.

	17-5C			
	core		rim	
	P (kbar)	**T (ºC)**	**P (kbar)**	**T (ºC)**
P(NP82)	8.3	651	6.9	546
P(EN91)	10.4	665	8.9	558
P(KS90, Mg)	10.2	728	9.5	628
P(KS90, Fe)	6.8	728	6.7	628

Table 6.7. PT results of retrogressed minerals in sample 17.5C.

	Sample: 17-5C, core			17-5C, rim			17-5C, kelephytic rim	
Linescan:	W17-5CL18	W17-5CP8	W17-5CP8	W17-5CL18	W17-5CP9	W17-5CP9	W17-5CL19	W17-5CP1
Spot #	59	3	5	2	4	3	2	1
Mineral	grt, core	cpx, wide	pl, wide	grt, rim	cpx, thin	pl, thin	amp	pl
compound (wt%)								
SiO2	41.33	52.50	62.12	40.49	53.17	62.41	40.68	60.24
Al2O3	22.39	1.76	23.07	21.68	1.66	22.31	15.34	24.11
FeO	16.82	4.67	0.18	20.05	4.23	0.20	8.41	0.14
MnO	0.79	0.12	0.03	1.67	0.07	-	0.14	0.01
MgO	14.93	14.90	0.02	12.27	15.04	0.35	15.04	-
CaO	3.70	21.79	3.90	3.84	22.03	3.94	11.44	5.49
K2O	-	-	0.14	-	-	0.18	0.35	0.10
Na2O	0.02	1.19	9.04	0.01	1.10	8.78	2.95	8.29
TiO	0.02	0.09	-	0.02	0.07	0.01	0.07	0.02
Cr2O3	0.56	0.52	0.01	0.63	0.52	0.01	0.57	0.01
Total	100.57	97.55	98.51	100.66	97.89	98.19	95.00	98.41
cations (p.f.u.)								
Si	3.04	1.96	2.79	3.04	1.98	2.81	5.98	2.72
Al	1.94	0.08	1.22	1.92	0.07	1.19	2.66	1.28
Fe2+	1.03	0.09	0.01	1.25	0.11	0.01	0.34	-
Fe3+	-	0.06	-	0.01	0.02	-	0.65	0.01
Mn	0.05	-	-	0.11	-	-	0.02	-
Mg	1.64	0.83	-	1.37	0.84	0.02	3.30	-
Ca	0.29	0.87	0.19	0.31	0.88	0.19	1.80	0.27
K	-	-	0.01	-	-	0.01	0.07	0.01
Na	-	0.09	0.79	-	0.08	0.77	0.84	0.73
Ti	-	-	-	-	-	-	0.01	-
Cr	-	0.02	-	-	0.02	-	0.07	-
total	8.00	4.00	5.00	8.00	4.00	5.00	15.78	5.00
Mg#	0.61	0.85	0.15	0.52	0.86	0.76	0.76	0.00
end-members								
Pyrope	54.34	-	-	45.06	-	-	-	-
Almandine	35.99	-	-	44.80	-	-	-	-
Grossular	9.68	-	-	10.15	-	-	-	-
Spessartine	1.64	-	-	3.49	-	-	-	-
Enstatite	-	44.90	-	-	45.23	-	-	-
Ferrosilite	-	7.90	-	-	7.14	-	-	-
Wollastonite	-	47.20	-	-	47.64	-	-	-
En+Fs+Wo	-	88.86	-	-	91.18	-	-	-
Jadeite	-	7.71	-	-	7.31	-	-	-
Aegirine	-	6.00	-	-	2.42	-	-	-
Albite	-	-	80.10	-	-	79.30	-	72.80
Anorthite	-	-	19.07	-	-	19.66	-	26.63
K-feldspar	-	-	0.83	-	-	1.04	-	0.56
… amphibole	-	-	-	-	-	-	Calcic	-
Si	-	-	-	-	-	-	5.98	-
Mg/(Mg+Fe2+)	-	-	-	-	-	-	0.91	-

Table 6.8. Measurements for granulite facies mineral assemblage of eclogite sample 17-5C.

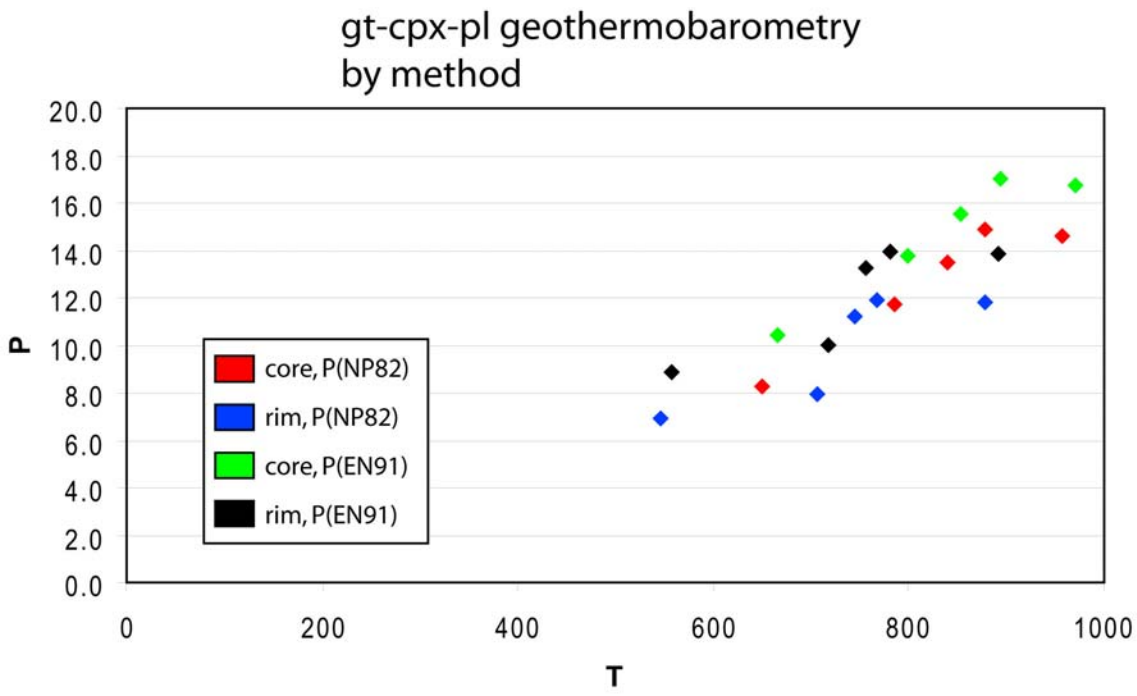

Figure 6.12. PT results of granulite facies in samples 11.3B, 11.5A, 16.3A, 17.5C, 19,3A by grt + cpx + pl geothermobarometry.

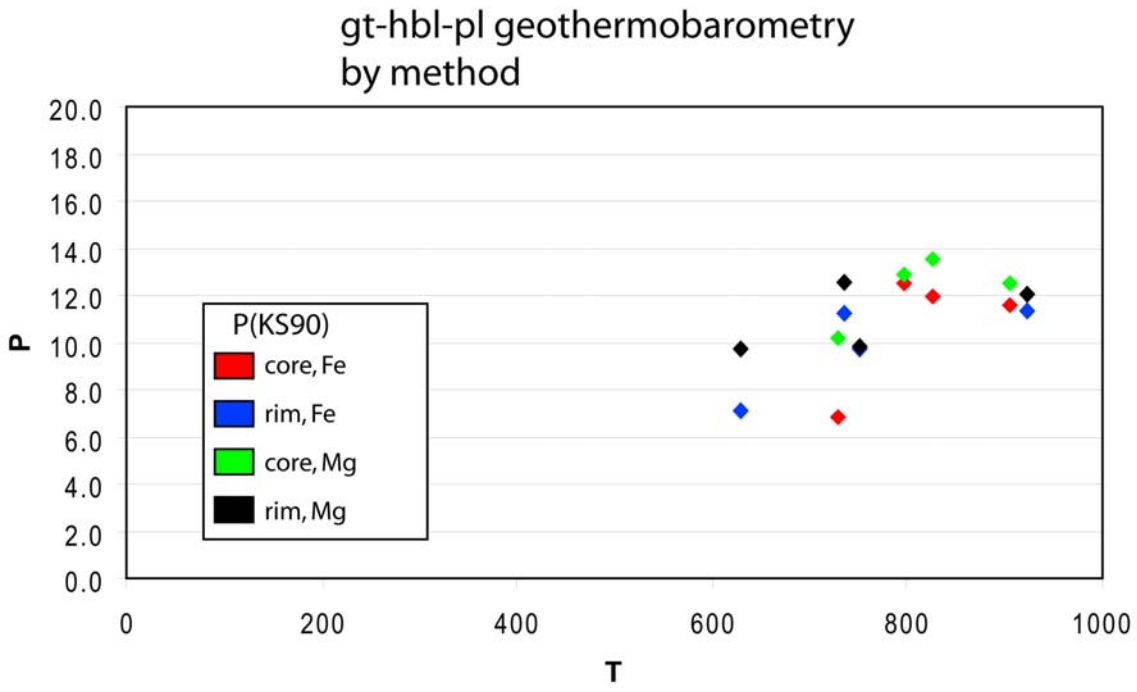

Figure 6.13. PT results of granulite facies in samples 11.3B, 11.5A, 17.5C, 19,3A by grt + amph + pl geothermobarometry.

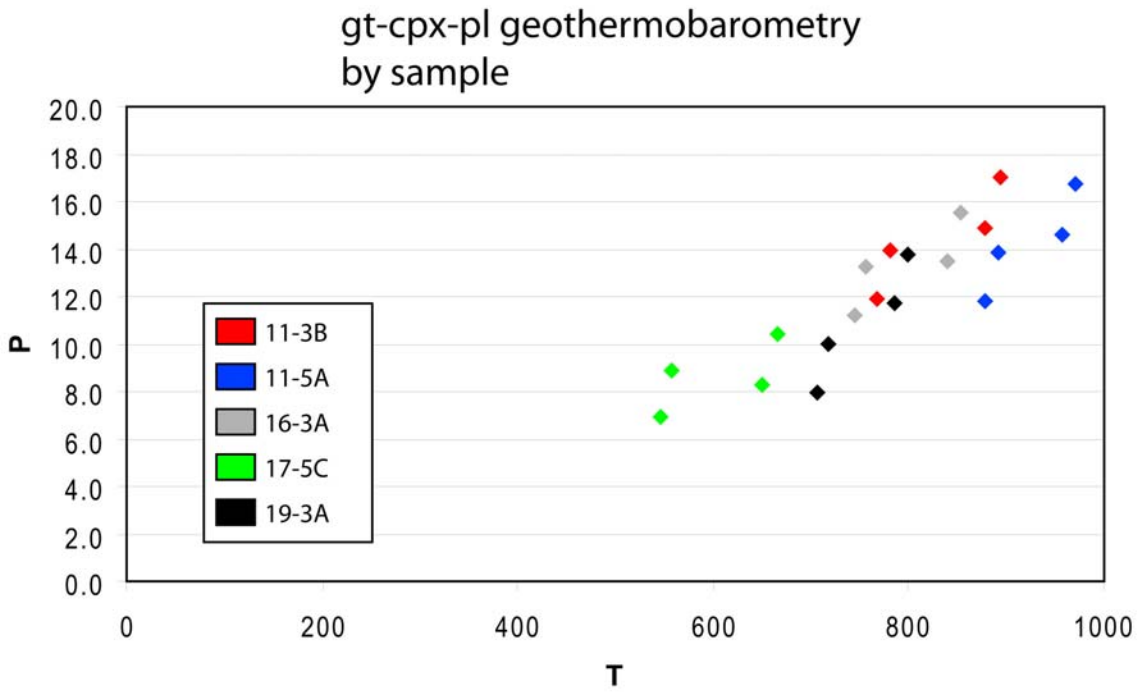

Figure 6.14. PT results of granulite facies of all core and rim calculations by grt + cpx + pl geothermobarometry.

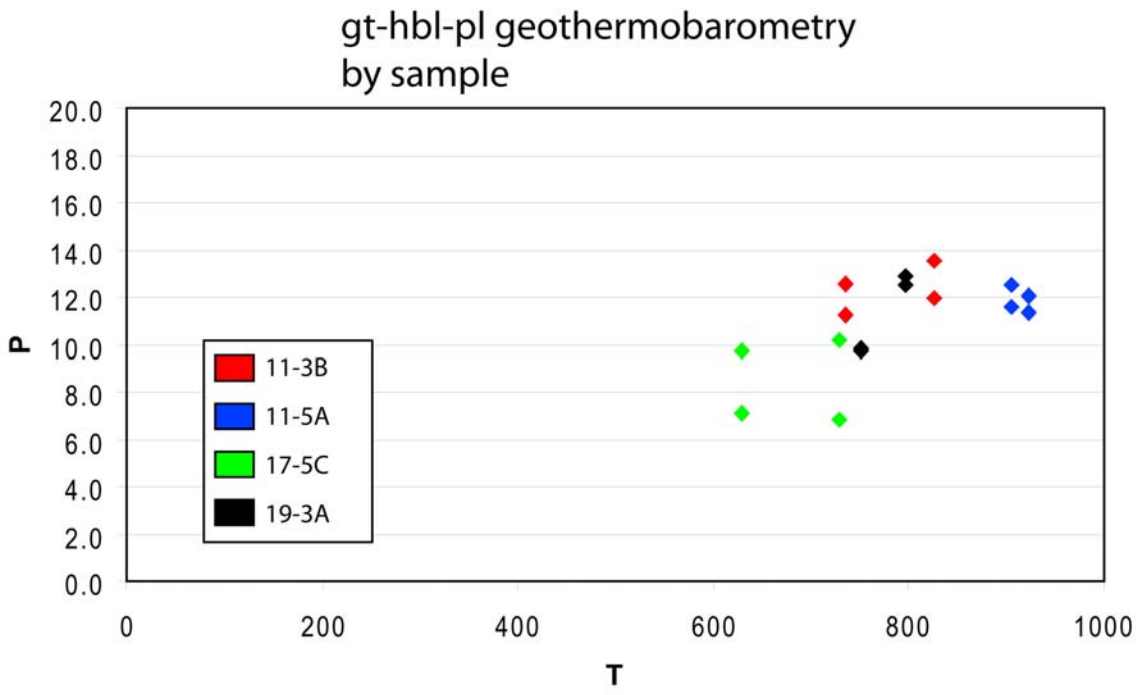

Figure 6.15. PT results of granulite facies of all core and rim calculations by grt + amph + pl geothermobarometry.

6.3 Additional features: possible coesite and relative timing

Possible coesite

The possible PCQ features that have been observed in sample 11.5A are investigated by EMP as well. Figure 6.16 shows approximately the same area as figure 4.12. The composition of the inclusion within cpx reveals that the inclusion is pl, instead if the inferred quartz. In this image the darkest shades are qtz, dark grey is pl, with cpx being a lighter shade of grey. The most hopeful example of coesite in all eclogite and granulite samples, with nice radial cracks, thus turns out to be a pl inclusion. Of course this does not mean that coesite/PCQ is not in these samples at all, but the absence of any PCQ features in quartz in any of the analysed samples indicates that it is likely that all quartz is just 'normal' quartz.

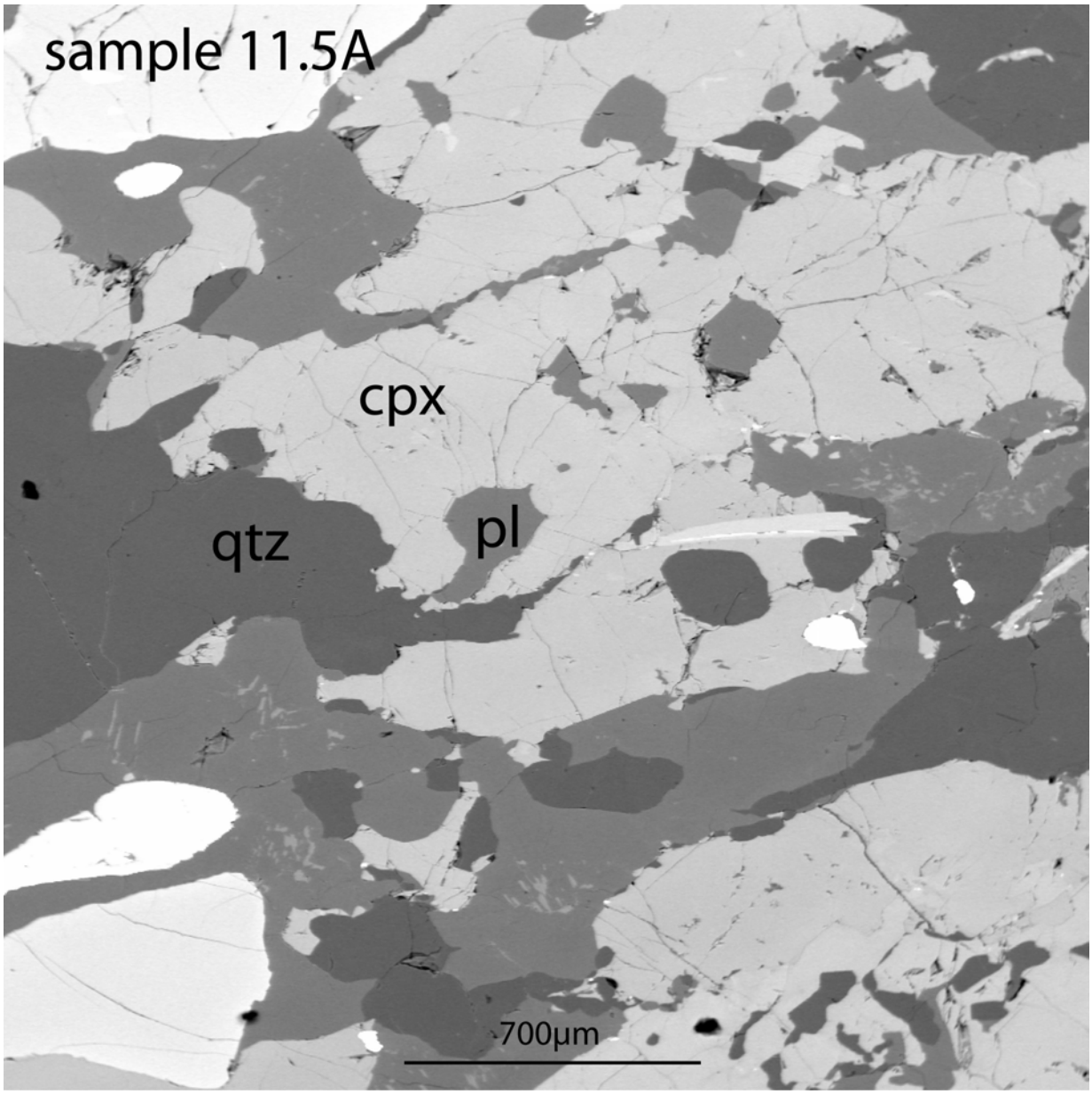

Figure 6.16. EMP image of same area as figure 4.12, qtz is black, pl is dark shade of grey.

Relative timing of cpx symplectites and cpx exsolution

The eclogite samples from outcrop 17-5C show both exsolution of qtz + amph in the centre of cpx grains, and the growth of cpx + pl symplectites at the grain boundaries of cpx. At some locations these features are show some overlap, an example is shown in figure 6.17.At these places there are no signs of any exsolution features present within the symplectites, This means that either the exsolution of qtz + amph has taken place after the formation of the symplectites or that exsolution minerals where recrystallized together with the cpx to form symplectites, thus destroying the exsolution features.

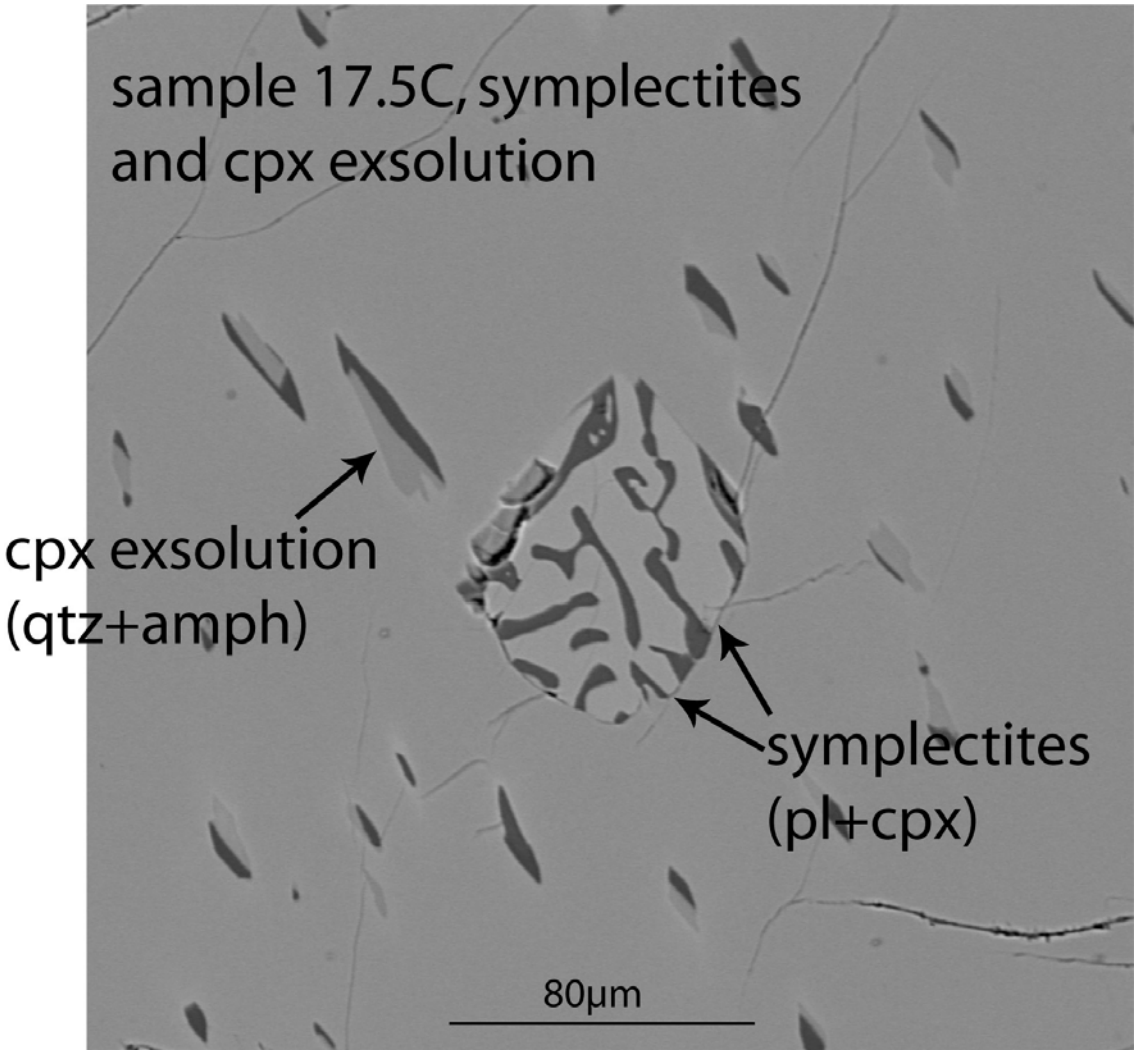

Figure 6.17. EMP image of qtz + amph exsolution and pl + cpx symplectites both form in cpx.

6.4 Results summary

All results of the granulite facies PT conditions in both the granulites and the eclogite sample are given in figure 6.18. Core measurements of grt + cpx + pl geothermobarometry give higher PT points than the rim measurements, but for the mineral combination grt + hbl + pl there is hardly any difference between core and rim measurements. PT points from the retrogressed minerals in eclogite are at lower PT conditions than the granulites.

There is a large variation in calculated PT conditions, from 18kbar and 950ºC for the highest conditions in granulite to 7kbar and 550ºC for the lowest conditions in eclogite. There are two possible explanations for this variation:

1. The different calibrations and different chemical systems that have been measured all contribute with their own error, which result in a large spread in PT conditions. The error margins of the different geothermo- and barometers are:
   P(NP82) 1.8 kbar
   P(EN91) 2.0 kbar
   P(KS90) 0.75kbar
   T(KoghRavna00) 100ºC
   T(GP84) 145ºC
   These errors might explain a significant part of the spread in PT conditions.
2. False assumptions have been made regarding the chemical equilibrium of different mineral combinations. Combining rim or core compositions of all minerals might not be the correct approach and the true equilibrium assemblages might be more subtle, e.g. by combining rim compositions of some minerals with core compositions of others. The current approach of the end-member situation of all core or all rim measurements obviously results in extreme PT conditions.
3. The results represent a PT path and mineral growth from high to low PT conditions has been recorded.

If the explanation is one of the reasons above, or a combination, the retrogressed minerals of the eclogite sample do indicate significantly lower PT conditions (with especially lower temperatures) than the granulites. This will be an important observation in the construction of the PT path in chapter 7.

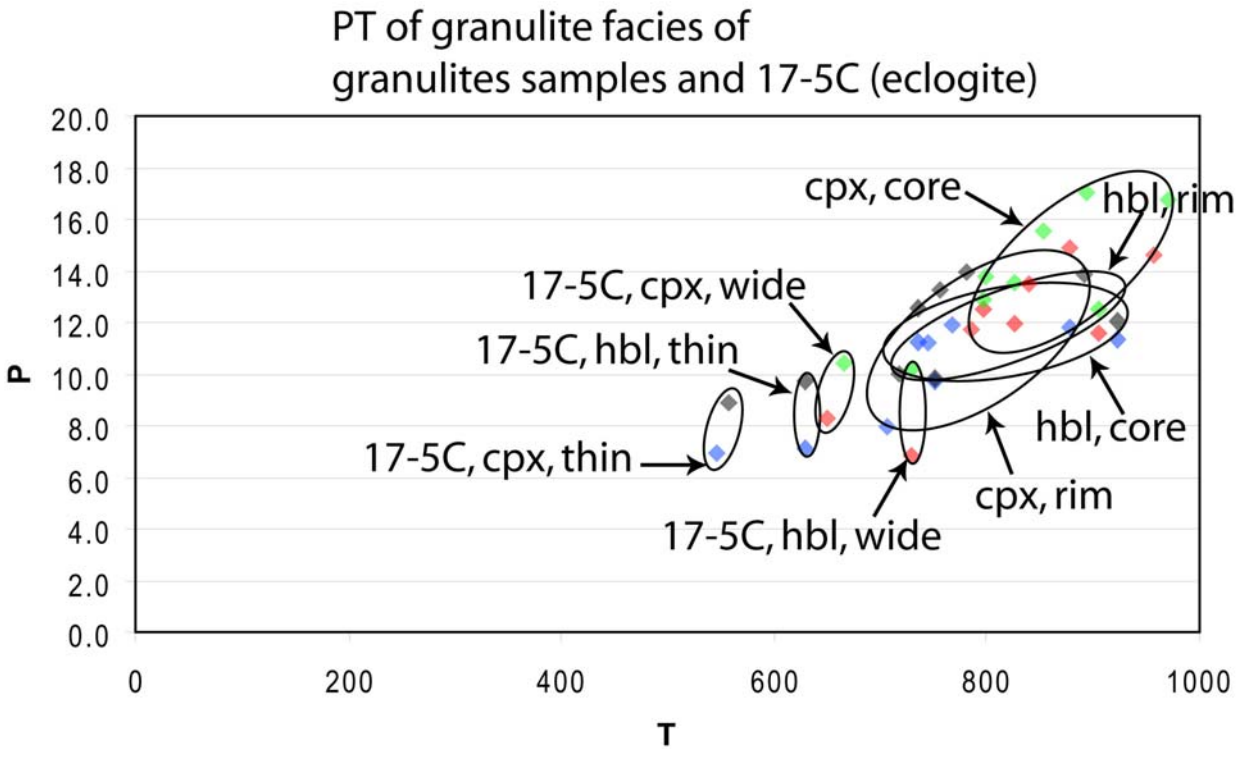

Figure 6.18. Summary of geothermobarometry of the granulite facies of the granulites samples and the granulite facies of 17-5C (eclogite).

7 The PT path

Before all PT results can be connected show to the PT history of the rocks on Gossa, it is vital to answer the question whether all rocks have experienced the same PT path or that rocks with different PT paths together make op the geology on Gossa. If all rock units have experienced the same PT path then the basement gneiss and granulite rocks have experienced eclogite facies metamorphic conditions, just like the eclogite rocks. If this is the case, then the granulites are retrogressed (partly recrystallized) UHP eclogites. Because of retrogression it is impossible to find UHP conditions within the granulites by geothermobarometric methods. Regarding other evidence, there are indications for both an UHP and a non-UHP origin of the granulites:

Arguments against an UHP origin of granulites:

1. If the granulites are retrogressed eclogites, then the eclogites apparently have not been effected by this phase of retrogression. But the retrograde minerals that are found in the eclogites indicate growth of these mineral at the same pressures, but at up to 200ºC lower temperatures (see figure 6.18). This is in accordance with observations done by optical microscopy, where it is shown that the symplectite lamellae in eclogites are much thinner that in granulites, indicating a lower temperature of formation (see e.g. figure 4.4 and figure 4.10). If the granulites are retrograde UHP eclogites, it would seem more likely that the retrogressed parts of the eclogites formed at the same PT conditions as the granulites.
2. Although the symplectites indicate retrogression of the high pressure cpx omphacite, there is no indication of retrogression in garnet. The garnets in granulites show little zoning from core to rim and a complete absence of a kelephytic rim (see e.g. figure 4.11, figure 6.1 and figure 6.2). The presence of zoning and a kelephytic rim are features of the more retrogressed parts of garnets in eclogites (see figure 4.3). If the granulites are retrograde UHP eclogites, then the retrograde reactions that are apparent in some eclogites have not effected the garnet in the granulites. The original garnet composition has been destroyed by complete recrystallization or by diffusion, and the recrystallization of the garnet rim which leads to the growth of a kelephytic rim has not taken place. Again this indicates different PT conditions for the formation of the granulites and the retrograde reactions that have taken place in the eclogites.

Arguments in favour of an UHP origin of the granulites:

1. The difference between temperature in the retrograde parts in eclogites and the formation of granulites is not very large. Considering the 100ºC error margin of the grt-cpx geothermometer and the 145ºC error margin of the grt-amph geothermometer, and the overlap that exists between measurements of the wide symplectites in eclogites and the rim measurements in granulites, the difference in temperature becomes almost negligible.
2. The symplectites in granulites indicate (almost) complete recrystallization of a precursor cpx. This means that the granulites are recrystallized from a former higher pressure rock, possibly the eclogites.
3. The basement rocks show stability in the sillimanite field, and have experienced the reaction sill + kfs → musc. Musc forms an overgrowth of foliation defining minerals, but is not oriented parallel to the foliation itself. This means that the foliation must have formed before the musc forming reaction. The foliation bends around the mafic lenses, both eclogites and granulites, which means that the mafic lenses have been inserted into the basement before the foliation was formed and thus before the musc forming reaction. Because the PT conditions of the retrograde parts of the eclogites are well into the musc stability field, this means that the eclogites where inserted into the basement before these retrograde reactions took place. So the eclogites where already part of the basement, together with the granulites, at higher temperatures

than the calculated PT conditions for the retrograde reactions in the eclogites. Both eclogites and granulites have therefore experienced the same PT history, at least from the time of formation of the foliation.

This last argument, a combination of evidence from field relations, optical microscopy and geothermobarometry, shows that the PT history of the eclogites is linked with the PT conditions that have been obtained for the granulites and the basement rocks. It cannot be proven or rejected that the granulites are retrogressed UHP eclogites. The eclogites, granulites and basement gneisses are proven to have made up one unit at the retrograde path at least from granulite facies conditions. This is an important observation, because it shows that the eclogites have experienced all PT conditions that have been obtained in this study.

The PT path for the eclogites on Gossa is shown in figure 7.1. The thick red arrow contains all PT results from the eclogites and granulites and it crosses the sill + kfs → musc line within the sillimanite field. It should be noted that the quartz-coesite and the graphite diamond line in figure 7.1 come from Ernst and Liou (2008). The positions of these lines are somewhat different from the position of these lines in the plots of the eclogite PT results that are obtained from Kohler (2007), and therefore the intersection of the circles that comprise the geothermobarometric results of the eclogites intersect the stability lines at different position than in figure 5.21.

Ideally the PT path of figure 7.1 would be exactly pinpointed and represented by a thin line. Instead, a thick line is needed to contain all PT data that is obtained in this study. There is an uncertainty of more than 200ºC in the UHP part of the PT path and several kbar in the lower part. There two explanations for this spread in PT results:

1. There is a large uncertainty caused by the methods used for geothermobarometry. The use of 7 geothermometers for the eclogites results in a large spread in both pressure and temperature. This causes the thickness of the PT part in the UHP field. For the lower part of the PT path several methods and mineral combinations have been used, all giving different results. Again, this causes the spread in PT results, and thus a thick PT path is drawn to contain all these results.
2. The lower part of the PT path shows a spread in pressure of several kbars. The lower end is in the sillimanite field, while the higher end is the result of some granulite PT results. This can possibly represent a metamorphic field gradient. The samples are collected at different places in Gossa. If these places, that are currently at the same horizontal level, have been tilted in such a way that they once where situated at different levels and thus different pressure. The maximum pressure difference that is possible between these samples is then the current horizontal distance between these samples, assuming that the current horizontal plane was tilted 90º at time the measured PT conditions. The sillimanite bearing basement samples 12-7, 17-1B and 20-7 are all from the southern basement, and all granulites except 19.3A are collected in the northern basement (see figure 3.7). 19-3A is the granulite sample with the lowest PT conditions, close to the sillimanite field (see figure 6.14 and figure 6.15). The current distance between basement sample 12-7 and granulite 16-3 (which are the closest sillimanite basement and high PT granulite samples) is only about 3 km, corresponding to 1 kbar difference in lithostatic pressure if placed above each other. However, the northern and southern basement probably are connected either by a fold, or represent different thrust units (see figure 3.38 and figure 3.39), which both can have resulted in a greater distance between these units in the past. A metamorphic field gradient as the explanation for the pressure difference between samples from the southern and the northern basement is therefore not ruled out.

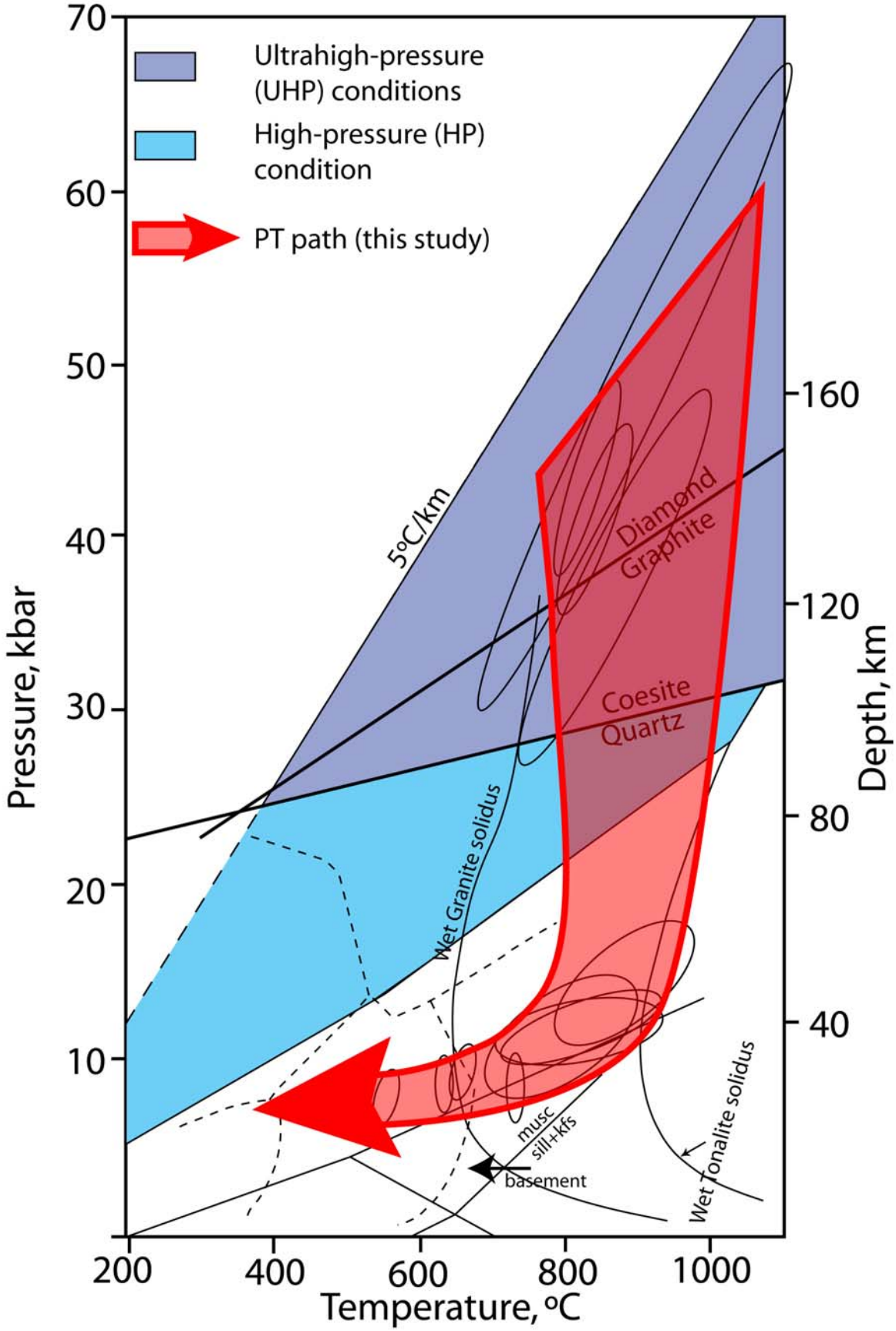

Figure 7.1. PT path obtained in this study (thick red line). Based on results from eclogite facies geobarometry (figure 5.21), granulite facies geobarometry (figure 6.18) and optical microscopy (figure 4.23). Metamorphic facies, Al_2O_3 polymorphs, (U)HP fields, metamorphic facies fields and solidi as in figure 2.2.

Relative timing of events

The construction of the PT path puts some constraints on the relative timing of the events that are discussed so far. The relative timing of events that is shown in figure 7.2 is based on:

1. UHP conditions are the oldest PT results that are obtained in this study, the formation of foliation of eclogite lenses must have been at these PT conditions. From the PT-path it can be deducted that these conditions were present before the crossing of the wet tonalite solidus. This is marked as t=1.
2. The timing between UHP conditions and the insertion of the mafic lenses in the basement is not constrained.
3. Insertion of the mafic lenses took place before the formation of the main basement foliation. This is marked t=2.
4. The conditions at which the granulites formed overlaps with the sill stable field, the tonalite solidus and the formation of retrograde rims in eclogites. Formation of granulite facies foliation has taken place in this timeframe.
5. Formation of the main basement foliation took place outside the musc stable field, but within the sillimanite field. It therefore could very well have started right of the wet tonalite solidus, and therefore overlaps with the wet tonalite melting.
6. The PT path reaches the sill stable field after it crossed the wet tonalite solidus. This is marked t=3.
7. Both folded and unfolded migmatites have been observed in the field. The partial melting of basement has started at least when the tonalite solidus is crossed, and continued until after the formation of the main foliation in the basement gneisses had ended. This means it continued until in the sillimanite stability field.
8. Musc is not a foliation defining mineral, and therefore formation of the foliation had already ended when the musc stable field was entered. This is marked t=4.
9. The retrograde reactions within the eclogites partly overlap with both the granulite formation and the sill stable field.

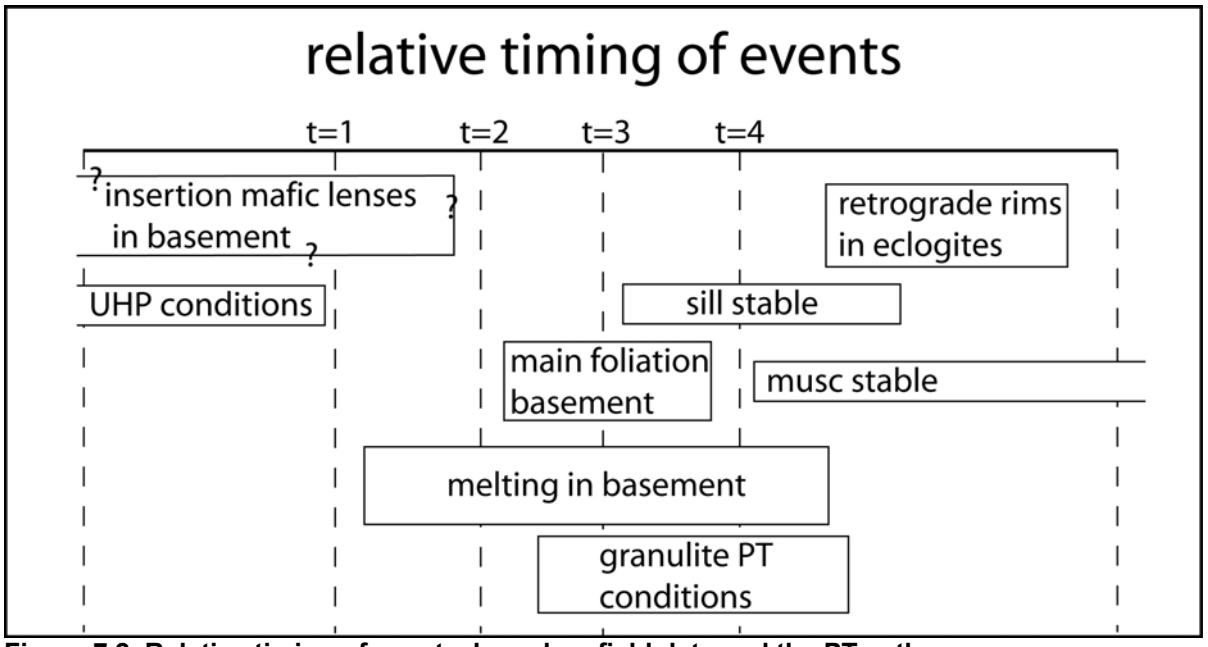

Figure 7.2. Relative timing of events, based on field data and the PT path.

Absence of coesite

Given the evidence that the eclogites have experienced PT conditions far into the coesite stability field and the presence quartz, it seems odd that no indication for the former presence coesite, radial cracks or PCQ, has been found. The presence of quartz in other UHP eclogites is mostly associated with the occurrence of coesite. It has even been argued that the formation of UHP eclogites is triggered by the influx of fluids which often contain Si, and coesite is therefore a common feature in UHP eclogites (Carswell et al., 2005).

However, because of the absence of any coesite/PCQ indications it seems likely that the quartz that is now present in the eclogites has never been coesite and thus was introduced in the eclogites at PT conditions lower than UHP.

One possible explanation is that the quartz is introduced in the eclogites from an external source, possibly from the surrounding granodioritic basement. Another possibility is that the quartz is an accumulation of the exsolution out of cpx. It is observed that the amph + quartz exsolution lamellae are present within the core of cpx, but the rim is relatively free of this (see e.g. figure 4.5 and figure 5.17). The cpx composition of the rim of cpx in eclogites is no different from the core, and so it is unlikely that the exsolution has not happened in the cpx rim as well. Possibly the qtz and amph have diffused out of the cpx crystals and quartz accumulated in the eclogite matrix to form larger quartz grains. This exsolution has happened outside the UHP field (because CaEs is stable within the UHP field) and the quartz therefore has never been coesite, the reason why there are no signs of PCQ found within the eclogites.

8 Comparison of results with literature

The PT path
Figure 8.1 shows the PT path from this study (red line), as well as the PT path obtained by Spengler et al. (in press) from geothermobarometry on peridotites from the island of Fjørtoft and Otrøy, and Svartberget on the mainland (black line). Because Spengler et al. (in press) have chosen to make a PT path based on a single geothermo- and geobarometer pair, the result is a thin line. Their data does, however, show a considerable spread in PT results when different geothermo- and geobarometers are used.

The PT path obtained by Spengler et al. (in press) resembles the PT path from this study. There is some deviation where higher pressures are found in the peridotites. At lower pressures, between 10-20kbar, the PT path by Spengler et al. (in press) indicates lower temperatures between 500-600ºC. Overall, however, the PT paths are not very different. They are quite similar in shape and the deviations are not very large considering that different kind of rocks are used in both studies, what will result in different geothermo- and geobarometers and different errors in the PT estimates.

Also plotted in figure 8.1 is the PT path by Terry et al. (2000b) based on geothermobarometry applied on kyanite bearing eclogites in the region of Fjørtoft and Flemsøy (solid blue line). As discussed in section 2.2.1, a history for this area is proposed where an UHP unit (indicated with 'Path 1') has been thrusted on top of the HP Ulla Gneiss (indicated with "Path 2"). The Ulla Gneiss, with enclosed mafic lenses, are inferred to be non-UHP. In chapter 3.7 it has been shown that the basement gneisses that are found on Gossa correlate with the Ulla Gneiss unit. It is clear that 'Path 1' correlates best with the PT path obtained in this study. This is opposite to the prediction by Terry et al. (2000b) who argue that 'Path 2' is the valid PT path for the Ulla Gneiss.

Is it possible that a setting exists on Gossa where UHP eclogites have been thrusted on top of the LP basement gneisses? No evidence for such a contact between eclogites and basement gneisses has been found. Also the amount of eclogites enclosed in basement gneisses would imply many such contacts in the southern basement. Therefore, in line with observation by Vrijmoed et al. (2006), the entire region from Nordøyane to Gossa to the Bud-Tornes area is better regarded as one coherent UHP province. On Gossa there is no evidence for thrusting of nappes with different PT conditions, as proposed by Terry et al. (2000b).

The reason that Terry et al. (2000b) have not found UHP conditions for the mafic lenses enclosed in the Ulla Gneiss might be because eclogites in that unit in Nordøyane have undergone more retrograde reactions compared to Gossa, or the absence of UHP conditions is due to bad luck. As we have seen not all samples from the UHP outcrops on Gossa do indeed contain low Al_2O_3 values, and by chance non-UHP samples can be collected from UHP outcrops. The absence of proof is in this case no proof of absence, and care should be taken with indicating a non-UHP origin of rock units in this area.

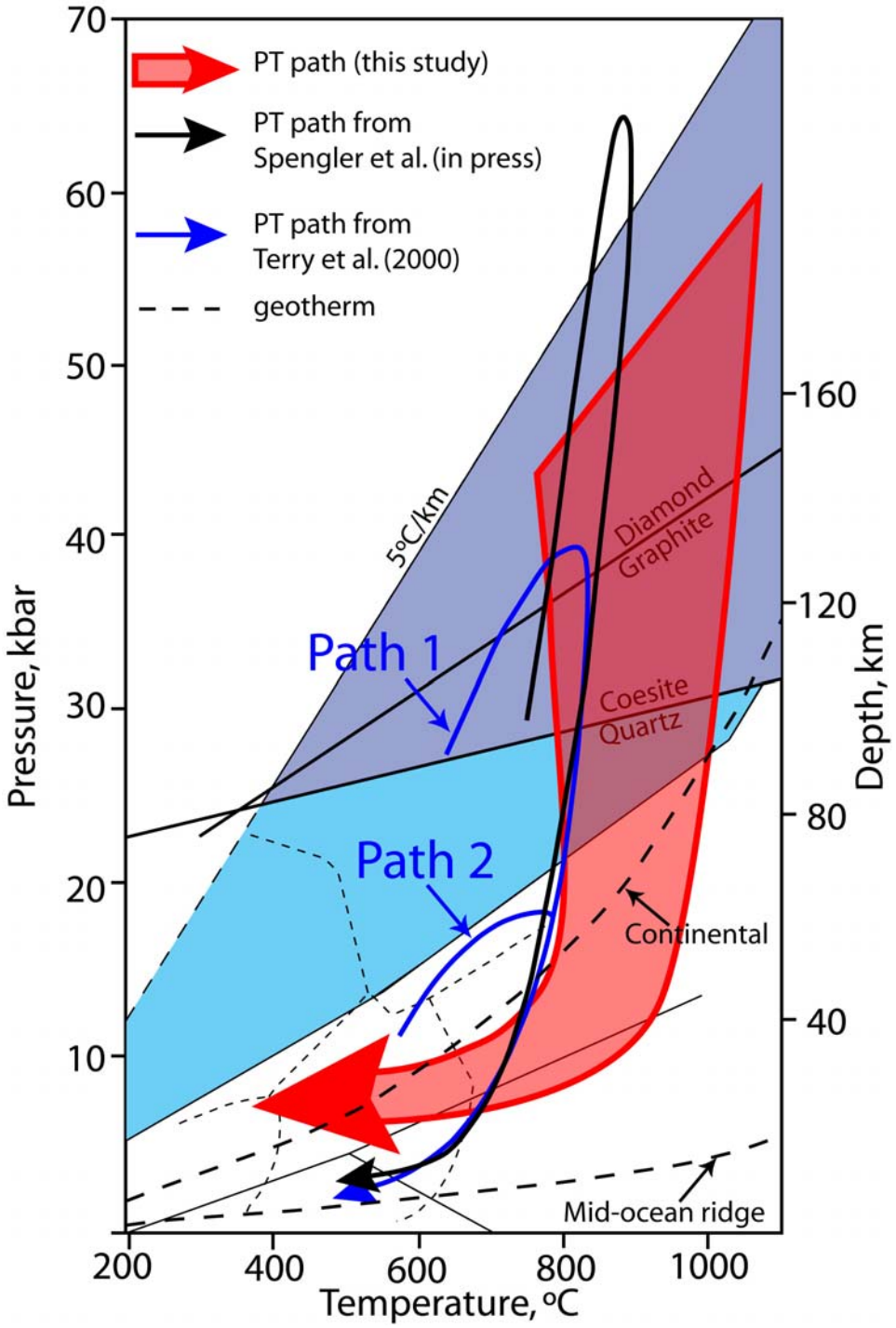

Figure 8.1. Comparison between the PT path that is obtained in this study, the PT path as published in Spengler et al. (in press), which is a composite of PT results from Otrøy, Fjørtoft and Svartberget, and the PT path for two units in Fjørtoft from Terry et al. (2000a). Geotherms from Blatt et al. (2006), metamorphic facies, Al_2O_3 polymorphs, (U)HP fields, metamorphic facies fields and solidi as in figure 2.2.

Tectonic implications of PT path

Also plotted in figure 8.1 are average geotherms for a stable continental crust and of a mid-ocean ridge (geotherms from Blatt et al. (2006)). The 5ºC/km is normally taken as the coldest possible geotherm, associated with cold (rapid) subduction.

Although because suitable inclusion minerals in grt no prograde path could be obtained from the samples in this study, the peak PT conditions indicate a subduction origin. The peak PT conditions are colder than what is expected for a normal, stable, continental geotherm and

are close to the 5ºC/km geotherm. After the peak PT conditions exhumation is isothermal until it crosses the continental geotherm. So from a very cold conditions, conditions with excess heat over the normal continental geotherm are achieved. This could implicate that exhumation was very fast within the subduction setting, resulting very little cooling time. Another explanation is that the cold subduction setting changed to a hot extensional setting. In that way the exhumation was not necessarily very fast, because the change in environment caused hotter conditions at lower pressures. In either case do the PT conditions change back to the continental geotherm by isobaric cooling before the mid-ocean ridge geotherm is reached. No PT information is present for the PT path after this point.
This PT path is in agreement with the dunk tectonics model by Brueckner and Van Roermund (2004), as discussed in chapter 2.1.4, where subduction is followed by rapid buoyancy driven eduction along the subduction path.

Observations from other parts of the WGR indicate that garnet in HP eclogites show prograde zoning with amphibolite facies inclusions, while garnet in UHP eclogites are unzoned with eclogite facies inclusions (Wain et al., 2000). The pressure gap between HP and UHP eclogite is explained to tectonic juxtaposition of different units. This is contradicted by Cuthbert et al. (2000) and Carswell and Cuthbert (2003) who state that the difference between the eclogites is very hard to tell, and therefore no different HP/UHP units exist and tectonics should not be introduced. Although Gossa is from another location than where these observations have been done, it is still interesting to compare the garnet from HP/UHP eclogites with the garnet in the UHP eclogites on Gossa. Prograde zoning is not observed, instead garnet compositions are flat with only some retrograde zoning at the outermost rim (see figure 5.4 and figure 5.5). Inclusions, on the other hand, consist of cpx, amph and sometimes bio. This is an amphibolite facies mineral assemblage, which according to (Wain et al., 2000) is a characteristic of HP eclogites, while these eclogites are shown to be UHP. This observation is in agreement with Cuthbert et al. (2000) and Carswell and Cuthbert (2003) who state that HP and UHP eclogites cannot be told apart based on the characteristics of garnet zoning and inclusions.
Again, like in the discussion about the thrust nappes in the northern UHP domain as envisioned by Terry et al. (2000b), this observation is an argument against tectonic juxtaposition of HP and UHP units in the WGR.

Constraints on timing of insertion of mafic lenses in the basement gneisses
Relatively little constraints can be made on the timing of the insertion of mafic lenses in the basement gneisses. So far it could only be concluded that it happened before the formation of the present day main foliation in the basement gneisses. The PT path that has been deducted on the basis of peridotites by Spengler et al. (in press) and the PT paths based on eclogites in this study show a very good similarity. If the eclogites and the peridotites have shared the same PT history, they are very likely to have been part of the same lithological unit. This means that they had probably also been inserted in the basement gneisses for all of their shared PT history, and the basement gneisses therefore also are likely to have experienced UHP conditions. It is, however, possible that the eclogites and peridotites became one unit at, or before, UHP conditions and where inserted after UHP conditions in the basement gneisses. This would imply that the basement gneisses have not been to UHP conditions.

Expansion of the UHP area
Evidence of UHP conditions has been demonstrated from two opx bearing eclogites on Gossa. Both eclogites are located in the southern basement. Because of reasons discussed above, the basement itself is thought to have witnessed UHP conditions. Because of the similarity of the basement gneisses that are found on Gossa, and the description of the inferred Ulla Gneiss in Nordøyane, it is likely that this is one large UHP unit. The best prediction of this UHP domain is given by Vrijmoed et al. (2006).
Figure 8.2 shows the UHP occurrences in the northern UHP domain of the WGR (similar as

figure 2.11) extended with the UHP evidence from this study. The UHP domain as indicated by Vrijmoed et al. (2006) closest resembles the observation of one continues UHP domain from the mainland in the Bud-Tornes area to Nordøyane. The UHP boundary on Gossa is best drawn between the southern basement unit and the allochthonous unit (red line). The allochthonous unit is a HP unit (Verberne, 2009) and in the northern basement no suitable rocks have been found for PT analysis. Therefore there is no indication for UHPM in that unit. The data of this study supports the outline of the UHP domain by Vrijmoed (2006) with the notion that the northern boundary on Gossa is located 1-2 km's more south in order to trace the boundary between the southern basement and the supracrustals.

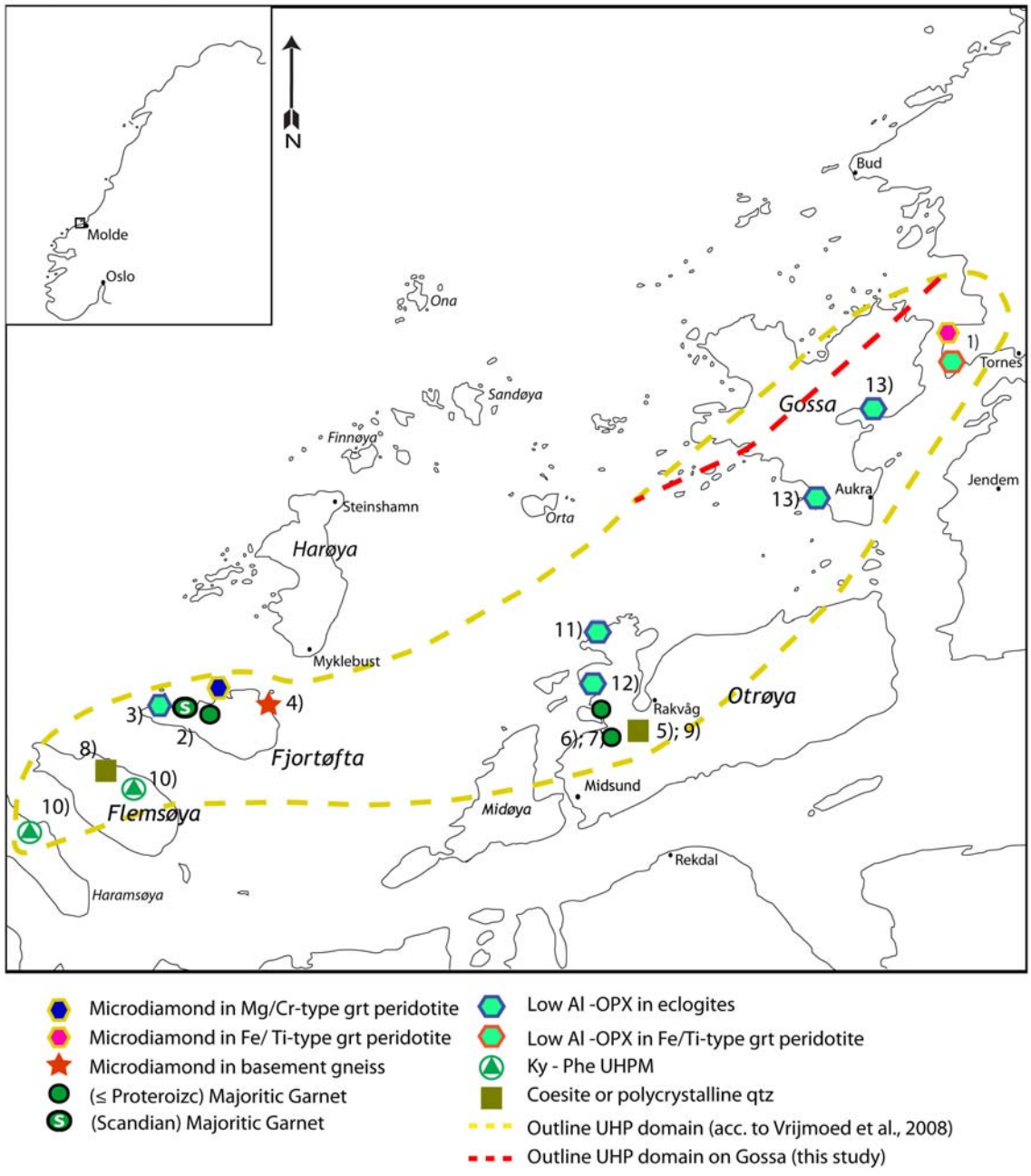

Figure 8.2. UHP occurrences in the vicinity of Gossa. Similar to figure 2.11, but extended with: 13) UHP evidence from this study and the dashed red line indicating a more detailed boundary between UHP and non-UHP units on Gossa.

9 Conclusions

- Samples from two opx bearing eclogites from the southwestern part of Gossa are investigated by EMP. Al_2O_3 contents in opx grains of 0.26 wt% (outcrop 17.5) and 0.30 wt% (outcrop 10.5) indicate diamond grade UHP metamorphic conditions.
- Qtz + amph exsolution has been found in cpx minerals in eclogites and granulites. This feature has by some authors been used as indication for (diamond grade) UHP metamorphic conditions. However, controversy in the literature is too great to assign this exsolution feature to UHP conditions.
- No indication for the presence of coesite/PCQ has been found in the opx bearing eclogites, even though geothermobarometric calculations show UHP metamorphic conditions for these rocks.
- A retrograde PT path is constructed based on optical microscopy and EMP analysis of eclogites, granulites and basement gneisses. The PT path that shows a good correlation with published PT paths from others locations within the UHP domain.
- Based on the UHP metamorphic conditions experienced by eclogites in the southwestern part of Gossa and the correlation of the PT path with other parts of the northern UHP domain, the southwestern part of Gossa can confidently be included in the northern UHP domain.
- The area of northern UHP has been determined by a few authors. The outline of the northern UHP domain by Vrijmoed et al. (2006) is found to be most accurate. A small correction is sufficient to incorporate the results from this study.
- The Ulla Gneiss on the islands of Fjørtoft and Flemsøy has not reached UHP metamorphic conditions according to Terry et al. (2000b). The tectonic model by Terry et al. (2000b) explained the existence of UHP units next to the LP Ulla Gneiss by tectonic thrusting. The discovery of UHP metamorphic conditions in opx bearing eclogites on two locations within the Ulla Gneiss on Gossa is a strong indication that the trusting theory of Terry et al. (2000b) is invalid.

10 Acknowledgements

I would like to thank Herman van Roermund for his supervision during this Master thesis. His company in the field was very inspiring and he was always generous with his time. Also his air mattress was very comfortable, after mine had exploded. I could not have survived the second part of the fieldwork without it. Auke Barnhoorn his help during the fieldwork and especially during the process of writing the thesis was indispensible. Our discussions have made me think clearer about the problems that I faced and made this a better thesis. Also I want to thank Bart Verberne for making the fieldwork such a good experience. The community of Aukra have very generously supplied us with high quality aerial photographs. This greatly contributed to the geological mapping on Gossa. The Molengraaff fonds has supported the fieldwork financially, and their contribution was vital for this research. Further I would like to thank Tilly Bouten for her help at the EMP, Hans de Bresser for discussions about the structural geology and Stijn Verhagen for his company in Norway. Everyone else who I shared the countless coffee breaks with have also, although in a relaxing way, contributed to this thesis.

11 References

Alden, A., 2009. http://geology.about.com/od/more_igrocks/ig/igroxdiagrams/.

Andersen, T.B. and Jamtveit, B., 1990. Uplift of deep crust during orogenic extensional collapse: a model based on field studies in the Sogn-Sunnfjord region, W. Norway. Tectonics, 9: 1097-1111.

Austrheim, H., 1991. Eclogite formation and dynamics of crustal roots under continental collision zones. Terra Nova, 120: 492-499.

Beyer, E., O'Reilly, S. and Griffin, B., 2001. GEMOC 2001 annual report.

Blatt, H., Tracy, R.J. and Owens, B.E., 2006. Petrology. W.H. Freeman and Company, New York.

Brandelik, A., in press. Calcmin - an EXCEL Visual Basic application for calculating mineral structural formulae from electron microprobe analyses. Computers & Geosciences.

Brey, G.P., Bulatov, V.K. and Girnis, A.V., 2008. Geobarometry for peridotites: Experiments in simple and natural systems from 6 to 10 GPa. Journal of Petrology, 49(1): 3-24.

Brey, G.P. and Kohler, T., 1990. Geothermobarometry in four-phase lherzolites II. New thermobarometers, and practical assessment of existing thermobarometers. Journal of Petrology, 31(6): 1313-1352.

Bromiley, G.D. and Keppler, H., 2004. An experimental investigation of hydroxyl solubility in jadeite and Na-rich clinopyroxenes. Contributions to Mineralogy & Petrology, 147(2): 189-200.

Brueckner, H.K. and van Roermund, H.L.M., 2004. Dunk tectonics: A multiple subduction/eduction model for the evolution of the Scandinavian Caledonides. Tectonics, 23(2).

Bucher, K. and Frey, M., 2002. Petrogenesis of Metamorphic Rocks. Springer-Verlag.

Carswell, D.A., 1991. The garnet ortho-pyroxene Al barometer - problematic application to natural garnet lherzolite assemblages. Mineralogical Magazine, 55(378): 19-31.

Carswell, D.A., Brueckner, H.K., Cuthbert, S.J., Mehta, K. and O'Brien, P.J., 2003. The timing of stabilisation and the exhumation rate for ultra-high pressure rocks in the Western Gneiss Region of Norway. Journal of Metamorphic Geology, 21(6): 601-612.

Carswell, D.A. and Cuthbert, S.J., 2003. Ultrahigh pressure metamorphism in the Western Gneiss Region of Norway. In: T. Carswell and R. Compagnoni (Editors), EMU notes in Mineralogy: Ultrahigh Pressure Metamorphism, pp. 51-73.

Carswell, D.A., Cuthbert, S.J. and Bruekner, H.K., 2005. Fluid-influx triggered formation of ultrahigh-pressure orthopyroxene eclogites at Arsheimneset and Grytting in the Western Gneiss Region of Norway. unpublished.

Carswell, D.A., van Roermund, H.L.M. and Wiggers de Vries, D.F., 2006. Scandian ultrahigh-pressure metamorphism of proterozoic basement rocks on Fjørtoft and Øtroy, Western Gneiss Region, Norway. International Geology Review, 48(11): 957-977.

Carswell, D.A., Wilson, R.N. and Zhai, M., 2000. Metamorphic evolution, mineral chemistry and thermobarometry of schists and orthogneisses hosting ultra-high pressure eclogites in the Dabieshan of central China. Lithos, 52(1-4): 121-155.

Carswell, D.A. and Zhang, R.Y., 1999. Petrographic characteristics and metamorphic evolution of ultrahigh-pressure eclogites in plate-collision belts. International Geology Review, 41(9): 781-798.

Chopin, C., 2003. Ultrahigh-pressure metamorphism: tracing continental crust into the mantle. Earth and Planetary Science Letters, 212(1-2): 1-14.

Cuthbert, S.J. and Carswell, D.A., 1990. Formation and exhumation of medium-temperature eclogites in the Scandinavian Caledonides. In: D.A. Carswell (Editor), Eclogite Facies Rocks. Blackie & Son, Glasgow, pp. 180-203.

Cuthbert, S.J., Carswell, D.A., Krogh-Ravna, E.J. and Wain, A., 2000. Eclogites and eclogites in the Western Gneiss Region, Norwegian Caledonides. Lithos, 52(1-4): 165-195.

Dobrzhinetskaya, L.F. et al., 1995. Microdiamond in high-grade metamorphic rocks of the Western Gneiss Region, Norway. Geology, 23(7): 597-600.

Droop, G.T.R., 1987. A general equation for estimating Fe^{3+} concentrations in ferromagnesian

silicates and oxides from microprobe analyses, using stoichiometric criteria. Mineralogical magazine, 51: 431-435.
Eckert, J.O., Newton, R.C. and Kleppa, O.J., 1991. The ΔH of reaction and recalibration of garnet-pyroxene-plagioclase=quartz geobarometers in the CMAS system by solution calorimetry. American Mineralogist, 76(1-2): 148-160.
Ellis, D.J. and Green, D.H., 1979. An experimental study of the effect of Calcium upon garnet-clinopyroxene iron-magnesium exchange equilibria. Contrib. Mineral. Petrol., 71: 13-22.
Ernst, W.G. and Liou, J.G., 2008. High- and ultrahigh-pressure metamorphism: Past results and future prospects. American Mineralogist, 93(11-12): 1771-1786.
Gasparik, T., 1985. Experimental study of subsolidus phase relations and mixing properties of pyroxene and plagioclase in the system Na2O-CaO-Al2O3-SiO2. Contributions to Mineralogy and Petrology, 89(4): 346-357.
Gasparik, T., 1986. Experimental study of subsolidus phase relations and mixing properties of clinopyroxene in the silica-saturated system CaO-MgO-Al2O3-SiO2. American Mineralogist, 71: 686-693.
Graham, C.M. and Powell, R., 1984. A garnet - hornblende geothermometer: calibration, testing and application to the Pelona Schist, Southern California. J. Metamorphic Geology, 2: 13-31.
Green, H.W., 2005. Psychology of a changing paradigm: 40+years of high-pressure metamorphism. International Geology Review, 47(5): 439-456.
Griffin, W.L. et al., 1985. High-pressure metamorphism in the Scandinavian Caledonides. In: D.G. Gee and B.A. Sturt (Editors), The Caledonian orogen Scandinavia and related areas, pp. 783-801.
Harley, S.L., 1984. An experimental study of the partitioning of iron and magnesium between garnet and orthopyroxene. Contr. Mineral. Petrol, 86: 359-373.
Hemingway, B.S., Bohlen, S.R., Hankins, W.B., Westrum, E.F. and Kuskov, O.L., 1998. Heat capacity and thermodynamic properties for coesite and jadeite, reexamination of the quartz-coesite equilibrium boundary. American Mineralogist, 83(5-6): 409-418.
Joanny, V., van Roermund, H. and Lardeaux, J.M., 1991. The clinopyroxene plagioclase symplectite in retrograde eclogites - a potential geothermobarometer, pp. 303-320.
Kennedy, C.S. and Kennedy, G.C., 1976. The Equilibrium Boundary Between Graphite and Diamond. J. Geophys. Res., 81.
Köhler, T., 2007. http://www.mineralogie.uni-frankfurt.de/index.html.
Kohn, M.J. and Spear, F.S., 1990. Two new barometers for the garnet amphibolites with applications to south-eastern Vermont. American Mineralogist, 75: 77-84.
Krabbendam, M. and Dewey, F., 1998. Exhumation of UHP rocks by transtension in the Western Gneiss Region, Scandinavian Caledonides, Continental Transpressional and Transtensional Tectonics.
Labrousse, L., Jolivet, L., Agard, P., Hebert, R. and Andersen, T.B., 2002. Crustal-scale boudinage and migmatization of gneiss during their exhumation in the UHP Province of Western Norway. Terra Nova, 14(4): 263-270.
Leake, B.E. et al., 1997. Nomenclature of amphiboles: Report of the subcommittee on amphiboles of the International Mineralogical Association, Commission on New Minerals and Mineral Names. Canadian Mineralogist, 35: 219-246.
Liou, J.G., Zhang, R.Y., Ernst, W.G., Rumble, D. and Maruyama, S., 1998. High-pressure minerals from deeply subducted metamorphic rocks. In: R.J. Hemley (Editor), pp. 33-96.
Mancktelow, N.S., 2008. Tectonic pressure: Theoretical concepts and modelled examples. Lithos, 103(1-2): 149-177.
Newton, R.C. and Perkins, D., 1982. Thermodynamic calibration of geobarometers based on the assemblages garnet - plagioclase - orthopyroxene (clinopyroxene) - quartz. American Mineralogist, 67: 203-222.
NGU, 2009. Bedrock Maps, 1:250,000 scale.
Nickel, K.G. and Green, D.H., 1985. Empirical geothermobarometry for garnet peridotites and

implications for the nature of the lithosphere, kimberlites and diamonds. Earth and Planetary Science Letters, 73(1): 158-170.
Page, F.Z., Essene, E.J. and Mukasa, S.B., 2003. Prograde and retrograde history of eclogites from the Eastern Blue Ridge, North Carolina, USA. Journal of Metamorphic Geology, 21(7): 685-698.
Page, F.Z., Essene, E.J. and Mukasa, S.B., 2005. Quartz exsolution in clinopyroxene is not proof of ultrahigh pressures: Evidence from eclogites from the Eastern Blue Ridge, Southern Appalachians, USA. American Mineralogist, 90(7): 1092-1099.
Poli, S. and Fumagalli, P., 2003. Mineral assemblages in ultrahigh pressure metamorphism: a review of experimentally determined phase diagrams. In: T. Carswell and R. Compagnoni (Editors), EMU notes in Mineralogy: Ultrahigh Pressure Metamorphism, pp. 307-340.
Powell, R., 1985. Regression diagnostics and robust regression in geothermometer/geobarometer calibration: the garnet-clinopyroxene geothermometer revisited. Journal of Metamorphic Geology, 3(3): 231-243.
Ravna, E.J.K., 1988. The garnet-clinopyroxene iron-magnesium geothermometer - a reinterpretation of existing experimental data. Contr. Mineral. Petrol, 99: 44-48.
Ravna, E.J.K., 2000. The garnet-clinopyroxene geothermometer: an updated calibration. Journal of Metamorphic Geology, 18: 211-219.
Ravna, E.J.K. and Paquin, J., 2003. Thermobarometric methodologies applicable to eclogites and garnet ultrabasites. In: T. Carswell and R. Compagnoni (Editors), EMU notes in Mineralogy: Ultrahigh Pressure Metamorphism, pp. 229-259.
Ravna, E.J.K. and Terry, M.P., 2004. Geothermobarometry of UHP and HP eclogites and schists - an evaluation of equilibria among garnet-clinopyroxene-kyanite-phengite-coesite/quartz. Journal of Metamorphic Geology, 22(6): 579-592.
Roermund, H.L.M.v., Carswell, D.A., Drury, M.R. and Heijboer, T.C., 2002. Microdiamonds in a megacrystic garnet websterite pod from Bardane on the island of Fjortoft, western Norway: Evidence for diamond formation in mantle rocks during deep continental subduction. Geology, 30(11): 959-962.
Roermund, H.L.M.v. and Drury, M.R., 1998. Ultra-high pressure (P > 6 GPa) garnet peridotites in Western Norway: exhumation of mantle rocks from > 185 km depth. Terra Nova, 10(6): 295-301.
Roermund, H.L.M.v., Drury, M.R., Barnhoorn, A. and De Ronde, A.A., 2000. Super-silicic garnet microstructures from an orogenic garnet peridotite, evidence for an ultra-deep (> 6 GPa) origin. Blackwell Science Inc, pp. 135-147.
Scambelluri, M., Pettke, T. and van Roermund, H.L.M., 2008. Majoritic garnets monitor deep subduction fluid flow and mantle dynamics. Geology, 36(1): 59-62.
Schumacher, J.C., 1991. Empirical ferric iron corrections: necessity, assumptions, and effects on selected geothermobarometers. Mineralogical Magazine, 55(378): 3-18.
Smith, D.C., 1984. Coesite in clinopyroxene in the Caledonides and its implications for geodynamics. Nature, 310: 641-644.
Smith, D.C., 1995. Microcoesites and microdiamonds in Norway: an overview. In: R.G. Coleman and X. Wang (Editors), Ultrahigh Pressure Metamorphism, pp. 299-355.
Spengler, D., 2006. Origin and Evolution of Deep Upper Mantle Rocks from Western Norway. PhD-thesis Thesis, Utrecht University, Utrecht.
Spengler, D., Brueckner, H.K., Roermund, H.L.M.v., Drury, M.R. and Mason, P.R.D., in press. Long-lived, cold burial of Baltica to 200km depth.
Spengler, D. et al., 2006. Deep origin and hot melting of an Archaean orogenic peridotite massif in Norway. Nature, 440(7086): 913-917.
Terry, M.P. and Robinson, P., 2003. Evolution of amphibolite-facies structural features and boundary conditions for deformation during exhumation of high- and ultrahigh-pressure rocks, Nordoyane, Western Gneiss Region, Norway. Tectonics, 22(4).
Terry, M.P. and Robinson, P., 2004. Geometry of eclogite-facies structural features: Implications for production and exhumation of ultrahigh-pressure and high-pressure rocks, Western Gneiss Region, Norway. Tectonics, 23(2): 23.

Terry, M.P., Robinson, P., Hamilton, M.A. and Jercinovic, M.J., 2000a. Monazite geochronology of UHP and HP metamorphism, deformation, and exhumation, Nordoyane, Western Gneiss Region, Norway. American Mineralogist, 85(11-12): 1651-1664.

Terry, M.P., Robinson, P. and Ravna, E.J.K., 2000b. Kyanite eclogite thermobarometry and evidence for thrusting of UHP over HP metamorphic rocks, Nordoyane, Western Gneiss Region, Norway. American Mineralogist, 85(11-12): 1637-1650.

Touret, J.L.R. and Frezzotti, M.-L., 2003. Fluid inclusions in high pressure and ultrahigh pressure metamorphic rocks. In: T. Carswell and R. Compagnoni (Editors), EMU notes in Mineralogy: Ultrahigh Pressure Metamorphism, pp. 467-487.

Verberne, B., 2009. Geobarometry & geochronology applied to allochthonous rocks of Gossa island, Western Gneiss Region, Norway.

Vrijmoed, J.C., Smith, D.C. and van Roermund, H.L.M., 2008. Raman confirmation of microdiamond in the Svartberget Fe-Ti type garnet peridotite, Western Gneiss Region, Western Norway. Terra Nova, 20(4): 295-301.

Vrijmoed, J.C., Van Roermund, H.L.M. and Davies, G.R., 2006. Evidence for diamond-grade ultra-high pressure metamorphism and fluid interaction in the Svartberget Fe-Ti garnet peridotite-websterite body, Western Gneiss Region, Norway. Mineralogy and Petrology, 88: 381-405.

Wain, A., 1997. New evidence for coesite in eclogite and gneisses: Defining an ultrahigh-pressure province in the Western Gneiss region of Norway. Geology, 25(10): 927-930.

Wain, A., Waters, D., Jephcoat, A. and Olijynk, H., 2000. The high-pressure to ultrahigh-pressure eclogite transition in the Western Gneiss Region, Norway. European Journal of Mineralogy, 12(3): 667-687.

Wain, A.L., Waters, D.J. and Austrheim, H., 2001. Metastability of granulites and processes of eclogitisation in the UHP region of western Norway. Journal of Metamorphic Geology, 19(5): 607-623.

Walsh, E.O. and Hacker, B.R., 2004. The fate of subducted continental margins: Two-stage exhumation of the high-pressure to ultrahigh-pressure Western Gneiss Region, Norway. Journal of Metamorphic Geology, 22(7): 671-687.

Wells, P.R.A., 1977. Pyroxene thermometry in simple and complex systems. Contr. Mineral. Petrol, 46: 129-139.

Young, D.J., Hacker, B.R., Andersen, T.B. and Corfu, F., 2007. Prograde amphibolite facies to ultrahigh-pressure transition along Nordfjord, western Norway: Implications for exhumation tectonics. Tectonics, 26(1): 15.